

Sheffield Hallam University

The microstructure and precipitation effects in Inconel alloy 690.

SMITH, Alan J.

Available from the Sheffield Hallam University Research Archive (SHURA) at:

<http://shura.shu.ac.uk/20371/>

A Sheffield Hallam University thesis

This thesis is protected by copyright which belongs to the author.

The content must not be changed in any way or sold commercially in any format or medium without the formal permission of the author.

When referring to this work, full bibliographic details including the author, title, awarding institution and date of the thesis must be given.

Please visit <http://shura.shu.ac.uk/20371/> and <http://shura.shu.ac.uk/information.html> for further details about copyright and re-use permissions.

POLYTECHNIC LIBRARY
POND STREET
SHEFFIELD S1 1WB

TELEPEN

100264957 9



~~26/4 - 20.55~~

- 5 MAY 2003 5pm

~~23.1. 18.26.~~

27/10 - 8.50 pm.

12/4 16:55

27 MAY 2004 9pm

17 AUG 2005 5pm

23 APR 2002

4.36pm

24 APR 2002

4.31

9.1. 8.56 pm

28 APR 2003

9pm

ProQuest Number: 10701017

All rights reserved

INFORMATION TO ALL USERS

The quality of this reproduction is dependent upon the quality of the copy submitted.

In the unlikely event that the author did not send a complete manuscript and there are missing pages, these will be noted. Also, if material had to be removed, a note will indicate the deletion.



ProQuest 10701017

Published by ProQuest LLC (2017). Copyright of the Dissertation is held by the Author.

All rights reserved.

This work is protected against unauthorized copying under Title 17, United States Code
Microform Edition © ProQuest LLC.

ProQuest LLC.
789 East Eisenhower Parkway
P.O. Box 1346
Ann Arbor, MI 48106 – 1346

THE MICROSTRUCTURE AND PRECIPITATION EFFECTS
IN INCONEL ALLOY 690.

by

ALAN JOHN SMITH

A THESIS SUBMITTED TO THE COUNCIL
FOR THE NATIONAL ACADEMIC AWARDS IN
PARTIAL FULFILMENT OF THE REQUIRMENTS
FOR THE DEGREE OF

DOCTOR OF PHILOSOPHY
MARCH 1990

SPONSORING ESTABLISHMENT:

DEPARTMENT OF METALS AND MATERIALS ENGINEERING.

SHEFFIELD CITY POLYTECHNIC.

SHEFFIELD.

ENGLAND.

COLLABORATING ESTABLISHMENT:

HEALTH AND SAFETY EXECUTIVE.

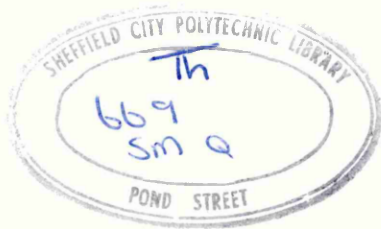
HER MAJESTY'S NUCLEAR INSTALLATIONS INSPECTORATE.

ST PETERS HOUSE.

BOOTLE.

LIVERPOOL.

ENGLAND.



PREFACE

The work described in this thesis was carried out at Sheffield City Polytechnic between the 1st October 1986 and 30th September 1989, under the supervision of Dr R.P. Stratton, Director of Studies, and Dr F.B. Pickering, who has acted in an advisory capacity. Dr B. Hemsworth, of H.M.N.I.I., acted as industrial supervisor.

In accordance with the regulations for the award of Ph.D. the relevant parts in the MSc. in Metallurgical Process Management were successfully completed. The details of the course are given below:

MODULE II

1. Numerical Methods
2. Computer Programming

MODULE III

1. Stainless Steels
2. Heat Treatment.

An advanced level course in Stress Corrosion Cracking and Corrosion Fatigue of Metals was also successfully completed at Newcastle University.

Two papers have been presented, from the research, at international conferences. The titles of the papers are given below:

Effects of Carbon Content and Heat Treatment on the Microstructure of Alloy 690 Steam Generator Tubing.

Presented at the NUCMAT 88 conference on Materials Engineering for High Risk Environments. 22 - 24 June 1988, Nice France.

Relationship Between Composition, Microstructure and Corrosion
Resistance of Alloy 690 Steam Generator Tubing for PWR Systems.
Presented at the Fourth International Symposium on Environmental
Degradation of Materials in Nuclear Power Systems - Water
Reactors. 6 - 10 August 1989 at Jekyll Island, U.S.A..

DECLARATION.

During the period of registration for the CNAA degree of Ph.D. the candidate has not been registered for any other CNAA award or for a university degree.

The results and theories presented in this thesis are original except where reference is made to previous work.

Signed :

Date :

26/3/90

ACKNOWLEDGEMENTS

The author would like to thank the Sponsoring Establishment , Sheffield City Polytechnic, and the Collaborating Establishment, The Health and Safety Executive - Nuclear Installations Inspectorate, for enabling this work to be carried out. Particular thanks are due to my academic supervisors Dr R.P.Stratton, my industrial supervisor Dr B. Hemsworth and to Dr F.B.Pickering who acted in an advisory capacity.

I would also like to thank the following establishments for either material, advice, or the use of equipment in specialised areas of the experimental work:

CEGB - Sizewell - England.

CERL - Leatherhead - England.

UKAEA - Harwell - England.

UKAEA - Risley - England

Framatome - Paris - France.

Vallourec - Montbard - France.

Sandvik - Sandviken - Sweden.

Newcastle University - Newcastle - England.

Thanks are also due to all the technical staff in the materials Dept with particular reference to Mr P Slingsby, Mr S.Creasy, Miss R. Colington, Dr B.Lewis, Dr J.Cawley and Mr G.Gregory. I am also grateful to Dr H. Adrian for his helpful discussion and invaluable assistance with computing.

Finally thanks are due to my family for their support and encouragement and to Fiona for doing the washing up when I needed to work.

ABSTRACT

Failure of Alloy 600 steam generator tubing in Pressurised Water Reactors (PWR's) has prompted the investigation of alloy 690 as an alternative material. Six commercially produced tubes and ten experimentally produced alloys have been examined with varying amounts of carbon, aluminium and titanium. Alloy compositions have been selected to investigate the individual and combined effects of these elements on the microstructure and corrosion behaviour in the environments of corrosion tests and simulated PWR conditions.

Alloys were subjected to simulated mill annealing treatments at varied temperatures. Microstructural characterisation using optical and electron microscopy has demonstrated the effects of composition and thermal treatment in controlling grain size and carbide precipitation together with the interdependence between these structural details.

Stress corrosion resistance of selected alloy 690 tubes has been examined with samples in an autoclave at fixed temperatures with environments based on pure water, sodium hydroxide and sodium hydroxide + sodium sulphate solutions. Susceptibility to intergranular attack has been related to aluminium contents of the alloy and to thermal treatments given. Results suggest a decreased resistance to IGA when aluminium is increased. Thermal treatments given to the samples appear not to be very significant to the amounts of IGA.

The compositions and heat treatments used in the corrosion study were further examined on a dedicated scanning transmission electron microscope in order to correlate the effects of, chromium depletion, nickel enrichment and impurity segregation at grain boundaries, with corrosion characteristics. These results have shown the effect of varying the special thermal treatment temperature and time on the degree of enrichment / depletion / segregation and the corrosion resistance of the alloy. The mechanism of protection afforded by the special thermal treatment can thus be elucidated.

TABLE OF CONTENTS.

	<u>Page</u>
1. <u>INTRODUCTION</u>	1
2.0 <u>LITERATURE REVIEW</u>	3 - 70
2.1 Historical Review.....	3
2.2 Austenitic Stainless Steel.....	17
2.3 Alloy 600.....	19
2.4 Alloy 690.....	34
2.5 Carbon.....	47
2.6 Process Parameters Which Exert the Greatest Influence Over Corrosion Resistance.....	53
2.7 Effect of Dispersed Particles on Grain Size.....	56
2.8 Precipitation.....	60
3. <u>EXPERIMENTAL METHOD</u>	71 - 81
3.1 Selection of Materials for Study.....	71
3.2 Preparation of Experimental Melts.....	72
3.3 Solution Treatment of Alloys.....	73
3.4 Hardness Determinations.....	73
3.5 Optical Metallography.....	74
3.6 Electron Microscopy.....	75
3.7 Thermal Ageing Studies.....	78
3.8 Corrosion Studies.....	78
3.9 Tensile Studies.....	81
4. <u>EXPERIMENTAL RESULTS</u>	82 - 94
4.1 Identification of Precipitates Present in Commercial Tubing.....	82
4.2 Identification of Inclusions Present in Experimental Alloys.....	83
4.3 Hall - Petch Relationship for As Received Commercial Tubing.....	84

4.4	Effect of Varying Carbon Content in the Absence of Both Aluminium and Titanium.....	84
4.5	Effect of Varying Carbon in Alloys Containing 0.03% Aluminium and 0.38 Titanium.....	87
4.6	Effect of Varying Aluminium with Constant 0.02% Carbon and 0.27% Titanium.....	88
4.7	Effect Of Varying Titanium in Alloys Containing 0.019% Carbon and 0.12 % Aluminium.....	90
4.8	Thermal Ageing Studies.....	91
4.9	Corrosion Studies.....	92
4.10	Tensile Tests.....	94
5.	<u>DISCUSSION</u>	95 - 140
5.1	Carbon Solubility.....	95
5.2	The Effect of Chromium Carbide Dispersion on Grain Size.....	98
5.3	The Difference in Hardness Between the As Received and the Experimentally Produced Alloys.....	101
5.4	Grain Size Inhomogeneity.....	103
5.5	Activation Energy for Recrystallisation and Grain Growth.....	106
5.6	The Effect of Varying Carbon in the Absence of both Aluminium and Titanium.....	108
5.7	The Effect of Varying Carbon with 0.03% Aluminium and 0.38% Titanium.....	110
5.8	The Effect of Varying Aluminium in the Presence of 0.02% Carbon and 0.27% Titanium.....	113
5.9	The Effect of Varying Titanium in the Presence of 0.02% Carbon and 0.14% Aluminium.....	115
5.10	Measurements of the Chromium Depletion Profile of Thermally Treated EM 12.....	120
5.11	Corrosion.....	127
5.12	Thermal Ageing Studies.....	132
5.13	Cellular Precipitation.....	134
5.14	Commercial Considerations.....	137

6.	<u>CONCLUSIONS</u>	141 - 147
7.	<u>SUGGESTIONS FOR FUTURE WORK</u>	148 - 149
8.	<u>REFERENCES</u>	150 - 156
9.	<u>TABLES</u>	157 - 176
10.	<u>FIGURES</u>	177 - 233
11.	<u>APPENDIX A</u>	I - VII

1. INTRODUCTION

A major area of concern in Pressurised Water Reactors (PWR) are the safety aspects of steam generator (SG) tubes. The safety functions of these tubes are concerned with containment of primary fluid and heat abstraction from the primary circuit. A variety of corrosion problems may arise from the environmental conditions in which the SG tubes operate and include such problems as denting, phosphate wastage, stress corrosion cracking (SCC) and intergranular attack (IGA). These problems have been overcome to a large extent by either modification of the environment/design, reducing stress levels, or selecting materials which are resistant to the particular form of corrosion.

Alloy 690 has a nominal composition of 60% Ni-30% Cr-10% Fe and has been recommended as a material for steam generator tubing in PWR systems. The carbon content has a significant effect upon the heat treatment required to produce material which is more resistant to various forms of degradation. The mill annealing temperature is critically dependent on carbon content because of the necessity to dissolve sufficient chromium carbides prior to the special thermal treatment which controls the size, shape and distribution of carbides. The more corrosion resistant materials are associated with moderately large grains (ASTM 6) semi-continuous grain boundary carbides and minimal intragranular carbides.

There is a requirement for a systematic investigation of the effects of minor alloying additions and thermal treatment upon

the precipitation of carbides. Corrosion tests may be carried out on materials treated to produce controlled microstructures with specific carbide configurations and the results of the corrosion tests may be related to the compositional and microstructural conditions.

2.0. LITERATURE REVIEW

Inconel Alloy 690 is a high chromium, nickel based fully austenitic alloy, designed to resist corrosion and oxidation in aggressive industrial environments at elevated temperatures. Rigorous laboratory tests on the alloy over the past 15 to 20 years have shown that the alloy has tremendous resistance to sensitisation and stress corrosion cracking (SCC) in caustic environments. The fundamental physical and chemical properties of the alloy, as outlined in the original copyright (1), are shown in table I.

Since the purpose of this literature review is to examine in a comparative way the work carried out on 690 so far, and since the bulk of 690 is used in the nuclear industry for steam generator tubes, it is appropriate to start with a brief account of how and why this material was developed, which was primarily to resist SCC in high temperature aqueous environments.

2.1. HISTORICAL REVIEW.

Long before the innovation of the pressurised water reactor (PWR), steam generator tubes were highly susceptible to corrosion problems. This is hardly surprising considering the working environment :- either hot water, furnace flames or hot gases on the primary side, with high temperature high velocity water on the secondary side. The two are separated by ordinary unprotected steel.

In the pressurised water reactor steam generators (fig 1), the primary side inlet water temperature is approximately 325°C, whilst the outlet temperature on the secondary side is typically 293°C. This super heated - water is being pumped at an average pressure of 157 bar and at a rate of 4685 kg/s (2). Obviously, liquid moving through the 5626, 17.48mm (OD) U-tubes at such velocity is going to cause considerable vibration and associated mechanical problems, including water hammer, fretting and wear of tubes, as well as erosion corrosion. For this reason, the tube bundles are fitted with anti- vibration bars and bound together with tube support plates. Finally, the tubes are connected in a variety of ways to the baseplate or tube sheet, which forms the division between the primary and secondary side.

The primary reactor coolant water is maintained in a purified condition. It has a dual purpose: it acts as a heat transport medium and as a moderator. By injecting a boron compound into the coolant, it is possible to slow down the faster moving neutrons produced in the fission process so that they might react with the fuel rod atoms (e.g. U_2O_5). This maintains and controls the process. Water purity and chemistry are maintained by circulating a portion of the water continuously through heat exchangers and by a deep bed ion exchange mixture in a demineraliser (3) .

Secondary side water chemistry is currently controlled by an All Volatile Treatment (AVT). How this treatment was arrived at will now be examined.

One of the original problems associated with SG's of PWR's was caustic induced stress corrosion cracking , which was attributed to a lack of rigorous control over the sodium-to-phosphate ratio (4). This co-ordinated phosphate water treatment was chosen since it was the conventional water treatment used in fossil fuel fired boilers with similar steam pressures. The inability to control the Na : PO₄ ratio resulted in the presence of free caustic , which in turn led to caustic induced stress corrosion cracking (SCC). The solution to this was to change to a low sodium to phosphate molar ratio control (from 2.8 to 2.0), which greatly reduced the incidence of SCC, but which ultimately led to a more general form of corrosion, now known as phosphate wastage. The postulated mechanism for this type of attack is similar to that suggested for the build up of high concentrations of NaOH (5). A sludge pile consisting of any solid contaminants inside the steam generator, such as phosphate corrosion, and erosion products, etc. builds up on the tube sheet. At some critical height liquid at the base of the pile is vaporised but not replenished. The temperature in this region would be approaching that of the primary coolant. This steam blanketing effect would prevent any build up of solids and, therefore, of any aggressive salts. Similarly, there would be no build up of salts at the top of the sludge pile, since there is sufficient circulation of water to prevent drying out. The remaining region - where there is just enough circulation of water to allow alternate wetting and drying and thus concentration of undesirable contaminants - is, however, that of maximum wastage, fig (2a). The attempt to control the deleterious effects of contaminant acidic salts had in itself produced a problem of water chemistry

which had to be overcome.

The solution to this problem involved a change in water chemistry control from the co-ordinated phosphate water treatment to the ammonia-hydrazine based AVT. This treatment was not universally adopted. The German KWU and Canadian CANDU reactors have both opted for a low phosphate treatment using Alloy 800 and have experienced a lower rate of wastage, although it is not clear whether this is due to the material used, to the low Na : PO₄ or to the comparatively low rates of in-leakage recorded in these plants. It is most likely the conjoint effect of all these. The adoption of AVT did not, however, eradicate corrosion problems in steam generators. In fact, the change heralded the introduction of a further problem - denting.

2.1.1 Denting

Denting has been defined as "plastic deformation of tubes resulting from the build up of carbon steel plate corrosion products (Magnetite) in the tube to tube support plate annuli" fig (2). This phenomenon first appeared in 1975 in plants which had changed to AVT and up until November 1984, approximately 24 PWR units in the USA had reported denting, with 8 plants being affected extensively. As can be ascertained from the definition, the cause of the stress, and ultimate denting of the tube, is the pressure provided by the increase in the volume of the corrosion product compared to the volume of metal corroded (6). The cause of this Potter-Mann type linear accelerated corrosion was found to be associated with the formation of a high concentration of an

acid and oxidising environment, which is highly corrosive to carbon steels, as well as with extremely high levels of chloride concentration found between the tube and tube support plate. The chloride, having originated from such sources as condenser in-leakage, could accumulate by local thermal hydraulic conditions.

The damage caused by denting includes: tube cracking and leakage at the constricted crevice, tube cracking and leakage at U bends, tube support ligament failure and tube support plate gross deformation. The short term solution to the problem involved " sleeving " the dented tubes, Fig (2b).

Denting was found to be so widespread by 1977 that the Steam Generators Owners Group was set up in an effort to eradicate the problem. Having identified the cause (ie the conjoint effect of an aggressive environment and, in that environment, unsuitable material/design), the solution was, inevitably, to improve the environment by reducing the impurity levels permissible in the secondary water. This has been achieved by reducing condenser in-leakage, reducing air in-leakage, producing purer make-up water by using condensate polishers to purify the water and by the use of boric acid to inhibit acid chloride attack. Other improvements, introduced as early as 1975 by Framatome, include a change in support plate design from the drilled to broached holes Fig (3). In the broached quatrefoil design, the fluid is forced to flow around the tubes (sweeping), thereby reducing the risk of dry out and

preventing the accumulation of corrosion products. A further design improvement was to change the material of manufacture from a plain or low alloy carbon steel to a 13% Cr. ferritic stainless steel. This latter change may have been prompted by the fact that KWU steam generators, which use 347 stainless steel in their support structures, have never reported denting (7). A problem which has affected the KWU SG's, as well as 29 other plants, is that of primary side stress corrosion cracking.

2.1.2 Primary Side Stress Corrosion Cracking.

Stress corrosion cracking (SCC) has been described in general terms as " stressed alloy failures that occur by the propagation of cracks in corrosive environments " (8). There are basically two different types of failure mechanism :-

- (1) The removal of material at the crack tip.
- (2) The separation of material at the crack tip.

Such is the complexity and, above all, lack of agreement as to which mechanism is operative - especially in stainless steels - that a more simplistic nomenclature, one that describes the environment that caused the SCC, has been adopted. Thus, terms like chloride cracking, caustic cracking and oxygen cracking are used to describe modes of failure in high temperature water environments which contain chloride, caustic or oxygen. The terms hydrogen embrittlement and sulphide cracking both relate to a cracking process which involves entry of hydrogen into the metal. The sulphide ion in the latter acts as a hydrogen ion recombination poison, promoting the entry of hydrogen into the metal.

This (sulphide ion) will be discussed later when considering resin intrusion as a cause of SCC in 600 in working PWR's and of 690 in test loops (51).

The first in-service failure attributed to primary side stress corrosion cracking (P.S.S.C.C.) occurred at the KWU built plant at Obrigheim in 1971, although the phenomenon of high nickel alloys cracking in high purity water had been reported by Coriou et al as early as 1966 (9). The areas most severely affected by this mechanism of failure are the inner U bends, roll transition, roll expansion and areas affected by denting. These are obviously areas of high stress, due either to manufacture, installation or corrosion. It should be noted, however, that thermal stress can also greatly affect cracking resistance. Several remedies have been suggested and tried to overcome the stress component contribution to P.S.S.C.C (10). These include :-

(1) In Situ stress relief. This involves using resistance heaters at U bends, induction heaters at roll transitions and/or a global treatment of the entire tube sheet area.

(2) Shot peening. (Either normal shot or Rotapeening.) Account must be taken of the total tube stress (ie not only the compressive ID stress, but also the tensile outside diameter stress.)

The environmental factor of greatest importance appears to be the temperature. The failures that occurred at the roll transition,

for example, did so only on the hot leg. Reducing the temperature difference between the hot and cold leg by some 30°C could increase the time for cracking by some 4 to 5 times (11). It has been demonstrated by Airey (12) and Bandy et al. (13) that further environmental problems include the presence of hydrogen gas and/or chemical contaminants. Their results show that pure water is more aggressive than primary water (with lithium hydroxide, boric acid and hydrogen added) at the same hydrogen concentration.

The final component of this stress corrosion system to be considered must be material with specific reference to Alloy 600, the predecessor and lower chromium version of Alloy 690. It has been shown by many workers (14) that the most susceptible microstructure for alloy 600 to P.S.S.C.C. is one with fine grains and predominantly intragranular carbide precipitation, which is the structure produced by a low final mill annealing temperature. Conversely, the structure with predominantly intergranular carbide precipitate, with or without grain boundary chromium depletion, shows improved high purity water S.C.C. resistance (15) (16). The optimum microstructural condition has been achieved by solution treating in the range 982-1010°C followed by a 704°C treatment for 15 hours to allow for back diffusion of chromium. This back diffusion is of importance when considering sensitisation and intergranular attack.

2.1.3 OD Intergranular Attack / Intergranular Stress Corrosion Cracking.

As the heading suggests, there are essentially two types of intergranular attack of steam generators. The first, I.G.A., is a uniform attack of all the grain boundaries over the surface of the tube. The second, known as intergranular stress corrosion cracking (I.G.S.C.C.), has a corrosion morphology which consists of a single, or multiple major cracks with moderate amounts of branching. The main difference between I.G.A. and I.G.S.C.C. is that there is no evidence of any stress contribution for the more uniform I.G.A. Cracks propagate intergranularly in both cases. Because this form of attack is mostly confined to crevice locations (ie tube to tube sheet crevice and tube/tube support plate crevice), it has, as yet, not resulted in a large rupture, although it has caused extensive and expensive outages in virtually all fresh water cooled P.W.R steam generators.

The mode of concentration of the aggressive chemicals is, again, a wetting and drying process and although the resulting contaminants from the process and the postulated effects of the contaminants are varied, ultimately, I.G.A. results. Five such classes of contaminant are listed below:-

- (1) High concentration of sodium and/or potassium hydroxide.
- (2) Reaction products from the reduction of the sulphate ions with hydrazine or hydrogen (this reaction may produce reactive

sulphur bearing species).

- (3) The products of thermal decomposition of ion exchange resins, sulphates and organic residuals.
- (4) Highly concentrated salt solutions at neutral or near neutral pH (these salts being the natural consequence of condenser leakage concentrated to a high level of salt by the boiling process in the steam generator).
- (5) Alkaline carbonates and/or their reaction products, or hydrolysed products. These are believed to affect the nature of the passive film on the surface of the alloy.

The corrective action for I.G.S.C.C. is initially going to be to reduce, or where possible eradicate, the stress component. In new generators this is achieved by either full bundle stress relief on completion of fabrication or by employing thermally treated alloy 600. More recently, thermally treated alloy 690 has been employed, although this method has not been universally adopted. The method employed for operating plants is to sleeve the tubes using a material which is resistant to a caustic environment. Modification of the environment has been the method for controlling I.G.A. and may well apply equally to I.G.S.C.C. The environmental remedies so far attempted include:-

- (1) Lowering the temperature (see P.S.S.C.C).
- (2) Adding a pH neutraliser (ie boric acid).
- (3) Removing the corrodent by flushing.

(4) Changing the concentration and/or ratio of bulk water
contaminants .

(5) Design modifications (ie the improvement of hydraulic flow
above the tube sheet to minimise areas of low flow velocity where
sludge can accumulate).

2.1.4 Pitting

The laminar pits encountered so far have occurred on the cold leg
side between the tube sheet and first support plate. The mechanism
is again believed to be due to the concentration effect of alter-
nate boiling and drying in sludge piles adjacent to the pitted
areas. The cause of the pitting has been attributed to chlorides
(either sea water or copper chlorides), low pH, and an oxidant such
as CuCl_2 or O_2 (17).

The solution to this problem is, again, to modify either the mate-
rial/design or the environment. For existing plants, sleeving has
been adopted using a bi-metallic alloy which can resist both OD
pitting and ID P.S.S.C.C. The environmental improvements are very
much as for other corrosion mechanisms which rely on a sludge pile
build up (ie minimise the ingress of solids and reduce air in
leakage, sludge lancing and chemical cleaning, and, where possible,
reduce the ingress of contaminants primarily by following the
secondary water chemistry guidelines).

2.1.5 Fatigue Cracks

Vibration within the generators can lead to loss of metal from the tubes by a process known as fretting. This is caused by small amplitude oscillations of the tube against support plates. This metal loss, though serious, can lead to the initiation of fatigue cracks, which in a detrimental environment can further lead to corrosion fatigue (18).

These cracks are primarily associated with the upper regions of the Once Through Steam Generators (O.T.S.G.), although, so far, it is felt that recirculating SG's are immune only because they have not been in service long enough. The corrosive environment thought to exist in the upper regions of the O.T.S.G's, and which is used in testing, is an acid sulphate/silicate solution. Tests carried out under these conditions at 289°C and 10^7 cycles resulted in a fatigue strength which was 56% of the value measured under similar conditions. in air.

The corrective action, in common with all the other environmentally related failure mechanisms, is to modify the environment by minimizing the ingress of impurities. Material improvements have been found to be somewhat more complicated, since the behaviour of the tubing material is affected by both environment and support plate material (19). For example, it has been found that alloy 600 wore the least against a ferritic alloy support plate in simulated secondary fluid compared to austenite and plain carbon steel support plates. In faulted sea water conditions, however, it was the corrosion behaviour of the tube support plate alloys which

dominated the fretting wear behaviour of both 600 and 690. The thermo-hydraulic characteristics have been modified by reducing the opening at the base of the wrapper, which increases the fluid momentum at penetration of the tube bundle, by introducing a flow distribution baffle, which creates a flow towards the centre of the tube sheet and so reduces upward flow velocities.

To bring this historical review up to-date, an examination of two plants, one recently commissioned, the other due for completion in 1992, will be made. These plants will draw, or have drawn together all the preventative measures mentioned (20).

2.1.6 Tsuruga 2

This plant entered commercial operation on 17.2.87. It is the first in a line of new generation four loop plants in Japan and has embodied many advanced features which include:-

- (1) The adoption of thermally treated alloy 600 for the tube materials.
- (2) The modification of the tube support plate hole.
- (3) Operation with high hydrazine concentration.
- (4) The installation of a full flow condensate demineraliser.
- (5) The keeping of alkaline metal ion concentration below 1ppb, or control of condensate and make up water to maintain molar ratio ($Na / Cl < 1$) where Na^+ concentrations exceeds 1 ppb.

(6) The minimal use of any materials during construction which contain alkaline metal ions (e.g. shielded electrodes for welding).

Other improvements at the design stage include improved materials and hole configuration for the tube support plate, as well as modification of secondary side thermal and hydraulic characteristics.

There has also been a good deal of work on achieving more effective tube inspection. More space is now provided for eddy current inspection, and the design of the steam generator nozzle lid has also been improved.

2.1.7 Guangdong

Guangdong nuclear power joint venture company (GNPJVC), recently signed contracts with Framatome, Electrite de France (EdF) and General Electric Company for the construction of two 900 MWe PWR's. The two units are due on stream in 1992 / 1993 and their design incorporates many of the features discussed, including:-

- (1) All-volatile treatment of secondary water.
- (2) Stainless steel support plates with quatrefoil broached holes to prevent denting.
- (3) Inconel 690 for the tube material to increase resistance to IGA and SCC.
- (4) Thermal heat treatment to reduce PSSCC.

(5) Full depth tube expansion, with complementary expansion "kiss" rolling in the tube sheet.

(6) Various thermal hydraulic improvements to preclude the formation of deposits above the tube sheet.

Since there is little published on alloy 690 it seems logical to look first at austenitic stainless steel for a general background and then more specifically at alloy 600 to examine more closely the parameters which have greatest effect on the performance of 690.

2.2. Austenitic Stainless Steels.

Austenitic stainless steels have an approximately equiaxed grain structure. Precipitation primarily occurs at grain boundaries, when cooling at industrial rates, and the type and quantity of precipitate will depend on the following variables; carbon and or nitrogen content, the presence of elements with a higher affinity for carbon/nitrogen than chromium, the austenite grain size or defect structure and the cooling rate from the solution treatment temperature. The precipitation of chromium carbides occurs at regions of fastest diffusion ie. grain boundaries. Precipitation of these chromium rich carbides causes the denudation of chromium in the adjacent areas. If the level of chromium falls below that required for passivation then the resulting chemical and physical differences between precipitate , matrix and impoverished grain boundary region , in a suitable corrosive environment , will promote intergranular attack. If a sensitised component is subject to even a small tensile stress, be it applied or residual, then an

intergranular stress corrosion crack can result. The chemical differences between carbide, denuded area and matrix will include segregation of minor alloying elements and impurities. The effect of these impurities on SCC resistance will depend on the test environment. For example stainless steel containing less than 0.003% P appears to be immune to SCC in boiling magnesium chloride, the effect becoming less pronounced as Ni content increases (21), yet in high temperature water containing chloride ions the beneficial effect of low phosphorous is not so pronounced. Carbon content has little effect on failure times and crack path in NaOH solutions (22) yet has a marked effect in pure water in alloys containing less than 26% Cr. Sulphur does not effect SCC in manganese chloride solutions directly but manganese sulphide inclusions have been known to give rise to pits and thus enhance the initiation of cracks. Kowaka et al. go on to suggest that besides phosphorous and nitrogen other detrimental elements for an 18%Cr - 10%Ni stainless include Mo, Cu and Cr (23).

As stated, a factor which will affect the precipitation and subsequent sensitisation of austenitic stainless steels is the addition of an element which has a higher affinity for carbon than chromium, ie a stabilising agent. Titanium and niobium are often used for this, promoting the precipitation of titanium and niobium carbides. Titanium additions are normally five times the carbon content, niobium is ten times (24). The niobium addition appears to be more effective at improving IGSCC resistance possibly because Ti(CN) precipitates at grain boundaries. It has been widely reported that TiC dissolves in nitric acid and Hanninen (25) has reported the

dissolution of TiC in oxygenated high temperature water in stabilised AISI 321 steel.

Finally it is possible to desensitise the microstructure by employing a special thermal treatment which promotes the back diffusion of chromium into the denuded areas thus homogenising the chromium content. Many heat treatments (26) have been tried in an attempt to not only homogenize the levels of chromium but also change the carbide distribution from continuous to discrete grain boundary particles.

2.3. Alloy 600.

Alloy 600 was designed for use in the dairy industry (27). It was selected for use in the PWR steam generators because of its good general corrosion resistance in high temperature water. Since alloy 600 is the higher nickel, lower chromium predecessor to 690 and is the closest material in terms of composition and working environment, it seems appropriate to examine alloy 600 in more detail.

2.3.1 Primary Side Stress Corrosion Cracking of Alloy 600.

The factors which have greatest influence over PSSCC have been identified as: environment, stress and microstructure. Environmental factors include temperature and hydrogen, water chemistry and purity having been dealt with previously. The temperature difference between the hot and cold leg in the steam generator (30 - 40°C) appears to influence significantly the initiation of PSSCC. This

suggests a thermally activated process whose rate can be expressed by an Arrhenius relationship, $\exp. (-Q/KT)$. Q = activation energy k = Boltzmann's constant and T = absolute temperature. Results suggest that a reduction of 30°C will increase the time to cracking by a factor of 4 to 5. The effect of hydrogen overpressure has been evaluated by Bulishech (28) and Airey (12). Bulishech found that, compared to pure water, the effect of the hydrogen overpressure was to promote shorter PSSCC initiation times. An examination by Airey of the composition and structure of the oxide layer showed that the oxide on the pure water specimen was thicker and the chromium content higher. Nickel was present in both the elemental and oxide form only on the pure water specimen, the oxide layer on the sample taken from the autoclave with a hydrogen overpressure had nickel present only in the elemental form. Airey suggests that it is the form and structure of the oxide film in the hydrogenated water compared to the pure water which influences the SCC initiation time.

The stress component of PSSCC can arise from a number of sources: residual stress inherent from tube manufacture/installation, water/steam pressure, thermally induced stresses and denting.

Experience has shown that (29) in those areas of highest stress i.e. row 1 U bends, expanded joints etc., where a microstructure is susceptible, attack can be rapid.

How the microstructure affects PSSCC has received a great deal of attention (30) and opinion is divided as to why the special thermal treatment (mill anneal at 1040°C followed by a 704°C 15

hour heat treatment) has such a profound effect on the SCC resistance of the alloy in deaerated high temperature water especially when considering that the opposite effect is afforded in aerated water under similar conditions. Many workers (30) (31) agree that the special thermal treatment enhances PSSCC resistance and have added that the improvement is evident with or without grain boundary chromium depletion. This is because deaerated water does not attack denuded areas and for this reason it has been suggested by Berge et al. (32) that the grain boundary carbide film physically blocks intergranular oxidation. Blanchet has suggested that sulphur may be an important impurity for PSSCC in pure water.

McIlree et al (33)(34) carried out corrosion tests on a series of Ni-Cr-Fe alloys with C, S and P at the upper limit for commercial materials and found that they did not impair alloy 600 corrosion resistance in high temperature deaerated water. these results also applied to low levels of C, S and P.

2.3.2. Effect of Metallurgical Parameters.

Recent work carried out by Norring (35) on PSSCC in pure water with a hydrogen over pressure at 365^oC on alloy 600 has shown the effect of the following metallurgical parameters on crack initiation time:

- (1) Annealing temperature.
- (2) Carbon content.
- (3) Amount of grain boundary carbide.
- (4) Grain size.

(5) Yield stress.

Norrington has shown that annealing temperature has considerable influence over crack initiation time. Increasing the temperature from 925°C to 1025°C increases the crack initiation time from 1200 hours to 10,000 hours. These results have been extrapolated to 320°C using an Arrhenius extrapolation with $Q = 50 \text{ Kcal/mol}$ which has shown that increasing the mill annealing temperature would increase the service life by 20 years.

The results from the study do not show a correlation between the total carbon of the alloy and the crack initiation time. However if the carbon contents of the experimental alloys are plotted against the final mill annealing temperature and the carbon solubility of alloy 600 is included on the same axis then a fairly good correlation between carbon content and crack initiation time is achieved.

This demonstrates that when annealing alloy 600 account must be taken of the carbon content since there is a strong correlation between increasing carbon not taken into solution and decreasing crack initiation time.

It follows from this that the amount of grain boundary carbide will also be of importance since the more carbon taken into solution the greater the carbon available for subsequent precipitation and Norrington's work confirms this.

A good correlation has also been shown between grain size, yield strength and crack initiation time. The larger the grains (ASTM 6) the lower the yield strength (250 MPa) and the longer the crack initiation time. However this may well reflect the effect of the higher mill annealing temperature since both grain size and yield strength are highly annealing temperature dependent.

A recent EPRI report (36) describes results gained, through the application of several microanalytical techniques, when examining microstructure, microchemistry and microdeformation aspects that may contribute to IGSCC susceptibility in alloy 600. Grain boundary Cr contents in the U bend region of steam generator tubes removed during shut down of a working PWR were found to be consistently lower than those measured in the straight sections. These differences, though small, appear statistically valid and are believed to be due to rapid diffusion paths present in the heavily deformed U bend region. This accelerated diffusion prompts a significant decrease in Cr content within a several-atom spacing of the boundary, but is not fast enough to affect the overall chromium depletion gradient.

Mill annealed and thermally treated material of alloy 600 were examined in the high voltage electron microscope (HVEM). Using dynamically strained specimens it was possible to monitor microdeformation events. Macroscopic deformation was accommodated by localised dislocation movement within planar arrays. Thermally treated specimens with higher densities of grain boundary carbides produced more homogeneous deformation. The grain boundary carbides

had been identified as primary dislocation sources, thus the thermally treated (TT) specimens produced many more dislocations with the consequence that shorter pile-ups resulted. The isolated grain boundary carbides in the mill annealed (MA) microstructure provided a limited number of carbides per grain resulting in longer pile-ups, less homogeneous deformation and higher local stress at grain boundaries. It is suggested that the differences in microdeformation characteristics between MA and TT conditions may have significant implications on the mechanism(s) controlling IGSCC of alloy 600 steam generator tubing. It is proposed that the microdeformation characteristics influence the intergranular crack tip stress distribution and, thereby the crack tip strain rate. Crack tip strain rate is an integral part in both dissolution controlled cracking and hydrogen embrittlement.

2.3.3 Secondary Side Intergranular Attack and Stress Corrosion Cracking.

Although all the steam generators which have exhibited intergranular attack, be it IGA, IGSCC or IGP (Intergranular penetration (IGP) is a hybrid of the previous two) have been tubed with alloy 600, it has been shown that alloy 800 and 690 MA are also susceptible.

Again the nature of the passive film has been examined to ascertain the effect of impurities. Hanson (37) exposed samples of alloy 600 at different potentials to caustic and borate solutions to simulate the effect of oxidising and reducing conditions that could arise by the presence of either impurity. Significant differences were noted at higher potentials. The oxide layer exposed to the borate solution showed no signs of

mechanical damage, whereas the oxide produced in the caustic environment was thicker and had cracked. Aluminium and silicon concentration of the oxide increased with increasing potential although it is not clear whether this is due to preferential dissolution of other metallic elements or deposition of contaminants. This study has shown how caustic can promote a damaged oxide layer which can allow further attack of the underlying parent metal. Pure borate water, similar to that used in a working PWR, does not appear to have an adverse effect on the alloy between the temperatures examined (290 °C - 325°C).

McIlree et al (33) (34), in a study carried out to examine the effects of C, S and P found that higher C reduced the SCC resistance in deaerated 50% NaOH at 316°C, but high S contents in combination with high C decreased the deleterious effects of the C. Phosphorus did not affect the NaOH SCC susceptibility.

A study of the effect of low temperature heat treatment on SCC resistance in high temperature water containing chloride ions, such as might occur under faulted sea water cooled conditions, has been carried out by Kowaka et al (38). The results suggest that a low temperature mill anneal (930°C) allows a shorter thermal treatment time (15 hours at 700°C) compared to a mill anneal at 1150°C which necessitated a TT of some 100 hours before IGA and IGSCC resistance was recovered. The microstructure of the low temperature MA alloys contained large and discrete carbides both at grain boundaries and in the matrix. The low MA temperature microstructure consisted of flaky and continuous carbide precipi-

tates only at grain boundaries. The inference from these results must be that the rate at which Cr diffuses through the matrix to the denuded areas is heavily dependent on carbide morphology and distribution. Since continuous grain boundary carbide must first break down and since the grain size of the higher temperature MA specimen is larger the time to desensitisation will be longer. It was also suggested that moderately high C should be used since this should allow faster IGA and IGSCC recovery.

Payne et al. (39) carried out a detailed study of the effect of mill annealing temperature and TT time at 704°C on commercial tubes in deaerated 10% NaOH and 30% NaOH + 10% Na₂SO₄. These results show that IGA/IGSCC resistance is critically dependent on solution treatment temperature. Commercial tubes mill annealed and thermally treated were found to be equally susceptible to IGA/IGSCC yet the same material given a high temperature mill anneal 1150°C (0.032%C) followed by a thermal treatment of 704°C for as little as 90 minutes demonstrated a much greater IGA/IGSCC resistance. The as received commercial material had a microstructure consisting of a high density of intragranular carbides with both discrete M₂₃C₆ growing at high angles to the boundary and colonies of cellular M₂₃C₆. After the laboratory MA and TT the microstructure consisted of a semicontinuous M₇C₃ precipitate at grain boundaries. A heat treatment of 90 minutes would not be sufficient time to ensure back diffusion of Cr to the denuded grain boundary areas to above the minimum 9% Cr minimum suggested by Was et al. (40). It must therefore be concluded that the results agree with (30), (31), who state that in

pure deaerated water corrosion resistance is improved with or without desensititation. This is an indication of why the results of Kowaka et al. are so markedly different to Payne et al.. Kowaka examined the effect of an acidic environment - one which might be expected to attack Cr denuded areas. Thus the lower mill annealing temperature would promote fewer grain boundary carbides and less time would be required for desensitisation. No mention is made of the carbide phase present but it must be assumed that it is $M_{23}C_6$ since nucleation of M_7C_3 is more dependent on the activity of carbon and a low mill annealing temperature would dissolve less carbon. This, in conjunction with the fact that precipitation of M_7C_3 is more difficult than $M_{23}C_6$, suggests an $M_{23}C_6$ carbide phase. Payne et al. have shown that precipitation of discrete $M_{23}C_6$ and filamentary and columnar $M_{23}C_6$ is indicative of a microstructure that is not resistant to attack in high temperature caustic. These results demonstrate the danger of extrapolating data obtained from one corrosive environment to another.

The mechanism of protection afforded by the high temperature mill anneal + thermal treatment is not fully understood. Payne et al. have noted a detrimental effect of large grains and has suggested that segregation of impurities to the grain boundaries in the MA only condition may be instrumental. A heat treatment which promotes isolated grain boundary carbides which incorporate solute impurities from grain boundaries regions has been shown to reduce susceptibility to IGA by interrupting its penetration path (26). This work was carried out on non - sensitised stainless steel in boiling nitric acid containing dichromates. Norring has shown

that a correlation exists between large grains and primary side IGA/IGSCC resistance. This is however following the TT. The large grains are in fact indicative of the high MA temperature which the alloy has undergone.

Airey (41) examined the effect of temperature on ageing times and found that the optimum thermal treatment was 705°C for 15 hours, although an ageing time of 10 hours was sufficient to restore Cr depleted areas at 705°C. Phosphorus and boron were both found to have segregated to grain boundaries and although the effect of boron is not reported, the effect of P was considered insignificant.

In a study carried out by EPRI (42) the time to failure as measured in the slow strain rate test conducted in a 1N sulphuric acid solution at room temperature and at an anodic potential (120 mV vs SHE) was found to be shortest for specimens heat treated at 600°C which corresponds to a maximum segregation of sulphur, silicon, nitrogen and titanium. Further corrosion results also show that precipitation at grain boundaries slightly enhances intergranular attack. These results are contrary to later work. The cause for this discrepancy is most likely due to a too low mill annealing temperature.

Much of the confusion which exists about the special thermal treatment applied to alloy 600 is due to the postulated in-service environment which the tubes will be subjected to and also to unspecified prior thermal-mechanical history. For example, in a sea water cooled reactor the build up of chlorine anions in

crevices, due to in leakage, can promote an acidic environment from which IGA/IGSCC can result. Alternatively as the tubes enter the base plate the sludge may, depending on local thermal/hydraulic conditions, be highly alkaline. In a simulated environment made up of 50% NaOH test results vary. Some have shown that a thermal treatment which promotes intergranular precipitation can slightly accelerate IGA (43), other workers have stated that the sensitised heat treatment has no effect on crack depth (51) and yet more results have shown that heating at 700°C greatly enhances IGA resistance (30). This latter conclusion is now the most widely accepted providing the material is mill annealed at a sufficiently high temperature to allow adequate carbon into solution prior to the special thermal treatment. Work by Coriou (9) has shown that it is the nickel content of the alloy which has the greatest influence over SCC resistance in deaerated NaOH and it has been suggested that the improvement in SCC resistance after the thermal treatment is due to the higher nickel concentration in the chromium denuded zones. Aspden et al. (44) has shown the importance of oxygen concentration on SCC characteristics. A comparison of alloy 600 and 690 showed that in oxygenated high temperature NaOH alloy 690 resisted SCC while 600 did not, but when oxygen was removed 690 cracked more readily than 600. These results would seem to suggest that sensitised 600 has enhanced SCC resistance due to nickel enrichment since 600 has a higher nickel content than 690.

Simulated corrosion tests in acidic environments have shown that heat treatment at 700°C for times of up to 3 hours promote severe IGA/IGSCC and it is not until the material has been heated for 10

hours that its structure is desensitised. Thus when examining the corrosion results after the special thermal treatment with particular regard to time at temperature, it is most important to consider the simulated corrosive environment.

Was et al. (40) have carried out measurements of chromium content in the chromium depleted areas using a Scanning Transmission Electron Microscope (STEM) in order to clarify the effect of heat treatment on corrosion resistance. From this study it was concluded that the depth and shape of the chromium depleted zone varies with thermal treatment, with the depth reaching a maximum after 10 hours. The depth refers to the degree of chromium denudation. The results are reported in terms of chromium content either side of the precipitate against perpendicular distance from the precipitate. Thus the deeper the attack the lower the chromium content in that area. After 100 hours the material was desensitised; unfortunately there were no intermediate times between 10 and 100 hours. The width of the depleted zone increases monotonically with time. It was found that preferential corrosion occurred at grain boundaries if the chromium content in the depleted zone fell below, or during healing failed to rise above 9% Cr. The only other element to segregate to grain boundaries in quantities significantly above the bulk was phosphorous. Was et al., however, conclude that it is chromium depletion which is primarily responsible for intergranular corrosion behaviour as a function of thermal treatment.

Kowaka et al. (38) and Kruger et al. (45) report that boron not only segregates it also precipitates at grain boundaries which enhances susceptibility to SCC by causing Cr depletion. After thermal

treatment corrosion resistance is recovered.

A further complication to the corrosion problems of alloy 600 may be in-service sensitisation. Work by Gane (27) has shown that precipitation of Ti(CN) occurs at grain boundaries and that that precipitation may be responsible for some grain boundary pinning. Work on alloy 800 (46) and other austenitic stainless steels has shown that decomposition of TiCN to chromium rich $M_{23}C_6$ can result in depletion of chromium in a narrow zone in the matrix adjacent to grain boundaries. Such in-service sensitisation would be highly deleterious. The decomposition in alloy 800 occurs at 800 °C which is somewhat higher than the working temperature of a PWR. However, given sufficient time at temperature decomposition has been shown to occur in austenitic alloys and such an occurrence would result in reduced tube life.

An advantage of the special thermal treatment is that it can help to overcome the wide heat to heat variability of the mill annealed alloy. Tests carried out by Bandy and Van Rooyen (47) using a range of mill annealing temperatures and static and dynamic tests, showed that when exposed to the polythionate SCC tests significant improvements, in SCC resistance, were observed following the special thermal treatment.

The most striking conclusion to draw when examining simulated corrosion data on alloy 600 is that the following factors must be taken into account:

- (1) Test environment and concentration. Acid, alkaline or neutral.
- (2) Oxygen potential. Aerated or deaerated.

- (3) Temperature of test.
- (4) Imposed potentials.
- (5) Prior thermo-mechanical history of test material.
- (6) Heat treatment. Precipitation/segregation.
- (7) Chemical composition. Particularly minor alloying additions.

From the above it is clear that data obtained for alloy 600 in a given corrosive media cannot be reliably extrapolated to another environment. This is clearly shown when considering the effect of sensitisation.

To summarise:

Alloy 600 has been shown to be susceptible to stress corrosion cracking in deaerated pure water and intergranular attack/stress corrosion cracking in the environment of secondary side water chemistry. The remedies used to combat these problems include: lowering the stress levels in the tube, preventing crevices by redesigning or by clearing crevices by mechanical means and finally by microstructural engineering. Work on control of the microstructure has shown that corrosion resistance of alloy 600 is critically dependent on:

Mill annealing temperature.

Ageing time and temperature.

Carbon content / solubility.

Possible segregation of minor alloying additions.

Since identifying these parameters, tighter control has been exercised over them. However, all the suggested remedies will increase either the steam generator production costs or PWR steam generator running costs.

An alternative material is alloy 690. It has acceptable mechanical properties including formability and by virtue of the higher chromium content ostensibly better corrosion resistance.

The vast majority of literature published to-date has concentrated on this corrosion resistance and, for this reason, the following section of the review will be sub - divided. Each division will be concerned with the envisaged mode of failure for a particular in-service application.

2.4. Alloy 690

2.4.1. Stress Corrosion Cracking (S.C.C.)

As stated, due to the complexity and lack of agreement concerning S.C.C. failures, a more simplistic nomenclature is used. It is one which describes the environment that caused the failure.

2.4.2. Chloride Environments

Austenitic stainless steels are known to suffer from catastrophic S.C.C, induced by chloride contaminants. The material currently employed in P.W.R steam generators, Alloy 600, has been shown by J.P.Hammond et al (48) to be susceptible to this type of attack. In fact, it has been suggested by Staehle et al (49) that the lowering of Chromium in Fe-Ni-Cr alloys to 10-15% increases resistance to cracking. Hammond et al (48) also examined a variety of commercially based Fe-Ni-Cr alloys, including 690, and arrived at the opposite conclusion. It is for this reason that Alloy 690 has been tested using a variety of procedures.

A.J.Sedriks et al (50) employed the following tests:

- (1) Boiling $MgCl_2$, $154^{\circ}C$, 13.9 weeks.
- (2) Undeaerated water + 500 ppm Chloride, $260^{\circ}C$, 18 weeks.
- (3) Vapour phase above environment No. 2, 8 weeks.
- (4) Undeaerated water + 875 ppm Chloride, $260^{\circ}C$. 8 weeks.
- (5) Vapour phase above environment No. 4, 8 weeks.
- (6) Undeaerated water + 660 ppm Chloride +150 ppm Na_2HPO_4 , $260^{\circ}C$, 8 weeks.

(7) Deaerated N_2H_4 water + 500 ppm Chloride, $316^{\circ}C$, 98 weeks.

Alloy 690 did not stress corrosion crack in any of these environments. Furthermore, in test No. 2, variables such as heat treatment, cold work, welding, and the presence of crevices did not promote S.C.C. No cracks were found by Hammond under cyclic steam environment tests and thus it was concluded that chromium in Ni-Cr-Fe alloys in the range 30 to 37% appears to impart immunity to chloride S.C.C. under these test conditions.

2.4.3. Caustic Environment

Alloy 600 suffers from caustic induced S.C.C. and does so to such an extent that it has been found necessary to treat thermally the tubes in-situ in order to promote a favourable carbide distribution. In fact, Sedriks (51) has shown that all commercially available nickel based alloys exhibit some degree of cracking in high temperature caustic environments. Aspden et al (44) carried out similar work and concluded that S.C.C. resistance increased with increasing nickel content. (600 has a higher nickel content than 690.) This view has been supported by many workers. McIlree et al (52), for example, went on to conclude that heat treatment had no consistent beneficial effect on the S.C.C. resistance of 690 and that it even had a deleterious one. These latter results are totally contrary to the more recent findings of Airey et al (53) and Gimond (54), who concluded that not only was the thermal treatment applied to 600 beneficial to 690, but that it would appear that thermal treatment parameters for 690 are much less critical than

those for 600. The cause of this disagreement is most likely the heat treatment used by McIlree et al (52) (1066-1121^oC), which produced a large grained microstructure with no grain boundary carbides. It has been suggested by many workers, including Gimond, that the most effective microstructure for resistance to S.C.C. in NaOH is a continuous and dense grain boundary precipitate, which is achieved at 700^oC after 5 hours, rather than the 15 hours required at temperature for 600. Airey (53) has gone on to suggest that this increased resistance may be associated with the phosphorous and boron which segregate to the grain boundaries and, it is suggested, alters the nature of the oxide film formed at those boundaries.

To summarise the results thus far published :-

- (1) Unde-aerated 50% NaOH, 300^oC, heat treated, cold worked and welded, no cracking.
- (2) De-aerated 10% NaOH, 316^oC, 20% crack penetration after 6 weeks. This was only just superior to 600. A variety of heat treated conditions were used without conclusive results as to their effects, except possibly that the least resistant treatment was the one also used by McIlree.
- (3) De-aerated 50% NaOH, 316^oC, 66% crack penetration, 5 weeks, slightly inferior to Alloy 600, although the differences are small and dependent on test temperature.

It has been suggested, again by McFlree,(52) that it is the nickel and the chromium which enhance the S.C.C. resistance of 690 in air and that in the absence of air, it is the nickel alone which is the predominant factor. This would explain the superior performance of 600 in 50% NaOH, deaerated, but not the results from the 10% NaOH deaerated.

Obviously, it is not just the corrosive environment which influences the S.C.C. behaviour of the alloy, but also the stress and the temperature at which that stress is applied. The effects of stress have been summarised by Gimond (54), whose results showed that cracking of Alloy 690 was possible in a concentrated caustic solution (100 g/l), providing the stress threshold of 80% yield strength is exceeded (measured at 350^o C) in the case of the mill annealed tubes and equal to, or above the yield stress for material in the thermally treated condition. Gimond (54) goes on to state that thermally treated 690 showed superior stress corrosion cracking resistance to mill annealed 690 and that optimum corrosion resistance is obtained using a high mill annealing temperature (1040^oC). The thermal treatment of 5 hours at 700^oC produces a coarse grained microstructure with a dense and semi-continuous grain boundary carbide (in agreement with the Westinghouse specification). Longer times at temperature do not increase the beneficial effect since it is maintained that 690 does not suffer from sensitisation (50).

2.4.4. High Temperature Water with Low Oxygen

Alloy 690 has been tested extensively in both low and high oxygen waters (ie 6 ppm - 10-20 ppb), and in pure and contaminated water. Tests include:(50)

- (1) Deaerated pH 10 water, 316^oC (48 weeks).
- (2) Deaerated pH 10 water + 60 ppm Na₂HPO₄, 326^oC, 96 weeks.
- (3) Deaerated water unadjusted pH , 316^oC, 48 weeks.
- (4) Deaerated water, unadjusted pH + Pb, 316^oC, 18 weeks.

Tests numbers 1 and 3 also incorporated a wide range of heat treatments, cold work, welding and the presence of crevices.

The results of these tests can be summarised by stating that under the condition of test, alloy 690 does not appear to be susceptible to S.C.C. in high temperature, low O₂ water. It should be remembered that crack initiation in Alloy 600 is highly temperature sensitive and it seems likely that 690 will have an even higher activation energy for crack initiation. Thus a more practical test temperature, still within the bounds of credibility for a working PWR, would be 340^oC. Page and McMinn (55) carried out tests aimed at simulating faulted conditions on the primary side of a Boiling Water Reactor (BWR) (ie neutral pH high purity water with an O₂ concentration of approximately 200 ppb + 1ppm H₂SO₄. H₂SO₄ is added, since resin from the demineraliser rapidly decomposes to form this compound). They also carried out similar tests without the resin intrusion, using

Alloy 600 for comparison. Both were carried out at 288°C using the slow strain rate method and crack growth rate studies were conducted in the simulated resin intrusion environment using pre-cracked constant displacement specimens. Both materials were as received and either low temperature or furnace sensitised. The carbon contents were 0.08% for 600, and between 0.012 and 0.02% for the two 690 melts. Alloy 600 and 690 exhibited surface cracking (creviced and uncreviced) during slow strain rate testing in the simulated resin intrusion environment, and crack growth during the constant displacement test, although the stress intensity required was higher for 690 (70 MPa m^{-1/2}) than for 600 (49 MPa m^{-1/2}), and the average crack growth rate for 690 was lower (2.2 x 10⁻⁸ mm s⁻¹ compared to 3.2 x 10⁻⁷ mm s⁻¹).

The effect of the resin intrusion is to lower the pH and increase the conductivity in the primary coolant system, and it has been shown by Andressen et al (56) that much more severe conditions can arise in service.

Electricity de France (EDF) (57) have specifically examined the primary side SCC resistance of Alloy 690 under a variety of test conditions. Tests at 360°C in pure water, pure water + H₂ and primary fluid failed to produce any SCC. The tubes were in the Mill annealed (1045 - 980°C) or thermally treated (700°C - 16 hrs) condition. Further tests by EDF include :

(A) Test on capsules - pure water 350°C, MA 1040°C.

(B) Test in Boucor loop - 325°C, 15 Bar, Li = 1.5 ppm, B = 1000 ppm

(C) U bend.

(D) C ring.

All of these produced no SCC after 27,000 hrs. It would appear from this evidence that 690 has excellent resistance to high temperature low oxygen pure water with a K_{iscc} of 70 MPa m^{-1/2} in a simulated resin intrusion environment.

2.4.5. Oxygenated Pure Water.

Stress corrosion resistance under these conditions was a major factor in the development of the composition of 690. It is not surprising, therefore, that 690 has shown excellent resistance to cracking when tested at various levels of aeration. Clarke et al. (58) have suggested, however, that cracking can be achieved at very high levels of O₂ (36 ppm), although the material used was not typical of wrought 690 and repeat tests using material with a well defined heat treatment yielded only one crack, most likely a weld defect. Therefore, with the exception of Clarke's work, 690 must be considered highly resistant to cracking in oxygenated pure water. Since such high levels of oxygen in an operating PWR are unlikely, this type of cracking should not arise.

2.4.6. Localised Corrosion

As stated, a major area of concern with 600 was intergranular attack or sensitisation. Briefly, sensitisation is due to the formation of chromium rich precipitates which form at grain boundaries. The high chromium concentration in the precipitate causes depletion of chromium in the metal adjacent to the precipitate. As a result, there is increased attack by those environments in which a decrease in chromium leads to an increase in corrosion rate (59). It is felt that the increase in chromium in 690 compared to 600 will reduce this problem by maintaining sufficiently high levels of chromium in the areas adjacent to the chromium rich precipitates. To test this theory, a series of intergranular corrosion tests have been carried out. The tests and results are given below.

2.4.7. Intergranular Corrosion Tests in Boiling 65% Nitric Acid

This test, known as the Huey test, (ASTM A262, Practice C) (60) is very severe. It attacks Cr depleted regions. Results from the Huey test show that the intergranular corrosion resistance of 690 is critically dependent on the carbon content of the alloy - fig (4a - 4b) . Fig (4a) shows the time temperature sensitisation diagram for 690 under Huey test conditions. Fig (4b) shows that the 0.02%C alloy (furnace sensitised) is resistant to sensitisation. High C levels which have been furnace sensitised, but which are still within the specified chemical composition range recommended for alloy 690, have given severe intergranular attack in boiling nitric acid, however. Welded samples of the lower

carbon alloy were also subjected to the Huey test and, again, very low rates of corrosion were recorded. The higher carbon alloy has yet to be evaluated under welded conditions.

Kai et al. (61) have examined chromium depletion around grain boundary carbides after thermal treatment. It was shown that chromium concentration first decreases then increases with heating time for the temperatures 538°C, 600°C and 700°C. At 800°C the chromium depletion profile always increases with increasing time. The minimum chromium content of all heats tested was 18% Cr. For alloy 600 the minimum chromium content required to ensure adequate intergranular corrosion resistance in an environment which would be expected to attack depleted grain boundary areas was 9% Cr. It is reasonable to assume that alloy 690 is highly resistant to sensitisation because of the high levels of chromium remaining in the areas adjacent to carbides despite heat treatments which would be expected to sensitise the structure. Kai et al. also examined the effect of heat treatment on carbide morphology and the results from this study are summarised in fig (4c).

Because of the severity of the Huey test, other tests have been tried in the hope that they might be more applicable to working conditions. These tests include the modified Huey, the Strauss, Streicher and Polythionic tests. The merits or otherwise of these tests are beyond the scope of this review, except to state that the modified Huey is the most used. This is despite the fact that predictions made from results gained using alloy 600 appear to be opposite to the trends found in practice .

A corrosion test which is claimed to be more discriminating than either the Huey or the Streicher tests is the Electrochemical Potentiokinetic Reactivation (EPR) method. The test is based on the relationship between the degree of sensitisation and the charge generated by the attack of the chromium deficient areas during a reactivation scan from the passive range. The test has been modified by Maday et al. (62) to ensure adequate sensitivity of testing for alloy 600. A solution composition of 0.1M H₂SO₄ + 0.001M KSCN has been selected in order to ensure the selectivity and sensitivity of the test.

2.4.8. Pitting in Chloride solutions.

Tests carried out at 316^oC in deaerated water containing 500 ppm chloride for 96 weeks revealed no evidence of pitting at 3000 x magnification (50). Research in this area continues and results suggest that 690 may be susceptible to attack in a number of corrosive environments.

2.4.9. Corrosion product release rates

Corrosion product release from the internal surfaces of steam generator tubes can contribute a significant amount to the total corrosion product release in the primary circuit of a PWR. Work carried out by Bodine et al (63) concentrated on tube manufacturing variables and their effect on the corrosion product release rate of alloy 600. It was concluded from the tests that production variables can affect the amount of corrosion product release, but the best overall trends were obtained using conventional PWR steam generator tube practices. It is desirable to keep steam generator corrosion product release to a minimum because nickel may transmute to a radioactive isotope of cobalt, Ni⁵⁸ (n,p)

Co⁵⁸, with a half life of 71 days

The behaviour of alloy 690 in ammoniated and borated simulated primary water, employing a high velocity test loop, has been examined. Results show that 690 loses less material to steam than any other material tested. These results suggest that the crude release rates of alloy 690 in an operating PWR could be very low. It should be noted that the data quoted should only be used as a guide since the results are subject to an error of some 25%.

2.4.10. Stress Corrosion Cracking Index.

Having discussed effectively three alloys - 690, 600 and, albeit briefly, 800 - it seems appropriate to end the corrosion section by reviewing a recent paper by R.J.Jacko (64). The paper sets out to evaluate the relative corrosion resistance of three alloys (mill annealed and thermally treated 600 and 690, and shot peened 800). All three alloys were tested under accelerated test conditions using several heats and various unspecified process parameters. The effect of welding on corrosion resistance was also studied. S.C.C. resistance was evaluated in both primary and faulted secondary environments at 332°C and Jacko suggests a decreasing severity ranking for the tests used:

(1) 10% NaOH.

(2) 10% NaOH + 1% CuO.

(3) 8% Na₂SO₄ pH 3.

(4) 12.7% FeCl₂.

(5) Pure water with dissolved O₂.

Two other indices were suggested:

(a) S.C.C. initiation index.

(b) S.C.C propagation index.

The highest value indicates greatest resistance and the results are given below:

Initiation Index.

Global avg.

Alloy 600.	37
Alloy 690.	90
Alloy 800.	80

Propagation Index.

Global avg.

Alloy 600.	67
Alloy 690.	99
Alloy 800.	80

There are, however, many factors which must cast doubt over the relevance of these indices. The most striking ones are listed below:

- (1) The paper does not state whether or not the faulted secondary environment has undergone deaeration, or how often over the 5000 hour period the solutions were replenished.

- (2) The assertion that all tests are equally relevant is preceded by a table of test environments ranked in order of decreasing severity.
- (3) No allowance was made for different stress or total exposure time when calculating the initiation index.
- (4) The practice of assuming that cracking would proceed at an average rate if a test was stopped in mid - term.
- (5) The 690 alloys used had carbon contents ranging from 0.015 - 0.02%, which has been shown to be the most resistant general carbon content. A wider spread of carbon contents, still within the compositional range recommended by the manufacturer, would have been more testing.
- (6) The idea of averaging the results gained from several environments makes a nonsense of the final global average.

This concludes the section on corrosion aspects of alloy 690. The following section will examine work published dealing with the physical metallurgy of the alloy. Since the importance of carbon has already been demonstrated, it seems appropriate to examine the effects of Carbon on the physical metallurgy separately.

2.5. Carbon

2.5.1. Carbon Solubility.

Gimond et al. (54) have stated that the best microstructure for SCC resistance is one with large grains, continuous grain boundary carbides, and as few intragranular carbides as possible. This can be achieved by ensuring that all the available carbon is in solution prior to the controlled ageing treatment. Knowledge of the carbon solubility of the alloy is, therefore, of utmost importance in order to ensure that the correct annealing temperature is used.

Norberg (65) Scarberry (66) and Nagano (67) have all produced solubility curves, Fig (5). The lower solubility of 690, compared to 600 has been attributed to the type of carbide formed. The predominant carbide formed in 690 is $M_{23}C_6$, which is more stable at high temperatures than the corresponding M_7C_3 in alloy 600. Thus, for a given carbon content, a higher annealing temperature is required to dissolve all the chromium carbides in 690 than in 600. Obviously, the three solubility curves for 690 differ considerably, especially at the lower carbon content range. This large difference is most likely due to the fact that Scarberry and Norberg used optical microscopy (Norberg at an unspecified magnification, Scarberry at x500) and Nagano used the SEM. These differences in conjunction with the associated problems of positive carbide identification must account for the discrepancy. This large difference of opinion suggests that a more detailed study is required, preferably using the TEM.

2.5.2 Effect of Carbon on Recrystallisation Characteristics

Norberg carried out a series of heat treatments, ranging from 800 - 1150°C in 50°C intervals using cold rolled strip (50% reduction). The experimental strip alloys used were those whose carbon contents were 0.006% - 0.017% and 0.053% C.

Recrystallisation in the low and medium carbon strip was completed in 5 mins at 800°C. The higher carbon strip required a temperature of at least 900°C. It seems likely that the overriding effect of prior cold work will have diminished the contrast between the high and low carbon levels. Further work seems necessary to examine the effects of both prior cold work and carbon content on the recrystallisation characteristics of the alloy. A further criticism of this work is that an average of only 3 hardness indentations were taken. Based on hardness indentations taken by the author, a standard deviation of 8 VPN could be expected. Such a large scatter may swamp the early trends (900 - 1050°C).

2.5.3. Effect of Carbon on Grain Coarsening Behaviour.

Norberg repeated the above experiment, but this time used the linear intercept method to examine the effects of annealing temperature on the grain size. As expected, the grain coarsening temperature increased with increasing carbon. This demonstrates the effective pinning of grain boundaries whilst sufficient carbon is present during annealing.

2.5.4. Effect of Titanium on Grain Coarsening Characteristics

Titanium is added to alloy 690 to tie up any nitrogen present, forming TiN or TiCN. This has the effect of improving hot workability. There has been some discussion in previous work that these precipitates may be responsible for grain boundary pinning in alloy 600 (27). Norberg has dismissed this notion and has stated that pinning due to TiN or TiCN is negligible in 690. This conclusion was arrived at by producing experimental melts in the absence and presence of titanium. These materials were then annealed as before and the grain coarsening characteristics examined, fig (6). There appeared to be no difference between the two.

This concludes the literature review of alloy 690. Since this alloy is most commonly used as steam generator tubing, it seems appropriate to examine the manufacturing procedures which can have the most profound effect on the product's in-service life. During the course of the research the author has visited two tube manufacturers, VALLOUREC, Montbard, France and SANDVIK, Sandviken, Sweden. The following section gives a brief account, by way of a flow diagram, of the typical process route for a steam generator tube and examines the possible effect each step may have on the quality and, thus, the in-service performance of the final product.

2.5.5. Summary.

A major area of concern in PWR's are the safety aspects of steam generator tubes. The safety functions of these tubes are concerned with containment of primary fluid and heat abstraction from the

primary circuit. A variety of corrosion problems may arise from the conditions in which the SG tubes operate.

Much of the research into alloy 600 has concentrated on microstructural engineering. Workers have shown that in a primary side environment 600 is more resistant to SCC if the grain boundaries are decorated with a semicontinuous network of carbides. The possible sensitisation associated with such a structure is not detrimental in a pure water environment. However, on the secondary side the build up of chloride anions, due to local thermo-hydraulic conditions can produce an environment which can readily attack a material in the sensitised state. This can be overcome by a special thermal treatment which allows sufficient time at temperature for the back diffusion of chromium from the matrix to the denuded grain boundary areas. Why this carbide morphology should enhance SCC resistance in deaerated pure water is not clear. It has been postulated that the carbide film physically blocks crack growth or that the carbides, by acting as primary sources for dislocations, influence microdeformation characteristics and crack tip strain rates. A further suggestion is that solute impurities segregate to grain boundary carbides thus removing these often deleterious impurities from the grain boundary.

The physical metallurgical factors which appear to exert the greatest influence over the suitability of alloy 600 for SG applications are, carbide shape, size and distribution, carbon content and final mill annealing temperature. In both deaerated pure water and deaerated NaOH, increasing mill annealing temperature increases IGA/SCC resistance.

Because of the problems associated with 600 work has gone into the development of more suitable alloys. The specified material for the Sizewell B project is alloy 690. Extensive corrosion tests have shown the alloy to be resistant to sensitisation in acidic environments and pure water but susceptible to attack in deaerated high temperature NaOH. As with alloy 600, a special thermal treatment has been shown to improve the alloy's corrosion resistance. Solubility of carbon in 690 is lower than alloy 600 due primarily to the higher chromium content of the former. It is for this reason that only the higher temperature chromium carbide has been reported in 690.

There has been comparatively little physical metallurgical work carried out on 690, most has concentrated on corrosion resistance. Data for carbon solubility have been presented but there is much scatter in the results and more work is needed in this area. No systematic study, both individual and synergistic, of minor alloying additions such as aluminium, titanium and carbon has been reported. There is a requirement for a systematic investigation of the effect of minor alloying additions and thermal treatments upon the precipitation of carbides. Corrosion studies carried out on this material could then relate compositional and microstructural variations to corrosion behaviour.

Key Manufacturing Steps According
to Vendors Experience.

Alloy Melting and Bar Forging
(220 mm dia)

Hot Extrusion to Hollow Shell.

Multi Cold Reduction Steps by Cold
Pilgering Process With Intermediate Mill
Annealing Between Steps.

Final Cold Reduction
Pilger or Drawing Process.

Final Anneal.

Roll Straightening.

Inside Diameter Sand Blasting
Outside Diameter Grinding.

Non Destructive Examination.

Special Thermal Treatment.

U Bending.

Non Stress
Relief
Items

Stress Relief Treatment on Small Radii.

Final Inspection and Packaging.

2.5.6. Process Parameters Which Exert the Greatest Influence Over Corrosion Resistance.

(1) The double melting process has been employed to optimize cleanliness and homogeneity. Chromium and nickel units are of the highest quality for nuclear applications. During pickling a lubricant is used which must be removed by de-greasing.

(2) The annealing process is carried out under a controlled atmosphere. Sandvik use hydrogen, Vallourec use cracked ammonia. A continuous annealing muffle furnace is used, the tubes have a typical residence time of 2-3 minutes before moving on to a rapid cooling section, Fig (7) shows a characteristic commercial heating/cooling curve. Cooling down between 800°C and 500°C is carried out in about 3 minutes to prevent uncontrolled precipitation. Mechanical properties depend on % carbon and final mill annealing temperature. The temperatures for commercial practice range from 1020°C to 1115°C. A typical yield strength after mill annealing at the higher temperature would be 278 MPa, the UTS would be 708 MPa and the hardness 161 VPN (5 kg) for a 0.02%C (68).

(3) After roller straightening the material should have consistent and reproducible mechanical properties and as low residual stress as possible. The process has a profound effect on the yield stress and tensile strength, typically increasing the former by 70 MPa and the latter by 25 MPa. Hardness increases to 168 VPN.

(4) Mechanical cleaning and smoothing of the inside diameter is usually achieved by sand blasting or Zircon blasting to a roughness of 63 microns rms.

(5) The removal of disturbed material from the outside diameter of the tube is achieved by grinding a minimum of 0.025mm of material away, approximately 1 ton of material per bundle. This ensures uniform surface aspects and roughness. Belt grinding is used with grit size spanning from 180-240 mesh. The yield stress and UTS both increase by 10 MPa.

(6) 100% NDE checks are carried out to ensure a defect-free and geometrically accurate tube.

(7) Commercial temperatures and soaking times for the special thermal treatment vary from vendor to vendor - from 700°C to 720°C and from 5 to 15 hours. It is felt that control over heat treatment is much less critical than for alloy 600 because of the higher chromium content of the former. Heat treatment is carried out in a vacuum furnace (10^{-6} - 10^{-7} Torr). Heat up from 25°C to 700°C takes approximately 6-8 hours. The two tube manufacturers visited by the author, Sandvik and Vallourec both favour the shortest Special Thermal Treatment (STT) time. Sandvik claim that stress relief is of primary importance and that adequate stress relief has occurred after 5 hours.

Vallourec maintain that carbide coalescence may occur after prolonged soaking times. Economic factors may exert considerable influence over this discussion. Other factors of concern during this treatment are dimensional stability, heat tinting due to

residual atmosphere and scratching. Mechanical properties after the STT are typically, yield strength = 335 MPa, UTS = 736 MPa and hardness 177 VHN, which represents an increase in the UTS but a decrease in the yield strength.

(8) The critical bending parameters are ovality control, wall thinning, smooth junction between straight leg and bent portion, which are specific defects associated with bending and dimensional control. If the tubes are of a satisfactory quality then the tightest U bends are stress relieved in a vacuum furnace.

(9) Finally the tubes are examined for any local defects. If any are found then they may be rectified by using 400 mesh abrasive. The tubes are then cleaned and boxed.

It is not known how well or badly the tubes are handled on site. Much of the effort expended in maintaining quality during manufacture can be negated by poor handling during installation.

The final section of the review will examine briefly the fundamentals of microstructural control.

2.5.7. The Effect of Dispersed Particles on Grain Size Control.

Normal Grain Growth.

At temperatures above the recrystallisation temperature grain growth occurs. The driving force for this process is the reduction of the grain boundary area/unit volume, since grain boundaries possess surface energies and raise the overall energy of the metal. Boundaries migrate towards the centre of curvature. The boundaries of grains containing fewer than six sides are usually concave towards their centre and therefore tend to disappear while those grains with more than six sides are convex towards their centre and tend to grow.

It is reasonable to assume that the rate of grain growth is proportional to the driving force which in turn is inversely proportional to the grain diameter. Beck et al (69) derived an equation for grain growth assuming that the rate of migration is proportional to the driving force (which in turn is caused by the capillary force of the curved grain boundary) as given by:

$$D^{1/n} - D_0^{1/n} = Kt \quad \dots\dots\dots\text{eqn (1)}.$$

Where :

D_0 = Average Grain Size at Start of Annealing.

D = Average Instantaneous Grain Diameter.

K = $A \exp -Q/RT$

t = Time

n = Parameter dependant on material and temperature. 0.5 maximum

Hillert (70) developed this and produced a model describing the rate of grain growth given by equation (2), where D_{cr} is the critical grain size when the driving force for grain growth is equal to zero.

$$\frac{dD}{dt} = 4M\gamma \left(\frac{1}{D_{cr}} - \frac{1}{D} \right) \dots\dots\dots\text{eqn (2)}.$$

γ = Surface Free Energy

$M = M_0 \exp (-Q/RT)$

M_0 = Rate Constant.

The solution to this equation leads to the parabolic growth law described by equation (3).

$$D_{cr}^2 - D_0^2 = 2M\gamma t \dots\dots\dots\text{eqn (3)}.$$

Where:

D_{cr} = is now 9/8 of the average grain size D_a

The calculation of this relationship, between critical and average grain size, was made possible by using the theory developed by Lifshitz et al. (91) who showed that there is a tendency for a fixed distribution, of relative sizes, of second phase particles during particle coalescence.

The Net Pinning Force from Ideal Particles.

Zener (71) assumed that the surface area of the particle is the same in the two adjoining grains and that the particle centre was distance ,r, behind the migrating boundary. The surface energy of the boundary being given by γ , so that the boundary acts with a maximum force:

$$B = \pi r \gamma \dots\dots\dots\text{eqn (4)}.$$

All the particles behind or in front of the rigid boundary though still in contact with the boundary were ignored. Hillert examined how pinning force varied with respect to particle

position on the boundary and arrived at a correction factor β which is dependent on the ratio:

$$\rho/r \dots\dots\dots \text{eqn (5)}.$$

Where;

ρ = Curvature of the boundary

r = Radius of the particle

β has been shown to attain a value of 2 at $\rho/r = 10^5$ and as a consequence is not of great importance. Other attempts at qualifying the effects of particles whose position is not equal to r behind the grain boundary have produced numerical factors such as 9/8, (72), 1.37 (73) and 1.1 (74), ~~for incorporation in eqn (4).~~

Non - Ideal Particles

Real particles do not necessarily behave according to Zener's estimate. They have shape or contact angle variations which cause them to exert higher pinning forces than the maximum predicted by Zener. It has been shown for example that pinning effects can be markedly different for low angle boundaries. To accommodate this Hillert has shown that correction for non - ideal particles can be made by using a correction factor α , which would be less than 2. Incorporating these modifications into the original model gives:

$$\frac{1}{Da} = \frac{3\alpha\beta f}{4r} \dots\dots\dots \text{eqn (6)}.$$

Where:

f = volume fraction of second phase particle

Hillert further extended the mean field treatment of grain growth to include the effect of second phase particles:

$$\frac{dD}{dt} = 4M\gamma \left(\frac{1}{D_{cr}} - \frac{1}{D} + \frac{z}{2} \right) \dots\dots\dots\text{eqn (7)}.$$

Where:

z = Heterogeneity factor (R/R_0)

R = Radius of growing grain in matrix of grains of diameter R_0 .

Gladman (75) also developed the Zener model in a more sophisticated manner using tetrakaidecahedron as the grains of distance $2R$ between opposite hexagonal faces, with r the radius of the pinning particles of volume fraction f and incorporating the heterogeneity factor, z . This more realistic analysis shows that a critical particle size, r_{crit} , is achieved when the driving force for grain growth is equal to the pinning force produced by the particles, thus:

$$r_{crit} = \frac{6R_0f}{\pi} \left(\frac{3}{2} - \frac{2}{z} \right)^{-1} \dots\dots\dots\text{eqn (8)}.$$

This can be rewritten in terms of grain diameter as:

$$Da < \frac{\pi r}{2f} \left(1 - \frac{4Da}{3D_{large}} \right) \dots\dots\dots\text{eqn (9)}.$$

where D_{large} is the diameter of the growing grain.

This formula can now be compared with eqn. (7) when rewritten in terms of D_{cr} ($dD/dt \leq 0$). Providing D_{cr} is < the result of eqn. (7) then abnormal grain growth will not occur.

$$D_{cr} < \frac{8r}{3f} \left(1 - \frac{D_{cr}}{D_{large}} \right) \dots\dots\dots\text{eqn (10)}.$$

Hillert suggests that allowing for the fact that Gladman uses $4\sigma r$ (where σ = surface energy) which is taken from an estimate of the maximum change of energy, rather than $\pi\sigma r$ and assuming that the ratio of D_{cr}/D_{large} is as Gladman suggests, $4/3$, then the two equations are identical.

Precipitation.

It is well established that precipitation of chromium carbides in Inconel alloy 600 plays an important role in corrosion resistance. An attempt has been made to derive the precipitation time/temperature relationship based on the thermodynamics of the system and diffusion controlled nucleation theory for both $Cr_{23}C_6$ and TiC/Ti(CN). It seems appropriate briefly to review both theories.

2.5.8. Thermodynamics of Precipitation.

In order to produce an embryo of α in a matrix of γ' , three conflicting energetic forces must be considered:

(a) The Chemical Driving Force.

The critical chemical driving force for the formation of a spherical embryo is given by:

$$\frac{4\pi r^3}{3} \Delta G_v \dots\dots\dots \text{eqn. (11)}$$

This will be negative below a critical temperature T_0 and thus the reaction will occur spontaneously. However this driving force for precipitation is opposed by two other energy terms.

(b) The Strain Energy Term. (W)

This is due to the change in volume accompanying the transformation which produces strain in the embryo and the matrix. Such strain raises the energy of the system and thus opposes transformation. The strain energy associated with a spherical embryo is given by:

$$\frac{4\pi r^3}{3} W \dots\dots\dots \text{eqn. (12)}$$

(c) Surface Energy (σ)

The creation of an embryo will produce an interface between α and γ'. The interface will have a surface energy which will raise the energy of the embryo above its surroundings and oppose transformation. For a spherical embryo this surface free energy term is given by:

$$4\pi r^2 \sigma \dots\dots\dots \text{eqn. (13)}$$

Thus the total free energy of the embryo above its surroundings is given by:

$$\Delta G = \frac{4\pi r^3}{3} (\Delta G_v + W) + 4\pi r^2 \sigma \dots\dots\dots \text{eqn. (14)}$$

The variation of ΔG with embryo size is given in fig (8).

In order to produce an embryo that will grow spontaneously an activation energy hump must be overcome. At small values of r:

the positive term, $4\pi r^2 \times \sigma$, predominates.

Thus at small values of r , an increase in embryo size will lead to an increase in free energy and, therefore, these tend to dissolve. At larger values the negative term predominates.

Thus there is a maximum value of both $\Delta G = \Delta G^*$ and $r = r^*$ beyond which an increase in r will produce a decrease in free energy and thus the embryo becomes stable.

$$\text{At } r^* \quad \frac{d\Delta G}{dr} = 0$$

This can be solved to find r^* in terms of $(\Delta G_v + W)$ and σ . Substituting r^* into equation (14) gives ΔG^* . Differentiating eqn (14) with respect to the radius of the embryo gives:

$$d\Delta G = \frac{4}{3} \pi r^3 \times (\Delta G_v + W) + 4\pi r^2 \sigma = 0 \text{ at } r^* \dots \text{eqn. (15)}$$

$$\frac{d\Delta G}{dr} = 0 \text{ at } r^*$$

$$\frac{d\Delta G}{dr} = 4\pi r^{*2} (\Delta G_v + W) + 8\pi r^* \sigma = 0 \dots \text{eqn (16)}$$

$$4\pi r^{*2} (\Delta G_v + W) = -8\pi r^* \sigma$$

$$r^* = \frac{-2\sigma}{(\Delta G_v + W)} \dots\dots\dots \text{eqn. (17)}$$

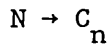
Substituting r^* into eqn (14) gives:

$$\Delta G^* = \frac{16\pi\sigma^3}{3(\Delta G_v + W)^2} \dots\dots\dots \text{eqn. (18)}$$

It is possible to ignore the strain energy term if the nucleus is incoherent or is at grain boundaries. For these reasons, the strain energy term has been removed for the purposes of the remainder of the calculations.

The Metastable Equilibrium Concentration of Embryos.

Embryos containing n atoms of total free energy ΔG_n can form on a possible N sites /unit volume of γ' . If the concentration of embryos of size n is C_n then the reaction for the formation of embryos of size n is:



with free energy ΔG_n accompanying the reaction.

The equilibrium constant for this reaction is given by:

$$K = \frac{C_n}{N}$$

$$\Delta G_n = - kT \ln \frac{C_n}{N}$$

Thus:

$$C_n = N \exp \left(\frac{- \Delta G_n}{kT} \right) \dots\dots\dots \text{eqn. (20)}$$

and the concentration of critical nuclei will be given by:

$$C^* = N \exp \left(\frac{- \Delta G^*}{kT} \right) \dots\dots\dots \text{eqn (21)}$$

The Classical Nucleation Rate

It has been shown by Volmer and Weber (76) that the rate of nucleation per unit volume, I, is equal to the number of critical nuclei per unit volume multiplied by the growth rate of each nucleus, β .

Thus incorporating this into equation (21)

$$I = N \exp - \frac{\Delta G^*}{kT} \times \beta^*$$

Where:

$$\beta^* = S^* \times N_{\gamma'}^{2/3} \times \nu \times p$$

where:

S^* = Surface area of critical nucleus.

$N_{\gamma'}$ = Number atoms /unit volume of γ' .

ν = Frequency of vibrations of atoms.

p = Probability that an atom is moving in the right direction

to join the nucleus.

Diffusion theory gives:

$$p\nu = \frac{D}{a_{\gamma'}^2} = \frac{D_0}{a_{\gamma'}^2} \exp - Q/RT$$

Where:

D = Appropriate diffusion coefficient for atoms joining the nucleus.

Q = Activation energy for atoms joining the nucleus.

$a_{\gamma'}$ = Lattice parameter of γ' .

Hence:

$$I = NS^* N_{\gamma'}^{2/3} \frac{D_0}{a_{\gamma'}^2} \exp \frac{-\Delta G^*}{kT} \exp \frac{-Q}{kT}$$

By plotting I against T the TTT type 'C' curve is produced. This demonstrates that at high temperatures the overall rate of nucleation is controlled by the slowest process, i.e. nucleation, even though diffusion will be fast. At lower temperatures nucleation is readily achieved but diffusion and thus growth is slow. Therefore the overall rate is controlled by the $\exp -Q/kt$ term.

Diffusion controlled nucleation in solids has recently been summarised by Russell (77) who shows that the steady state nucleation rate J_s can be expressed as:

$$J_s = \left(\frac{N}{a_{\gamma'}^2} \right) D_{\text{eff}} X_{\alpha} \exp \left(\frac{-\Delta G^*}{kT} \right) \dots \dots \dots \text{eqn (22)}$$

Where:

N = Number of nucleation sites of a particular type/unit volume.

$a_{\gamma'}$ = Lattice parameter of matrix phase.

D_{eff} = Effective diffusion coefficient

X_{α} = Solute concentration.

ΔG^* = Free enthalpy of forming a critical nucleus.

k = Boltzmann constant.

For heterogeneous nucleation the value of ΔG^* must be modified to account for nucleation on preferential sites such as dislocation or grain boundaries.

Thus:

$$\Delta G^* = \frac{16\pi\sigma^3 f}{3 (\Delta G_v)^2} \dots \dots \dots \text{eqn (23)}$$

where f is a modifying factor which is less than unity for heterogeneous nucleation.

The chemical driving force ΔG_v can be written:

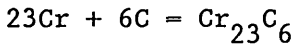
$$\Delta G_v = -(RT/V_m) \ln k_s \dots\dots\dots \text{eqn (24)}$$

where:

V_m = Molar volume precipitate.

k_s = Supersaturation ratio.

This supersaturation ratio determines the free enthalpy change for precipitation to occur. It can be defined as the actual amount of, for example [Cr] [C], in solution at a given temperature, compared to the equilibrium amount given by the solubility product equation. The basic reaction for carbide formation may be written as:



Thus for Cr_{23}C_6 :

$$k_s = [\text{Cr}][\text{C}]_{\text{soln}} / 10^{(T-2555)/233} \quad (79).$$

The Cr in solution was calculated based on Scarberrys et al. (66) solubility product for Cr_{23}C_6 . The % Cr in solution at any given temperature may be calculated using a mass balance of the elements forming the carbide, ie.

$$\text{Cr} = [\text{Cr}] + \frac{(\text{Cr})}{(\text{Cr}_{23}\text{C}_6)} \cdot \langle \text{Cr}_{23}\text{C}_6 \rangle$$

$$\text{C} = [\text{C}] + \frac{(\text{C})}{(\text{Cr}_{23}\text{C}_6)} \cdot \langle \text{Cr}_{23}\text{C}_6 \rangle$$

The final form of the eqn. enabling the calculation of Cr in solution is given below:

$$[\text{Cr}] = \text{Cr} - \frac{(\text{Cr})}{(\text{C})} \cdot \{ \text{C} - [\text{C}] \}, \text{ where: } () = \text{atomic or molar weight}$$

[] = element in solution
no brackets = total content Cr or C.

In order that nucleation occurs, a critical supersaturation must be exceeded and in undeformed austenite this is expected to be high (78). The introduction of strain via cold work provides sites for

nucleation so that precipitation is observed at lower supersaturation. Cohen and Hanson (79) observed precipitation in a single pass rolling experiment with a supersaturation ratio between 5 and 7.5.

Incorporating eqn.(24) into eqn.(22) and using a value of Q_d of 273 kJ mol^{-1} [89] for the activation energy of diffusion for Cr in Ni produces:

$$J_s = \alpha [Cr] \exp \frac{(-273,000)}{RT} \exp \frac{(16\pi\sigma^3 V_m^2 Nof)}{3RT (-RT \ln k_s)^2} \text{ .eqn (26)}$$

$$\alpha = \left(\frac{N}{a_{Cr}} \right) D_0$$

A number of nuclei/unit volume must be formed in time t for nucleation and thus precipitation to be detected:

$$t \propto N^*/J_s$$

Eqn (26) can be rewritten as:

$$t = C [Cr]^{-1} \exp \frac{(273,000)}{RT} \exp \frac{B}{T^3 (\ln k_s)^2} \text{eqn (27)}$$

Where:

$$C = N^*/\alpha$$

$$B = 16\pi\sigma^3 V_m^2 Nof / 3R^2$$

Substituting a value of $V_m = 1.82 \times 10^{-5} \text{ m}^3 \text{ mol}^{-1}$, a typical value of $\gamma = 0.5 \text{ Jm}^{-2}$, a value of f of 0.5 and a value of $C = 6 \times 10^{-30}$

gives the curve shown in fig (9). Figs (10) and (11) show the effect of increasing f for constant C and C for constant f . As would be expected increasing f from 0.1 to 0.7 increases the time and reduces the temperature for precipitation.

The effect of increasing C is also as expected. Assuming α in eqn (26) is given in nuclei/unit time then increasing the number of nuclei will increase the time required for those nuclei to form. The model has also been useful in demonstrating the effect of increasing the supersaturation ratio on precipitation temperature and time. Again the behaviour predicted by the model is as would be expected, increasing the supersaturation ratio by increasing the amount of solute in solution compared to the equilibrium amount decreases the precipitation temperature and time.

By comparing values gained in experimental work it should be possible to define more accurately the theoretical precipitation C curve for alloy 690. This model can be used for qualitative predictions of precipitation of TiC and Cr₂₃C₆.

As the model stands the following inaccuracies are present:

- (a) The solubility product equation for Ti(CN) is based on a stainless steel rather than on alloy 690.
- (b) The activity of chromium is based on ideal behaviour of dilute solutions. There is no suitable data on the thermodynamics of non dilute multicomponent systems.

(c) No account has been taken of the effect of temperature on the molar volume fraction. Clearly heating would increase the volume of a given precipitate compared to the volume calculated at room temperature.

(d) The diffusion Coefficients for Ti and Cr used in eqn (26) are based on diffusion of these elements in pure Ni not in a Ni-Cr-Fe alloy.

It is felt that the effect of point (b) is of greatest importance when considering the accuracy of this model, which at best could only be described as semi-quantitative. The model does however demonstrate how :

(1) Prior deformation reduces the precipitation time and temperature by increasing the density of preferred nucleation sites.

(2) Increasing the mill annealing temperature again reduces the precipitation time and temperature by increasing the super saturation ratio.

3. EXPERIMENTAL METHODS.

3.1 Selection of Materials for Study.

Six as received commercially produced steam generator tube sections were supplied. The tubes all had nominal 690 compositions, Table II, with elemental variations within the specification laid down by the CEGB for nuclear applications. The tubes had been subjected to a variety of thermal treatments, Table III, which consisted of mill annealing between the temperatures 965°C - 1080°C followed by the special thermal treatment at 715°C - 725°C for between 5 and 15 hours.

In order to examine systematic compositional changes of Al, Ti and C, the as received tubes were supplemented with 10 experimental melts. These casts all had nominal 690 chemical compositions, Table IV. The rationale behind the choice of composition is outlined. The first 4 melts, EM 1, 3, 5 and 6 were chosen to examine the effect of varying carbon in the absence of both Ti and Al, group (1). Alloys in group (2) were chosen to examine the effects of varying C with constant Al and Ti, the % Al and Ti in conjunction with tube A giving a high, medium and low carbon content. Alloys 12 and 13 in conjunction with the as received tubes C and D give a range of Ti with constant carbon, group (3). Finally, melts 7 and 11 in conjunction with tubes C and D, provide a range of Al contents with constant carbon and Ti compositions, group (4)

Experimental work initially centred around the characterisation of the as received tubes in terms of hardness, grain size and the identification of precipitates. Tubes A and E,

which represent the highest and lowest carbon content respectively, were further selected to examine the effect of simulated mill annealing schedules on the hardness, grain size, grain coarsening characteristics and temperature for the complete solution of carbon. The range of temperatures chosen for this simulation was between 900°C - 1200°C at 50°C intervals. This represents the mill annealing temperatures required to facilitate hot working across the entire carbon contents specified by the tube manufacturers.

As received commercial wire has also been supplied and an unsuccessful attempt has been made to try to measure the precipitation kinetics of $M_{23}C_6$ carbide in 690 using the electrical resistivity method. The Wheatstone bridge used could not differentiate between solution treated and aged for 15 hours at 700°C, and solution treated only.

3.2. Preparation of Experimental Melts.

All the experimental melts were produced using vacuum melting. The 5Kg ingots were surface dressed and the top and bottoms were removed prior to hot working. The mill annealing temperatures used were based on the Scarberry et al (59) carbon solubility data with a further allowance of 50°C for the rapid heat loss during the latter stages of rolling. In this way edge cracking was controlled. The rolled strip was air cooled prior to the edges being removed. The finished strip was 2mm thick.

Despite the allowance in temperature made when selecting the mill annealing schedule, none of the as rolled strip was fully

recrystallised.

3.3. Solution Treatment of Alloys.

Tubes A and E - the highest and lowest carbon contents respectively of the as received tubes - were subjected to a simulated mill annealing schedule between the temperatures 900° - 1200°C at 50°C intervals. Quarter sections of the tubes, approximately 20mm long, were sealed under a partial pressure of Argon (100mm Hg) in silica tubes. Sealing the tubes prevents both oxidation and nitrogen pick up during heat treatment. In order to examine the effects of cooling rate, two sets of 7 samples were prepared. One was water quenched after heat treatment, the silica being broken under water. The other set was air cooled. The experimental melts were also subjected to an identical mill annealing schedule.

3.4. Hardness determinations

3.4.1. Commercial Tubes.

During the initial characterisation of the as received tubes it was noted that grain size varied through the wall thickness with a layer, at both the inner and outer surfaces, of fine grained recrystallised material. It was felt that the grain size inhomogeneity would lead to hardness variations depending on the depth to which the tubes were polished. For this reason micro hardness traverses were carried out on the as received tubes. It was felt that providing at least four indentations were taken across the polished flat surface of the tube, ensuring two on the extreme edges and two in the middle sections, this would even out the effect of the inhomogeneity. The results from the

microhardness traverse, though it is appreciated that it is difficult to compare micro hardness with Vickers hardness, seem to bear the accuracy of the approximation out. A minimum of 5 hardness indentations were taken, using a 10kg load on a Vickers diamond indenter hardness testing machine. Extreme care was taken to ensure that excessive thinning of the tube wall did not occur due to over polishing: this may not only result in too little of the tube wall remaining for an indentation to be taken, but could also lead to excessive work hardening. All samples were polished to a 1 micron finish.

3.4.2. Experimental Melts.

The experimental melts were mounted in bakelite and polished to a 1 μm finish. The extra thickness of these samples enabled indentations to be taken from both the outer surface and through the thickness. The results given are an average of at least 5 indentations.

3.5. Optical Metallography.

A variety of optical microscopes were used in order to examine precipitates, precipitate morphology, grain structure and grain size.

As received and experimentally produced samples were mounted in bakelite, polished to a 1 μm finish and etched. The etchant used depended on the nature of the optical examination, ie: Nimonic etch reveals twinning; 10 % oxalic reveals grain boundaries, but dissolves carbides; bromine / methanol dissolves the matrix, but leaves carbides in relief (SEM only); electrolytic 8:1 phosphoric: water, dissolves the matrix and leaves carbides in

relief but is more suitable for optical microscopy; 2-6% Nital also reveals grain boundaries. Schaffmeister's reagent, which has been widely used for alloy 600, was found to be too unreliable for 690.

Grain size work was carried out using the Vickers Fifty - Five microscope. Samples were polished to $1\ \mu\text{m}$ ($1/4\ \mu\text{m}$ for photo microscopy) and electrolytically etched in 10% oxalic. Due to the grain size inhomogeneity problem, microhardnesses were carried out on all the as received tubes. Grain size measurements were then made through the wall thickness using the hardness indentations as a means to facilitate correlation with the grain size and hardness. All grain size measurements were made using the mean linear intercept method and are quoted to within 95% confidence limits.

3.6. Electron Microscopy.

3.6.1 Auger Electron Spectroscopy.

Auger electron spectroscopy has been employed to identify positively precipitates present in the microstructure. It has also been employed in an attempt to examine whether or not precipitation of either chromium nitride or carbide occur preferentially on the inner or outer layers of the tube. It has been suggested that these precipitates act to pin surface grains, thus producing the grain size inhomogeneity. A sample of tube A was conventionally ground down in order to expose a surface which consisted of fine grains adjacent to the comparatively coarser central grains. AES examination of the type and predominance of precipitates across the surface was then made.

3.6.2 Scanning Electron Microscope

The Scanning Electron Microscope has been employed to examine the microstructure of lightly etched as received and experimental samples, as well as stress corrosion cracking samples. Energy Dispersive X-ray Analysis has been used to identify inclusions present. Samples were mounted in conductive bakelite, polished to 1 micron and etched in a suitable etchant depending on the purpose of analysis. A limitation of the SEM / EDX system is the diameter of the beam and the depth to which it penetrates. If the precipitate of interest is too small or too thin then excitation of the matrix will occur, with consequent inaccuracies in the recorded spectrum.

3.6.3 Transmission Electron Microscope.

The Transmission Electron Microscope (TEM) has been employed to examine precipitates present, the interactions of precipitates with dislocations and grain boundaries, and the effect that solution treatment temperature has on carbide shape, size and distribution. Both thin foils and carbon extraction replicas have been employed in this analysis. The EDX facility on the TEM has also been employed when using carbon replicas. Selected Area X Ray Diffraction (SAED) has been used to identify the phases present, both light and dark field having been used to ascertain orientation relationships.

Thin foils were produced in the conventional way. Coupons were spark eroded from tubes before being hand polished to a thickness of 0.2mm. The thinned samples were then placed in a Struers electropolishing cell to be electrochemically polished and dished. The solution used was 6% perchloric acid in glacial acetic acid at

-50°C at a current of 1.7mA. In this way a transparent region at the centre of the foil was produced. A problem associated with the production of carbon extraction replicas was that of finding a suitable etchant. The electrolytic etchants tend to remove the carbon layer too rapidly, due to hydrogen evolution and subsequent bubble formation, leaving the carbides still in the structure. The most effective solution found to this problem was to use a dilute solution of bromine/methanol (<2%) and having scored the surface carbon layer on the sample leave it in this solution until the carbon is removed. The solution can then be filtered and the replica retrieved.

3.6.4 Scanning Transmission Electron Microscopy

The United Kingdom Atomic Energy Authorities (U.K.A.E.A.) dedicated scanning transmission electron microscope (STEM), the HB501, has been used in order to measure grain boundary chromium denudation, impurity segregation and nickel enrichment in an experimental alloy (EM12) thermally treated at 720°C for 1, 5, 10 and 15 hours, having been solution treated at 1200°C. The results from this study are compared to results from as received tube C which underwent the lowest mill annealing temperature of the as received tube. The HB501 has guaranteed resolution of 0.204 nm with sufficient current in a typical 0.5nm probe diameter to give accurate data very close to a grain boundary. The amount of work which can be carried out on the HB501 is very limited due to the cost of hire time and it is for this reason that only the commercial temperature has been examined.

3.7. Thermal Ageing Studies.

The type of thermal treatment carried out has been dictated primarily by the corrosion studies. Although an attempt has been made, in conjunction with a mathematical model, to more accurately define the nose of the precipitation C curve using thermal ageing study results. Three as received tubes and six experimental melts have been examined. All have been mill annealed at 1200°C. The ageing treatment consists of heating at temperatures ranging from 650 - 850°C for times of between 5 minutes and 24 hours. Hardness tests have been carried out though this has proved to be insufficiently sensitive to pinpoint the onset of precipitation. Both optical and electron microscopy has been employed to examine how carbide type and morphology change with time and temperature.

3.8. Corrosion Studies

In order to examine the effect precipitation has on the all important corrosion characteristics of alloy 690, corrosion tests have been instigated. The object of these tests is to measure the effects systematic changes in composition, (C, Ti and Al) solution treatment temperature and ageing times have on the corrosion resistance of the alloy. Corrosion tests thus far carried out are outlined below. Two autoclaves were used one at the U.K.A.E.R.E. at Harwell, the other at the Central Electricity Research Laboratories (C.E.R.L.) at Leatherhead.

(1) Stress Corrosion Cracking Tests.

As received tubes A and E, the highest and lowest carbon contents respectively of the as received tubes and tube F, were selected.

Stress corrosion cracking specimens were produced in accordance with ASTM G36 - 73 . Due to a lack of availability of alloy 690 bolts, it was necessary to use bolts made from alloy 600. Prior to testing these bolts were annealed at 1040°C followed by thermally treating at 700°C for 15 hours . The C ring specimens were deflected until the legs of the C rings touched. Samples of each tube type were then placed in the following corrosive environment:

(a) Pure Water with Hydrogen Over Pressure. (A6 and E6).

The autoclave was pressurised to 100 bar, depressurised and then pressurised to 10 bar with hydrogen, which was then depressurised to 2 bar. The autoclave was then heated to 340°C, which attained a pressure of about 160 bar.

(b) Deaerated 50% NaOH. (A1, 2, 3, E1, 2, 3.).

Specimens were placed in a capsule with 50 wt.% NaOH, the capsules were then deaerated by bubbling argon through for 20 minutes and then placed in an autoclave and heated to 340°C.

Tubes A and E were in the as received condition.

(c) Deaerated 30 wt.% NaOH + 10 wt.% Na₂SO₄. (A4, 5, E4, 5, F)

See b above for procedure. Tubes A, E and F were all in the as received condition. Samples of tube F were also solution treated at 1200°C and water quenched followed by ageing at 650 - 700 - 750°C for 1 and 14 hours. Where comparable tests are carried out in two different autoclaves a control sample is included so that immediate comparison from the two systems can be made.

(2) Intergranular Attack Corrosion Test.

The propensity for intergranular attack has been examined using unstressed specimens in deaerated 30% NaOH + 10% Na₂SO₄ at 350°C. It is appreciated that the more commonly used IGA test procedures are the Huey or the Streicher tests. However results from these tests have been shown to be misleading in alloy 600 when considering the working environment of a PWR SG tube. Also alloy 690 has been shown to be immune to sensitisation within the chemical composition outlined for nuclear applications when exposed to these environments. It seems more appropriate to examine IGA resistance in an environment which has been shown to attack 690 intergranularly.

The experimental melts examined and the rationale behind their selection are given below:

EM 7 and EM11. These were chosen to examine the effect of varying aluminium for constant carbon and titanium.

EM 12 and EM 13. Selected to examine the effect of varying the titanium to carbon ratio.

EM 5 and EM 6. These represent the highest and lowest carbon content of the alloys which contain neither aluminium nor titanium. Thus they can be used as a comparison to measure the effect, if any, of compositional variations in the preceding two groups of alloys.

All the above experimental melts were solution annealed at 1200°C and water quenched. One sample from each group was tested in this

condition, the rest were heat treated for 1, 5, 10 and 15 hours and water quenched prior to testing.

3.9. Tensile Tests

Tensile test specimens have been produced from experimental material; these specimens have been used to examine the effect of cold work on recrystallisation temperature. Tensile specimens solution treated at 1200°C have been strained to between 5 and 40% elongation at 5% intervals and have been subjected to mill annealing temperatures between 900°C and 1100°C at 50 °C intervals.

4. EXPERIMENTAL RESULTS.

4.1. Identification of Precipitates Present in Commercial Tubing

All as received tubes were examined both optically and with either SEM, TEM or AES to identify precipitates present. The most predominant intergranular precipitate present in all tubes was identified as chromium rich $M_{23}C_6$, figs 12 and 13. The metallic content of this phase is given in Tables V - IX. This carbide, though mainly intergranular, was also present intragranularly, fig 14. EDAX spectrum taken from this precipitate using carbide extraction replicas is shown in fig 15. It would appear that impurities associated with this phase include Al, Ti and P. Small Ti(CN) were also found on grain boundaries, fig 16.

Other particles present and identified are the larger angular particles, fig 17. These Ti rich cuboids have been identified using AES, SEM - EDAX, figs 18, and 19, as TiN and Ti(CN). TiN and Ti(CN) appear orange under optical light microscopy and occur both intra and intergranularly. They will have formed at temperatures above the mill annealing temperatures and are thus occasionally banded in the direction of rolling. The larger cubic particles are the TiN. The angularity of particles does not automatically denote the presence of Ti, since angular Cr rich particles have been identified using SEM, fig 20. Other trace elements associated with the Ti rich particles include P and S. The thermally treated as received tubes were also examined using the TEM in order to define accurately the carbon solubility of 690. From this study the effectiveness of the undissolved $Cr_{23}C_6$ grain boundary carbide particle for grain boundary pinning is

clearly demonstrated, fig 21. Extraction replicas taken from tube A show the cellular nature of some precipitates taken from this material, fig 22. This type of precipitate was not noted in tube E. There was also evidence of a very fine intragranular carbide phase in both A and E, but this has not yet been positively identified.

4.1.1. Effect of Simulated Mill Annealing.

The effect of increasing mill annealing temperature is as expected. As the temperature increases the grain boundary carbides ripen and spheroidise (1100°C) and many of the smaller intragranular carbides go into solution. The remaining predominantly intragranular - angular - particles left undissolved at the highest mill annealing temperatures have been identified as Ti rich, most likely $\text{Ti}(\text{CN})$. Fig.23 shows a typical precipitate - free grain boundary after solution treating at 1200°C followed by water quenching.

4.2. Identification of Inclusions Present in Experimental Alloys.

In the experimental melts the types of precipitate identified depended on the presence or absence of Al and Ti. In those alloys containing no Al or Ti the predominant intragranular carbide was an angular Cr rich precipitate, most likely $\text{Cr}_2(\text{CN})$, fig 24. In those alloys containing both Al and Ti, the predominant intragranular precipitate was again Ti rich TiC/CN with traces of Al. The Al may have been due to AlN precipitating on the surface of the $\text{Ti}(\text{CN})$. There is also evidence of a very fine (20nm) Ti rich grain boundary carbide most likely TiC , fig 25, as well as a

slightly coarser (44nm), Ti rich grain boundary precipitate associated with Cr rich $M_{23}C_6$. Alloys subjected to a high mill annealing temperature have been found to have large colonies of cellular chromium carbides at the grain boundaries, fig 26, after thermal treatment at 700°C

4.3. Hall - Petch Relationship for As Received Commercial Tubing.

Tubes A and E - the highest and lowest carbon respectively - were selected to examine the grain size vs. hardness relationship for alloy 690. Hardness is correlated to yield strength via the Meyer relationship, thus producing a Hall - Petch type graph, figs 27 and 28. The slopes for the two carbon levels (.022 and .015%C) are very similar. The wider scatter of results for tube E is due to the lack of intergranular carbide owing to its lower carbon content, which leads to indistinct grain boundary etching. The oxalic acid etch attacks the carbide phase, thus producing relief at grain boundaries. Without adequate grain boundary carbide, poor etching, and thus less accurate grain measurements, results. Material A, the higher carbon, was found to be consistently approximately 5 VPN harder. Water quenching produced a slightly harder material than air cooling. These results will be discussed.

4.4. Effect of Varying Carbon Content in the Absence of both Aluminium and Titanium.

Four experimental melts were produced in order to examine the effect of increasing carbon in the absence of both Al and Ti on grain size, grain coarsening, and, using this information in conjunction with as received material, carbon solubility. All four casts were subjected to the simulated mill annealing schedule

with temperatures ranging from 900 - 1200°C at 50°C intervals . The melts were then characterised in terms of hardness and grain size and the precipitates identified using SEM. The results are as follows:

4.4.1. Hardness vs. Solution Treatment Temperature.

This series of graphs, fig 29, shows that the hardness of the higher carbon alloy, EM6, is markedly higher than that of the lower carbon alloy, EM5; the hardness increases progressively from EM5 up to EM6 with carbon content. These graphs also demonstrate how increasing carbon content increases the temperature at which softening due to grain coarsening occurs. The hardness levels of EM6 are maintained up to 1100°C. EM5, the lowest carbon, shows no clearly defined grain coarsening temperature, indicating relatively ineffective grain boundary carbide pinning by those carbides present. The effect carbon has on the recrystallisation temperature is clearly shown in fig 30. By using these softening effects due to grain coarsening, in conjunction with those from the as received tubes, it has been possible to describe more accurately the carbon solubility temperature. The effect solution treatment temperature has on grain size, hardness and $d^{-1/2}$ is shown in Table X.

4.4.2 Hardness vs. Grain size.

Due to the rapid heat loss during the final pass of the hot rolling sequence, the rolling temperature dropped well below that required for dynamic recrystallisation. For this reason, none of

the experimental melts showed a fully recrystallised as rolled structure. For the Petch type analysis shown in fig 31, grain size and hardness measurements were taken only from those specimens which were fully recrystallised. As stated, increasing carbon increases the recrystallisation temperature. Thus as the carbon content increases, the mill annealing temperature required to promote complete recrystallisation increases. It is for this reason that no grain size measurements have been taken from EM6 (fig 30) and the number of measurements taken progressively decreases as the carbon content increases. However, the Petch analysis of the three remaining carbon contents are shown in fig 31. They are plotted on the same axis as the as received tube so that immediate comparisons are possible. The general trends from the analysis are as follows:

(a) The slopes (K_y) are all very similar and can be considered identical within the bounds of experimental error.

(b) Increasing carbon content increases the hardness for a given grain size, though the effect may be only slight when considering the large variation in grain size which produces a correspondingly large scatter band of results.

(c) The as received thermally treated material is markedly harder for a given grain size.

All postulated linear graphs drawn in this report have been statistically analysed using regression analysis; the slopes and R^2 values are given in Table XI.

4.5. Effects of varying Carbon in Alloys Containing 0.03% Aluminium and 0.38% Titanium.

This analysis was chosen to correspond to as received tubes in order to maximise the use of commercially supplied material. Three alloys have been examined two experimental casts, EM 8 and EM 10, and tube A.

4.5.1. Hardness vs. Solution Treatment Temperature

Samples were again subjected to a simulated mill annealing schedule between the temperatures 900 - 1200°C at 50°C intervals and water quenched. The results of the hardness, grain size and $d^{-1/2}$ are given in Table XII. A graphical representation of hardness vs. mill annealing temperature is shown in fig 32. It is clear that the higher carbon, EM 10, has a higher grain coarsening temperature than the lower carbon EM 8. However, EM 10 has a higher carbon content than tube A, yet has a lower grain coarsening temperature. This will be discussed.

4.5.2. Grain Size vs. Hardness.

Again, the as rolled material was not fully recrystallised during hot working and did not fully recrystallise until a mill annealing temperature of between 1000 and 1050°C was reached. For this reason, only the fully recrystallised grain size has been counted. A Petch type plot for EM 10 and EM 8 is shown in fig 33 and is compared with tube A. The slopes of each line and the R^2 values are given in Table XI. The most striking difference between the two compositions is the considerably higher hardness for a given grain size of the commercially produced tube compared to the experimentally produced material. This will be discussed.

4.6. Effects of Varying Aluminium With Constant 0.02% C and 0.27% Ti.

For this analysis EM 7 and 11 were used in conjunction with material C, Group 4 in the tables. EM 7 and 11 represent high and low Al contents respectively. The composition of material C is very similar to that of EM 11, but has been included to demonstrate the fact that for a similar composition and grain size, the thermally treated commercial tubing has a consistently higher hardness than the experimentally produced material. All alloys were subjected to the simulated mill annealing schedule outlined previously and the results of grain size and hardness measurements are shown in Tables XIII and XIIIa.

4.6.1. Hardness vs. Solution Treatment Temperature.

Hardness vs. solution treatment temperature graphs for the three alloys are shown in fig 34. Again, the most striking result is the difference in hardness of the as received tube compared to the two experimental melts. This will be due in part to the much lower mill annealing temperature used for processing tube C. The lower the mill annealing temperature the greater the volume fraction of undissolved carbides available to pin grain boundaries. Thus dynamic recrystallisation will be retarded and a more work hardened structure is produced. However, a further contribution to the hardness may be from the precipitation, and subsequent dislocation generation from those precipitates, of Cr_{23}C_6 . This will be discussed.

The higher Al alloy, EM 11, appears to be slightly softer for a given grain size and solution treatment temperature than EM 7.

Also, EM 11 has a considerably larger grain size at the higher mill annealing temperatures than EM 7, Table XIII. This may at first appear to be an unusual result considering the role Al, and more specifically AlN, plays in the grain refining of HSLA steel. However, using data taken from experimentally determined solubilities (61) of carbides and nitrides, it must be assumed that all the nitrogen in the material is associated with the Ti present, forming TiN. These nitrides form at very high temperatures, are virtually insoluble in austenite and commonly appear as large cuboids which are generally incapable of contributing to grain refinement. Aluminium has been found to be associated with Ti rich cuboid inclusions, most likely TiN(CN), in both as received and experimentally produced alloys, fig 17. The cause of the apparent softening of the Al containing alloy is at present unclear. In alloys which precipitate AlN for the purpose of grain refinement, it has been observed that the increasing Al content to beyond optimum decreases its grain refining potential. If any grain refining is occurring due to the presence of TiC(CN), it may be that the association of Al with those precipitates causes a coarsening of them and thus prevents grain boundary pinning by them. There is, however, no evidence to support this hypothesis.

4.6.2. Hardness vs. Grain Size.

Petch type plots of the three alloys are shown in fig 35. The slopes of tube C and EM 11 are very similar, reflecting the similarity in composition. The main difference is the higher hardness for a given grain size of the commercially produced

tube. The smaller gradient of the slope of the high Al EM 7 reflects the increasing grain size at the higher solution treatment temperatures, compared to the other two alloys. The cause of this apparent accelerated grain growth will be considered in the discussion.

4.7. Effects of Varying Ti in Alloys Containing 0.019% C and 0.12% Al

This group consists of alloys with high (EM 13), medium (Tube C) and low (EM 12) Ti contents. The composition was chosen in order to include, and thus maximise the use of, as received commercial tubing. The Hall - Petch type plots and hardness vs. solution treatment graphs produced from the results of the simulated mill annealing programme are shown in Figs 36 and 37. Table XIV gives details of hardness and grain size results.

4.7.1. Hardness vs. Solution Treatment Temperature.

Again, the commercial steam generator tubing, tube C, is considerably harder at the lower mill annealing temperatures and this hardness difference, though not as pronounced, is maintained at the higher mill annealing temperatures, fig 36. The only difference between the two experimentally produced alloys is that the higher Ti alloy, EM 13, appears to have a higher grain coarsening temperature. This temperature, 1000°C , coincides with that for tube C, which during its production received a final mill anneal of only 965°C . As with all the experimentally produced alloys, dynamic recrystallisation had not occurred during rolling and did not occur until a suitably high solution

treatment temperature was arrived at. It is interesting to note that the grain sizes of the two experimental melts, EM 12 and EM 13, are very similar (39 - 43 μm at recrystallisation ie. 1050 $^{\circ}\text{C}$) and indeed at 1100 $^{\circ}\text{C}$ the grain sizes are virtually identical (104 - 105 μm). However, from that temperature upwards the grain size of the low Ti alloy (EM 12, 0.1% Ti) increases to 170 and then to 355 μm for the two remaining mill annealing temperatures. The final grain size for EM 12 of 355 μm is considerably larger than any other alloy examined. These results will be considered in the discussion.

4.7.2. Grain Size vs. Hardness

Graphs representing the results from grain size and hardness measurements taken after the simulated mill annealing schedule had been completed are shown in fig (37), tube C was given earlier. The slopes for the three compositions, EM12, EM13 and tube C, are all very similar and are given in table XI. It should be noted that the R^2 value for EM 12, due to the wide scatter of results, suggests the least linearity of all the alloys examined. As with all the other groups of alloys examined, the commercial tubing exhibited a marked higher hardness for a given grain size than did the experimental casts.

4.8. Thermal Ageing Studies.

The graphs representing the hardness of tube F, having been solution treated at 1200 $^{\circ}\text{C}$, at ageing times between 5 and 30 minutes at 5 minute intervals, and at ageing temperatures between 550 and 700 $^{\circ}\text{C}$ at 50 $^{\circ}\text{C}$ intervals are shown in fig 38.

Initially it was felt that the hardness test (10 kg) was sufficiently sensitive to indicate the onset of precipitation. Results from the thermal treatments showed an increase in hardness at 550°C after 20 minutes. However repeat tests on the same alloy have not shown the same increase in hardness and it is for this reason that the hardness was not used for the remainder of the work.

A limited examination of thermally treated material has been carried out on the TEM in an effort to produce a precipitation C curve for a given solution treatment temperature and chemical composition, fig 39. Further optical microscopy work has been carried out to depict the effect ageing time and temperature have on carbide morphology. The results from this study are summarised in table XV and figs. 40 and 41. The effect of heat treatment on grain boundary chemical composition, with particular reference to Cr, Ni, Al, P and S, is shown in Tables XVI - XX. Graphical representations of the effects of Cr depletion and Ni enrichment at grain boundaries are given figs in 42 - 51. These show the effect of increasing the ageing time from 1 to 15 hours at 720°C on Ni enrichment and Cr depletion in areas adjacent to the grain boundary. EM 12 was used having been solution annealed at 1200°C. As received tube C was also examined and fig 46 shows the results from this latter examination.

4.9. Corrosion Studies.

4.9.1. Stress Corrosion Cracking.

The results from the C ring stress corrosion cracking tests carried out at both Harwell laboratories and CERL at Leatherhead

are summarised in tables XXI and XXII. All samples except those in the pure water environment had undergone intergranular attack after 1800 hours or less, figs 52 and 53 . Tests on tubes A and E were allowed to continue for a further 6200 hours to ascertain the effect further exposure would have once corrosive attack had commenced. The results from the effect of ageing time and temperature on the intergranular resistance of tube F after 1500 hours exposure are shown in table XXII. The samples removed after 1800 hours exposure from the deaerated NaOH environment were examined (A 2 and E 2) under the SEM for any evidence of cracking. The micrograph shown in Fig 54 shows striations running perpendicular to the tube length. All the stress corrosion cracking samples were polished to a 6 micron finish to remove the effect of belt polishing during the final stages of production. The samples were not examined on the SEM prior to immersion, only an optical examination was carried out. It is possible that the deeper belt polishing marks remained since the tubes are commercially polished to only a 240 grit finish.

The bolts used to stress the C rings were as stated made from alloy 600. On removal from the test environment it was found that IGA/SCC had completely penetrated through the bolts in many places. The most pronounced attack occurred in the highly stressed areas such as the root of the nut/bolt thread, Figs 55, 56 and 57. This demonstrates the increased corrosion resistance of alloy 690 compared to alloy 600 in this test environment.

4.9.2. Intergranular Attack.

The tests outlined in the experimental procedure have been carried out and are dealt with in appendix A.

4.10. Tensile Tests

Tensile test specimens have been machined from experimental melt EM 12. Results from the examination of the effect of cold work on recrystallisation temperature are shown in Fig. 58. As would be expected, increasing cold work reduces the recrystallisation temperature of EM 12.

5.1. Carbon Solubility

In alloy 600 it has now been well established that in order to produce a sufficiently corrosion resistant microstructure, it is necessary to ensure adequate solution of carbon prior to the special thermal treatment (35)(39). However, the solution treatment temperature is critically dependent on carbon content and quite minor compositional variations could result in too low an annealing temperature and thus a microstructure susceptible to attack in a suitably corrosive environment. It has been demonstrated that the corrosion resistance of alloy 690 can be enhanced by a similar thermal treatment to alloy 600 (53)(54). Thus in order to optimise a heat treatment which will produce a consistently corrosion resistant microstructure, it is necessary to obtain carbon solubility data for alloy 690. Three such sets of data exist (65)(66)(67) and are shown in Fig.5. Using the equations fitted to these curves, eqn 1, 2 and 3 below, the following solvus temperatures were arrived at for the experimental melts and the as received tubes, Table XXIII. The first group of experimental melts has been produced to examine the effects of carbon in the absence of both Ti and Al.

$$\text{Scarberry et al.} \dots T^{\circ}\text{F} = 1.0 \log \% \text{C} \times 233 + 2555 \dots\dots\dots(1)$$

$$\text{Nogano et al.} \dots T \text{ (K)} = -5999 / (\log \% \text{C} - 2.93) \dots\dots\dots(2)$$

$$\text{Norberg et al.} \dots T^{\circ}\text{C} = \log \% \text{C} + 6.819 / 4.771 \times 10^{-3} \dots\dots\dots(3)$$

This table also contains the solvus temperature for TiC, arrived at using the solubility equation derived from work on austenitic

stainless steels, equation 4 (81).

$$\text{Log [Ti] [C]} = (-6780 / T) + 2.97 \dots\dots\dots(4)$$

Where [C] is the wt% of carbon and T is in ° K.

The temperatures given in table XXIII for the solubility of TiC assumes that all the nitrogen present is associated with Ti, thus reducing the effective Ti available for precipitation as TiC.

It is appreciated that in stainless steel, TiC is a more thermodynamicly stable phase than chromium carbide. The results of the calculations shown in table XXIII suggest that in alloy 690 it is Cr_{23}C_6 which is more stable. While the case for doing this may be weak, in the absence of any other appropriate data, an attempt has been made to relate grain growth characteristics to the precipitation of TiC based on the only available TiC solubility data. The justification for using this solubility data is that it has been successfully used in work on alloy 600. Again it is appreciated that the expected TiC solubility of alloy 600 should be closer to an austenitic stainless than is alloy 690.

Results from the group of experimental melts produced to examine the effects of carbon in the absence of both Al and Ti showed how increasing carbon increased the hardness, for a given composition and grain size, and also increased the temperature at which softening due to grain coarsening occurred, Fig. 29. This demonstrates the effectiveness of the chromium carbide for grain boundary pinning. Therefore, as long as there are appreciable amounts of carbide phase present grain coarsening is severely

restricted. Fig. 30 shows the effect carbon has on the microstructure of 690. Fig. 30 (a) is EM 5 (0.004%C at 128X mag), fig. 30 (b) is EM 6 (0.05% C at 100-500X mag). Both these alloys have undergone the solution treatments previously outlined; EM 5 shows a recrystallised structure at or below 950°C, whereas EM 6 has only just recrystallised at 1100°C. Examination of the grain coarsening temperatures of all four experimental melts and plotting them against carbon content on a logarithmic scale would produce a graph approximately 50°C below the Nagano plot. Allowing for the fact that grain coarsening occurs prior to the complete solution of carbon ie. ripening of carbides precedes their complete solution, the solution temperature is put somewhere in the region of the Nagano data. This data, however does not take into account the effect of prior cold work as evidenced by the fact that hardness values are reduced from the as rolled to the first solution treatment temperature level.

The as received tubes were in the heat treated condition and therefore stress relieved so that the grain coarsening temperatures of these tubes are more indicative of the effects of carbide rather than the effects of carbide and a large residual stress. Using the grain coarsening temperature as a starting point a TEM study of the above alloys has been carried out. This limited study has shown that of the three postulated solubility curves the Scarberry et al. (66) data is in closest agreement with the results obtained. Additionally, the micrograph taken using the TEM, Fig.21, of tube A after solution treatment at 1100°C indicates that even Scarberry's curve may be slightly low, although this is by no means conclusive. It is for the reasons outlined above that

solubility data given by Scarberry et al. (66) have been used and will continue to be used throughout the remainder of the work. These findings have been supported by Sarver et al. (82) who, in a recent paper on the thermal treatment of alloy 690, quoted the Scarberry et al. data.

5.2. The Effect of Chromium Carbide Dispersion on Grain Size.

The results from group 1 experimental melts demonstrate how increasing carbon decreases the grain size for a given composition and prior cold work. It has been shown in previous work on alloy 600 (27) that the grain boundary pinning particle size in the higher carbon alloy will be larger than in the lower carbon alloy. The effect of this is offset by the fact that the critical particle size, at which the driving force for grain growth is equal to the pinning force exerted by the particles, is also larger.

A similar examination has been carried out on alloy 690 using tubes A and E the highest and lowest carbon of the as received tubes. The Zener (71) equation (eqn 5) has been used to estimate the radius of the grain boundary pinning particles and the Gladman (75) modification to estimate the critical undissolved particle radius (eqn 6). These equations are given below.

$$R = \frac{4}{3} \cdot \frac{r}{f} \dots\dots\dots \text{eqn. 5}$$

Where:

R = Grain radius.

r = Radius of grain boundary pinning particle.

f = Volume fraction of pinning particle.

$$r_c = \frac{6R_0 f}{\pi} \left(\frac{3}{2} - \frac{2}{z} \right)^{-1} \dots \dots \dots \text{eqn. 6}$$

Where:

R_0 = The matrix grain radius.

f = the volume fraction of undissolved particles.

z = Heterogeneity factor for grain size.

The mass fraction of undissolved Cr_{23}C_6 and TiC for all the alloys examined are shown in Table XXIV. From the Zener equation it can be calculated that tube A will have on average a particle size 1.75 times bigger than tube E for a given mill annealing temperature below the solvus temperature. Using the Gladman modification the critical particle size, above which grain coarsening occurs spontaneously, has been calculated and is given in table XXV and XXVa. Table XXVa gives the calculated TiC critical particle size and these results will be considered later. The heterogeneity factor for grain size, z , has been estimated between 2 and -2. It is clear from this analysis that the critical particle radius (r_{crit}) is some 1.8 times bigger for the higher carbon alloy tube A. To summarise, the higher carbon experimental alloys have shown smaller grain size and subsequently higher hardness than the lower carbon alloys. The numerical analysis used shows that for increasing volume fraction the carbide radius increases and this has been supported by experimental results. Further, the analysis shows that increasing carbon increases the critical particle size above which grain coarsening occurs spontaneously and this too has been borne out by experimental results. Thus, as the volume fraction of undissolved carbide increases, so the grain size is reduced and the hardness increased. From these results it would be expected that tube A

would have a smaller grain size than tube E; however, this appears not to be the case. The above rationale applies to the experimental melts in group 1, in that it is clear that the alloy with the highest carbon has the smallest grain size and highest hardness. Tube E, however, which has a 1.8 times smaller carbide size and was, therefore, extremely difficult to etch, appears to have a smaller grain size. Examination of the 0.2% yield strength and the U.T.S of both tubes would suggest that unless some other strengthening mechanism is occurring the grain size of E should be, and most likely is, larger than A and it is an inability to etch the alloy adequately which is at fault.

A study carried out on alloy 600 (27) has suggested that $TiC/(CN)$ are the predominant grain boundary pinning particles. An analysis of the reciprocal mass % undissolved carbide, below the grain coarsening temperature, versus grain size showed a linear relationship for both the experimental melts and the as received tube. No clearly defined relationship was shown to exist for the predominant carbide phase Cr_7C_3 in alloy 600.

Alloy 690 has lower solubility for carbon than alloy 600 (66). Thus grain growth and recrystallisation, for a given carbon content and cold work, will occur at lower temperatures in alloy 600, than 690. In the study of alloy 600 dynamic recrystallisation had occurred during hot working, in the majority of the alloys, thus grain size measurements could be made from the lowest mill annealing temperature up to the onset of grain growth. In alloy 690 dynamic recrystallisation did not occur. In fact recrystallisation coincided with grain growth in some of the

alloys so that no grain size measurements could be made on those experimental melts below the grain coarsening temperature. The as received tubes were in the recrystallised condition. A graph of grain size vs the reciprocal mass fraction of undissolved carbides is shown in fig.59a and compared, fig 59b, with a limited number of data points available for the reciprocal mass fraction of undissolved TiC. The results from the $Cr_{23}C_6$ analysis are similar to those from alloy 600 in that each composition shows a linear relationship with grain size rather than a clear relationship between grain size and carbide type. The TiC data are too limited to be considered in any way conclusive. Further examination of the results gained will be presented later and will elucidate the role of TiC for grain size control.

5.3. The Difference in Hardness Between the As Received and the Experimentally Produced Alloys.

Results show that the as received tubes are consistently some 20 VPN harder than the mill annealed experimental melts of a similar composition. The opposite was reported (27) for as received (mill annealed only) and thermally treated alloy 600. In the case of alloy 600 the reason was attributed to the effect of cold work. The mill annealed only tubes, it was postulated, were subjected to a straightening operation after the final mill anneal which left considerable cold work in the tubes, approximately 30 VPN. The as received alloy 690 tubes have, however, undergone a special thermal treatment designed not just to optimise precipitation but also to promote stress relief, thus much of the effect of the cold work will, it must be assumed, have been removed. The

increase in the hardness of the thermally treated tubes must therefore be associated with some other strengthening mechanism other than cold work. Solid solution hardening seems the least likely since there will be considerably more precipitation in the specially thermally treated material than in the mill annealed only. In fact it may be that the mill annealed samples have undergone some solid solution hardening (eg. by carbon from carbide taken into solution) which has reduced the apparent difference between the two types of thermal treatment. Results from alloy 600, using an empirical relationship to examine the effects of different elements in solution, suggest that solid solution hardening by carbon is negligible and since 690 has an even lower solubility for carbon, it would seem that the effect of carbon on solid solution hardening would be minimal. Attempts have been made to use this and other structure / property relationships, but as yet unsuccessfully. For example, the equation used in the alloy 600 work gives a yield strength for a typical 690 composition, some 100 MPa too high. Since the tube manufacturers insist that no straightening is carried out after the TT, it was initially assumed that cold work was not the cause of the increased hardness. Also, if the tubes had undergone such a degree of cold work, then a more pronounced decrease in the hardness from the as received to the first solution treatment temperature might be expected. The results actually suggest that slight hardening has occurred. Within experimental error the effect is negligible, but it does demonstrate the fact that softening has not occurred due to stress relief after cold work.

The alternative mechanisms are either precipitation strengthening or dislocation strengthening due to precipitation. Precipitation strengthening seems unlikely, since precipitation occurs predominantly on grain boundaries. The carbides have been shown to have an orientation relationship with only one grain (83) and there is a small misfit between FCC austenite and $M_{23}C_6$. This would suggest that little precipitation hardening will result and insufficient dislocation generation will occur, to affect hardness profoundly. Results issued by Sandvik concerning a trial production of 690 steam generator tubing (68) shows a steady increase in hardness from the final mill anneal (161 VPN) to the straightening operation (168 VPN) and on to the belt grinding (179 VPN). The greatest increase comes from the belt grinding. After the thermal treatment (725°C / 15 hours) the hardness has dropped to 176 VPN with a standard deviation of 7.4 VPN. Since the hardness level of the as received tube has not dropped after a thermal treatment of 900°C , it must be assumed that the special thermal treatment temperature of 704°C is not sufficiently high to promote any form of recrystallisation. Therefore, the higher hardness of the as received tube must be due to the effect of cold work, with the greatest contribution coming from the belt grinding.

5.4. Grain Size inhomogeneity

Grain size inhomogeneity has been widely reported in both alloy 600 and 690 (84)(85)(65) Fig.60. It has yet to be established whether the fine grained recrystallised layer, both at the inside and outside surfaces, has any effect on the postulated lifespan of the tubing in its working environment. Collaborative work with

Risley laboratories, National Centre of Tribology (U.K.A.E.A.) has shown a rapid surface wear effect. It has been shown that work hardening increases, for a given material, with decreasing grain size, though the effect in austenitic stainless steel is only slight.

The general trends from the impact slide and rubbing fretting test, supplied by Risley, show 690 to be superior, from a tribological view point, to 600. This CEGB sponsored work continues.

There have been a number of suggestions as to the cause of the variation in grain size. These are given below:

(1). The pilgering process concentrates more work at the surface of the tube than through the wall thickness, resulting in a recrystallised layer of small surface grains.

(2). Surface contamination due to the pick up of grease during the manufacturing process results in surface carburisation. Alloy 690 has been shown to be susceptible to this effect .

(3). The protective atmosphere used during the special thermal treatment (cracked ammonia) promotes the formation of chromium nitrides at the surface, causing preferential pinning of the surface grains.

(4). The straightening, polishing and sand blasting carried out prior to the special thermal treatment reduces the recrystallisation temperature in those worked areas so that recrystallisation occurs in the outer layers during the special thermal treatment.

To ascertain whether Cr or Ti nitrides were responsible for any preferential grain boundary pinning at the surface layers of the tube, a specimen was prepared as outlined in the experimental method. No evidence was found of any preferential pinning by either nitrides or carbides. The results from the analysis are shown in fig 61, 62 and 63. Positive identification of Cr carbides and Ti (C/N) were made, figs 61 and 62. A problem associated with the positive identification of TiN is that the titanium and nitrogen peaks are very close so that it is difficult to see how much nitrogen is associated with the titanium. By using a standard Ti and TiN sample and comparing the ratio of the peaks (TiN = 3:1, Ti = 1.6:1) with those recorded, it is possible to identify positively TiN. An interesting analysis came from stringers on the polished surface, fig 63. Based on literature it was assumed that these were TiN which, having formed at the higher temperatures, were strung out in the rolling direction. However, results from fig 63 suggest that these stringers are chromium rich spinels with some Ni, Fe and C also present. The carbon may be associated with the pre-treatment of the sample and not necessarily associated with the stringer.

Grain size inhomogeneity has been noted in both Sandvik Steels and Valnox (Vallourec) tubing. Cracked ammonia is used by Valnox (Vallourec) as a protective atmosphere during thermal treatment - Sandvik Steels use high purity argon. From these results it seems unlikely that Cr or Ti nitrides or carbonitrides are responsible for the grain size inhomogeneity.

The as rolled experimental melts have all shown this surface effect, fig (64). The only treatment these alloys have undergone is rolling in air. The conclusion to draw from this is that the fine grained recrystallised layer is due to the concentration of cold work at the surface layers.

5.5. Activation Energy for Recrystallisation and Grain Growth.

The activation energy for normal grain growth is given by the following equation: (86)

$$D = Kt^{1/2} \cdot e^{-Q/RT} \dots \dots \dots \text{eqn (7)}.$$

Where:

- | | |
|-------------------------------|------------------------|
| D = Grain Size, μm | Q = Activation energy. |
| K = Rate constant. | R = Gas constant |
| t = Time at temperature. | T = Temperature (K) |

Factors which can exert an influence over activation energy for recrystallisation / grain growth include:

Impurities.

When a grain boundary moves, solute atoms can migrate along with the boundary and exert a drag that reduces the boundary velocity. The magnitude of the drag will depend on the binding energy and the concentration in the boundary.

Prior Deformation.

The activation energy for recrystallisation varies linearly with % deformation. This in turn is related to the hot working temperature and in the case of alloy 690, the carbon content. If an alloy which contains grain boundary pinning particles is rolled just above the grain coarsening temperature, it will contain less % deformation than a higher carbon alloy worked at the same temperature. This is, however, complicated by the fact that the higher the carbon, the larger the carbides and the larger is r_{crit} . It has already been shown that these latter two factors tend to cancel each other out and it is the overall effect of carbon which predominates.

The activation energies for all the alloys have been calculated using equation (7) and are given in Table XXVI and Fig.65 - 74. The R^2 values calculated from the lines of best fit are given in Table XXVII. The effect the systematic changes in composition have on these energies will be discussed when each variable is examined later. It is appropriate to examine in general terms the plots for tubes A and E now. It is clear from Fig.65 that the grain growth characteristics of the as received materials change at about 1050°C and that this change coincides with the carbide ripening temperatures. The slopes of the lines above 1050°C are considerably steeper than the original, reflecting the fact that the grains are no longer pinned and thus grain growth at these higher temperatures is more rapid than at the lower temperatures when carbide pinning was occurring. It is important to note that the slopes of the high temperature grain growth, Fig.65, are very

similar to the slopes of the experimental melts in the absence of both Al and Ti, Fig.68a., and further that the slopes of the experimental alloys which contain Al and Ti, Fig.69, are also much steeper than the as received material. These results will be discussed later.

5.6.The Effect of Varying Carbon in the Absence of Both Aluminium and Titanium.

From thermodynamic data (81) and from experimental results, it is shown that in the absence of both Al and Ti the predominant intragranular precipitate is Cr rich, most likely chromium nitride / carbonitride. The carbon is therefore almost entirely available for precipitation of chromium carbide. The effect carbon has on the hardness, grain size and grain coarsening temperature has already been examined under the heading of carbon solubility and will not be repeated here. It is interesting to note that the grain size of EM 1 (0.015% C) is markedly larger than any of the other alloys in this group, including the lowest carbon EM 5 (0.004% C). It might be expected that the lowest carbon alloy, whose total carbon would go into solution at a lower temperature than the higher carbon alloy, would thus have the largest grain size since it should have the greatest time at temperature for grain growth. However, this is clearly not the case since EM 1 had recrystallised at 1000^oC whereas EM 5 recrystallised at 1050^oC. EM 1, therefore, had the greatest time at temperature for grain growth to occur. A phenomenon noted in all the alloys is a general variation in grain size not just associated with the outer layers of the material. This is not

uncommon in alloys which use grain boundary pinning particles for grain size control - for example, the pinning of grain boundaries by AlN in HSLA steel. If some sub grain boundaries become unpinned before others, then these may grow to form the nuclei for recrystallised grains. These sub - grains grains would then grow at the expense of the surrounding unrecrystallised matrix and thus large grains in a matrix of smaller grains result (87).

Examining the activation energies, the slopes of EM 5 and EM 1 are very similar, Fig.68. Work on alloy 600 (27) suggests that increasing carbon increases the activation energy for grain growth in the absence of both Al and Ti, an effect not demonstrated in these results. This may be due to the lower carbon solubility of 690 in that the lower % carbon in solution exerts a smaller drag on the grain boundaries. Alternatively, it may be that the effect the small change in carbon has had on the activation energy is swamped by some other overriding mechanism such as cold work due to a lower mill annealing temperature and the effect this has on recrystallisation and subsequent grain growth. It is unfortunate that the higher carbon alloy EM 3 has so few points to plot since this renders the results unreliable.

The Petch relationships for the three alloys are shown in Fig. 31. All the slopes are very similar. The only slight difference between the three alloys is a progressively increasing hardness for a given grain size, with increasing carbon. The effect is only slight and within experimental error is considered insignificant.

5.7. The Effect of Varying Carbon with 0.03%Al and 0.38% Ti.

This alloy group consists of high, medium and low carbon alloys. The difference between the high and low carbon experimental melt and the medium carbon as received tube is immediately apparent when examining the Petch plots, Fig.33. The as received material, for reasons already discussed, is considerably harder for a given grain size than the experimentally produced alloy. The slopes of the plots are, however, very similar.

The effect of solution treatment temperature on hardness is shown in Fig. 32. Initially the higher carbon alloy is harder, as would be expected considering the effect carbon has been shown to have on grain size and hardness. It has been suggested that the higher the carbon for a given mill annealing temperature, below the solvus temperature, the greater the stored energy and thus the lower the recrystallisation temperature. It has also been shown that the as received material is consistently harder than the mill annealed material due to cold work. The 0.05% carbon alloy has an as rolled hardness of 207 VPN: the same carbon content in the absence of both Al and Ti had a hardness of 212 VPN. EM 13, which has a similar composition to tube A, has a hardness of 166 VPN after the lowest solution treatment temperature and tube A has a hardness after the same treatment of 202 VPN. Assuming the comparison of composition between tube A and EM 13 is acceptable, it can be shown that the increase in hardness due to cold work in A is 36 VPN. It would not be unreasonable to assume that such a degree of cold work might have some effect on the material's recrystallisation temperature, yet this 0.022% C alloy does not undergo grain

growth until 1050°C - 1100°C , which is at the most only 50°C below that which would be predicted. Although it is appreciated that the greater % carbon the greater the discrepancy between the carbide solvus and the grain coarsening temperature, a difference of some 231°C , as seen in the case of EM 10, would not be expected. The cause of this discrepancy may well be associated with the special thermal treatment. This treatment promotes grain boundary carbide precipitation, the time and temperature being chosen to optimise both nucleation and growth of the precipitate. It can be assumed that the thermally treated microstructure will have a much larger volume fraction of grain boundary carbide than the mill annealed samples and it has been shown that the critical particle size above which grain growth can occur spontaneously increases with increasing volume fraction of particles. The mill annealed sample will have cooled very quickly through the optimum precipitation range and will thus have fewer carbides present. On heating at between 900°C - 1200°C , those carbides present will tend to become more coarse, since it is assumed that at these temperatures nucleation of new precipitates will be slow, whereas growth of existing ones will be rapid and increase with increasing temperature. In this way the carbides acting as grain boundary pinning particles will grow rapidly and thus cease to pin the boundaries. The thermally treated material with its larger volume fraction of carbides can be heated to a higher temperature before grain growth occurs, and once grain growth has occurred the smaller starting grain size will mean that for a given heat treatment smaller grains, and thus higher hardness, will result. It is for this reason that the lower

carbon tube A has a higher grain coarsening temperature and why its hardness levels are maintained at higher temperatures. However, an alternative explanation for this phenomenon may be associated with the as received tubes previous mill annealing temperature. It has been found that the grain growth temperature, of a reannealed sample of commercially produced 690 tubing, coincides with the previous mill annealing temperature. Thus tube A, which was mill annealed at 1040°C, would be expected to undergo grain growth at approximately that temperature, as was the case (92).

The effect carbon has on activation energy may not be a simple one, Table XXVI. With increasing carbon the activation energy increases from 124.6 - 167.3 - 197.5. However the results from the group (1) alloys have already shown that increasing carbon in the absence of both Al and Ti has no discernible effect on activation energy. This would suggest a conjoint effect of carbon with either or both Al and Ti.

Recent work has shown that segregation of V in austenite in the presence of C and or N is due to the presence of V - C - N clusters (88) which cause large local strains in and around the clusters. The clusters segregated to austenite grain boundaries can act as considerable inhibitors to grain boundary nucleation. In the same way such clusters may be increasing the activation energy for grain growth by increasing solute drag. It has been suggested that nitrogen enhances segregation in two ways. The first is by the formation of grain boundary pinning particles such as TiN. These immobilise grain boundaries allowing elemental

segregation to occur. The second is by the formation of X - C - N clusters, where X is a strong nitride former such as Al, Ti, V etc. Aluminium and titanium both have great affinity for nitrogen and if clusters of Al - N or Ti - C - N are increasing the activation energy then this will become apparent in the following sections which will examine the alloys in groups (3) and (4).

An alternative explanation for the increase in activation energy with increasing carbon is that the precipitation of TiC / Ti(CN) immobilises grain boundaries. The results show that the increase in activation energy corresponds to a decrease in the Ti:C ratio. It is well established that the greatest temperature dependency for the solution of carbide occurs at the stoichiometric ratio of the carbide (75). The greater the temperature dependency the greater the volume fraction of precipitated carbide for a given temperature below the solvus temperature, and thus the higher the activation energy for grain growth. As stated this effect has also been noted in alloy 600 though no TiC was actually found to support this hypothesis. Small TiC / Ti(CN) particles have been found at grain boundaries in this study and will be discussed later when examining the effect of titanium.

5.8. The Effect of Varying Aluminium in the Presence of 0.02% C and 0.27% Ti.

The alloys chosen for this analysis are EM 7, EM 11 and tube C. A graphical representation of hardness vs solution treatment temperature for all three alloys is given in Fig.34. Again, the as received material has a higher grain coarsening temperature than the experimentally produced alloys, for reasons already

outlined. It is interesting to note that the difference is not as pronounced as the difference between tube A and EM 10. This is as expected when considering tube C's lower mill annealing temperature. The grain coarsening temperatures of EM 7 and EM 11, the highest and lowest Al contents respectively, are both 50°C below the TiC solvus temperature so it is again possible that TiC has some effect on grain boundary pinning. This will be discussed later when considering the effect of varying Ti.

The Petch relationships for the three alloys are shown in Fig.35 Again, the commercially produced tube is harder for a given grain size than the experimentally produced alloy. The slopes for tube C and EM 11 are virtually identical, which is not surprising considering the similarity in composition. The alloy with less than 0.05% Al has a slightly shallower gradient although within the bounds of experimental error the effect is insignificant.

The activation energies for EM 7 and EM 11, the highest and lowest Al contents in the group, are very similar, 140 and 145 kJ mol^{-1} respectively, suggesting that Al exerts no influence over activation energy for grain growth. Tube C has an activation energy of approximately 29 kJ mol^{-1} higher than EM 11. It is felt that this increase reflects the effect of the different thermomechanical treatments undergone by the commercially produced alloy.

An important conclusion which can be drawn from this group of alloys is that Al does not appear to have a demonstrable effect on activation energy for grain growth. It is unlikely that Al-N clusters are forming which again points to a synergistic effect of Ti and C on the activation energies calculated for group (2) alloys.

5.9. The Effect of Varying Titanium in the presence of 0.02% C and 0.14% Al.

It has been suggested throughout the preceding text that a compound of Ti such as TiC/TiCN may be responsible for the immobilisation or part immobilisation of grain boundaries or sub grain boundaries thus preventing recrystallisation or normal grain growth. This will be now examined.

The results of the effect of Ti on the hardness for a given grain size (Petch, Fig.37) are inconclusive. As would now be expected the commercially produced material has a higher hardness for a given grain size than the two experimental melts. The slopes for the three alloys are very similar, with the low Ti EM 12 demonstrating a slightly higher hardness for a given grain size than the higher Ti EM 13.

The activation energies for grain growth for all the Ti containing alloys are given in Table XXVI and plotted in Fig.67 - 74. On preliminary examination of Table XXVI the mass % Ti does not appear to have any consistent effect. In alloy 600 (27) the grain size was shown to increase and then decrease with increasing mass % Ti. This is not the case in alloy 690. Assuming, for reasons already discussed, that the mid range Ti alloy tube C, is ignored due to its prior thermo-mechanical history, then it can be seen that the grain size of the highest and lowest Ti alloys are very similar for a given mill annealing temperature upto 1100°C. Beyond this the grain size in EM 12 increases, compared to EM 13, by 71% at 1150°C and a further 57% at 1200°C. Examining Fig.65 it would appear that EM 12 undergoes a secondary grain growth which occurs

at a temperature approximately 50°C - 100°C below the solvus temperature for chromium carbide. This apparent change in mechanism is more evident in EM 13, yet this alloy has an identical carbon content and thus an identical chromium carbide solvus temperature. If, as the results have so far indicated, TiC/CN are pinning grain boundaries, then the greatest increase in activation energy should occur at the stoichiometric ratio for that carbide. Fig. 75 shows a graph of activation energy for all the Ti containing alloys vs the stoichiometric ratio of those alloys and Table XXVI shows the activation energies of all the alloys examined. The most immediate difference to note from the table is that between those alloys with and without Ti.

It has been concluded from group (1) that carbon has no pronounced effect on activation energy for grain growth. Therefore the fact that the activation energies calculated in the Ti containing alloys are consistently higher than those alloys with no Al or Ti, adds further support to the assertion that TiC/CN are pinning grain boundaries.

Fig. 75 shows how, as the compositions of the alloys approach the stoichiometric ratio for TiC, the activation energy increases markedly. A linear regression analysis has been carried out on the data to ascertain a best fit curve. From this, the effect the Ti:C ratio has on activation energy for grain growth can be predicted. The formula is given below:

$$Y = A \times (X^B)$$

where:

Y = Activation Energy for Grain Growth

X = TiC Ratio

Where:

$$A = 148.23$$

$$B = - 0.804$$

The correlation coefficient = 0.9

The standard error = 10%

The activation energies plotted do not represent only the effect of TiC/CN. It has already been established that chromium carbides act to pin grain boundaries. It will therefore be necessary to estimate the contribution to the total activation energy supplied by carbon alone. Returning to group 1 alloys, which examined the effect of increasing carbon in the absence of both Al and Ti, and assuming that it is reasonable to ignore EM 3 due to too few data points and further assuming that it is acceptable to average the remaining two carbon contents and activation energies, then this activation energy for the given carbon content can be subtracted from the total activation energy for the Ti containing alloys. This will represent the effect Ti, and in particular the effect the Ti:C ratio is having on the activation energy. The average of the activation energies of the two remaining alloys in group 1 was 100 kJ mol^{-1} . This has been subtracted from the total activation energy and the result from this is also given in Fig.75.

These results clearly suggest that TiC/CN are pinning grain boundaries. This explains why the lowest Ti alloy in group (3) has the highest activation energy and the exaggerated grain growth. It also explains why increasing carbon in the group (2) alloys increased activation energy; the increase corresponding to a

decrease in the molar Ti:C stoichiometric ratio towards unity.

If this information is to be of any practical value it is important at least to estimate the temperature at which TiC/CN ceases to pin grain boundaries / sub grain boundaries. Table XXVIII shows the grain coarsening temperature for all the alloys examined compared to the TiC and Cr_{23}C_6 solvus temperatures; there appears to be no clear relationship between the TiC solvus temperature and the grain coarsening temperature. If the polygonisation temperature is plotted against the TiC solvus then there appears to be some correlation. Tables XXVIII and XXIX and Fig 76 show the TiC solvus vs polygonisation temperature and the Cr_{23}C_6 solvus vs grain growth temperature. These would suggest that TiC/CN are pinning subgrain boundaries and retarding recrystallisation. Once the material reaches a sufficiently high temperature, at which time carbide coarsening / dissolution occurs or decomposition has occurred, the material recrystallises. Grain growth appears to coincide with carbide ripening of Cr_{23}C_6 , suggesting that grain growth after recrystallisation is prevented by the precipitation of Cr_{23}C_6 . This would indicate a dual pinning process with both TiC and Cr_{23}C_6 taking part. Fig 77 shows both a TiC and a Cr_{23}C_6 adjacent to one another on a grain boundary. The material was as received tube C. Judging by the past thermo mechanical history of tube C and the morphology of the TiC it is possible that the grain boundary migrated to the particle rather than precipitation of TiC occurring at the grain boundary.

Very fine TiC have been found, in both the as received tubes and the experimentally produced alloys, at grain boundaries. These

carbides were identified using the HB501 STEM. Coarser Ti rich grain boundary carbides have also been identified using the JEOL STEM, Fig.78.

The volume fraction of TiC either calculated or found is not large yet the data analysis clearly suggests that TiC is responsible for some grain boundary pinning. The reason for the lack of positive identification of the finer precipitates noted may be associated with the difference in readily attainable resolution between the JEOL and the HB501 microscopes. The resolution of the JEOL is 0.34 nm in gold at 100 KV. The HB501 resolution, again using gold at 100KV, is 0.14 nm. The very fine TiC has only been identified using the higher resolution microscope. Thus the lack of positive identification of the fine carbide phase noted in the alloy 600 work using the more readily available JEOL microscope does not necessarily disprove the hypothesis that TiC is pinning grain boundaries.

The higher volume fraction of Cr_{23}C_6 might normally be expected to exert a greater influence over the grain size than the lower volume fraction of TiC. However the much finer TiC will be more effective for grain boundary immobilisation. This size difference is clearly shown in Fig.25.

It is interesting to refer back to the work carried out by Norberg (65) who found that the effect of pinning by TiN/Ti(CN) was negligible. Two compositions were examined in this work, one with Ti the other without. The grain coarsening temperatures were very similar, as were the grain growth characteristics which led to the conclusion that TiN/Ti(CN) play little part in grain

boundary pinning. Examining these results in the light of the present work offers a second possible interpretation. The Ti : C ratio of the Ti containing alloy was very high, approximately 20. By employing the regression analysis produced from this research and subtracting the postulated effect of carbon, an increase in activation energy of only 15 kJ/mol would be expected for this composition. Allowing for the 10% standard error, the increase in activation energy for grain growth would be negligible for this Ti : C ratio. The findings of Norberg (65) confirm, to some extent, those given here and the conclusion from the earlier work can now be updated in view of these more recent results.

From the Petch analysis, the slopes and hardness for a given grain size for EM 12 and EM 13 are very similar, the main difference being the larger grain size and thus lower hardness of EM 13 at the higher solution treatment temperatures. The experimentally produced material was again softer for a given grain size compared to the commercially produced tube for reasons already discussed.

5.10. Measurement of the Chromium Depletion Profile of Thermally Treated EM 12

Much of the research into alloy 690 has concentrated on the corrosion resistance of the alloy in certain accelerated environments as well as more realistic and thus longer term tests (51)(52)(53). In the Huey test Cr depletion at grain boundaries, in alloy 600, has been shown to enhance corrosive attack (29). However in deaerated pure water and NaOH the opposite has been

shown to be true . In this latter environment it has been suggested that this improvement may be due to Ni enrichment in areas adjacent to grain boundaries. The special thermal treatment used on alloy 600 improves IGA resistance in an acidic environment providing back diffusion of Cr from the matrix to the denuded grain boundary areas occurs. Such a heat treatment should not be so beneficial to the corrosion resistance of the alloy in a deaerated NaOH environment since Cr enrichment infers Ni depletion.

Alloy 690 has been shown to be immune to IGA in an acidic environment providing the carbon content of the alloy is kept below 0.02%C (50). This would suggest that the corrosion resistance of 690 would be greatly improved by a heat treatment which promotes grain boundary carbides but does not allow time for back diffusion of Cr to the denuded grain boundary areas. However this has not been shown to be the case with alloy 600. Payne et al. have shown that IGA resistance is improved by a thermal treatment which promotes back diffusion of Cr (39).

In order to investigate this further the degree of Cr depletion and Ni enrichment in areas adjacent to the grain boundary have been measured for a series of heat treatments . The results from this study will be correlated with corrosion tests carried out in deaerated 50% NaOH^{*} and deaerated 30 % NaOH + 10% Na₂SO₄ at 350°C. The results from the STEM study are shown in fig (42) - (51) and Tables XVI - XX.

The Cr depletion profiles observed are due to the precipitation of Cr rich carbides at grain boundaries during thermal treatment. The

* At 340°C ,

shape of the profile is due to the time and temperature of the thermal treatment as well as the level of carbon in the material. Higher temperatures result in faster Cr diffusion and less carbon available for precipitation because of the lower supersaturation. These two factors lead to the production of a wider and more shallow Cr depletion zone. Lower temperatures result in slower Cr diffusion and more carbon available for precipitation. These two factors lead to the production of a deeper and narrower Cr depletion zone, as would an increase in the C content of an alloy. Since the chemical composition, mill annealing temperature and thermal treatment temperature for the four samples are constant - the Cr depletion profile will depend entirely on ageing time. All the depletion profiles have been plotted on the same axis so that immediate comparison is possible. It is evident that as the ageing time increases so the width of depletion either side of the boundary increases and the depth decreases. The Cr levels in areas adjacent to the grain boundary do not fall below 20.5%, showing clearly why a 0.02% C alloy 690 is immune to IGA in an acidic environment. Ni enrichment is almost a mirror image of the Cr depletion profiles, the greatest degree of enrichment occurring after 1 hour (68% Ni). These results are not entirely indicative of what might be expected in a commercially produced material. The mill annealing temperature of 1200°C will promote very high supersaturation which will tend to push the nose of a precipitation C curve to high temperatures and shorter times. This will develop a narrower and deeper Cr depletion profile. The as received material examined on the STEM was tube C. This was mill annealed at 965°C followed by the STT. The Cr depletion

profile is very much shallower and wider than any of the experimental melts. Work on alloy 600 has shown that recovery from sensitisation occurs most rapidly in alloys which have undergone a low temperature mill anneal (38). The reasons for this are associated with carbide morphology, grain size and the comparatively small amounts of carbon in solution. The microstructure in alloy 600 after a high temperature mill anneal has been shown to consist of semi-continuous grain boundary carbides and large grains. Before desensitisation can occur the carbides must first spheroidise and this in conjunction with the large grain size, mitigates towards a long desensitisation time. A low mill anneal temperature will produce a finer grained material with large and discrete carbides, both inter and intra granular, thus promoting shorter desensitisation times. Thus when considering an acidic environment, a low temperature mill anneal would be advantageous. This is contrary to the microstructural requirements of the material in deaerated water and NaOH. Whatever mechanism is occurring in alloy 600 which causes the improved corrosion resistance in deaerated pure water when the microstructure has been sensitised, is opposite to the microstructural requirements of the alloy in an acidic environment. Yet in alloy 690 it has been possible to subject the material to a sensitizing heat treatment without rendering it susceptible to attack in an acidic environment. However, the benefits afforded by the thermal treatment may be due to segregation of impurities to grain boundaries. If this is the case the prolonged thermal treatment may still be required. This will now be considered.

An analysis for minor alloying additions and impurities was made, using the EDAX facility of the STEM, on grain boundary precipitates and up to 1000nm either side of the grain boundary. The results are given in Tables XVI - XX. Due to the limited number of tests possible the results of the analysis for impurities such as phosphorous and sulphur are inconclusive. The greatest degree of segregation of P occurred after 15 hours at 720°C in EM 12. The P content of the alloy was < 0.05 yet as much as 0.2% P was found adjacent to a grain boundary and as much as 0.3% (+ or - 0.078%) at 500nm from the grain boundary. There was little consistent evidence of P, up to but not including 15 hours, though the P which was evident was invariably only a few nm from the grain boundary. suggesting that some segregation of P to grain boundaries may be occurring. Airey (53), Was (40) and McIllree (34) have all reported segregation of P to grain boundaries though opinion as to its effect is divided. Airey suggests that P segregated to grain boundaries alters the nature of the oxide film formed at those boundaries. McIllree states that P segregation has no effect on corrosion resistance. The results from this study are inconclusive; if P is affecting the corrosion resistance of the alloy then it must be assumed from the corrosion results that the effect is a minor one. Samples of tube F solution treated at 1200°C and aged for between 1 and 15 hours at temperatures between 650°C and 750°C showed no discernible effect of heat treatment time or temperature on IGA resistance, table XXII. After 15 hours there has been an increase in the P concentration of as much as 30 times, in areas adjacent

to the grain boundaries. This must be considered significant in terms of segregation, yet the corrosion results show no apparent correlation after 1800 hours in the corrosive environment.

Again, these results may not be directly applicable to commercial practices due to the high solution treatment temperature used. Segregation of impurities in the highly deformed, lower mill annealed and thus smaller grained commercially produced material may be wholly different. However it should be noted that the two control test specimens, tube A and F (as received), have undergone very similar rates of IGA.

The level of P in precipitates also varied. 35% of the Ti rich precipitates had between 0.2 and 0.3% P present. None of the Cr rich particles contained detectable amounts. It would be beneficial to examine further ageing times and temperatures to ascertain the optimum thermal treatment for P segregation. In this way it would be possible to see if a correlation exists between P segregation and corrosion resistance.

Sulphur was not detected in areas adjacent to grain boundaries but was present in a small number of grain boundary precipitates. Opinion is divided as to what effect segregation of S may have on corrosion resistance. Airey (53) maintains that the effect of S is insignificant; McIllree (34) states that S improves the deleterious effect of high carbon levels in alloy 600, and earlier work on alloy 600 (42) showed that maximum corrosive attack coincides with maximum segregation of S, Si, N and Ti. Since S has not been detected on the grain boundary and since there was no effect of ageing time at temperature on the corrosion resistance of a material subjected to the same thermal treatment, it can be

concluded that under the conditions of test, S has no effect on corrosion resistance, assuming that the compositional differences between EM 12 and Tube F are not significant.

An element which appears to have segregated to the grain boundary region in quantities well above the bulk composition is Al.

The amount of segregation may be heat treatment dependant. The greatest degree of segregation of Al occurs at the shortest ageing time of 1 hour. After 1 hour the average Al content upto 180 nm from the grain boundary is approximately 5 times that of the bulk composition, reaching a maximum of 0.7% Al (+ or - 0.1%) compared to the matrix composition of 0.1% Al. After 15 hours the grain boundary Al levels are similar to the bulk composition of the alloy, 0.13% (+ or - 0.1%). The two intermediate levels range from between 0.14 - 0.34% Al for 5 hours and 0.3 - 0.5% Al for 10 hours ageing time. The mechanism by which Al could segregate to grain boundaries and the driving force for such segregation has already been discussed under the heading of the effects of varying Al for constant C and Ti (88).

It has been suggested that Al may exert some influence over the intergranular crack resistance of alloy 690 in a deaerated high temperature caustic environment. Crum et al. examined the effect of varying Al in four nominal 690 alloys and found that the highest Al content underwent IGA (89): the remaining 3 alloys did not.

Results from the study carried out on as received tubes A and E suggest that increasing Al may increase the depth of IGA. This will be discussed in more detail under the corrosion section which

follows. The data from the corrosion tests carried out on the group 3 alloys are at present not available so that confirmation of the role of Al can not be given.

It would seem logical that if Al is exerting an influence over IGA resistance then its presence in quantities above the bulk composition at grain boundaries should be significant. This however does not appear to be the case. The greatest degree of segregation occurred after 1 hour yet the amount of IGA after this time is virtually no different to the depth of IGA after 15 hours thermal treatment at the same temperature. These results would suggest that if Al has an affect on IGA resistance then either longer exposure to the corrosive medium is required or it is the bulk Al content which is of greatest importance.

Why Al should effect IGA resistance, if indeed it does, is unclear.

5.11. Corrosion.

5.11.1. As Received Tube.

Deaerated Pure Water With Hydrogen Over Pressure.

None of the stress corrosion C-ring samples have undergone any cracking or intergranular attack after 1200 hours.

Deaerated 50% NaOH and Deaerated 30% NaOH + 10% Na₂SO₄.

Both at 340°C.

The 50% deaerated NaOH test carried out at 340°C represents a theoretical extreme for in service conditions (5). The 30% NaOH + 10% Na₂SO₄ was chosen to simulate the effect of resin intrusion from the demineraliser during service in a PWR (55). Extensive

intergranular attack has occurred around the entire circumference of the tube on both internal and external surfaces. It is interesting to note that the belt grinding marks on the outside diameter of the tube appear to have deepened after exposure to the corrosion tests, Fig.54. It is possible that the grinding marks are acting either as occluded cells where concentration of the corrosive environment may be occurring, or in the case of SCC as crack initiators. It has been suggested that crack initiation in alloy 600 occurs at the root of the grinding striations.

Due to problems of availability it was necessary to use alloy 600 bolts as a means of stressing the C-ring specimens. These bolts have undergone extensive stress corrosion cracking, Fig.55 - 57. The cracks occurred in the highly stressed areas such as the root of the thread and nut and bolt thread contact areas. The bolts were in the thermally treated condition.

With alloy 690 intergranular attack growth rate appears to slow rapidly once the crack has developed. The crack morphology after 1200 hours shows a general IGA at the surface of the tube between 5-10 microns deep with branches approximately 50-100 microns apart to a maximum depth in the high carbon material of 41 microns. If this growth rate were maintained the tube would perforate fairly rapidly. However after 8000 hours the attack has not developed beyond 60 microns maximum. There is evidence of a thicker corrosion product in the attacked areas in alloy 690 compared to 600, which may be preventing further attack. As far as is possible the corrosion product has been examined

using the SEM. The Be window was left open so that the lighter elements such as oxygen carbon and nitrogen could be analysed for. The EDAX results are given in Figs.79 - 82. It is evident that the predominant oxide in the intergranularly attacked areas of the alloy 690 C ring is chromium rich compared to both the matrix of alloy 690 and the matrix and the corrosion product in the crack of the alloy 600 bolt. It is difficult to Speculate why this should be. The chemical composition of alloy 690 is higher in chromium than alloy 600 thus it may be that an oxide higher in chromium is forming on alloy 690 which is retarding crack growth. It is also interesting to note that the Ti content of the corrosion product in alloy 690 is appreciably above both the matrix concentration and the concentration found in the oxide of alloy 600. Again it is difficult to Speculate why this should be. The simple solution would be that excitation of an underlying Ti rich precipitate has occurred though this is not backed up by the EDAX results which do not show a marked increase in the carbon or nitrogen levels in the crack compared to the matrix. A more systematic study of the corrosion products of alloy 690, using a more surface sensitive analytical technique such as Auger, is required.

The higher carbon alloy tube A (0.022% C) appears to have consistently corroded less than the lower carbon alloy tube E. This would not normally be expected. Work on alloy 600 (39) has shown that IGA resistance is critically dependent on mill annealing temperature, in a deaerated 30% NaOH + 10% Na_2SO_4 environment.

Norrington et al (35) in a pure water environment, which would also not be expected to attack chromium denuded areas, has shown that corrosion resistance is dependent on carbon content in conjunction with mill annealing temperature. The higher the carbon content the higher the mill annealing temperature required to optimise corrosion resistance. Thus for a given special thermal treatment and mill annealing temperature below the solution treatment temperature a higher carbon alloy would be expected to be less IGA resistant than a lower carbon alloy. Tube A the higher carbon alloy has consistently corroded less than tube E. It is interesting to note that the lower carbon tube E has a much higher aluminium content than tube A. It has been suggested (90) that Al may play an active role in the corrosion process by increasing the propensity for intergranular attack. These results bear this out and it was for this reason that EM 7 and EM 11 have been chosen to examine the effect of varying Al on the depth of IGA. Further work in this area is to be carried out.

5.11.2. Effect of Heat Treatment on Intergranular Resistance in a Deaerated 30% NaOH + 10% Na₂SO₄ Environment at 350°C

Table XXII gives the results from this study. A sample of as received tube A was included in this exposure to ensure that the results from the two different autoclaves were comparable. The depth of attack of samples taken from the same tube and exposed to the two different autoclaves are similar. The results from this study suggest that under the conditions of test the thermal treatment has little effect on the degree of IGA. This would be

expected if the corrosion mechanism is linked to the degree of Cr depletion in areas adjacent to grain boundaries. It has been shown in alloy 600 that the corrosion resistance of the alloy in a similar environment (39) is linked to the thermal treatment. Payne et al. (39) have shown that providing a sufficiently high mill annealing temperature is used then IGA resistance can be recovered after as little as 90 minutes TT at 700°C. According to Was et al. (40) the Cr concentration in a high purity alloy 600 type material would be as low as 7% Cr at the grain boundary after 30 minutes TT at the same temperature. The Cr concentration in alloy 690 after 1 hour at 700°C has been shown to be no less than 20% Cr which is almost 3 times that which has been shown to improve IGA resistance and is in fact equivalent to the matrix concentration of alloy 600. These results confirm the hypothesis that if the corrosion resistance of alloy 690 in a deaerated 50% NaOH environment is unaffected by the special thermal treatment carried out between 1 and 15 hours, then there is no need to thermally treat the material for beyond 1 hour and possibly less. The TT is however used for stress relief as well as to promote the requisite carbide morphology. Further, the mill annealing temperature used in this study (1200°C) is considerably higher than that commonly used in industry and it has already been shown in alloy 600 that crack initiation time is critically dependant upon the total carbon - the carbon in solution (35). The smaller this figure is the longer the crack initiation time. More work is needed to examine mill annealing temperatures closer to those used in commercial practice.

The results from table XXI and XXII show that the 50% NaOH environment is more corrosively aggressive towards alloy 690 than the 30% NaOH + 10% Na₂SO₄, suggesting that under the conditions of test it was the NaOH concentration which exerts the greatest influence.

5.12. Thermal Ageing Studies

Work has been carried out on thermal ageing studies to identify the optimum time and temperature for precipitation which will maximise corrosion resistance. Work on alloy 600 (27) showed that the hardness test was not sufficiently sensitive to identify the onset of precipitation. This was also confirmed in alloy 690, Fig 38.

It is well established that a relationship exists between carbide morphology and corrosion resistance. Whether this effect is due to Cr depletion, Ni enrichment, or a mechanical effect of the carbides, ie. fewer carbides causing a localisation of stress and thus increasing the crack susceptibility, is not known. To investigate the effect of ageing time and temperature tube F, having been solution treated at 1200°C was aged at temperatures between 550°C and 850°C for times between 1 minute up to 24 hours.

At the inception of this study it was hoped that carbide morphology after thermal treatment could be examined using the TEM. However, owing to insufficient time, a complete TEM examination has not been possible. A qualitative summary of the results taken from an optical examination is given in table XV.

The types of precipitate noted have been categorised into three groups: continuous - semi-continuous - discrete, which in turn have been subdivided into fine and coarse. Another carbide type commonly observed at grain boundaries was a cellular or discontinuous carbide of Cr_{23}C_6 . The cause for and ramifications of this carbide type will be considered later. How the different morphologies were arrived at will now be considered.

The nucleation and growth of grain boundary carbides are a function of time and temperature. In general higher temperatures produce few carbide nucleation sites and semi continuous carbide nucleation is favoured, Fig 39c. At shorter times the carbides which have nucleated do not have time to grow and completely cover the grain boundaries. At lower temperatures nucleation is favoured but growth is not and again discrete precipitation is favoured. Other factors which influence carbide morphology are the degree of supersaturation and prior deformation. Increasing supersaturation increases the driving force for nucleation and growth of precipitation. The greater the amount of cold work the greater the number of nucleation sites and thus the greater the rate of nucleation. These effects are clearly demonstrated in Figs 9, 10 and 11. These are computer simulations of precipitation C curves.

Precipitation C curves for alloy 690 exist but different methods of detection, different compositions and different conditions of deformation all make quantification of each of the variables impossible. In this work an attempt has been made to determine the

precipitation time temperature relationship on the basis of the thermodynamics of the system and diffusion controlled nucleation theory and then to correlate the predicted relationship to observations made during this study and by other workers. In this way it was hoped that appropriate values of unknown constants in the relationship could be established. Evidently, since a detailed examination of the thermally treated specimens could not be made it has not been possible to update the model.

5.13. Cellular Precipitation

Grain boundary precipitation with concurrent boundary migration is known as discontinuous or cellular precipitation. It can be caused in one of two ways. The first is the precipitation on boundaries migrating under some external force. The second is precipitation induced boundary migration (86). It has been shown that these precipitates possess no orientation relationship with the matrix in the direction of growth (83), suggesting that the second mechanism is responsible for this morphology.

Cellular or discontinuous precipitation has been reported in both alloy 600 and 690. It has been associated with increased susceptibility to IGA, in alloy 600, in 30% NaOH + 10% Na₂SO₄ (39). Evidence of this type of precipitate, in alloy 600, has been attributed to a low mill annealing temperature. In alloy 690 this precipitation was found in thermally treated material which had been subject to a high temperature mill anneal. This reasons for this difference will be discussed.

If a material is subjected to a low temperature mill anneal then too little carbon will be taken into solution prior to the special

thermal treatment. The subsequent low activity of carbon will enhance the likelihood of $M_{23}C_6$ precipitation. Alloy 600 has a high solubility of carbon compared to 690 so that despite the fact that the mill annealing temperature is low the supersaturation of carbon may be sufficient to promote discontinuous precipitation.

In alloy 690 the predominant grain boundary carbide is $M_{23}C_6$. A high temperature mill anneal will ensure high supersaturation of carbon, especially considering the low solubility of 690 for carbon. Thus on thermally treating the precipitation of cellular $M_{23}C_6$ is possible.

The amount of cellular precipitation appears to depend on ageing time and temperature for a given composition and mill annealing temperature. The lower ageing temperatures maintain a higher degree of supersaturation but slow diffusion rates. So for example at 650°C for 24 hours there is little evidence of cellular precipitation, Fig 40. Yet at 800°C the quantity and size of the cellular precipitate cells increase with ageing time reflecting the increase in boundary and volume diffusion.

Smaller amounts of cellular precipitation were observed in the commercially produced material. This is most likely due to the lower mill annealing temperature of the as received tubes promoting lower carbon supersaturation.

Whether this type of precipitation will effect corrosion resistance in alloy 690 is not clear. In alloy 600 the cellular precipitate associated with a low mill anneal temperature was also associated with small discrete M_7C_3 particles. In alloy 690 after a

mill anneal of 1200°C the grain boundaries will be decorated with a semi continuous grain boundary network of M_{23}C_6 carbides, after a commercial ageing treatment. If the mopping up of solute impurities by grain boundary precipitates is responsible for the improved corrosion resistance after thermal treatment then the cellular precipitation on ageing after a high temperature mill anneal will have no effect on corrosion resistance, providing it is accompanied by a semi-continuous grain boundary network.

This is confirmed by experimental results. Table XXII shows that ageing time at temperature has no effect on IGA resistance up to 12 hours. It has already been shown that the amount of cellular precipitation depends on the ageing time at a given temperature and therefore the specimens aged for 12 hours will have considerably more cellular precipitation than after 1 hour. The latter has corroded no more than the former.

A TEM examination of the effect of ageing time and temperature has been carried out on EM 12. This examination qualitatively confirms the optical microscopy data. For instance, the carbide morphology of the as received tube was predominantly semi-continuous yet EM 12 thermally treated for 15 hours at 700°C shows discrete grain boundary particles. This trend continues at the higher ageing temperatures, Figs 39d and 39e. After ageing at 800°C for between 1 and 15 hours the particles are again predominantly discrete. Another factor which affects the rate of precipitation of M_{23}C_6 at grain boundaries is cold work prior to ageing. Grain boundary precipitation increases with the degree of cold work. This is because cold work generates a large number of extrinsic grain boundary dislocations or grain boundary ledges which are

often preferential sites for intergranular precipitation.

At short ageing times the grain boundaries were found to be decorated with fine discrete triangular platelets of $M_{23}C_6$, Fig. 39b. This type of carbide morphology has been reported in alloys which have undergone a thermally induced decomposition of TiC to $M_{23}C_6$. It is not known whether such a decomposition has occurred after such a short thermal treatment, (10 mins at $700^{\circ}C$), but it was noted if only qualitatively that the amount of TiC at grain boundaries diminished with increasing ageing time at $700^{\circ}C$. This may be due to the fact that the TiC is on average considerably smaller than the chromium carbides, Fig 25. Alternatively it may be that a decomposition of the TiC is occurring. As already stated the effect such a decomposition would have in service is not known.

Very little intragranular precipitation of TiC or $M_{23}C_6$ has been observed in the experimental melts solution treated at $1200^{\circ}C$ compared to the as received tubes. This could well be a consequence of the paucity of the heterogeneous nucleation sites due to the high mill annealing temperature of the experimentally produced alloys.

5.14. Commercial Considerations.

The three suggested mechanisms by which the thermal treatment of alloy 600 improves corrosion resistance are :

(1) Promoting the segregation of impurities to grain boundary carbides. The presence of the carbides interrupts the penetration path of the advancing IGA.

(2) Ni enrichment in areas adjacent to grain boundaries has been used to explain the increased corrosion resistance of sensitised alloy 600 on the primary side.

(3) Preventing the localisation of stress, due to discrete grain boundary carbides, by promoting a semi-continuous grain boundary carbide network.

It has been shown in alloy 600 that segregation of impurities occurs at the special thermal treatment temperature though work has not shown whether the amount of segregate increases linearly with time. Viewing the results of chemical analysis of the precipitates presented here in alloy 690 in conjunction with corrosion test data it is evident that segregation of impurities to grain boundary carbides has no effect on IGA resistance under the conditions of test. This would suggest that a prolonged thermal treatment is not necessary if it were used only to promote impurity segregation to grain boundary carbides.

It has been shown in alloy 600 that a suitably high mill annealing temperature must be used, prior to the special thermal treatment, to ensure adequate corrosion resistance. Too high a mill annealing temperature would promote too low a yield strength due to exaggerated grain growth. Work by Payne et al. (39) has shown that large grains can be deleterious to IGA resistance so that a compromise must be reached between carbon taken into solution and grain size. In alloy 690 it has been shown that precipitation of TiC increases the activation energy for grain growth and that the greatest increase occurs at the stoichiometric ratio of the carbide. It has also been shown that a dual

pinning process is occurring and that once the TiC ceases to prevent polygonisation, grain growth is controlled by $M_{23}C_6$. Thus the grain size in an alloy which has the molar stoichiometric ratio should be smaller for a given mill annealing temperature, below the grain coarsening temperature, than an alloy with a molar TiC ratio appreciably greater than 1. In this way a higher mill annealing temperature can be used in order to produce a greater solution of carbon whilst still achieving the required yield strength and IGA resistance. Alloy 600 has been shown to be susceptible to corrosive attack in acidic environments if insufficient time is given at temperature during the thermal treatment. Cr levels as low as 7% Cr have been reported in areas adjacent to grain boundaries after a short thermal treatment. This would have severe implications for corrosion resistance on the secondary side of a sea water cooled reactor but may be beneficial to corrosion resistance on the primary side.

It has been shown in the preceding text that Cr levels, in alloy 690, in areas adjacent to the grain boundary, do not fall below 20% Cr which is why the alloy is immune to IGA in acidic environments providing the carbon is maintained at $< 0.02\%$ C. This would suggest that a shorter thermal treatment should be used since the shorter the thermal treatment the greater the Ni enrichment and thus the greater the corrosion resistance on the primary side. However the thermal treatment is also used to reduce stress levels in the tube. Experience has shown that 5 hours at temperature will bring residual stress down to an acceptable level. It seems likely that at higher temperatures stress relief will occur at shorter times and providing that an

adequate carbide morphology could also be produced it is possible that the special thermal treatment time could be reduced still further.

The severe attack experienced by alloy 600 bolts demonstrates the improved corrosion resistance of alloy 690 compared to 600.

Further, it is clear from the corrosion test that control of thermal treatment temperature and time is much less critical for alloy 690 than 600. A wide range of mill annealing temperature and ageing times and temperatures have failed to produce a change in corrosion resistance in the extreme PWR simulated environments used.

For the reasons discussed, alloy 690 must be considered a most suitable material for steam generator tube applications.

6. CONCLUSIONS.

The second phase particles present in commercially produced alloy 690 have been examined. The tubes were in the thermally treated condition. It can be concluded that:

- (1) The most predominant intergranular phase has been identified as Cr rich $M_{23}C_6$. The composition of this compound has been shown to be approximately 80% Cr, 15.6% Ni and 3.6% Fe. The elements associated with this phase include Mn, Si and Al.
- (2) The large intragranular precipitates have been identified as Ti(CN). Impurities associated with this phase include S and P.
- (3) Cellular precipitates have been found in as received material though it is felt that there are insufficient to affect ductility.
- (4) The second phase particles responsible for grain boundary pinning in the thermally treated commercially produced alloy are $Cr_{23}C_6$ and Ti(CN).
- (5) It has been suggested that the Ti(CN) are pinning sub grain boundaries thus retarding polygonisation.
- (6) Hardness has been correlated to grain size and via the Meyer relationship to the Hall - Petch type plot. There is a linear relationship between hardness and reciprocal root grain size in as received alloy 690.

(7) The stringers orientated in the pilgering direction have been identified as $(\text{FeNi})\text{OCr}_2\text{O}_3$ spinels.

(8) The solubility of Cr_{23}C_6 in alloy 690 has been defined more clearly and is close to that defined by Scarberry.

Experimentally Produced Material.

The type of precipitate identified depends on the composition of the melt.

(9) In group (1) alloys the large intragranular carbide phase was Cr rich most likely Cr_2CN .

(10) In group (2) alloys the intragranular phase was Ti rich $\text{Ti}(\text{CN})$ with traces of Al.

(11) The predominant intergranular phase in all the experimental groups was Cr rich M_{23}C_6 .

(12) Very fine grain boundary $\text{Ti}(\text{CN})$ was found in alloys containing Ti.

(13) Alloys subjected to a mill anneal followed by thermal treatment between 650°C - 850°C were found to have colonies of cellular M_{23}C_6 , the size of the colony depending on the time and temperature of thermal treatment.

Effect of Composition on Hardness, Grain Size and Grain Coarsening Temperature After a Simulated Solution Treatment Schedule.

An examination of the hardness and grain size of the as received and experimentally produced alloys has been carried out. The conclusions have been divided into the four alloy groups.

Effect of Varying Carbon in the Absence of Both Al and Ti.

- (14) Increasing carbon in the absence of both Al and Ti increases both hardness and grain coarsening temperature and reduces grain size for a given solution treatment temperature.
- (15) Increasing carbon has no demonstrable effect on the activation energy for grain growth.
- (16) The hardness of the experimentally produced alloys was consistently some 20 - 30 VPN lower than the as received tube. This is due to the effect of cold work prior to the special thermal treatment. The greatest contribution to the hardness comes from the belt grinding. These hardness levels were maintained upto the carbide coarsening temperature.

Effect of Varying Aluminium in the Presence of 0.02% C and 0.27% Ti.

- (17) Varying Al within the specified composition has no pronounced effect on hardness, grain size or grain coarsening temperature.

The Effect of Varying Ti in the Presence of 0.02% C
and 0.14% Al.

- (18) The most pronounced effect of Ti on grain size, grain coarsening temperature and hardness occurs at the stoichiometric ratio for the TiC.
- (19) There is a clear relationship between activation energy for grain growth and the stoichiometric ratio of TiC - being maximum activation energy at the stoichiometric ratio.
- (20) A quantitative estimate of the effect that the Ti:C ratio has on the activation energy for grain growth has been produced. Published data, concerning the effect of Ti, has been reappraised on the basis of the estimate and a good correlation has been found.

Thermal Ageing Studies

- (21) The hardness test and the electrical resistivity method proved too insensitive to identify the onset of precipitation during thermal ageing after solution treatment.
- (22) Thermal ageing studies have qualitatively demonstrated how ageing time and temperature affects carbide morphology. Carbide shape size and distribution has been described for temperatures between 650°C - 850°C for times between 1 min and 24 hours.
- (23) The special thermal treatment markedly increases the grain coarsening temperature for a given composition providing

sufficient carbon is taken into solution during mill annealing.

- (24) Numerical analysis has shown that the average Cr carbide size increases with carbon content and that the critical particle radius above which grain growth occurs spontaneously also increases.
- (25) Grain size inhomogeneity has been observed in both as received and experimentally produced material. The cause of this phenomenon is the concentration of cold work at the surface of the material.
- (26) The amount of cellular precipitation appears to depend on ageing time at temperature for a given composition and thermal treatment at temperature.

Chromium Depletion

- (27) For a constant composition, solution treatment temperature and ageing temperature, the width of the Cr depletion zone either side of the grain boundary increases and the depth decreases with increasing ageing time.
- (28) The lowest Cr level recorded was 20.5% Cr, at the grain boundary, after solution treating at 1200°C followed by ageing at 700°C for 1 hour. This coincided with the highest level of Ni enrichment, 68% Ni, again adjacent to the carbide at the grain boundary.

(29) The lower the mill annealing temperature prior to the special thermal treatment the shallower the Cr depletion profile. The maximum Cr depletion recorded after the lower mill annealing temperature was 0.3 of the matrix Cr content.

(30) Maximum segregation of phosphorous occurred after 15 hours special thermal treatment. There was no consistent effect of time at temperature on the segregation of phosphorous up to 15 hours.

(31) Significant segregation of aluminium to areas adjacent to grain boundaries was noted.

Corrosion.

(32) As received tubes A and E showed no sign of cracking in deaerated pure water with a hydrogen over pressure at 340°C after 1500 hours.

(33) C ring SCC samples of as received tubes A, E and F all corroded intergranularly when subjected to a deaerated 30% NaOH + 10% Na₂SO₄ environment at 340°C and to a 50% NaOH environment also at 340°C.

(34) Alloy 600 bolts used for stressing the C ring specimens underwent severe IGA and SCC during the corrosion tests in both NaOH environments.

(35) Results suggest that crack growth rate in alloy 690 slows with time. There is evidence of a Cr rich oxide product within the cracks.

- (36) The higher carbon alloy tube A consistently corroded less than the lower carbon alloy tube E. It has been suggested that this is due to the higher Al content of the latter alloy .
- (37) Thermal treatment between 1 - 15 hours at 720°C following a 1200°C mill annealing treatment had no consistent effect on corrosion resistance for a given composition and corrosive environment.
- (38) The deaerated 50% NaOH environment at 340°C is more corrosively aggressive towards alloy 690 than is the 30% NaOH + 10% Na₂SO₄.

It has been shown that thermal treatment time between 1 and 15 hours at temperatures between 650°C and 750°C has no discernible effect on the corrosion resistance of alloy 690 in a given corrosive environment after mill annealing at 1200°C . It would be appropriate to examine the effect of mill annealing temperatures more indicative of those used during manufacture of steam generator tubing. The subsequent examination of an alloy, subjected to such a mill annealing treatment and aged at temperatures between 650°C to 850°C , on the STEM could be correlated to corrosion resistance. This would reveal the effect of mill annealing temperature and ageing time at temperature on the Cr depletion, Ni enrichment and degree of segregation of impurities to grain boundaries. The correlation of these thermally induced microstructural changes with corrosion test results should enable a narrowing of the range of mechanisms suggested for improved corrosion resistance following the special thermal treatment.

This work has shown that Ti can have a pronounced effect on the microstructure of alloy 690. It would be beneficial to examine the effects, either individual or synergistic, of nitrogen, vanadium and niobium on the microstructural characteristics of the alloy to see if further improvements can be made to the corrosion resistance of the alloy via thermal treatment without sacrificing mechanical properties.

... increases in the degree of cold work should be examined to ascertain the effect this has on precipitation during thermal treatment and ultimately on corrosion resistance.

It is interesting to note that the crack growth rate slows during exposure to the corrosive environments used. The mechanism/s which are acting to reduce the growth of the fingers of intergranular attack should be examined. If this reduced crack growth rate is due to the physical blocking of the crack by the formation of an oxide film then consideration of the conditions within a working steam generator ie. vibration and rapid flow rates, should be incorporated into the test procedure.

REFERENCES

1. Alloy digest Inconel alloy 690 copyright. Filing code: Ni-266, March 1981.
2. A technical outline of Sizewell B. The British pressurised water reactor. CEGB. Department of information and public affairs.
3. M.A. Cordovi. Corrosion considerations in light water cooled nuclear power plants. International Nickel power conference, Kyoto, Japan 1972.
4. S.J.Green and D.A.Steininger. Pressurised water steam generators - problems and progress. ASME (Nuclear engineering division). Century 2 nuclear engineering conference. San Francisco. Calif. August 19-21 1980.
5. M.Hecht et al., in " The Corrosion Handbook " (ed., H.H.Uhlig), p. 530, John Wiley & Sons, Inc, New York, (1963).
6. C.Buchalet. Framatomes Continuous Efforts to Improve Steam Generator Corrosion Resistance. Nuclear Eng and Design 86 (1985).
7. S.J.Green. 'Methods for Preventing SG Failure or Degredation', EPRI, Presented at Post SMIRT Conference, ISPRA Italy, August 26-27,1985.
8. A..Sedriks. Stress Corrosion Cracking - an Overview. Pergamon press. 1980.
9. H. Coriou, L.Graill, C.Mahieu and M.Pelas. Sensitivity to Stress Corrosion and Intergranular Attack of High - Nickel Austenitic alloys. Corrosion , 1966, 22 p 280-290.
10. G. Frederick. Comparative Evaluation of Preventative Measures Against P.S.S.C.C of MA I 600 Steam Generator Tubing. Presented at post SMIRT conference seminar No.3. Ispra Italy aug 26 - 27 1985.
11. A.Stein "Stress Corrosion Cracking of Alloy 600 in Primary Water". Presented at EPRI workshop on primary side stress corrosion cracking and secondary side SCC and IGC of PWR steam generator tubing, Clearwater Beach, Florida Nov.28 Dec. 2, 1983.
12. G.P.Airey. "The Stress Corrosion Performance of Inconel Alloy 600 in Pure and Primary Water Environments" . Proceedings of the International Symposium on Environmental Degradation of Materials in Nuclear Power Systems - Water Reactors, Myrtle Beach South Carolina, August 22- 25, 1983. NACE, 1984.

14. A.A.Stein, A.Deleon, and A.R.McIlree. "Prediction of Intergranular Stress Corrosion Cracking of Alloy 600 Steam Generator Tubing in Primary Water and the Influence of Mill Annealing Temperature on the Susceptibility of Alloy 600 Steam Generator Tubing to Primary Water SCC". Second International conference on Degradation of Materials in Nuclear power systems - Water Reactors, Monterey, Calif., Sept 9 - 12, 1985.
15. H. Domain, R.H Emanuelson, L.W.Sarver and G.J.Theus. "Effect of Microstructure on Stress Corrosion Cracking of alloy 600 in High Purity Water." Corrosion 1977, Vol. 33, p. 26.
16. "Optimisation of Metallurgical Variables to Improve Corrosion Resistance of Inconel Alloy 600". EPRI Research Project. 1708-1, Final Report. Palo Alto, Calif.: Electric Power Research Institute , July 1983 NP- 3051.
17. J.F.Sykes and M.J.Angwin. "The Causes of Major Pitting of Alloy 600 Steam Generator Tubing in Pressurised Water Reactors". Second International Symposium on Environmental Degradation of Materials in Nuclear Power Systems - Water Reactors, Monterey, Calif.,Sept 9-12, 1985.
18. "Fatigue Performance of Ni-Cr-Fe Alloy 600 Under Typical PWR Steam Generator Conditions". EPRI Steam Generators Owners Group, Research Project S110-1, Final Report. Palo Alto, Calif.: Electric Power Research Institute , March 1983. NP-2957.
19. P.L.Ko ASME Publications. "Experimental Study of the Tube Fretting in Steam Generators and Heat Exchangers". Chalk River Nuclear labs Ontario Canada.
20. B.Fert. "Guangdong Nuclear Power Joint Venture Company". Nuclear Engineering International, Sept 1987 p 26-38.
21. M.Kowaka and H.Fujikawa. Sumitomo search 1972, 7,10.
22. I.L.W.Wilson and R.G.Aspden. "Stress Corrosion and Hydrogen Embrittlement of Iron Nickel Chromium Alloys". 1189, 1977, Houston, Texas, NACE.
23. J.E.Antil Int Metall Rev., 1974, 19, 252.
24. S.R.Keown and F.B.Pickering. Niobium in Stainless Steels. Niobium Proceedings of the International Symposium - Niobium 81, San Francisco Calif, Nov 8-11,1981.

25. H.E.Hanninen, International Metals Review, 1979, Vol 24, no.3.
26. K.T. Aust, J.S Armijo, J.S. Westbrook. Trans ASM 1966, vol 59, p 544 - 556.
27. P.Gane, Transfer Report Sheffield Polytechnic. 1986. Supervisor Dr F.B.Pickering.
28. T.S. Bulischech and Van Rooyen. Nuclear Technology, vol 55. p.383, 1981.
29. D.Van Rooyen. "Review of Stress Corrosion Cracking". Corrosion NACE vol 31 no. 9, Sept 1975.
30. "Optimization of Metallurgical Variables to Improve Corrosion Resistance of Inconel Alloy 600", EPRI Research Project,1707-1, Final Report. Palo Alto, Calif.: EPRI , July 1983. 3051.
31. "Stress Corrosion Cracking of Alloy 600 and Alloy 690 in AVT Water at Elevated Temperatures". EPRI Steam Generators Owners Group , Research Project, S192-2, Final Report EPRI, May 1983. NP-3061.
32. Ph. Berge. J.R Donati. B. Prioux. and D. Villard. Corrosion Vol. 33, No. 12, p 425 - 435, Dec. 1977.
33. A.R.McIlree et al.' Corrosion Problems in Energy Conversion and Generation.' In 1974, Prince Town, N.J., The Electrochemical Society.
34. A.R. McIlree et al. "Effects of Variation of Carbon Sulphur and Phosphorous on the Corrosion Behaviour of Alloy 600". The International Nickel Company. Paul. D. Mercia, Research Laboratory, Sterling Forest : Suffern, N.Y. 10901.
35. K. Norring, J. Engstrom and P. Norberg. "Intergranular Stress Corrosion Cracking in Steam Generator Tubing. Testing of Alloy 690 and 600 Tubes". Environmental Degradation of Materials in Nuclear Power Systems - Water Reactors. Edited by G.J.Theus and J.R. Weeks. The Metallurgical Society of AIME 1988.
36. "Microstructure, Microchemistry and Microdeformation of Alloy 600 Tubing". Steam Generator Owners Group/Nuclear Power Division. Project, RP S303-9. Final report, Feb. 1986.
37. A.L.Hanson, H.S.Isaacs and H.W.Craner. Corrosion-NACE Vol.41, No.6, June 1985.
38. M.Kowaka et al. Nuclear Technology Vol. 55, p.394, 1981.

- Microstructure on the Susceptibility of Alloy 600 to Intergranular Attack and Stress Corrosion Cracking". Corrosion Vol. 44, No.5, p 314-319. May 1988.
40. G.S.Was, H.H. Tischner, and R.N.Latanision. "The Influence of Thermal Treatment on the Chemistry and Structure of Grain Boundaries". Metall. Trans., 1981. vol. 12A, p 1396-1408.
 41. G.P. Airey. Metallography, 13, p 21-41, 1980.
 42. "Surface and Grain Boundary Segregation, Stress Corrosion Cracking and Corrosion Fatigue of Inconel 600". EPRI, NP 3949M Project 1166-1. Intrim Report March 1985.
 43. D. Lea and A. Vermilyea , "The Initiation of Intergranular Failure in Inconel - 600". Met Trans. Vol. 2, p, 2566 - 2571. Sept 1971.
 44. R.G. Aspden , R.T.Begley, F.W. Pement, I.L.W. Wilson, "Caustic Stress Corrosion Behaviour of Fe-Ni-Cr Nuclear Steam Generator Tubing." Nucl. Tech., Oct. 1976, 31, (1), p 70-84.
 45. R.M. Kruger and G.S. Was. "The Influence of Boron on Grain Boundary Chemistry and Microstructure of Ni-16Cr-9Fe-0.03%C." Metall. Trans A. 1988. Vol.19A, p 2555- 2566.
 46. P.R. Howell, J.O.Nilsson, G.L.Dunlop. "The Effect of Creep Deformation on the Stability of Intergranular Carbide Dispersion in an Austenitic Stainless Steel." Journal Mats. Sci. 13(1978), p 2022-2028.
 47. R.Bandy and D.Van Rooyen. "Effect of Thermal Stabilization on the Low Temperaturer Stress Corrosion Cracking of Inconel 600." Corrosion NACE Vol.40, No.6, June 1984.
 48. J.P.Hammond P. Patriarca, G.M.Slaughter and W.A.Maxwell. "Comparative Results on Chloride Stress Corrosion Cracking of Steam Generator Materials in Cyclic Steam Environment. Materials Performance, Nov 1975, p.41 - 52.
 49. R.W.Staehle, J.J.Ruyela, T.L.Raredon, E Serrate, C.R.Morin and R.V.Farrar. "Effects of Alloy Composition on Stress Corrosion Cracking of Fe-Cr-Ni Base Alloys." Corrosion, Vol.26, p.451. 1970.
 50. A.J.Sedriks. Inconel 690. "A new High Nickel Alloy for Corrosive Environments at Elevated Temperatures." Japan Society of Corrosion Engineering, Vol.28, No.2. 1979.
 51. A.J.Sedriks S.Floreen and A.R.McIlree. "The effect of Nickel Content on the Stress Corrosion Resistance of Fe-Cr-Ni Alloys in an Elevated Temperature Caustic Environment." Corrosion-NACE Vol.32, No.4, April, 1976.

51. ... Fe-Ni-Cr and Other Alloys in High Temperature Caustic Solutions." Corrosion NACE. Vol.33 No.2 Feb 1977.
53. G.P.Airey, A.R.Vaia, R.G.Aspden. "A stress Corrosion Cracking Evaluation of Inconel 690 for Steam Generator Tubing Applications." Nucl Tech Vol. 55, Nov 1981 p.436-448.
54. C.Gimond."Corrosion Performance of Alloy 690. EPRI Workshop on Thermally Treated Alloy 690 For Nuclear Steam Generators." Pittsburgh. June 1985.
55. R.A.Page and A.McMinn. "Relative Stress Corrosion Cracking of Alloys 690 and 600 in Simulated Boiling Water Reactor Environments." Metallurgical Transactions A Vol 17A May 1986.
56. P.L.Andressen. "A Mechanism for the Effects of Ionic Impurities in Austenitic Iron and Nickel Based Alloys in High Temperature Water." Corrosion/85, Paper No. 101. NACE Houston Texas 1985.
57. Electricite' De France (EDF). Private Communication. 1986.
58. W.L. Clarke et al.."Corrosion Problems in Energy Conversions and Generation". The Electrochemical Society. Princeton NJ, p. 410 (1974).
59. F.B.Pickering. Evolution of Stainless Steel. ASTM. 1978.
60. ASTM 262-79 ." Standard Recommended Practices for Detecting Susceptibility to Intergranular Attack in Stainless Steel." Reapproved 1982.
61. J.J.Kai and M.N.Liu. "Effects of Heat Treatment on the Carbide Evolution and the Chromium Depletion Along Grain Boundaries of Inconel 690 Alloy." Scripta Metallurgica, Vol.23 p 17-22, 1989.
62. A.J.Maday et al. Corrosion Science. May 1988, 887-900.
63. G.C.Bodine." Relation of Tube Manufacturing Variables to Corrosion and Corrosion Product Release Rates of a NiCrFe Alloy in a Simulated PWR Primary Water." Corrosion 74 Paper No. 53.
64. R.J.Jacko." Stress Corrosion Cracking of Alloy 690." EPRI Workshop on "Thermally Treated Alloy 690 Tubes For Nuclear Steam Generators." EPRI NP-4665M-SR. July 1986 Pittsburgh Pennsylvania. June 26-28 1986.
65. P.Norberg." The Influence of Composition and Heat Treatment on Microstructure and Material Properties of Sandvik Sanicro 69 (Alloy 690)." EPRI (See proceedings 64. above.).

66. R.S. Scarborough, W.L. Mankins, H.S. Ferovey. H.S. Carbon Solubility in Alloy 690." EPRI. (See Proceedings 64. above.).
67. H.Nagano, K.Yamanaka, T.Minami, M.Inoue, T.Yonezawa, K.Onimura N.Sasaguri, T.Kusakabe. " Effect of Alloying Elements and Heat Treatments on Corrosion Resistance of Alloy 690." (See Proceedings 64. above).
68. Sandvik Technical Report. "Trial Production of Steam Generator Tubing." Sample Testing Report. 13.6.1986.
69. P.A.Beck, J.C.Kremer and M.L. Holzworth: Trans. AIME 175 (1948) p 372.
70. M. Hillert. Acta Met. 13 (1965) p 227.
71. C.S.Smith. Trans. Amer. Inst. Min. Metall. Engrs. 175, (1949) 15.
72. N. Louat. Acta. Met.,30 (1982), 1291.
73. C.H. Worner and A. Cabo. Acta. Met. 35 (1987), p 2801.
74. P.M.Hazeldine, P.B.Hirsch and N Louat. First Riso. Int. Symp. p.159 (1980).
75. T.Gladman." On the Theory of the Effect of Precipitate Particles on Grain Growth in Metals." Proc. Roy. Soc. A 294 (1966) 298.
76. M.Volmer and A.Weber Phy, Chem, 1925, 119 p 277.
77. K.C.Russell, Adv. Colloid. Interface. Sci. 1980. 13, p 205-318
78. B.Dutta and C.M.Sellers. "Effect of Composition and Process Variables on Nb(CN) Precipitation in Niobium Microalloyed Steel." Material Science and Technology, Mar. 1987, Vol. 3, p 197.
79. M.Cohen and S.S.Hansen. STP 672, Micon 78. 34, 1979. Philadelphia P.A. ATSM.
80. K.J. Irvine, F.B.Pickering and T. Gladman JISI, 1967,vol 205, p 161-82.
81. Micro alloying 1975. Oct 1-3 1975. Washington DC, USA. Proceedings - Union Carbide Corp. N.Y.
82. J.M. Sarver, J.R.Crum and W.L. Mankins. "Carbide Precipitation and SCC Behaviour of Inconel Alloy 690." Corrosion NACE 1987. Vol 44, No 5, May 1988.

83. P. Mingos, and G. S. Was. "Grain Boundary Chemistry and Precipitation in Controlled Purity Alloy 690." Presented at the Fourth International Symposium on "Environmental Degradation of Materials in Nuclear Systems - Water Reactors." 6 - 10 Aug 1989. Jekyll Island U.S.A.
84. A.J. Smith and R.P. Stratton. "Effect of Carbon Content and Heat Treatment on the Microstructure of alloy 690 Steam Generator Tubing." Presented at the NUCMAT 88 Conference on "Materials Engineering for High Risk Environments." 22 - 24 June 1988, Nice France.
85. Hans Tornbloom. Sandvik Steels. Private Communication. 1989.
86. D.A. Porter and K.E. Easterling. "Phase Transformations in Metals and Alloys." Van Nostrand Reinhold (UK).
87. D.T. Gawne and G.T. Higgins. JISI, 209 (1971), 562.
88. G. Garbarz and F.B. Pickering. "Effect of Austenite Grain Boundary Mobility on Hardenability of Steels Containing Vanadium." Materials Science and Technology. Nov. 1988 vol. 4, 967 - 975.
89. J. Crum. Inco alloys. Private Communication. 1989.
90. P. McIntyre. National Power and Grid, Leatherhead, U.K. Private Communication. 1989.
91. I.M. Lifshitz and V.V. Slyozov: Zh. Eksp. Teor. Fiz. 35 (1958) 473.
92. P. McIntyre National Power and Grid, Leatherhead U.K. Private communication 1990.

INCONEL Alloy 690

Filing Code: Ni-266
Nickel Alloy

MARCH 1981

© Copyright 1980, Engineering Publications, Inc. All rights reserved.
ISSN: 002-614X

Published by
Engineering Alloys Digest, Inc.
Post Office Box 823
Upper Merion, New Jersey

DATA ON WORLD WIDE METALS AND ALLOYS

INCONEL* Alloy 690

(Corrosion-Resistant High-Chromium Nickel Alloy)

INCONEL Alloy 690 is a wrought nickel-base alloy with excellent resistance to many corrosive aqueous media and high-temperature atmospheres. It also has high strength, good metallurgical stability, and favorable fabrication characteristics. It has excellent resistance to stress-corrosion cracking in chloride-containing solutions and to sodium hydroxide solutions. INCONEL Alloy 690 is useful for various applications involving nitric or nitric/hydrofluoric acid solutions, sulfur-containing gases and various types of high-temperature water such as in nuclear generators.

*INCONEL is a registered trademark for products of Huntington Alloys, Inc.

Composition:

	Limiting*
Nickel	58.0 min.
Chromium	27-31
Iron	7-11
Carbon	0.05 max.
Silicon	0.50 max.
Manganese	0.50 max.
Sulfur	0.015 max.
Copper	0.50 max.

*Amendments for nuclear applications:
28-31 Cr, 0.04 max. C and 0.10 max. Co.

Physical Constants: (At room temperature)(Annealed)

Density, lb/cu in.	0.296
g/cu cm	8.19
Melting range, °F (°C)	2450-2510(1343-1377)
Specific heat, Btu/lb/°F	0.107
Thermal coef. expansion	See Table 1
Thermal conductivity	See Table 1
Electrical resistivity, ohm-circ mil/ft	691
Magnetic permeability at 200 oersteds	1.001
Modulus of elasticity, psi (Tension)	30.6 x 10 ⁶
Poisson's ratio	0.289

PROPERTIES

Table 1 - THERMAL EXPANSION, THERMAL CONDUCTIVITY, SPECIFIC HEAT, ELECTRICAL RESISTIVITY AND MODULUS OF ELASTICITY - Annealed Condition

Temperature °F	Thermal Coef. of Expansion* Per °F	Thermal Conductivity Btu/ft ² in./hr/°F	Specific Heat Btu/lb/°F	Electrical Resistivity ohm-circ mil/ft	Modulus of Elasticity** (Tension), psi
75	-	-	0.107	691	30.6 x 10 ⁶
200	7.80 x 10 ⁻⁶	93	0.112	698	30.0
400	7.97	107	0.119	710	29.1
600	8.11	122	0.126	723	28.1
800	8.29	136	0.133	736	27.1
1000	8.53	151	0.140	745	26.0
1200	8.87	165	0.148	745	24.8
1400	9.14	179	0.155	749	23.5
1600	9.38	194	0.162	753	22.2
1800	9.63†	207	0.169	760	
2000	9.87†	-	0.176	768	

*Between 75°F and temperature shown.
**Determined by a dynamic method.
†Extrapolated value.

Table 2 - ROOM-TEMPERATURE TENSILE PROPERTIES - Annealed at 1900°F

Form	Size		Tensile Strength psi (MPa)	Yield Strength (0.2% Offset) psi (MPa)	Elongation (2 in.) %
	in.	mm			
Tube, cold drawn	0.50 x 0.050	12.7 x 1.27	110000(758)	66800(461)	39
Tube, cold drawn	0.75 x 0.063	19.0 x 1.65	101500(700)	55000(379)	46
Tube, cold drawn	3.50 x 0.216	88.9 x 5.49	94000(648)	40900(282)	52
Flat, hot rolled	0.5 x 2.0	13 x 51	102000(703)	51000(352)	46
Rod, hot rolled	2.0 dia.	51 dia.	100000(690)	48500(334)	50
Rod, hot rolled	0.62 dia.	16 dia.	107000(738)	54000(372)	44
Strip, cold rolled	0.150 thick	3.81 thick	105000(724)	50500(348)	41

*Dimensions are outside diameter and wall thickness.

Table 3 - CORROSION RATES IN AQUEOUS NITRIC/HYDROFLUORIC ACID SOLUTIONS

Acid Solution	Corrosion Rate*	
	mpy†	mm/y†
10% Nitric/3% Hydrofluoric	6	0.15
15% Nitric/3% Hydrofluoric	10	0.25
20% Nitric/2% Hydrofluoric	6	0.15

*Average for duplicate specimens tested at 140°F (60°C).
†mpy = mils per year. mm/y = millimeters per year.

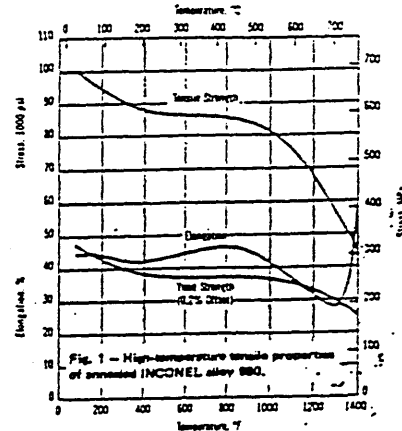


Fig. 1 - High-temperature tensile properties of annealed INCONEL alloy 690.

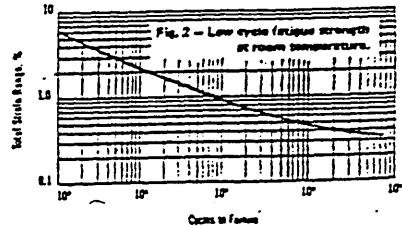


Fig. 2 - Low cycle fatigue strength of INCONEL alloy 690 at room temperature.

Table II.

Inconel 690 Steam Generator Tubing: Chemical Composition.

Tube	C	Ni	Cr	Fe	Si	Mn	P	S	Co	Cu	N	Al	Ti
A	.022	60.	30.	9.0	.25	.35	.01	.003	.01	.01	.03	.03	.38
B	.020	60.	30.	9.2	.31	.32	.01	.003	.01	.01	.03	.02	.39
C	.019	60.	29.	10.	.32	.36	.01	.001	.02	.01	.03	.14	.27
D	.019	60.	29.	10.	.32	.36	.01	.001	.02	.01	.03	.14	.27
E	.015	60.	29.	10.	.28	.36	.01	.001	.02	.01	.03	.13	.27
F	.019	60.	30.	9.2	.35	.35	.01	.003	.01	.01	.02	.02	.36

Table III.

Inconel 690 Generator Tubing: Processing History and mechanical Properties.

Tubes	Mill anneal Temperature. (°C)	Thermal Treatment (°C/hour)	0.2% Yield Strength. (MPa)	U.T.S (MPa)
A	1040	715/12	357	771
B	1080	715/5	318	712
C	965	715/12	452	798
D	1040	715/12	314	716
E	1040	715/12	320	724
F	1070	725/15	335	736

Table III.cont..

Tube	%C	Grain size.	Hardness (VPN)
A	.022	27.66	197
B	.020	30.36	194
C	.019	6.47	228
D	.019	25.32	192
E	.015	28.35	193
F	.019	30.40	179

Grain size to 95% confidence limits.

Table IV. Chemical compositions of Experimental Melts Of Alloy 690.

Group (1)

Melt	C	Ni	Cr	Fe	Si	S	Mn	P	Co	Cu	Nitrogen
EM5	.004	61.5	28.6	9.4	<.1	.001	<.1	.005	<.05	<.02	45 ppm
EM1	.015	61.3	28.6	9.4	<.1	.002	<.1	.005	<.05	.04	45 ppm
EM3	.029	62.0	28.8	9.5	<.1	.003	<.1	.005	<.05	<.02	67 ppm
EM6	.050	61.0	29.3	9.2	<.1	.003	<.1	.005	<.05	.03	53 ppm

*Both Al and Ti contents are < 0.05%.

Group (2)

Melt	C	Ni	Cr	Fe	Si	S	Mn	P	Co	Cu	N	Al	Ti
A	.022	60.0	30.0	9.0	0.25	.003	0.35	0.01	0.01	0.01	0.03	0.03	.38
EM10	.048	bal	28.6	9.43	<.1	.004	<.1	0.05	<.05	<.02	.004	<.05	.40
EM 8	.008	bal	28.8	9.40	<.1	.004	<.1	0.05	<.05	<.02	.004	<.05	.33

Group (3)

Melt	C	Ni	Cr	Fe	Si	S	Mn	P	Co	Cu	N PPM	Al	Ti
EM12	.02	bal	28.6	9.4	<.1	.005	<.1	0.05	<.05	<.02	49	0.11	.14
EM13	.02	bal	28.6	9.4	<.1	.004	<.1	0.05	<.05	<.02	52	0.11	.42
C	.02	bal	29.0	10.0	0.32	.001	0.36	0.01	0.02	<.01	300	0.14	.27

Group (4)

Melt	C	Ni	Cr	Fe	Si	S	Mn	P	Co	Cu	N PPM	Al	Ti
EM11	.02	bal	28.6	9.5	<.1	.004	<.1	0.05	<.05	<.02	51	.14	.27
EM 7	.02	bal	28.7	9.6	<.1	.004	<.1	0.05	<.05	<.02	46	<.05	.28
C	.02	bal	29.0	10.0	<.1	.001	<.1	0.01	<.05	<.02	300	.14	.27

Results from STEM Analysis.

Table V. Sample. EM 12. ST. 1200°C. TT. 720°C/1 Hour.

Precipitate	Si	% er	P	% er	Al	% er	Ti	% er	Cr	% er	Mn	% er	Fe	% er	Ni	% er
1	/	/	/	/	0.4	42.0	/	/	66.4	1.0	/	/	5.1	5.0	27.2	2.0
2	/	/	/	/	/	/	/	/	75.5	1.0	0.8	45.0	3.7	5.0	19.5	2.0
3	/	/	/	/	0.3	45.0	/	/	61.0	1.0	/	/	5.0	5.0	32.7	2.0
4	/	/	/	/	/	/	/	/	88.6	1.0	/	/	2.2	11.0	7.6	5.0
5	/	/	/	/	/	/	/	/	88.9	1.0	/	/	2.5	9.0	7.7	5.0

Table VI. Sample. EM. 12. ST. 1200°C. TT. 720°C/5 Hours.

Precipitate	Si	% er	P	% er	Al	% er	Ti	% er	Cr	% er	Mn	% er	Fe	% er	Ni	% er
1	0.1	49.0	/	/	0.2	32.0	9.7	1.5	22.6	1.0	/	/	9.6	2.0	57.5	1.0
2	/	/	/	/	/	/	/	/	88.4	1.0	0.5	48.0	3.0	4.3	7.8	2.5

Table VII. Sample. As Received Tube C.

Precipitate	Si	% er	P	% er	Al	% er	Ti	% er	Cr	% er	Mn	% er	Fe	% er	Ni	% er	S	% er
1	/	/	/	/	/	/	/	/	89.8	1.0	1.4	24.0	2.4	7.0	6.1	4.0	/	/
2	0.2	50.0	/	/	/	/	/	/	87.2	1.0	1.1	24.0	2.5	8.0	8.8	3.0	/	/
3	0.2	23.0	/	/	/	0.1	36.0	1.0	71.4	1.0	1.6	8.0	4.4	2.0	22.3	1.0	/	/
4	0.4	13.0	/	/	0.1	47.0	1.0	26.1	26.1	1.0	0.8	13.0	9.2	1.0	48.7	1.0	0.9	/
5	/	/	0.2	50.0	/	/	78.5	1.0	13.4	2.0	0.4	40.0	1.2	12.0	6.1	5.0	/	/

Table VIII. Sample. EM.12. ST.1200°C. TT. 720°C/10.

Precipitate	Si	% er	P	% er	Al	% er	Ti	% er	Cr	% er	Mn	% er	Fe	% er	Ni	% er	S	% er
1	/	/	/	/	/	/	/	/	90.6	1.0	/	/	2.3	6.0	7.2	3.0	/	/
2	0.2	38.0	/	/	0.3	39.0	41.7	1.0	17.0	2.0	/	/	5.6	3.2	35.2	1.2	/	/
3	/	/	/	/	/	/	36.1	1.0	17.2	1.0	/	/	6.15	3.0	37.7	1.0	2.7	5.0

Table IX. Sample. EM.12. ST.1200°C. TT.720°C/15 Hours.

Precipitate	Si	% er	P	% er	Al	% er	Ti	% er	Cr	% er	Mn	% er	Fe	% er	Ni	% er	S	% er
1	/	/	0.3	25.0	0.2	41.0	10.4	2.0	21.2	1.0	/	/	9.2	2.0	58.5	1.0	/	/
2	/	/	/	/	/	/	/	/	69.9	0.5	/	/	5.1	2.0	24.8	1.0	0.1	45.0

Table X.

Grain Size and Hardness Measurements Obtained After Solution Treating Alloys Containing Varying Carbon in the Absence of Both Aluminium and Titanium.

Solution Treatment Temp °C	Experimental Melt One.			Experimental Melt Three.		
	Water Quenched.			Water Quenched.		
	HV	d (um)	d ^{-1/2}	HV	d (um)	d ^{-1/2}
900	181			187		
950	177			186		
1000	142	42.1	0.1534	183		
1050	138	65.8	0.1233	172		
1100	135	77.65	0.1135	151	84.6	0.1082
1150	126	117.0	0.0925	135	92.2	0.1041
1200	127	141.0	0.0842	133	102.2	0.0989

Table X. cont..

Solution Treatment Temp °C	Experimental Melt Five			Experimental Melt Six		
	Water Quenched.			Water Quenched.		
	HV	d (um)	d ^{-1/2}	HV	d (um)	d ^{-1/2}
900	181			212		
950	173			199		
1000	160			195		
1050	142	43.5	0.1541	182		
1100	139	57.6	0.1437	182		
1150	132	91.5	0.1183	149		
1200	130	112.0	0.1041	151		

Table XI. Regression Output.

Material.	Constant.	X Coefficient. (x 10 ⁴)	R Squared.
Tube A	-0.32453	25.98	0.921
Tube E	-0.19657	20.18	0.894
Tube C	-0.45929	35.61	1.000
EM 1	-0.39229	37.84	0.927
EM 3	-0.30411	30.28	0.983
EM 5	-0.41428	40.09	0.987
EM 10	-0.28596	26.56	0.979
EM 7	-0.34680	33.56	0.964
EM 11	-0.55129	50.34	0.949
EM 12	-0.45838	42.39	0.712
EM13	-0.40206	39.13	0.985

Table XII.

Grain Size and Hardness Measurements From Alloys Containing 0.03% Aluminium 0.38% Titanium and Varying Carbon.

Solution Treatment Temp °C	Experimental Melt Ten			As Received Tube A		
	Water Quenched.			Water Quenched.		
	HV	d (um)	d ^{-1/2}	HV	d (um)	d ^{-1/2}
900	207			201	29.0	0.1857
950	199			194	30.4	0.1815
1000	198			194	30.2	0.1819
1050	183	25.1	0.1996	192	32.9	0.1744
1100	165	40.2	0.1581	183	34.4	0.1705
1150	151	92.5	0.1043	164	93.0	0.1037
1200	137	144.3	0.0833	160	108.1	0.0962

Table XII. cont..

Solution Treatment Temp °C	EM 8		
	HV	d (um)	d ^{-1/2}
900	185		
950	186		
1000	156	27.8	
1050	145	46.9	0.1460
1100	148	65.7	0.1233
1150	140	88.1	0.1065
1200	131	149.9	0.0817

Table XIII. Grain Size and Hardness Measurements Obtained After Solution Treating Alloys Containing 0.02% Carbon 0.27% Titanium and Varying Aluminium.

Solution Treatment Temp °C	Experimental Melt Seven			Experimental Melt Eleven		
	Water Quenched.			Water Quenched.		
	HV	d (um)	d ^{-1/2}	HV	d (um)	d ^{-1/2}
900	183			172		
950	171			170		
1000	155			142	35.2	0.1686
1050	151	40.3	0.1580	135	58.5	0.1308
1100	142	63.4	0.1260	131	118.6	0.0918
1150	135	75.8	0.1147	124	166.3	0.0775
1200	128	170.2	0.0767	123	192.5	0.0721

Table XIII. cont..

Solution Treatment Temp °C	As Received Tube C		
	Water Quenched.		
	HV	d (um)	d ^{-1/2}
900	230		
950	225		
1000	217		
1050	181	28.9	0.1857
1100	174	39.2	0.1601
1150	162	73.4	0.1170
1200	153	134.8	0.0861

Table XIV.

Grain Size and Hardness Measurements Obtained After Solution Treating Alloys Containing 0.019% Carbon 0.14% Aluminium and Varying Titanium.

Solution Treatment Temp °C	Experimental Melt Twelve.			Experimental Melt Thirteen.		
	Water Quenched.			Water Quenched.		
	HV	d (um)	d ^{-1/2}	HV	d (um)	d ^{-1/2}
900	178			166		
950	169			170		
1000	151			163		
1050	139	39.2	0.1601	142	43.4	0.1525
1100	135	104.4	0.0981	127	105.8	0.0971
1150	132	168.9	0.0769	125	119.3	0.0917
1200	118	354.7	0.0531	122	204.0	0.0700

Table XV.
Carbide Morphology Following Thermal Treatment.

Ageing Temp.	Ageing Time (Minutes)					
	5	30	60	300	900	1440
550	NP	NP	NP	NP	SCf	SCf
650	NP	NP	D	D	D	D
700	D/SC	D/SC	SC	SC	SCc	SCc
750	SC	SCc	SCc	SCc	SCc	SCc
800	SC	SC	D	D	D	D

NP = No Precipitation.

SC = Semi Continuous.

D = Discrete.

c = Coarse.

f = Fine

Table XVI. Change in Chemical Composition with Distance From Grain Boundary. EM 12 ST 1200°C TT 720°C/1 Hour.

Distance (nm)	Si	% er	P	% er	Al	% er	Ti	% er	Cr	% er	Mn	% er	Fe	% er	Ni	% er
180	/	/	/	/	0.6	19.0	0.2	47.0	29.4	1.0	/	/	9.44	2.3	59.7	1.0
160	/	/	/	/	0.6	21.0	/	/	29.2	1.0	/	/	9.5	2.0	60.0	1.0
120	/	/	/	/	0.4	27.0	0.2	34.0	28.1	1.0	/	/	9.9	2.0	60.9	1.0
100	/	/	/	/	0.5	24.0	0.2	33.0	26.9	1.0	/	/	9.6	2.0	62.2	1.0
80	/	/	/	/	0.6	21.0	/	/	25.5	1.00	/	/	9.9	2.0	63.1	1.0
60	/	/	/	/	0.6	22.0	0.2	36.0	25.1	1.0	/	/	9.6	2.00	63.7	1.0
50	/	/	/	/	0.7	15.0	0.1	49.0	22.9	1.0	/	/	9.8	2.0	65.4	1.0
40	/	/	/	/	0.7	16.0	0.2	41.0	23.1	1.0	/	/	9.9	2.0	65.6	1.0
30	/	/	/	/	0.7	17.0	/	/	21.9	1.0	0.5	32.0	10.0	2.0	66.4	1.0
20	/	/	/	/	0.6	18.0	/	/	21.7	1.0	/	/	10.4	2.0	66.7	1.0
10	/	/	/	/	0.7	16.0	/	/	21.2	1.0	0.3	41.0	10.3	2.0	66.9	1.0
0	/	/	/	/	0.5	38.0	/	/	21.0	2.0	/	/	10.1	3.50	67.8	1.0
10	0.3	34.0	/	/	/	/	/	/	22.7	1.5	/	/	10.2	3.0	66.8	1.0
20	0.3	38.0	/	/	/	/	/	/	24.3	1.0	/	/	10.1	3.0	65.1	1.0
30	0.3	34.0	/	/	/	/	/	/	24.1	1.0	/	/	9.6	3.0	62.5	1.0
40	0.3	35.0	/	/	0.3	36.0	0.2	47.0	26.7	1.0	/	/	9.8	3.0	63.7	1.0
100	0.3	35.0	/	/	0.30	41.0	/	/	29.6	1.0	/	/	9.6	3.0	60.0	1.0

Table XVII. Change in Chemical Composition With Distance From Grain Boundary. EM 12, ST 1200°C, TT 720°C/5 Hours.

Distance (nm)	Si	% er	P	% er	Al	% er	Ti	% er	Cr	% er	Mn	% er	Fe	% er	Ni	% er	S	% er
1000	0.2	35.0	/	/	0.2	31.0	0.1	33.0	30.1	1.0	/	/	9.6	2.3	59.6	1.0	/	/
500	/	/	/	/	0.2	38.0	0.1	33.0	30.4	1.0	/	/	9.8	2.0	59.2	1.0	/	/
300	/	/	/	/	0.2	39.0	0.2	28.0	30.4	1.0	/	/	10.0	2.0	58.8	1.0	0.3	26.0
200	/	/	/	/	0.5	24.0	0.1	48.0	29.4	1.0	/	/	10.0	2.0	60.2	1.0	/	/
100	/	/	/	/	0.2	48.0	/	/	27.2	1.0	/	/	10.2	2.0	62.1	1.0	/	/
50	/	/	/	/	0.2	33.0	/	/	25.6	1.0	/	/	10.2	2.0	63.7	1.0	0.3	26.0
20	/	/	0.2	32.0	0.2	45.0	/	/	24.2	1.0	/	/	10.4	2.0	64.9	1.0	/	/
10	/	/	0.2	38.0	0.3	32.0	/	/	24.1	1.0	/	/	10.3	2.0	65.0	1.0	/	/
5	/	/	/	/	0.2	37.0	/	/	23.9	1.0	/	/	10.3	2.0	65.1	1.0	/	/
2.5	/	/	0.3	33.0	0.3	29.0	/	/	23.5	1.0	/	/	10.4	2.0	65.1	1.0	0.2	48.0
0	0.2	31.0	/	/	0.3	33.0	/	/	23.8	1.0	/	/	10.3	2.0	65.1	1.0	/	/
2.5	/	/	/	/	0.2	38.0	/	/	23.9	1.0	/	/	10.4	2.0	65.5	1.0	/	/
5	0.2	30.0	/	/	0.2	48.0	0.1	42.0	23.6	1.0	/	/	10.4	2.0	65.2	1.0	0.2	42.0
10	0.2	31.0	/	/	0.2	49.0	/	/	24.1	1.0	/	/	10.4	2.0	65.2	1.0	/	/
20	0.2	32.0	/	/	/	/	0.2	35.0	24.3	1.0	/	/	10.3	2.0	64.7	1.0	/	/
50	0.2	44.0	/	/	0.2	48.0	0.1	50.0	25.7	1.0	/	/	10.3	2.0	63.8	1.0	/	/
100	/	/	/	/	/	/	/	/	27.2	1.0	/	/	10.0	2.0	62.5	1.0	/	/

Table XVIII. Change in Chemical Composition With Distance From Grain Boundary. EM12. ST 1200°C, TT 720/10hours.

Distance (nm)	Si	% er	P	% er	Al	% er	Ti	% er	Cr	% er	Mn	% er	Fe	% er	Ni	% er	S	% er
500	0.2	35.0	/	/	0.7	14.0	/	/	30.2	1.0	/	/	9.7	2.3	59.4	1.0	/	/
300	/	/	/	/	0.6	18.0	0.3	25.0	29.5	1.0	/	/	9.8	2.0	59.9	1.0	/	/
200	/	/	/	/	0.6	17.0	0.1	50.0	28.4	1.0	/	/	9.7	2.0	61.3	1.0	/	/
100	/	/	/	/	0.5	20.0	/	/	26.1	1.0	/	/	10.3	2.0	63.2	1.0	/	/
80	/	/	/	/	0.6	17.0	/	/	25.6	1.0	/	/	10.1	2.0	63.6	1.0	/	/
60	/	/	/	/	0.5	19.0	/	/	24.7	1.0	/	/	10.2	2.0	64.4	1.0	/	/
40	/	/	/	/	0.4	25.0	/	/	24.0	1.0	/	/	10.5	2.0	64.8	1.0	/	/
30	/	/	/	/	0.7	17.0	0.1	49.0	24.5	1.0	/	/	10.6	2.0	64.4	1.0	/	/
20	/	/	/	/	0.5	21.0	/	/	24.2	1.0	/	/	10.3	2.0	65.0	1.0	/	/
10	/	/	/	/	0.6	19.0	/	/	23.3	1.0	/	/	10.3	2.0	65.7	1.0	/	/
0	/	/	/	/	0.3	37.0	/	/	22.6	1.0	/	/	10.4	2.0	66.4	1.0	0.3	32.0
10	/	/	/	/	/	/	/	/	23.0	1.0	/	/	10.4	2.0	66.0	1.0	/	/
20	/	/	/	/	/	/	/	/	23.5	1.0	/	/	10.6	2.0	65.7	1.0	/	/
30	/	/	/	/	0.3	34.0	0.2	43.0	23.4	1.0	/	/	10.3	2.0	65.3	1.0	/	/
40	/	/	/	/	0.3	38.0	/	/	23.9	1.0	/	/	10.3	2.0	65.3	1.0	/	/
60	/	/	/	/	0.3	38.0	/	/	24.3	1.0	/	/	10.4	2.0	64.6	1.0	/	/
80	/	/	/	/	/	/	/	/	24.6	1.0	/	/	10.2	2.0	65.2	1.0	0.2	45.0

Table XIX. Change in Chemical Composition With Distance From Grain Boundary. EM 12. ST 1200°C, TT 720°C/ 15 Hours.

Distance (nm)	Si	% er	P	% er	Al	% er	Ti	% er	Cr	% er	Mn	% er	Fe	% er	Ni	% er	S	% er
500	/	/	/	/	/	/	0.2	27.0	30.2	1.0	/	/	9.6	2.3	60.0	1.0	/	/
300	/	/	/	/	/	/	/	/	28.5	1.0	/	/	10.0	2.0	61.3	1.0	/	/
200	/	/	/	/	/	/	/	/	26.8	1.0	/	/	9.9	2.0	62.6	1.0	0.2	43.0
100	/	/	/	/	0.2	49.0	0.1	43.0	24.5	1.0	/	/	10.5	2.0	64.6	1.0	/	/
80	/	/	/	/	/	/	/	/	23.1	1.0	/	/	10.1	2.0	66.3	1.0	0.2	35.0
60	0.2	32.0	/	/	/	/	0.1	47.0	22.9	1.0	/	/	10.4	2.0	66.0	1.0	0.2	28.0
40	/	/	/	/	/	/	/	/	23.2	1.0	/	/	10.3	2.0	66.3	1.0	0.2	32.0
20	/	/	/	/	/	/	/	/	22.9	1.0	/	/	10.4	2.0	66.2	1.0	0.1	44.0
10	/	/	/	/	/	/	/	/	22.7	1.0	/	/	10.7	2.0	66.4	1.0	0.2	29.0
5	/	/	/	/	/	/	/	/	22.2	1.0	/	/	10.4	2.0	66.9	1.0	0.2	29.0
0	/	/	0.2	39.0	0.4	23.0	0.1	44.0	23.0	1.0	/	/	10.3	2.0	65.8	1.0	0.2	31.0
5	/	/	0.2	45.0	0.3	30.0	/	/	22.6	1.0	/	/	10.8	2.0	65.7	1.0	0.2	28.0
10	/	/	0.2	32.0	0.3	27.0	/	/	22.9	1.0	/	/	10.6	2.0	65.9	1.0	/	/
20	/	/	0.3	26.0	0.3	30.0	/	/	22.9	1.0	/	/	10.4	2.0	65.8	1.0	/	/
40	/	/	0.2	30.0	0.2	39.0	/	/	23.3	1.0	/	/	10.6	2.0	65.4	1.0	/	/
60	/	/	0.2	35.0	0.3	25.0	/	/	24.1	1.0	/	/	10.5	2.0	64.8	1.0	/	/
500	/	/	0.3	26.0	0.2	19.0	0.1	44.0	30.1	1.0	/	/	9.6	2.0	59.6	1.0	/	/

Table XX. Change in Chemical Composition With Distance From Grain Boundary. Tube C, As Received.

Distance (nm)	Si	% er	P	% er	Al	% er	Ti	% er	Cr	% er	Mn	% er	Fe	% er	Ni	% er	S	% er
1000	0.6	16.0	0.2	48.0	0.6	20.0	0.2	38.0	31.3	1.0	0.7	24.0	10.8	2.0	55.6	1.0	/	/
250	0.6	16.0	/	/	0.3	40.0	0.2	43.0	30.9	1.0	1.1	24.0	10.6	2.0	56.4	1.0	/	/
50	0.6	17.0	/	/	0.3	39.0	0.2	34.0	30.3	1.0	0.3	23.0	10.9	2.0	56.7	1.0	/	/
20	0.7	14.0	/	/	0.3	34.0	0.2	41.0	30.2	1.0	0.9	19.0	10.5	2.0	57.3	1.0	/	/
10	0.7	14.0	/	/	0.5	24.0	/	/	29.9	1.0	0.9	18.0	10.7	2.0	57.0	1.0	/	/
5	0.6	16.0	0.3	31.0	0.3	35.0	0.2	37.0	30.0	1.0	0.7	26.0	10.9	2.0	57.1	1.0	/	/
2.5	0.6	15.0	/	/	0.4	26.0	/	/	29.8	1.0	1.1	15.0	10.7	2.0	57.2	1.0	/	/
0	0.7	13.9	/	/	0.3	41.0	0.2	40.0	30.3	1.0	1.1	15.0	10.5	2.0	56.8	1.0	/	/
2.5	/	/	/	/	0.4	30.0	0.2	39.0	29.9	1.0	0.8	21.0	10.9	2.0	57.3	1.0	0.2	39.0
5	0.3	29.0	/	/	0.3	37.0	0.2	32.0	29.8	1.0	1.0	17.0	10.7	2.0	57.4	1.0	/	/
10	0.3	33.0	/	/	0.3	40.0	0.2	40.0	30.8	1.0	0.8	18.0	10.7	2.0	57.5	1.0	/	/
20	0.3	32.0	/	/	0.4	30.0	0.2	40.0	29.8	1.0	1.1	18.0	10.9	2.0	57.2	1.0	/	/
50	0.3	31.0	/	/	0.4	29.0	/	/	30.1	1.0	0.8	21.0	10.8	2.0	57.2	1.0	0.3	30.0
250	0.4	27.0	/	/	0.4	27.0	0.2	39.0	30.9	1.0	0.9	23.0	10.7	2.0	56.5	1.0	/	/
1000	0.4	37.0	/	/	0.3	37.0	0.2	49.0	31.3	1.0	0.9	21.0	10.8	2.0	56.0	1.0	0.2	49.0

Table XXI.
Results of C Ring Stress Corrosion Cracking Tests of As
Received Tubes A and E

SAMPLE	ENVIRONMENT	MEAN CRACK LENGTH (microns)	S D	MAXIMUM PENETRATION (microns)	TIME hrs
E1	Deaerated				
	50% NaOH	38.4	17	157	8000
A1	Deaerated				
	50% NaOH	26.1	10	56	8000
E4	Deaerated				
	30% NaOH + 10% Na ₂ SO ₄	29.4	9	75	8000
A5	Deaerated	17.4	8	59.2	8000
	30% NaOH + 10% Na ₂ SO ₄				
A4	As for A5	10.9	5	41	1200
E3	As for A5	26.0	12	88	1200

Tube A = 0.022% C.
 Tube E = 0.015% C.

Table XXII.
Effect of Heat Treatment on IGA Resistance in a
Deaerated 30% NaOH + 10% Na₂SO₄ Environment at 350°C.

Material	Ageing Temp. °C	Ageing Time in hours	Crack Depth (um)	Standard Deviation.
Tube F	650	1	20	6
" "	700	1	22	5
" "	750	1	26	4
" "	650	15	24	6
" "	700	15	21	5
" "	750	5	22	6
" " *	715	15	16	6
Tube A *	725	12	24	6

* Tested in the as received condition. All other samples were solution treated at 1200°C and water quenched. Test duration for all samples was 1500 hours.

Table XXIII.

Material.	Chemical Composition.				Effective Ti	Effective Ti:C	Cr ₂₃ C ₆ Solvus °C
	C	Al	Ti	N			
Tube A	.022	.03	0.38	300	0.277	12.6	1187
Tube C	.019	.14	0.27	300	0.167	8.8	1178
Tube E	.015	.13	0.27	300	0.167	11.1	1166
EM 7	.017	<.05	0.28	46	0.264	15.5	1173
EM 8	.008	<.05	0.33	40	0.316	79.0	1091
EM 10	.048	.025	0.40	47	0.404	8.4	1231
EM 11	.020	.14	0.27	51	0.253	9.7	1182
EM 12	.020	.12	0.14	49	0.113	5.7	1182
EM 13	.020	.11	0.42	52	0.402	22.3	1182
EM 1	.015	.14	0.27	51	NA	NA	1166
EM 3	.029	.12	0.14	49	NA	NA	1202
EM 5	.004	<.05	0.05	52	NA	NA	1091

Table XXIII cont..

Material.	Chemical Composition.				Effective Ti	Effective Ti:C	TiC Solvus °C
	C	Al	Ti	N			
Tube A	.022	.03	0.38	300	0.277	12.6	1035
Tube C	.019	.14	0.27	300	0.167	8.8	914
Tube E	.015	.13	0.27	300	0.167	11.1	967
EM 7	.017	<.05	0.28	46	0.264	15.5	1002
EM 8	.008	<.05	0.33	40	0.316	79.0	886
EM 10	.048	.025	0.40	47	0.404	8.4	1175
EM 11	.020	.14	0.27	51	0.253	9.7	1015
EM 12	.020	.12	0.14	49	0.113	5.7	955
EM 13	.020	.11	0.42	52	0.402	22.3	1066

Table XXIV.

Mass Fraction Undissolved Titanium Carbides.

Material	Analysis m/o		Solution Treatment Temp °C	TiC		Grain Size (um)
	C	Effective Ti		f _m	1/f _m	
Tube A	0.022	0.277	900	0.0048	676	29.0
			950	0.0011	942	30.4
			1000	0.0005	2047	30.2
Tube E	0.015	0.167	900	0.0046	2174	24.3
EM 10	0.048	0.384	1050	0.0250	400	21.1
			1100	0.0162	615	40.2
			1150	0.0060	1667	92.5
EM 11	0.020	0.253	1000	0.0020	4975	35.2

Table XXIV cont..

Mass Fraction of Undissolved Chromium Carbides

Material	Analysis m/o		Solution Treatment Temp oC	Cr ₂₃ C ₆		Grain Size (um)
	C	Ti		f _m	1/f _m	
Tube A	0.022	0.38	900	0.0219	457	29
			950	0.0217	461	30.4
			1000	0.0212	472	30.2
			1050	0.0201	498	32.9
			1100	0.0173	578	34.4
			1150	0.0076	1316	93.0
Tube E	0.015	0.27	900	0.0149	670	24.3
			950	0.0147	681	26.0
			1000	0.0142	704	25.3
			1050	0.0131	765	26.2
			1100	0.0103	968	26.5
			1150	0.0036	2777	36.3
Tube C	0.019	0.27	1050	0.0171	586	29.8
			1100	0.0142	702	39.2
			1150	0.0076	1316	73.4
EM 7	0.020	0.28	1050	0.0181	553	29.8
			1100	0.0153	652	39.2
			1150	0.0086	1162	75.8
EM 11	0.020	0.27	1000	0.0192	521	35.2
			1050	0.0181	553	58.5
			1100	0.0153	652	118.6
			1150	0.0086	1162	166.3
EM 10	0.048	0.40	1050	0.0461	217	25.1
			1100	0.0433	231	40.2
			1150	0.0394	254	92.5
			1200	0.0202	495	144.3
EM 12	0.020	0.14	1050	0.0181	553	39.2
			1100	0.0153	652	104.0
			1150	0.0086	1162	168.9
EM 13	0.020	0.42	1050	0.0181	553	43.4
			1100	0.0153	652	105.0
			1150	0.0086	1162	119.0
EM 8	0.008	0.33	1000	0.0072	1387	27.8
			1050	0.0061	1645	47.0
			1100	0.0033	3003	66.0
EM 1	0.015	<0.05	1000	0.0142	704	42.1
			1050	0.0131	763	65.8
			1100	0.0103	971	77.7
			1150	0.0036	2755	117.0
EM 3	0.029	<0.05	1100	0.0240	417	84.6
			1150	0.0180	556	92.2
			1200	0.0012	8333	102.2

Table XXV.

Calculated Cr_{23}C_6 Critical Particle Size (rc) for Z values of 2 to -2.

Temp	Grain	Volume	rc	rc	Material
$^{\circ}\text{C}$	Radius	Fraction	Z = 2	Z = -2	
900	14.5	0.00452	0.25	0.050	Tube A
950	15.2	0.00448	0.26	0.052	
1000	15.1	0.00438	0.253	0.051	
1050	16.45	0.00416	0.261	0.052	
900	12.1	0.00308	0.142	0.028	Tube E
950	13.0	0.00304	0.151	0.030	
1000	12.7	0.00294	0.142	0.028	
1050	13.1	0.00271	0.136	0.027	

Table XXVa.

Calculated TiC Critical Particle Size for Z Values of 2 to -2

Temp	Grain	Volume	rc	rc	Material
$^{\circ}\text{C}$	Radius	Fraction	Z = 2	Z = -2	
900	14.5	0.00028	0.022	0.0044	Tube A
950	15.2	0.00007	0.005	0.0011	
1000	15.1	0.00003	0.002	0.0005	
900	12.15	0.00040	0.018	0.0035	Tube E

Table XXVI.

Activation Energies for Grain Growth.

Material	Activation Energy kJ/mol	C	Al	Ti Eff.	Ti:C Ratio. Stoichiometric
EM 1	93.5	.015	<.05	<.05	—
EM 3	31.7	.029	<.05	<.05	—
EM 5	107.5	.004	<.05	<.05	—
EM 7	145.0	.020	<.05	0.26	3.3
EM 8	124.6	.008	<.05	0.32	10.0
EM 10	197.5	.048	<.05	0.38	2.0
EM 11	140.6	.020	0.14	0.25	3.1
EM 12	230.8	.020	0.11	0.11	1.4
EM 13	155.3	.020	0.11	0.40	5.0
Tube A	167.3	.022	0.03	0.28	3.2
Tube E	160.2	.015	0.13	0.17	2.8
Tube C	169.2	.019	0.14	0.17	2.2

Table XXVII.

Statistical Analysis of Activation Energies for Grain Growth

Material.	X Coeff.	Standard Error of X Coeff	R Squared.
Tube A	-8735	2236 (25%)	0.88
Tube E	-8368	1831 (21%)	0.95
Tube C	-8837	1092 (12%)	0.97
EM 1	-4886	369 (8%)	0.98
EM 3	-1657	119 (7%)	0.99
EM 5	-5590	539 (10%)	0.98
EM 10	-10286	919 (9%)	0.98
EM 7	-7570	1557 (21%)	0.92
EM 11	-7292	825 (8%)	0.96
EM 12	-12020	723 (6%)	0.99
EM13	-8110	1610 (20%)	0.93
EM 8	-6511	420 (6%)	0.98

Table XXVIII.

Grain Coarsening Temperature Compared with Titanium and Chromium Carbide Solvus Temperature.

Material			Grain coarsening	TiC	Cr carbide
	C	Ti	temperature (°c)	Solvus (°c)	solvus (°c)
EM12	.020	0.14	1000-1050	955	1182
C	.020	0.27	1000	969	1178
EM 7	.020	0.27	950-1000	1002	1173
EM 8	.00	0.33	950-1000	886	1091
EM11	.020	0.28	950-1000	1015	1182
EM10	.048	0.40	1000-1050	1175	1231
EM13	.020	0.42	1000-1050	1065	1182

Table XXIX.

Polygonisation Temperature Compared to Titanium Carbide Solvus Temperature.

Material			Polygonisation	TiC	Cr carbide
	C	Ti	temperature (°c)	Solvus (°c)	solvus (°c)
EM12	.020	0.14	1000-1050	955	1182
C	.020	0.27	1000	969	1178
EM 7	.020	0.27	1000-1050	1002	1173
EM 8	.008	0.33	950-1000	886	1091
EM11	.020	0.28	950-1000	1015	1182
EM10	.048	0.40	1000-1050	1175	1231
EM13	.020	0.42	1000-1050	1065	1182

Table XXX.

Grain Size and Hardness Measurements Taken After Solution treating As - Received Tubes A, and E.

Solution Treatment Temp °C	Tube A.					
	Water Quenched.			Air Cooled.		
	HV	d (um)	d ^{-1/2}	HV	d (um)	d ^{-1/2}
900	201	29.0	0.1857	202	30.8	0.1801
950	194	30.4	0.1815	205	32.3	0.1759
1000	194	30.2	0.1819	192	30.8	0.1801
1050	192	32.9	0.1744	189	33.3	0.1733
1100	183	34.4	0.1705	180	39.6	0.1589
1150	164	93.0	0.1037	157	116.1	0.0928
1200	160	108.1	0.0962	147	130.0	0.0877

Table XXXI.

Solution Treatment Temp °C	Tube E.					
	Water Quenched.			Air Cooled.		
	HV	d (um)	d ^{-1/2}	HV	d (um)	d ^{-1/2}
900	203	23.5	0.2063	198	24.3	0.2029
950	199	21.2	0.2172	197	26.0	0.1961
1000	197	28.6	0.1870	193	25.3	0.1988
1050	197	24.7	0.2012	195	26.2	0.1954
1100	185	27.4	0.1910	195	26.5	0.1943
1150	166	48.5	0.1436	180	36.3	0.1660
1200	165	63.4	0.1256	171	69.0	0.1204

SIZEWELL B POWER STATION

MODEL F STEAM GENERATOR

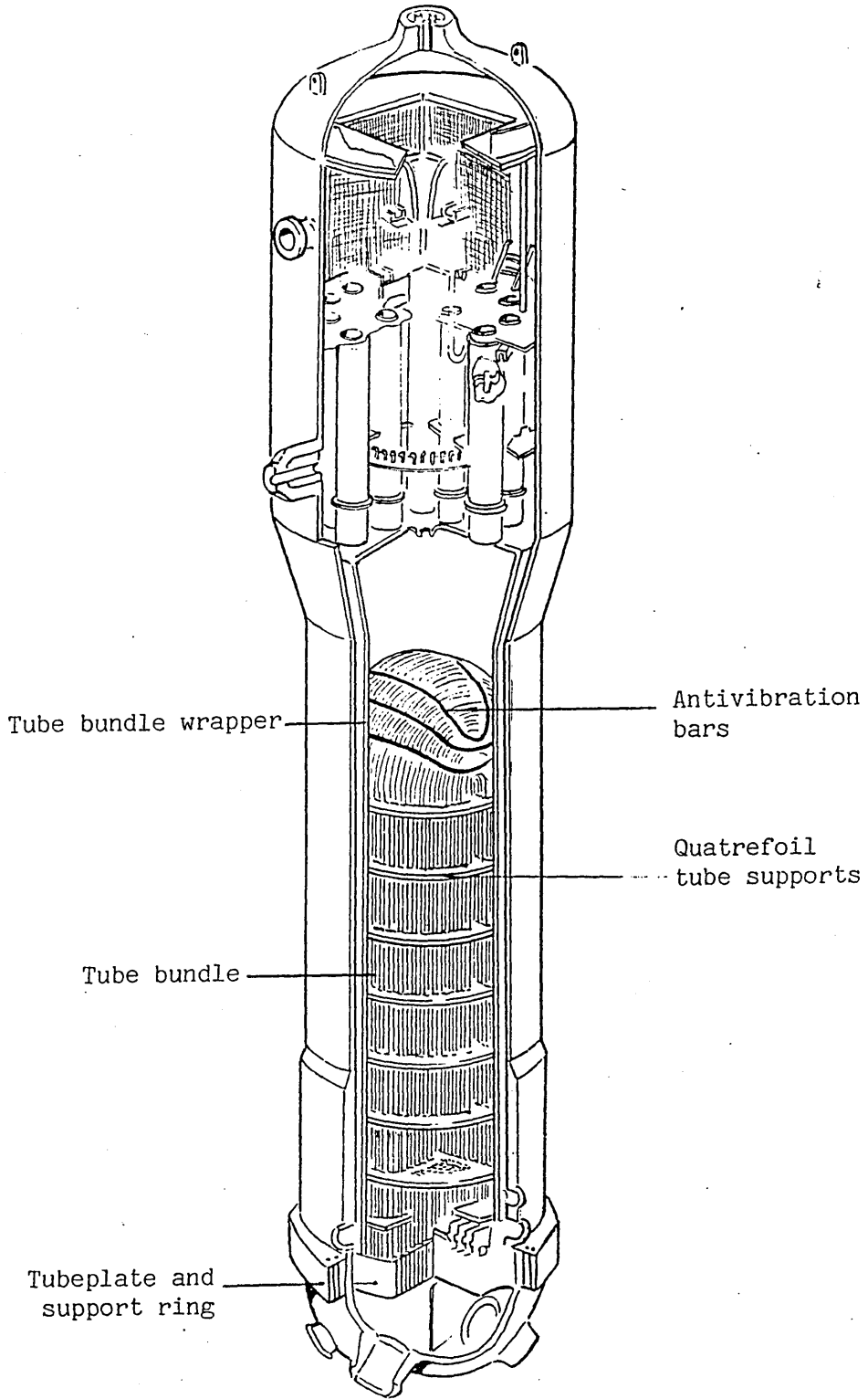
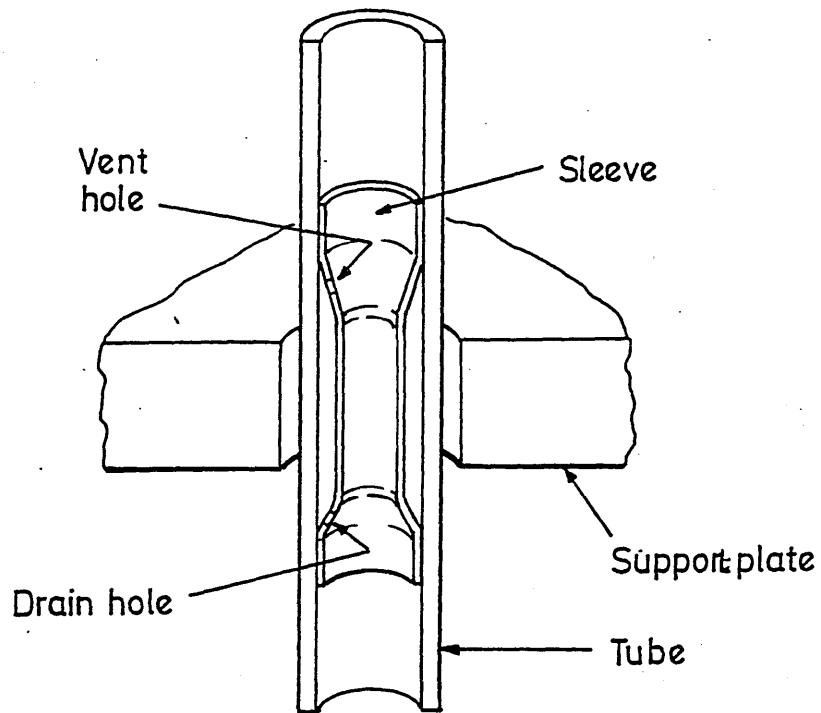
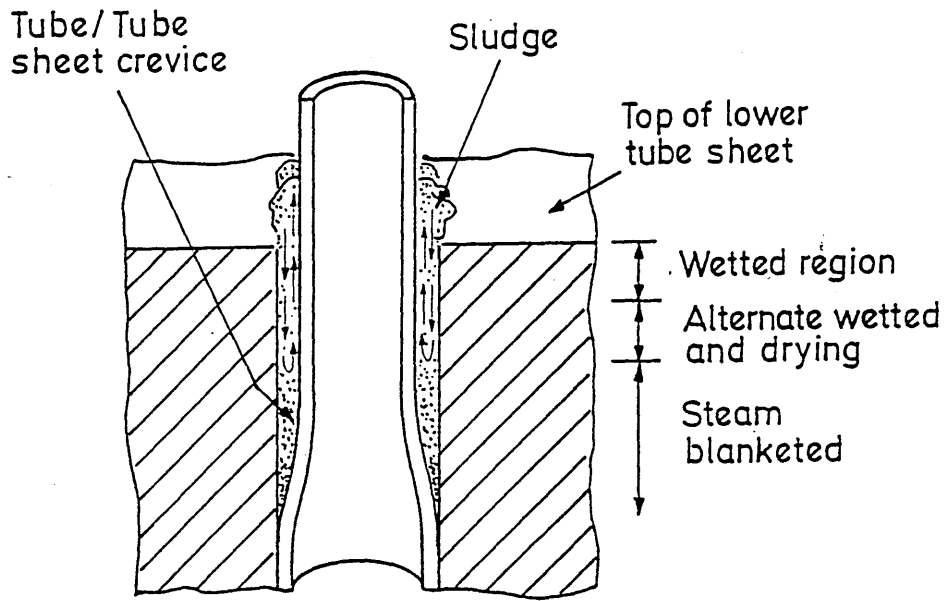


FIG.1

FIG.2

(a) Mechanism for concentration of deleterious corrosive species in occluded areas of steam generators



(b) Sleeving of corrosion-induced 'dented' tube

FIG. 3 Broached holes in Tube Support Plate

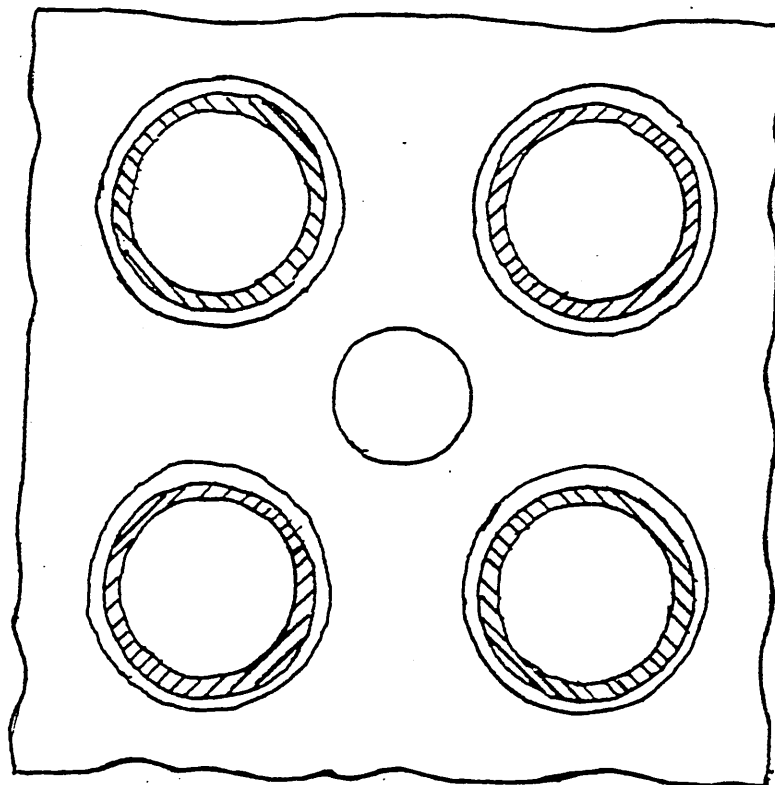
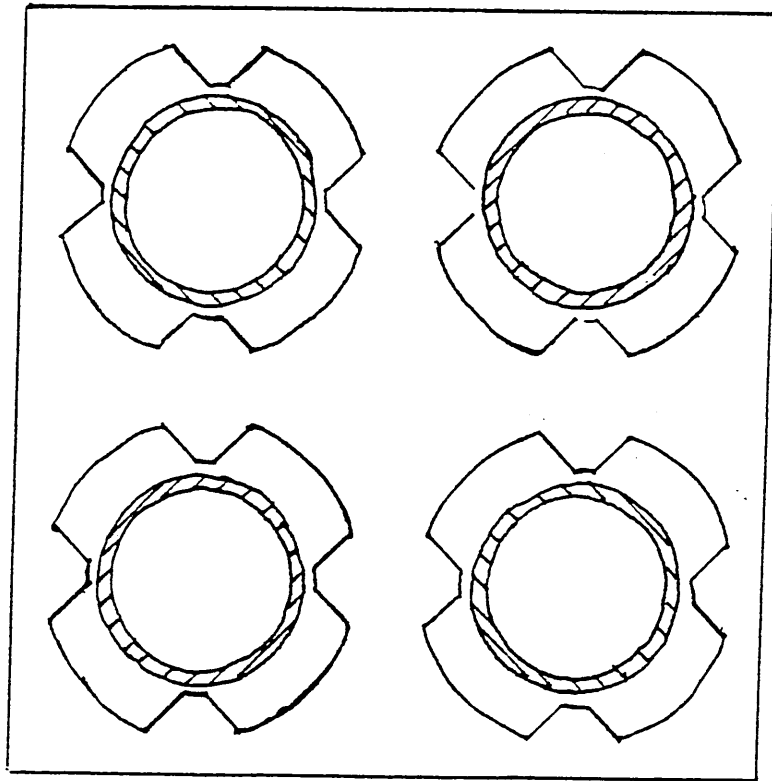
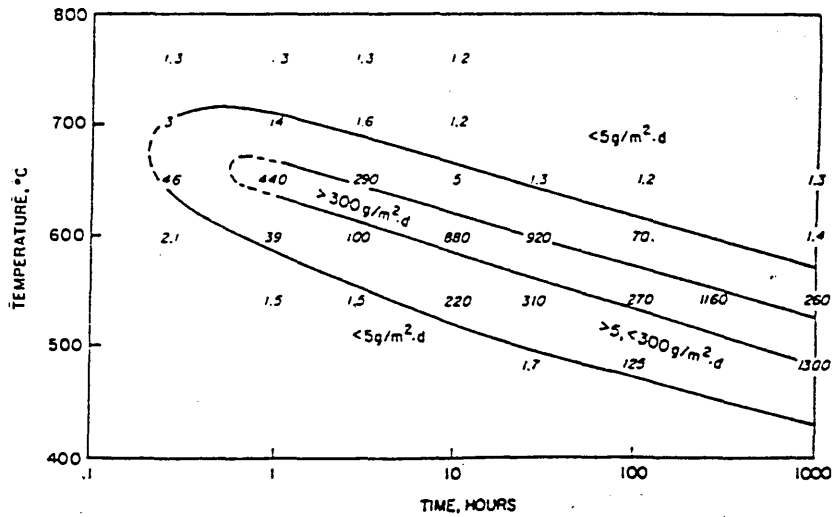


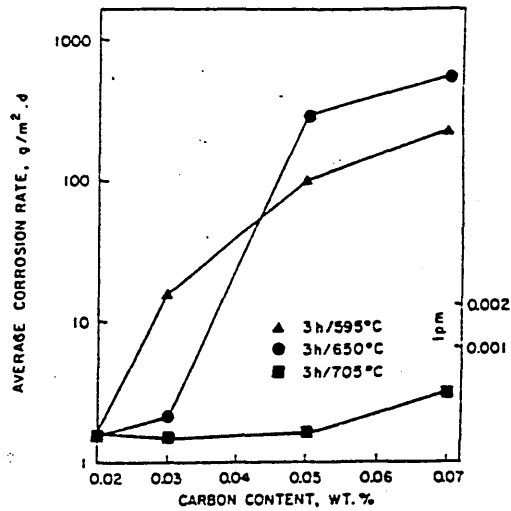
FIG. 3 Drilled holes in Tube Support Plate

Fig. (4a)



Time-temperature-sensitization diagram for Alloy 690 in boiling 65% Nitric acid. Heat T-57177 containing 0.05% c, solution annealed 1 h/1150°C/WQ.

Fig. (4b)



The effect of carbon content on the corrosion rate of Alloy 690 in the huey test. Material annealed 1 h/1150°C/WQ before sensitizing.

Fig. (4C) The Carbide Morphology of Inconel 690 after Various Heat Treatments

Temp.	Fine discrete	fine semi-continuous	large semi-continuous	course discrete
538°C	48h -----	100h -----	200h -----	
600°C		5h -----	10h 24h 48h -----	100h 215h -----
700°C		1h -----	5h 10h 24h 48h -----	100h -----
800°C			1h -----	10h -----

FIG.5

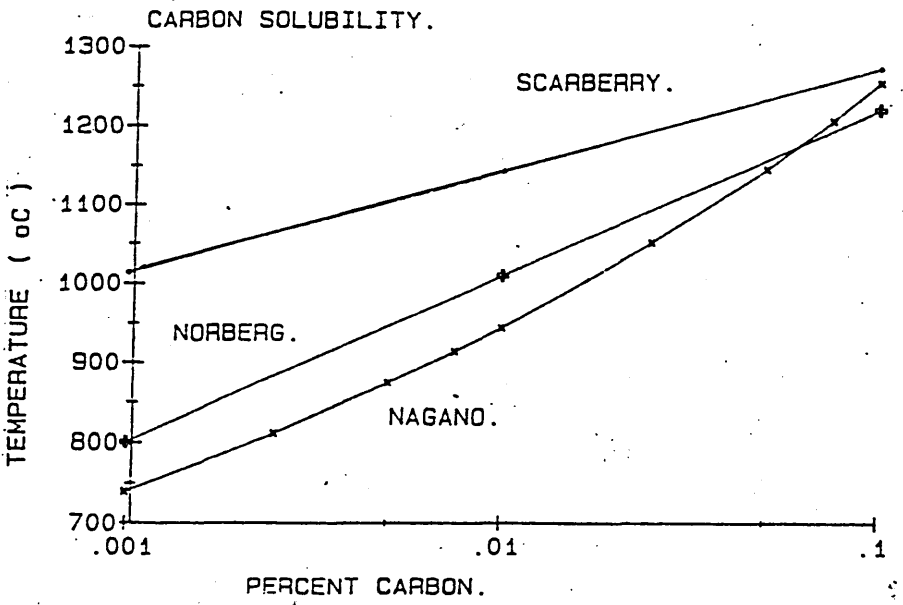
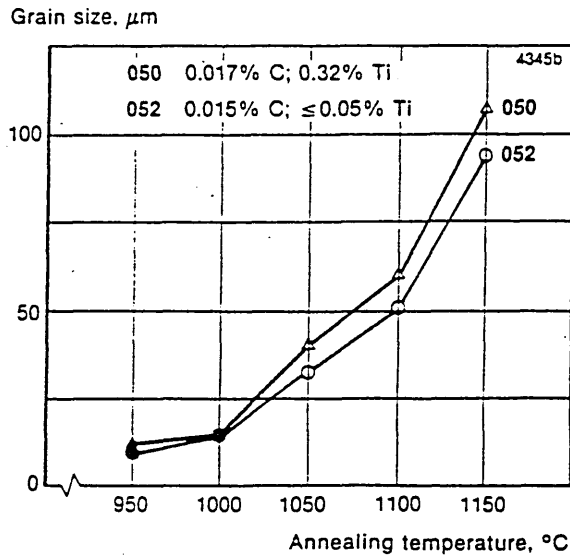
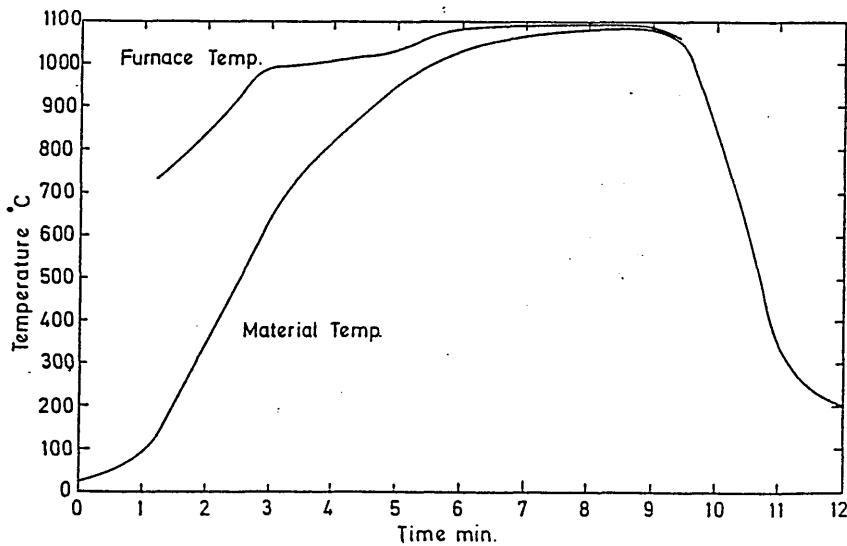


FIG. 6



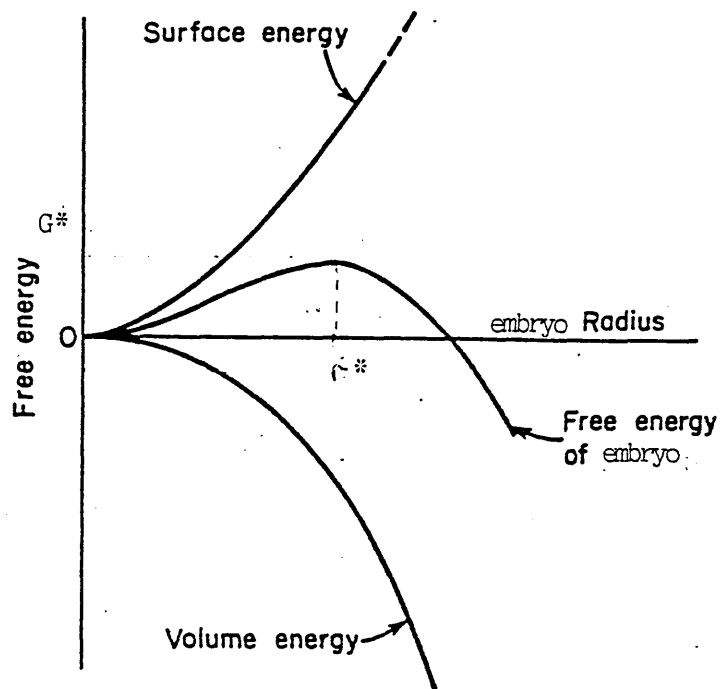
Grain coarsening characteristics of heats Nos 050 and 052, containing 0.32 and $\leq 0.05\%$ Ti, respectively. Filled legends indicate presence of undissolved chromium carbides. Annealing time 20 min.

FIG. 7



Typical heating/cooling curve for a commercial mill annealing muffle furnace, during production of alloy 690

FIG.8



Free energy of embryo as a function of embryo size

Fig (9). Computer simulation of precipitation of Cr_{23}C_6 .
 $c = 6 \times 10^{-30}$, $f = 0.7$. $ST = 1200^\circ\text{C}$, aged at between $650^\circ - 950^\circ\text{C}$.
 $0.022\% \text{C}$

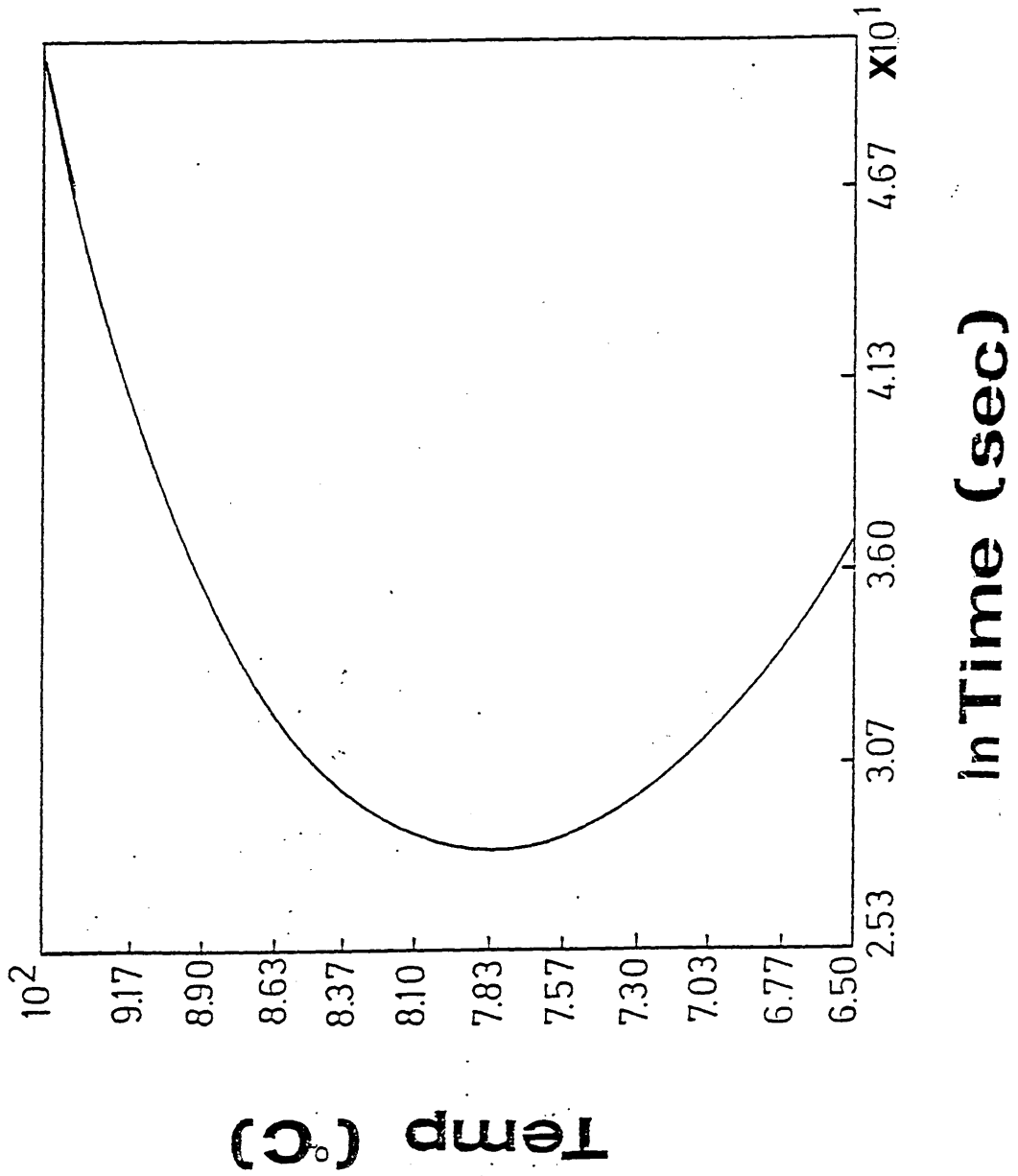


Fig (10).

Computer simulation of the precipitation of Cr₂₃C₆.
Constant $C=6 \times 10^{-34}$, varying f from 0.4 to 0.8.

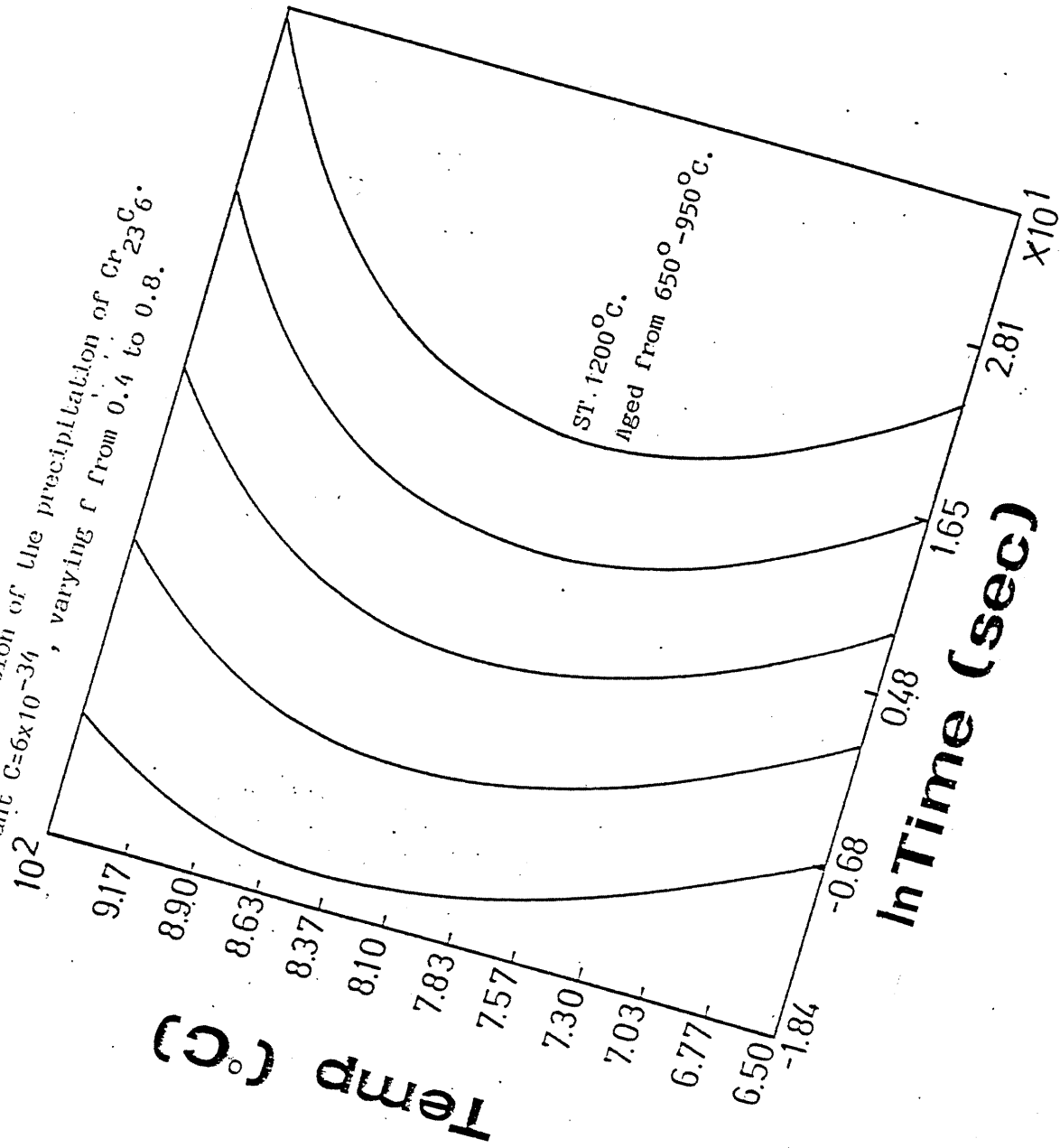


Fig. 11

Computer simulation of the precipitation of Cr_{23}C_6 .

Constant f , $C = 6 \times 10^{-34}$ to 6×10^{-29} in steps of

6×10^{-2} . ST 1200°C , aged between 650° and 950°C .

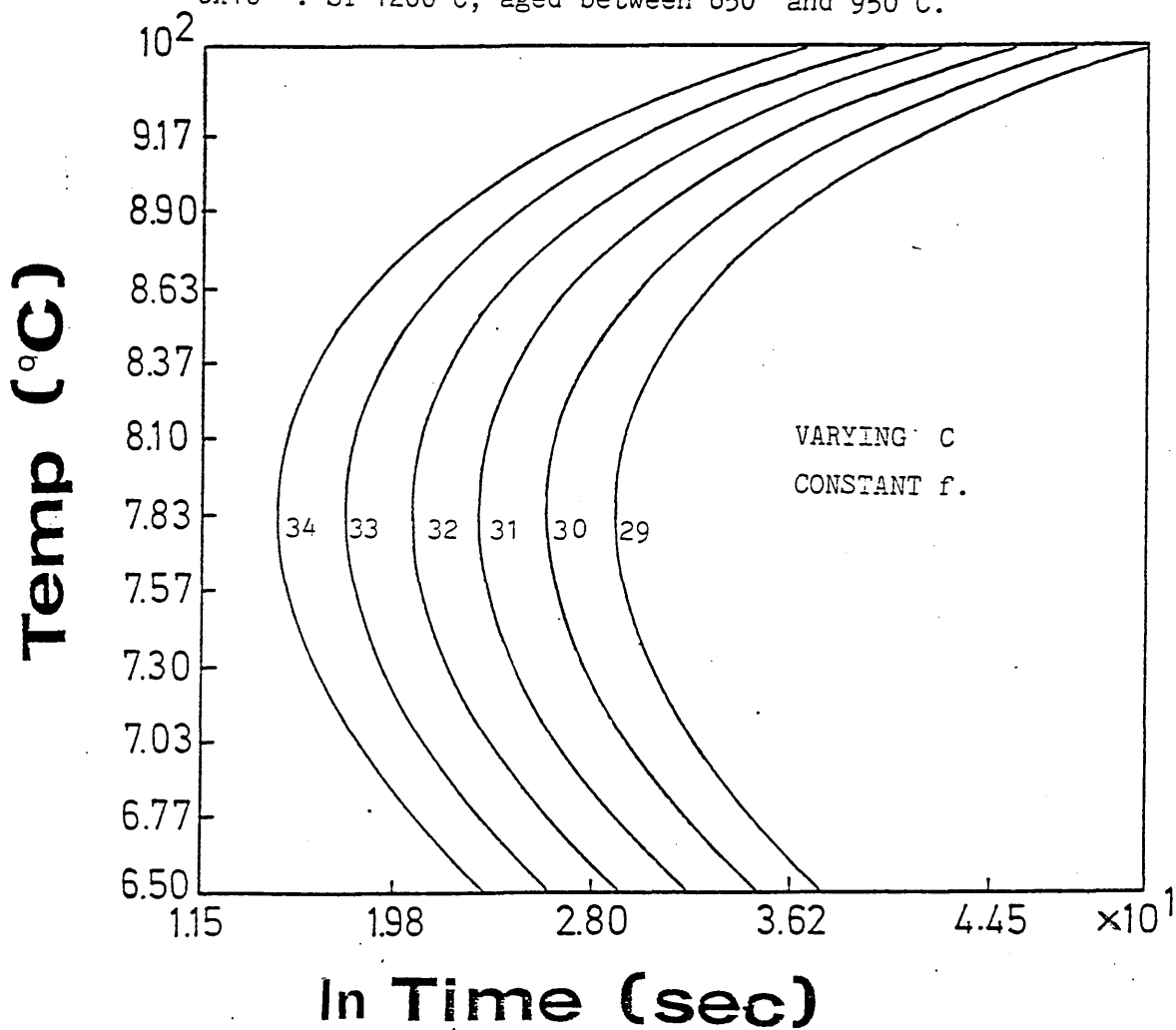




FIG.12(a) TEM Grain Boundary Carbide
taken from as-received
Tube A 66K

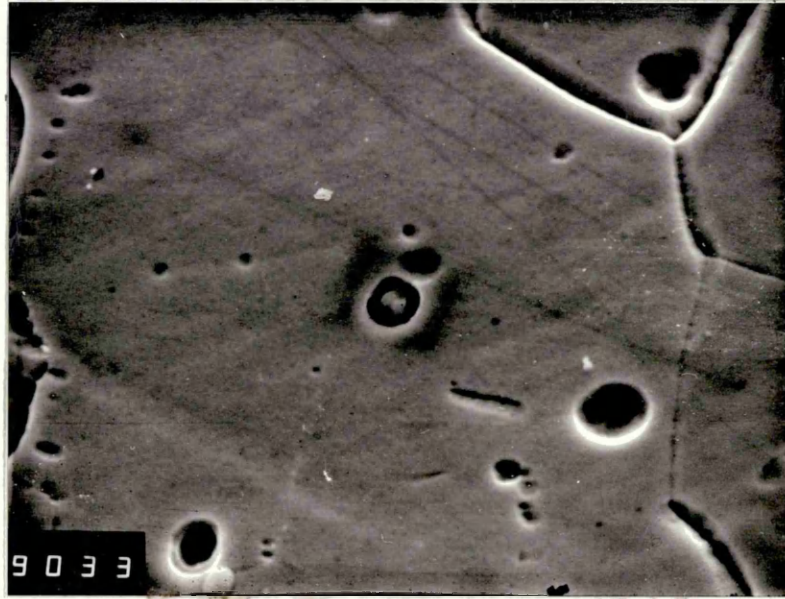


FIG.12(b) Dark field of above particle
66K



FIG.13 Diffraction pattern taken from
12(a) and 12(b) and identified
as $M_{23}C_6$ 187

FIG.14



Intragranular chromium carbide, (6400x mag.)
as-received Tube A S.E.M.

FIG.15 Index to spectra

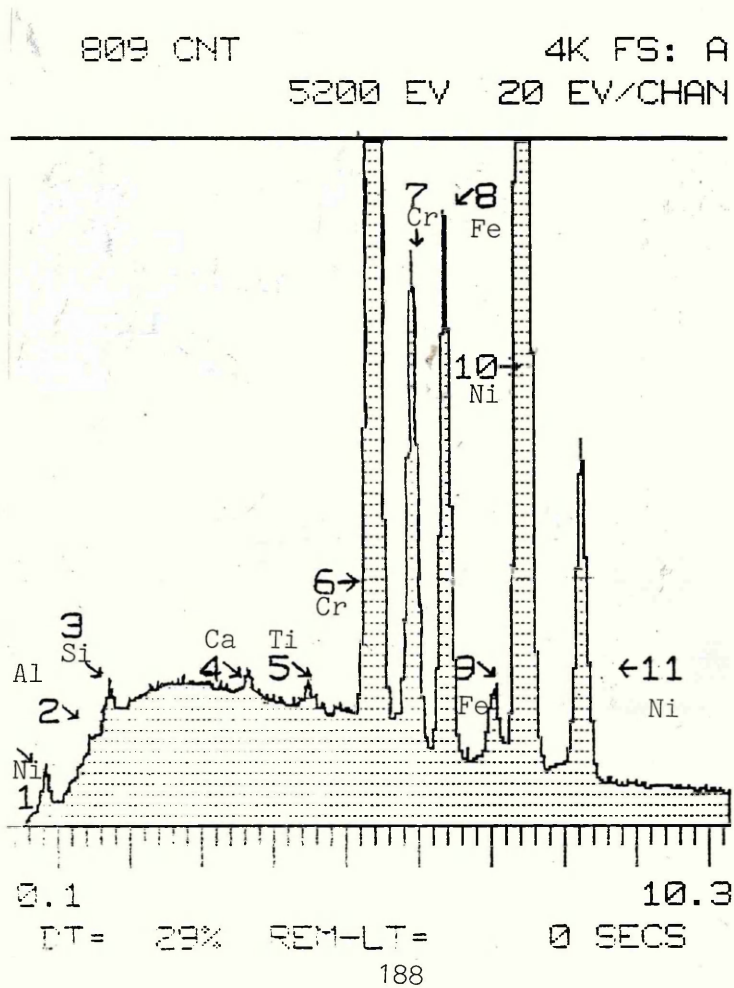


FIG.16 Small grain boundary Ti(CN) (0.02 μm)
100k mag. As-received Tube C, S.T.E.M.



FIG.17 Large intragranular TiN. As-received
Tube A. Longest axis 15 μm . S.E.M

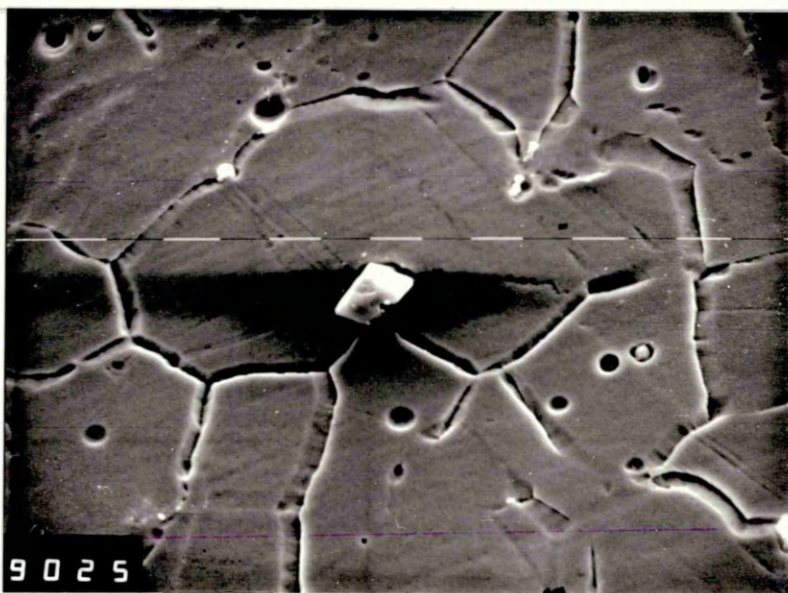


FIG.18 Auger Electron Spectroscopy. Spectrograph showing that larger intergranular particles are TiN

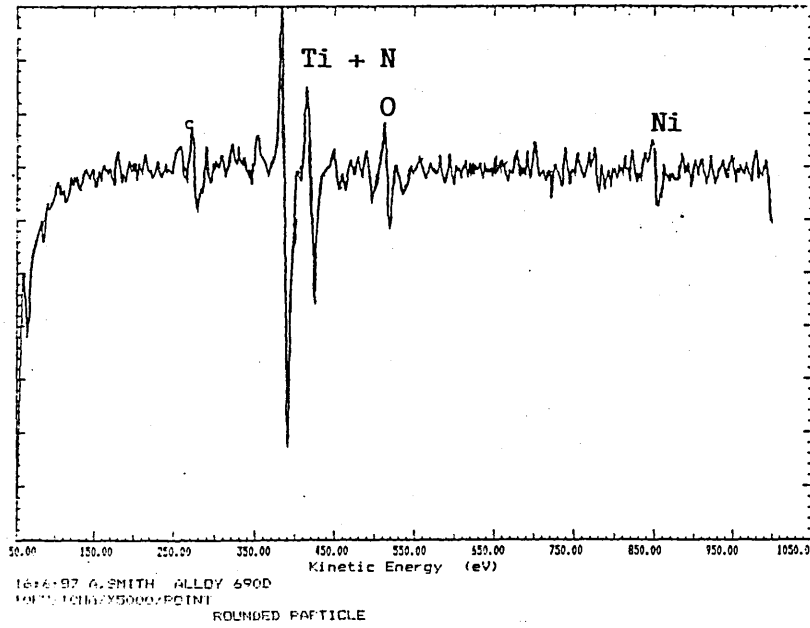


FIG.19 Intergranular angular particle identified as Ti-rich using SEM EDX

88 CNT 4K FS: A
 8888 EV 28 EV/CHAN

SAMPLE B ALLOY 690
 (TIC)

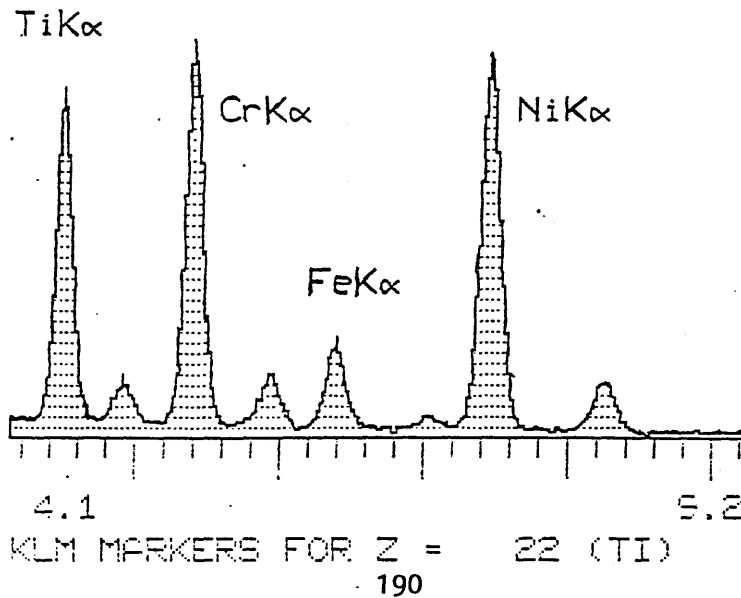
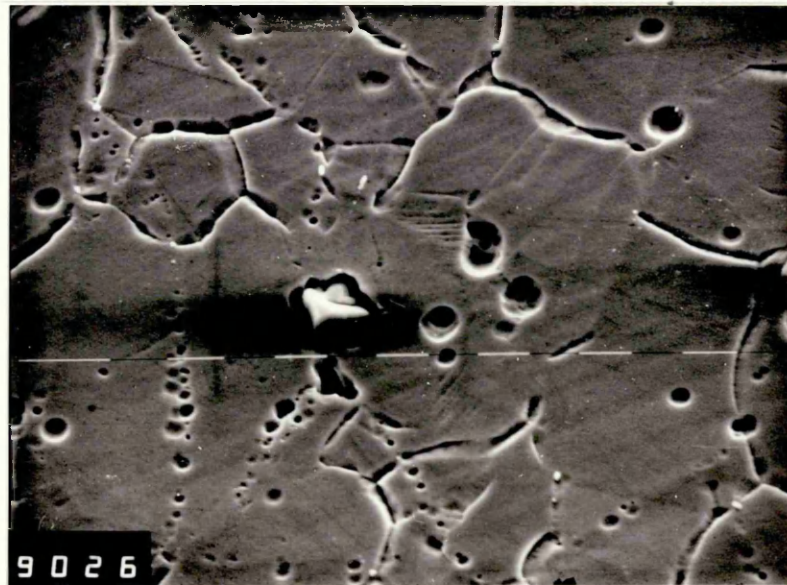
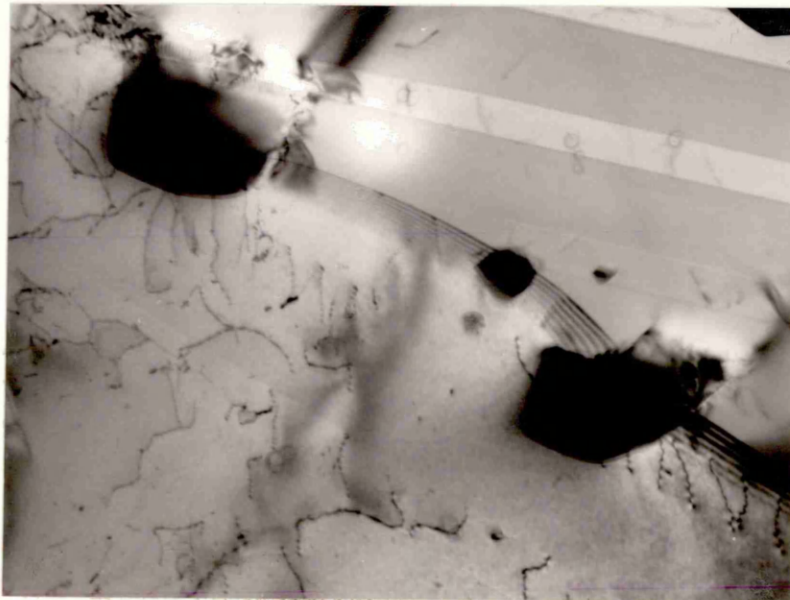


FIG.20



Angular Cr-rich intragranular precipitate.
As-received Tube B. S.E.M. x1 000

FIG.21



Chromium-rich $M_{23}C_6$ particle still pinning a
grain boundary after mill annealing at $1100^{\circ}C$
As-received Tube A. T.E.M. x330K

FIG.22 Filamentary Grain Boundary $M_{23}C_6$. As received
Tube A. T.E.M. x66K

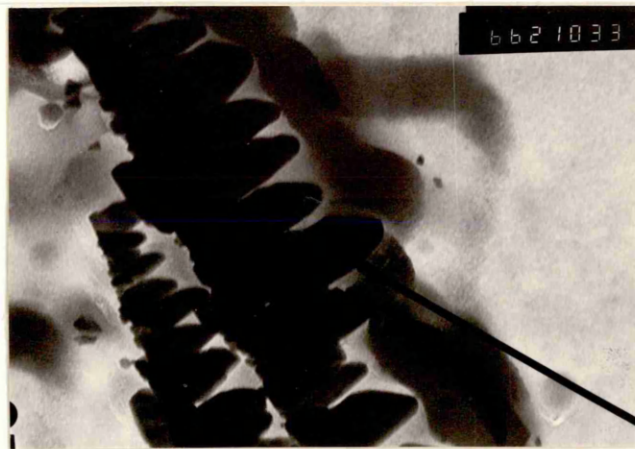
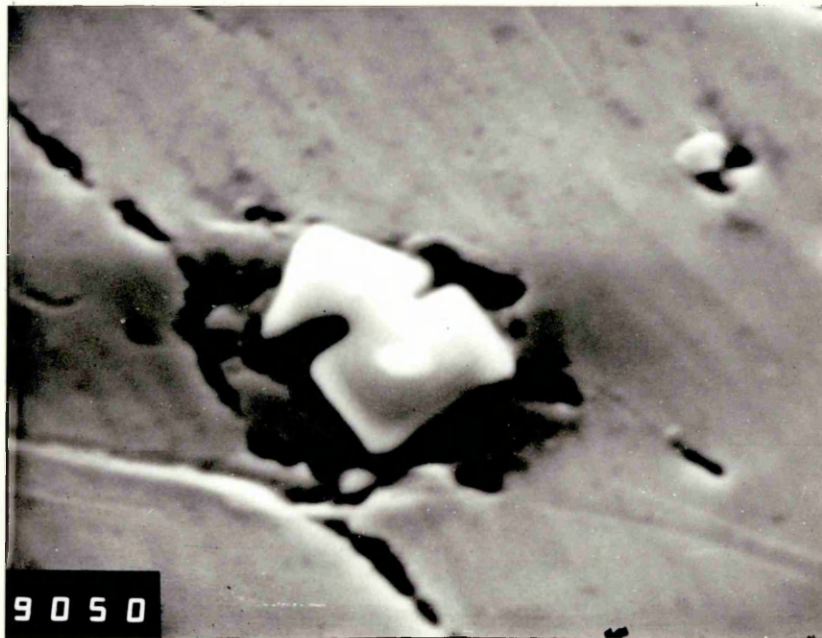


FIG.23 Typical precipitate free grain boundary
after solution treating at 1200°C
followed by water quenching. T.E.M. x130K

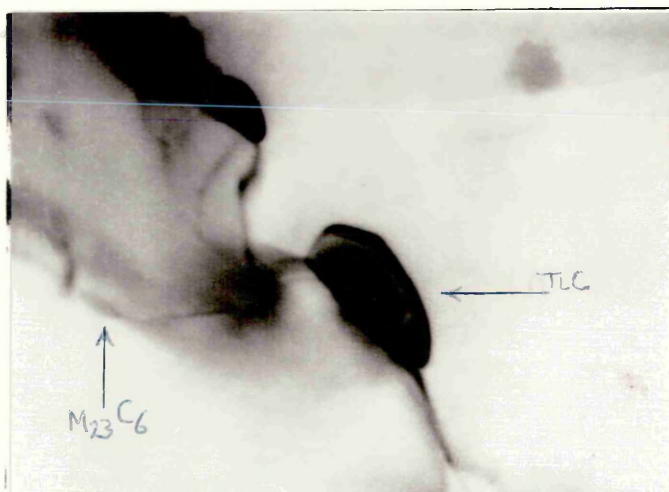


FIG.24



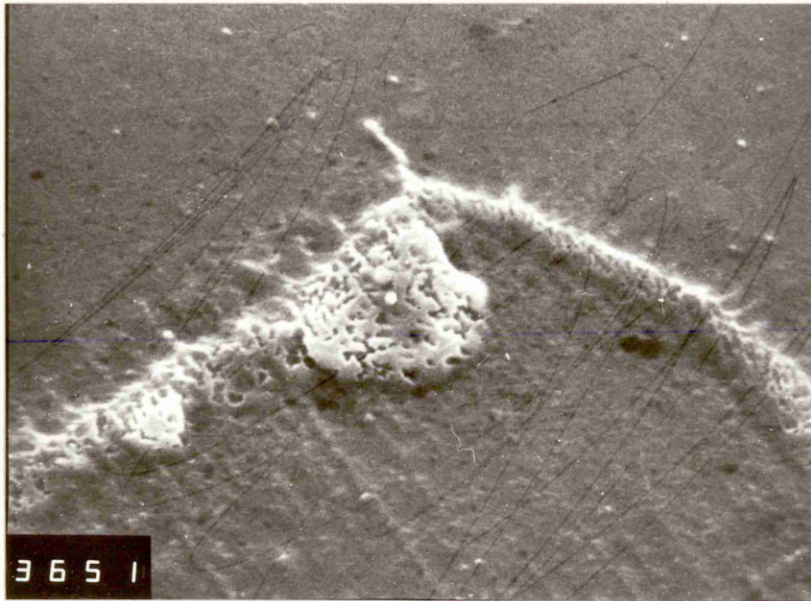
Angular Chromium-rich intragranular precipitate found in EM3. 6400x mag. S.E.M.

FIG.25



Fine Ti-rich carbide phase adjacent to a large chromium-rich $M_{23}C_6$ grain boundary precipitate. S.T.E.M. 100K

FIG.26



Colonies of cellular grain boundary chromium carbides
EM12 solution treated at 1200°C and aged at 700°C
for 10 hours. S.E.M. x 1000

FIG. 27

PETCH, TUBE E.

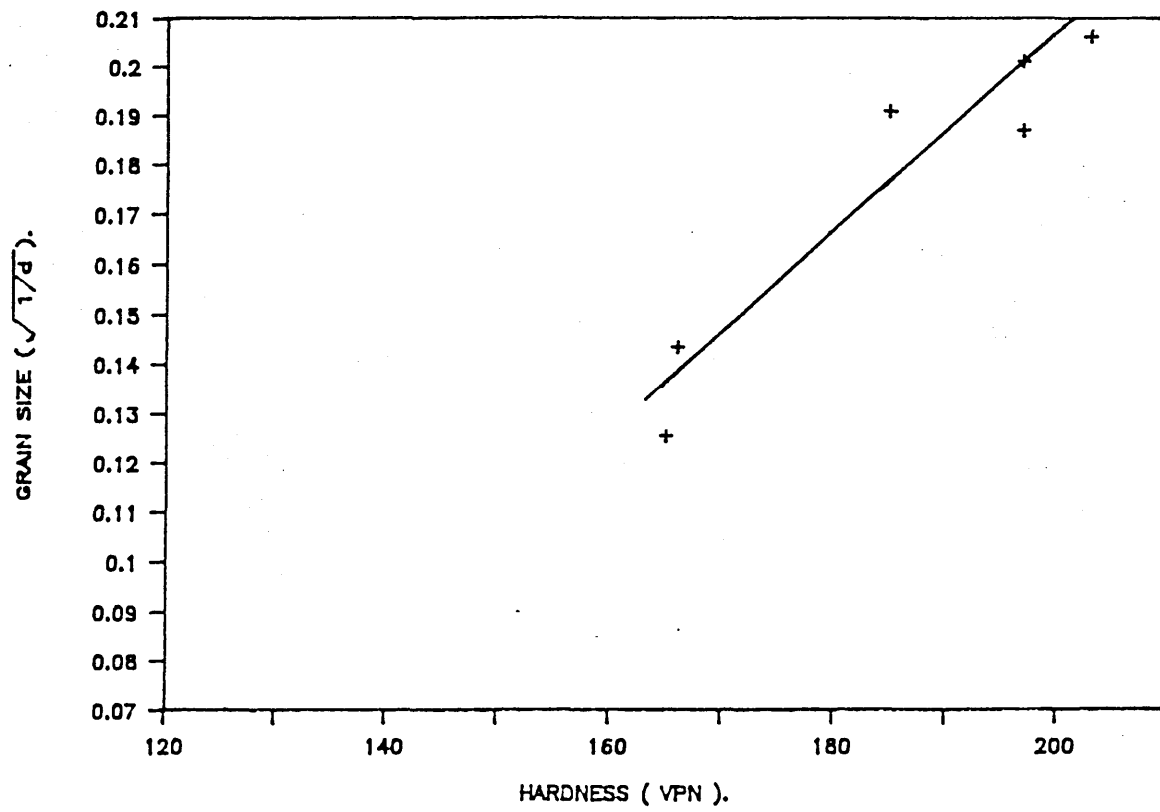


FIG. 28

PETCH, TUBE A.

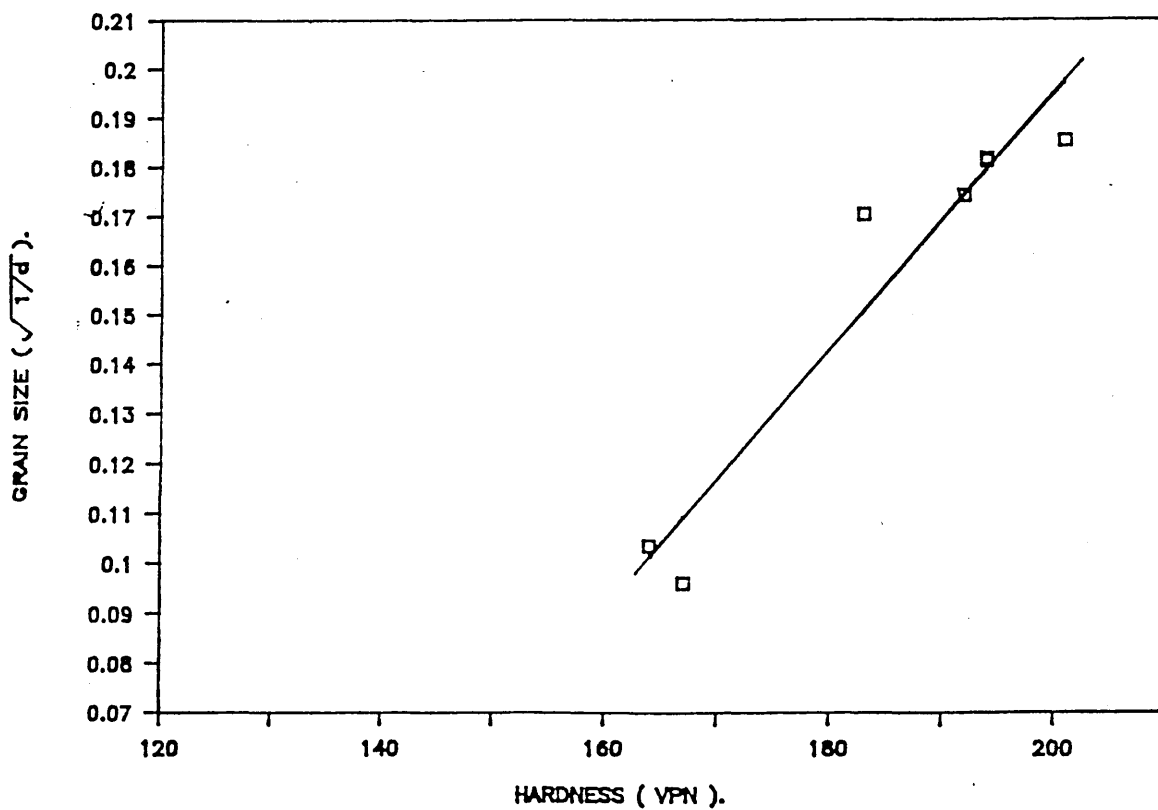
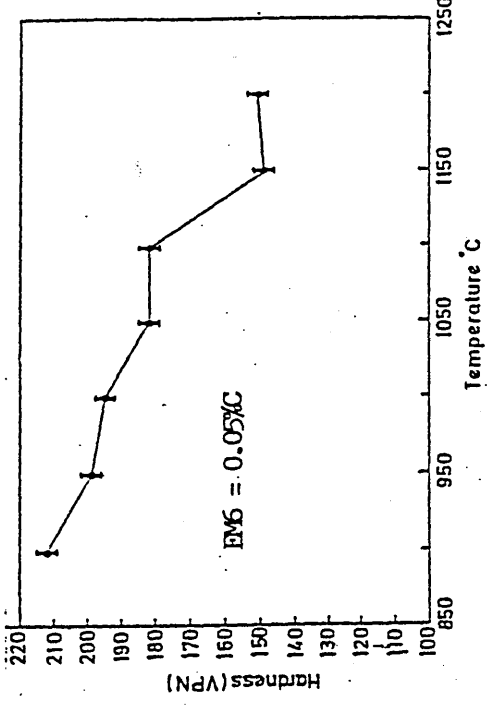
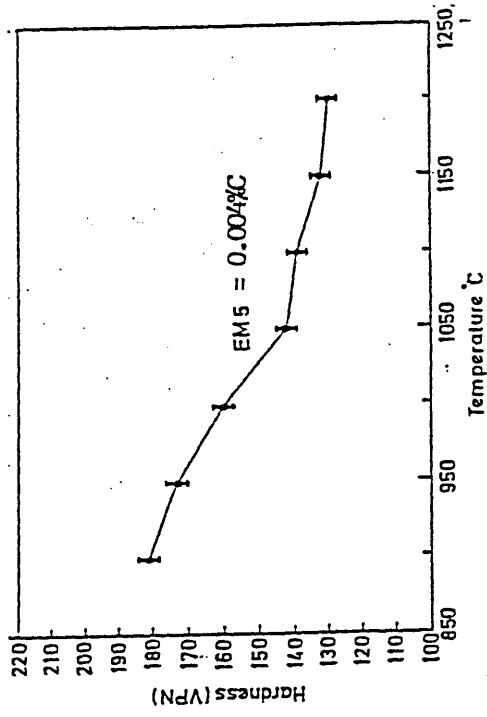
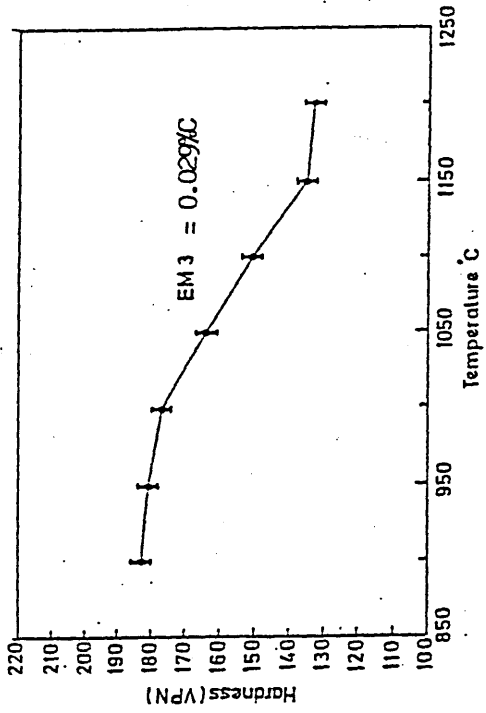
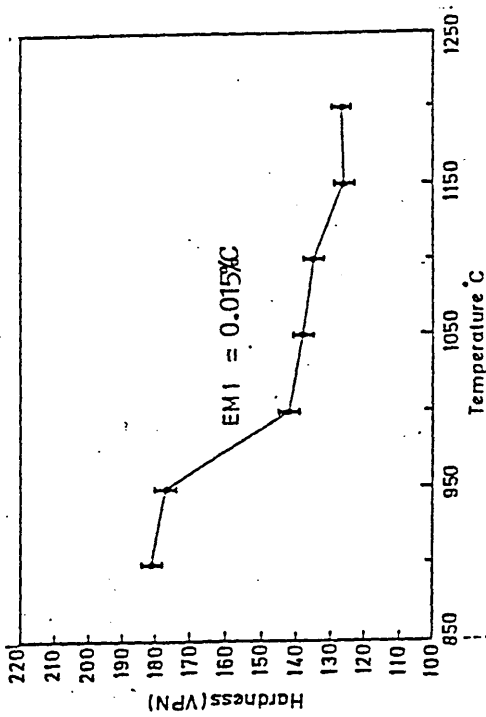
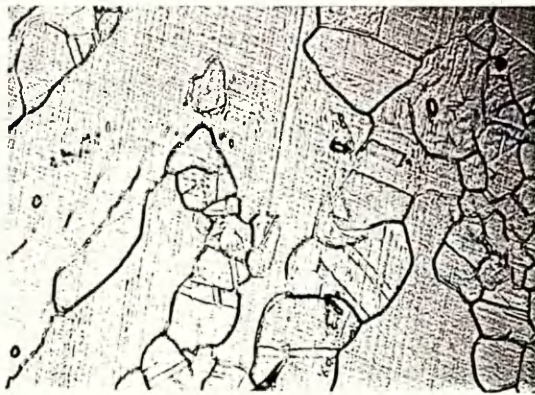


FIG. 29



Hardness versus solution treatment temperature. Effect of increasing carbon in the absence of titanium and aluminum



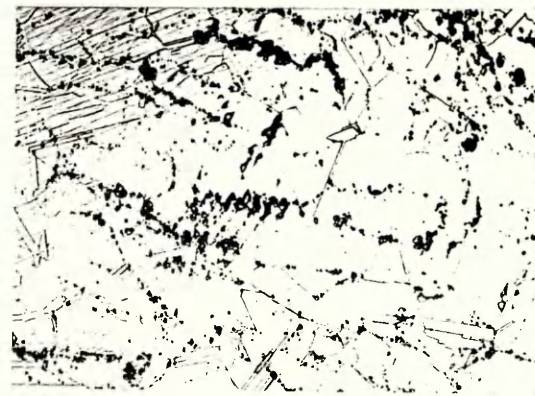
EM 5 heat treated 900°C
(128x mag)



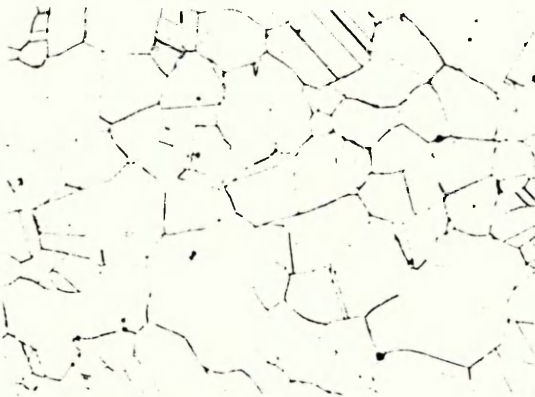
EM 6 heat treated 900°C
(500x mag)



EM 5 heat treated 1000°C
(128x mag)



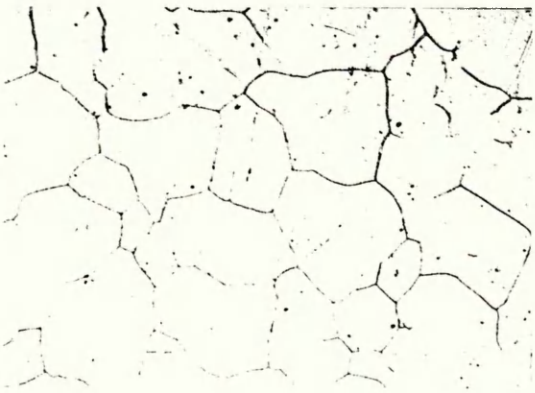
EM 6 heat treated 1000°C
(500x mag)



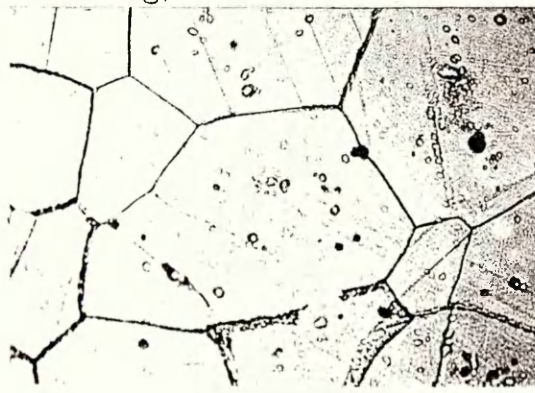
EM 5 heat treated 1100°C
(128x mag)



EM6 heat treated 1100°C
(500x mag)

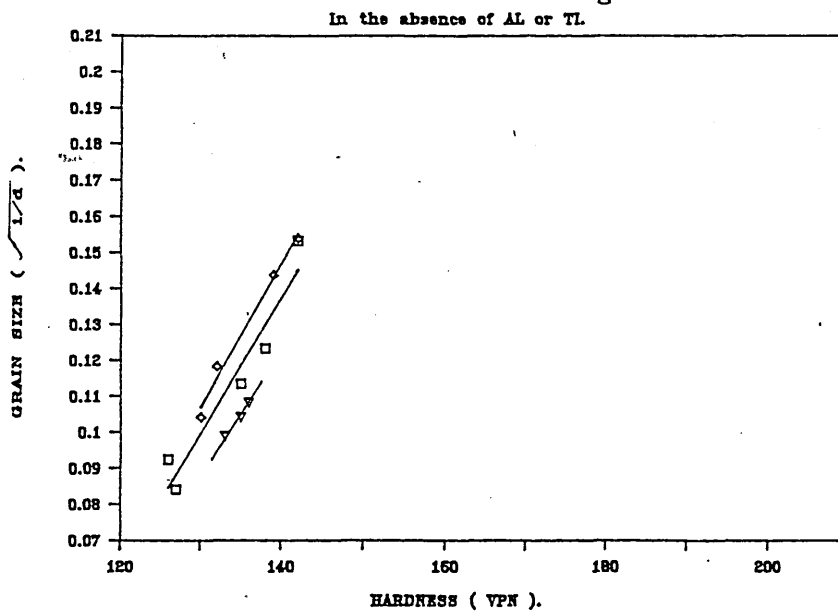


EM5 heat treated 1200°C (128x)



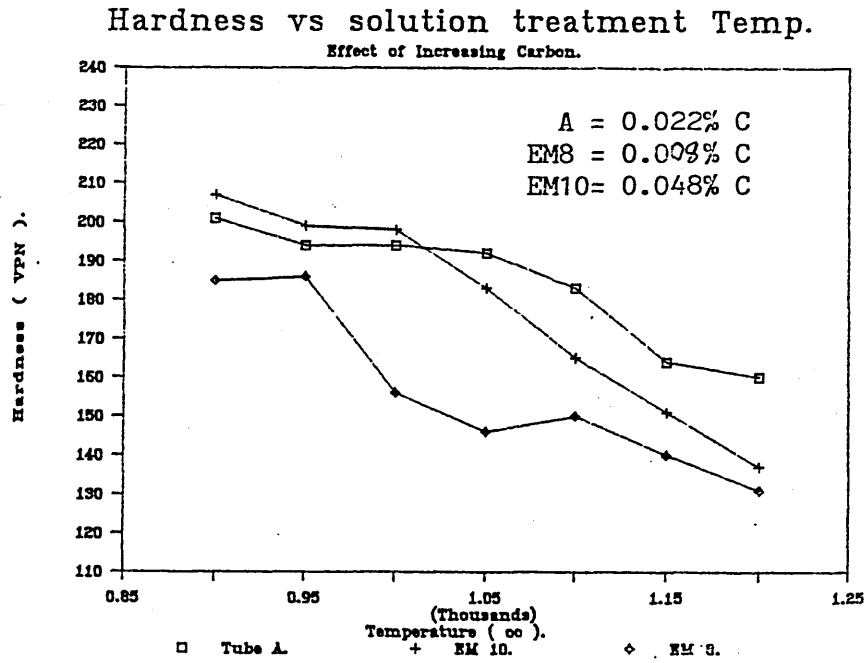
EM6 heat treated 1200°C (200x)

FIG.31 Petch. Effect of increasing carbon.



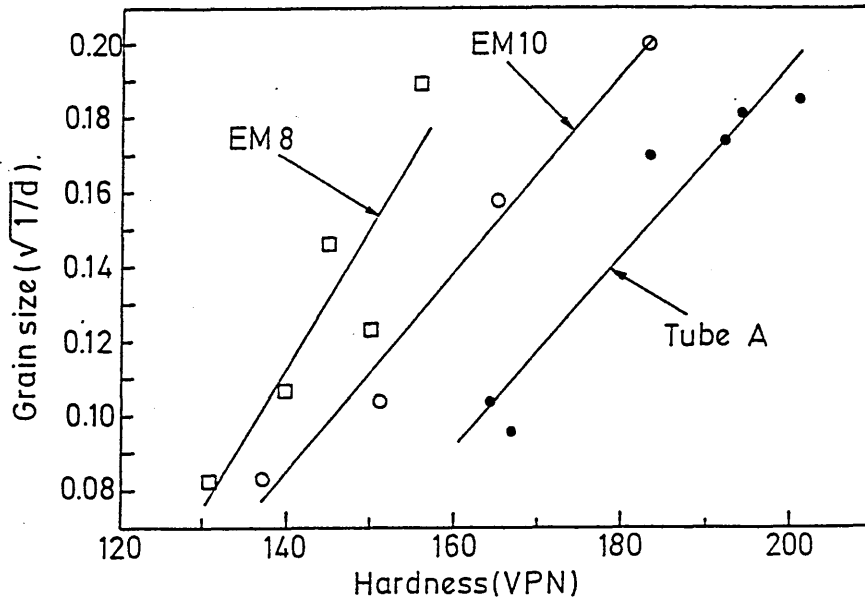
◇ = EM5
 □ = EM1
 ▽ = EM3

FIG.32



The effect of varying carbon in alloys containing 0.03% Al and 0.38% Ti

FIG.33



Petch effect increasing carbon in alloys containing 0.03% Al and 0.38% Ti

FIG.34 Hardness versus solution treatment temperature. Effect of varying Al with 0.02% C and 0.27% Ti

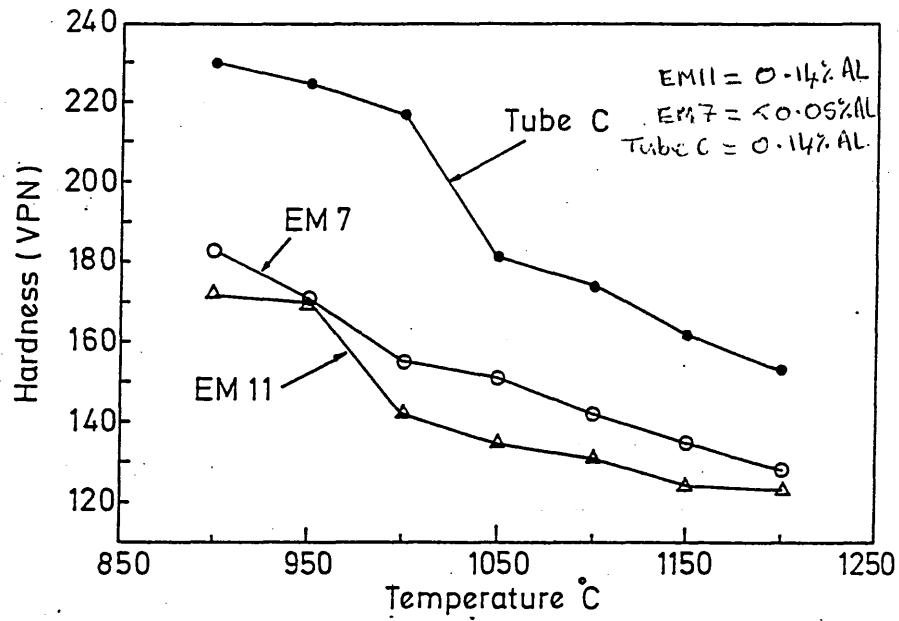


FIG.35 Patch. Effect of varying Al with 0.02% C and 0.27% Ti

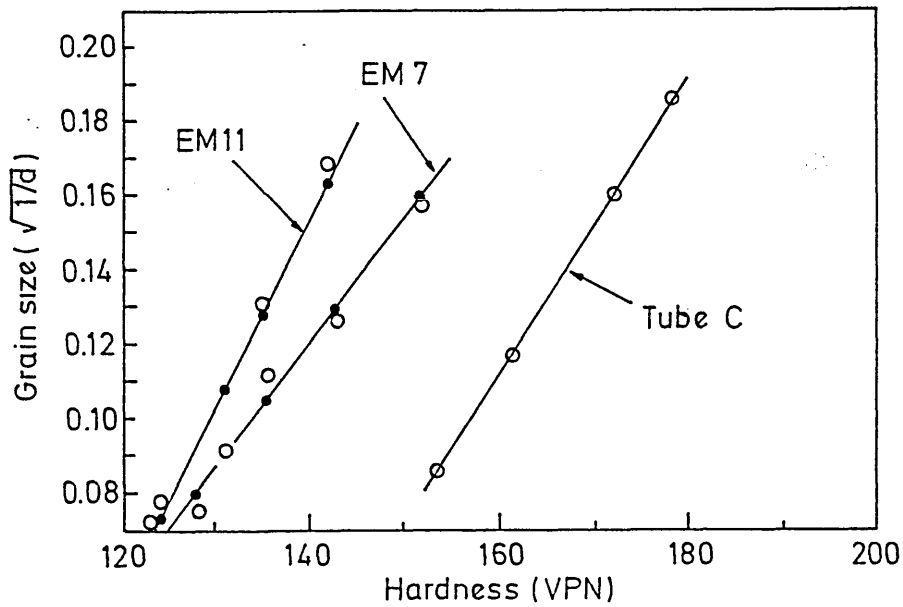


FIG.36 Hardness versus solution treatment temperature
 Effect of varying Ti in alloy containing
 0.019% C and 0.12% Al

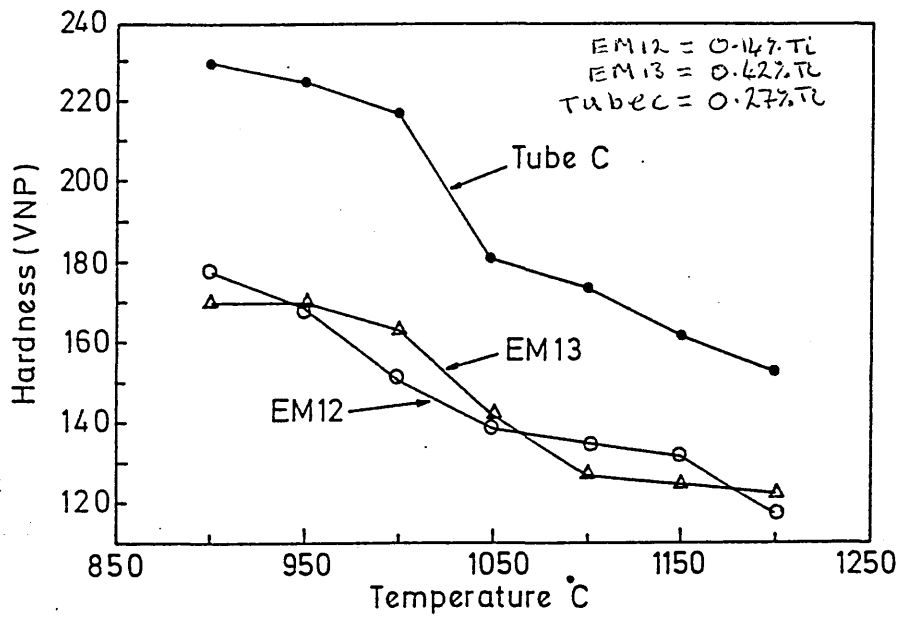


FIG.37 Petch. Effect of varying Ti in alloys
 containing 0.019% C and 0.12% Al

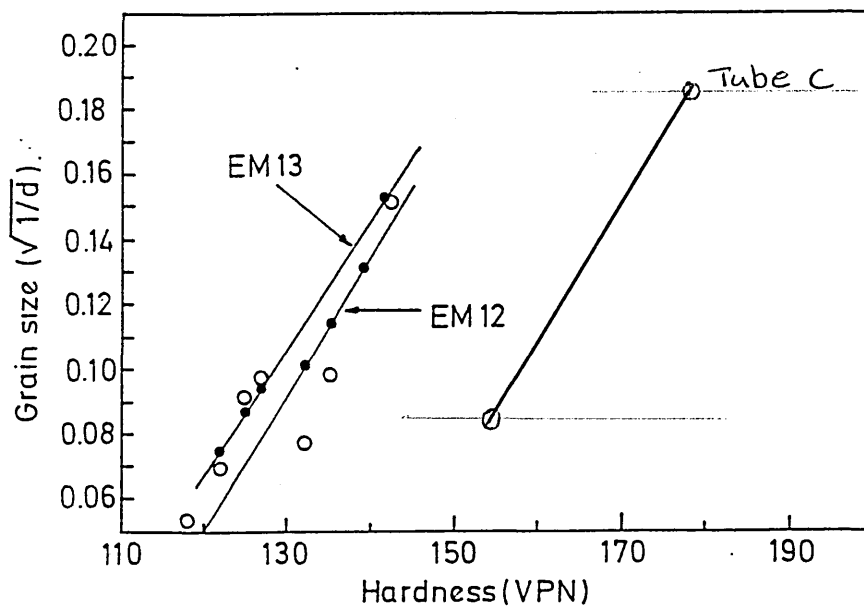


FIG. 38 Hardness versus ageing time at temperatures between 550°C and 700°C.
 Tube F. Solution Treated 1200 c.
 Time - Temperature Ageing Diagrams.

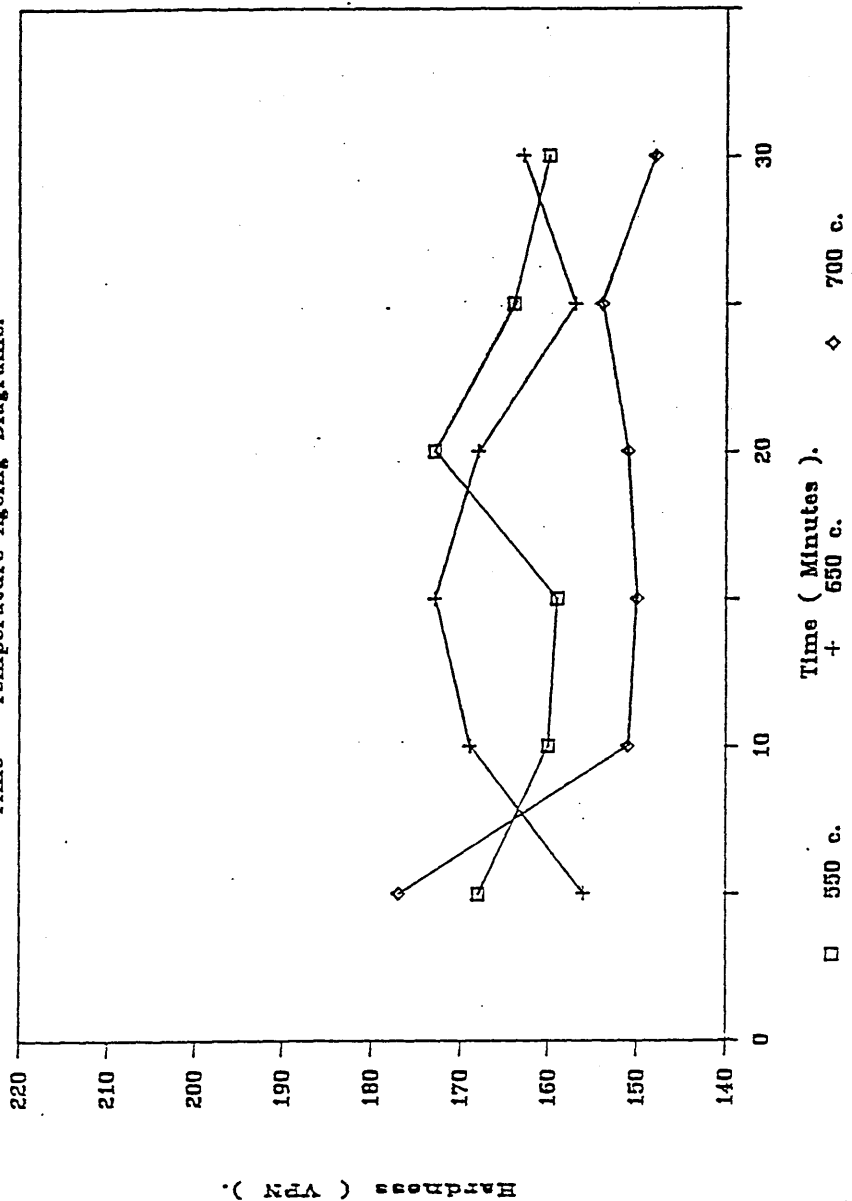


FIG.39(a) EM12 solution treated 1200°C (WQ). Aged at 700°C for 10 min. Carbon replica. Early stages of grain boundary chromium carbide precipitation with filamentary or cellular outcrop (33k mag)

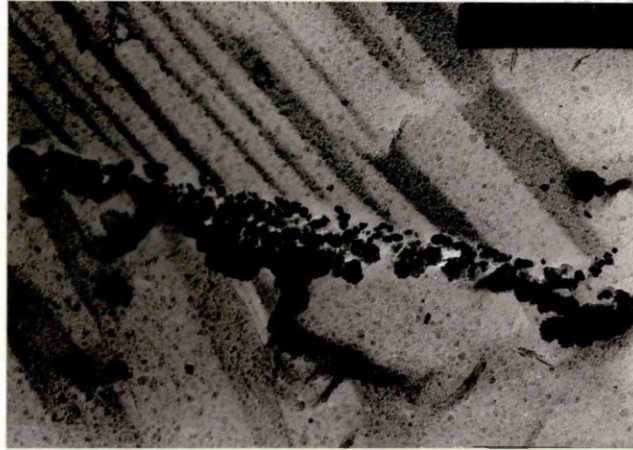


FIG.39(b) Higher magnification of above showing triangular platelets of $M_{23}C_6$. T.E.M. 66K



FIG.39(c) EM12 solution treated 1200°C. Aged at 800°C for 1 hour. Semi-continuous grain boundary carbide of $M_{23}C_6$. 66K T.E.M.

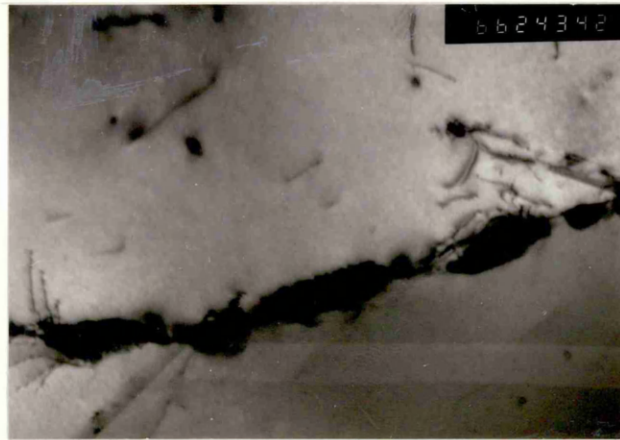
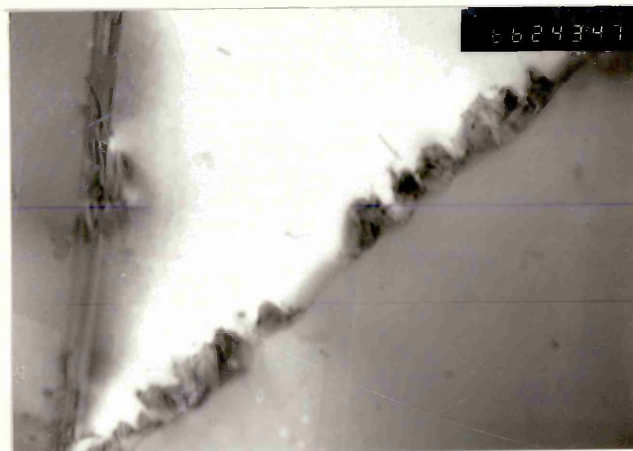


FIG.39(d) EM12 solution treated 1200°C. Aged at 800°C for 5 hours small discrete $M_{23}C_6$ grain boundary carbides. Early stages of spheroidising from the semi-continuous morphology



T.E.M. x66K

FIG.39(e) EM12 solution treated 1200°C. Aged at 800°C for 15 hours Large discrete grain boundary $M_{23}C_6$ carbides. T.E.M. 33K



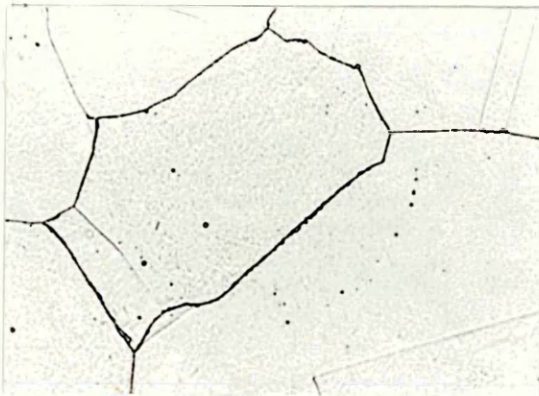
FIG. 40



EM12 Solution treated 1200°C.
Aged at 650°C for 1 hour
(25x mag)



EM12 Solution treated 1200°C
Aged at 700°C for 1 hour
(250x mag)



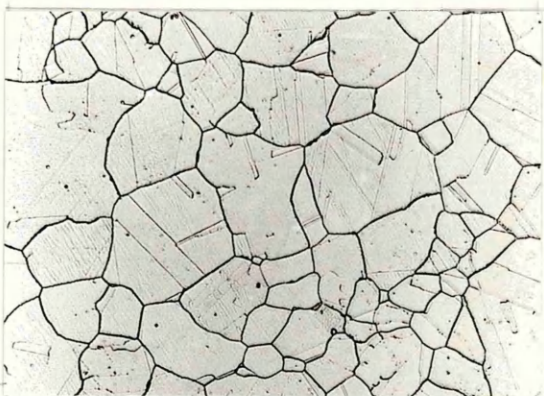
EM12 Solution treated 1200°C
Aged at 650°C for 5 hours
(250x mag)



EM12 Solution treated 1200°C
Aged at 700°C for 5 hours
(250x mag)

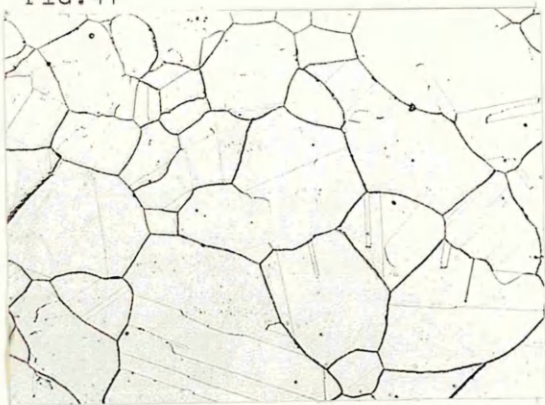


EM12 Solution treated 1200°C
Aged at 650°C for 15 hours
(100x mag)

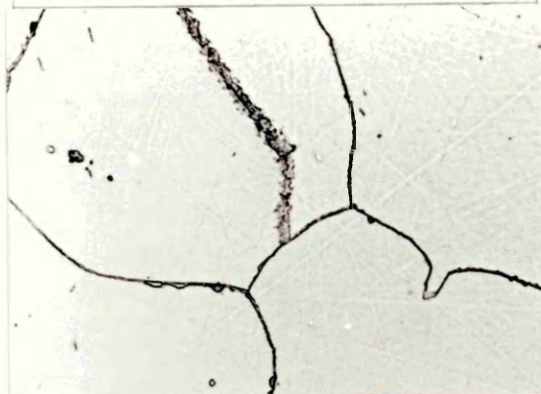


EM12 Solution treated 1200°C
Aged at 700°C for 15 hours
(75 x mag)

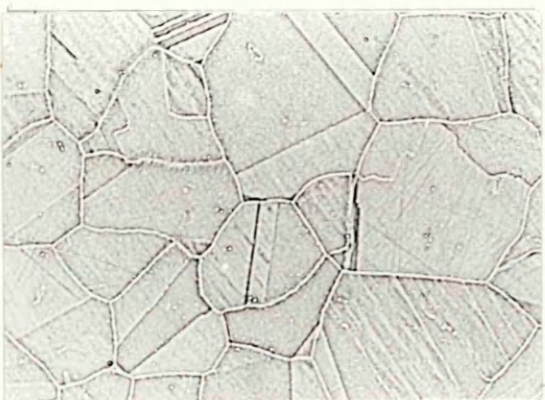
FIG.41



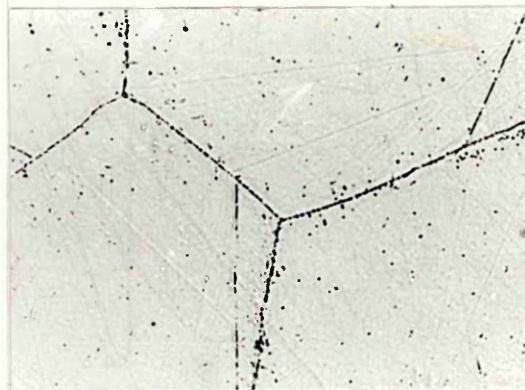
EM12 Solution treated 1200°C
Aged at 750°C for 1 hour
(100x mag)



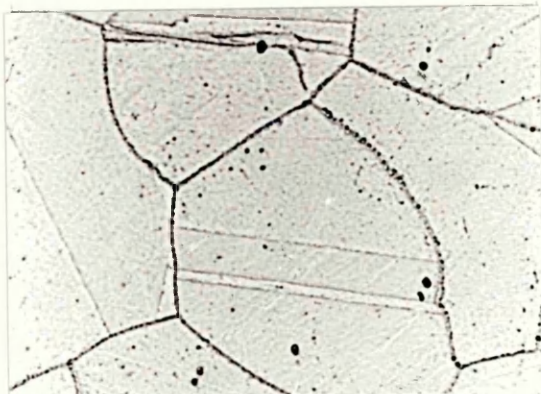
EM12 Solution treated 1200°C
Aged at 800°C for 1 hour
(250x mag)



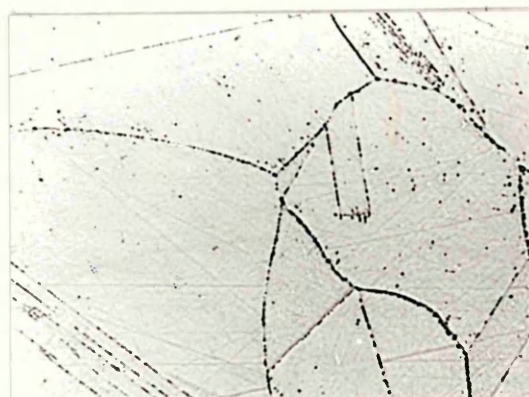
EM12 Solution treated 1200°C
Aged at 750°C for 5 hours
(100x mag)



EM12 Solution treated 1200°C
Aged at 800°C for 5 hours
(250x mag)



EM12 Solution treated 1200°C
Aged at 750°C for 15 hours
(250x mag)



EM12 Solution treated 1200°C
Aged at 800°C for 15 hours
(250x mag)

FIG. 42

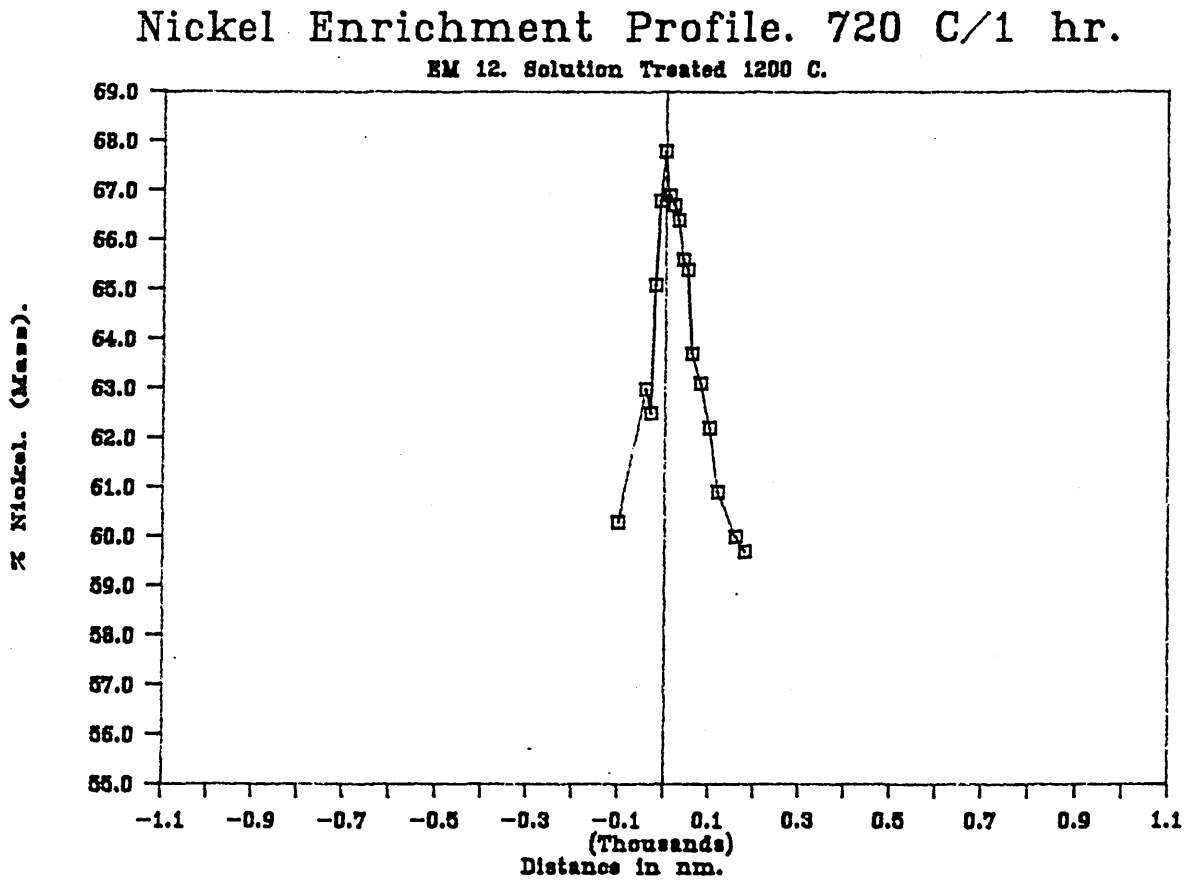


FIG. 43

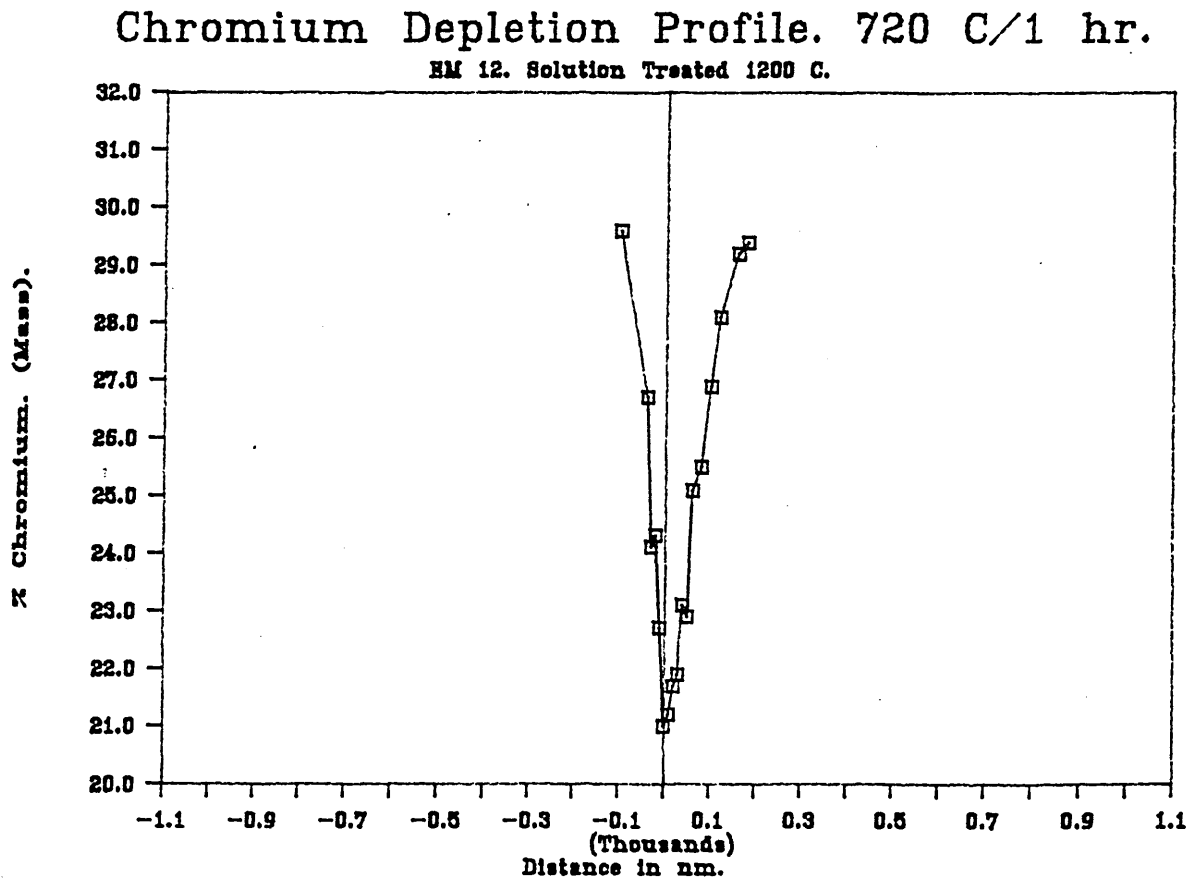


FIG.44

Nickel Enrichment Profile. 720 C/5 hr.

HM 12. Solution Treated 1200 C.

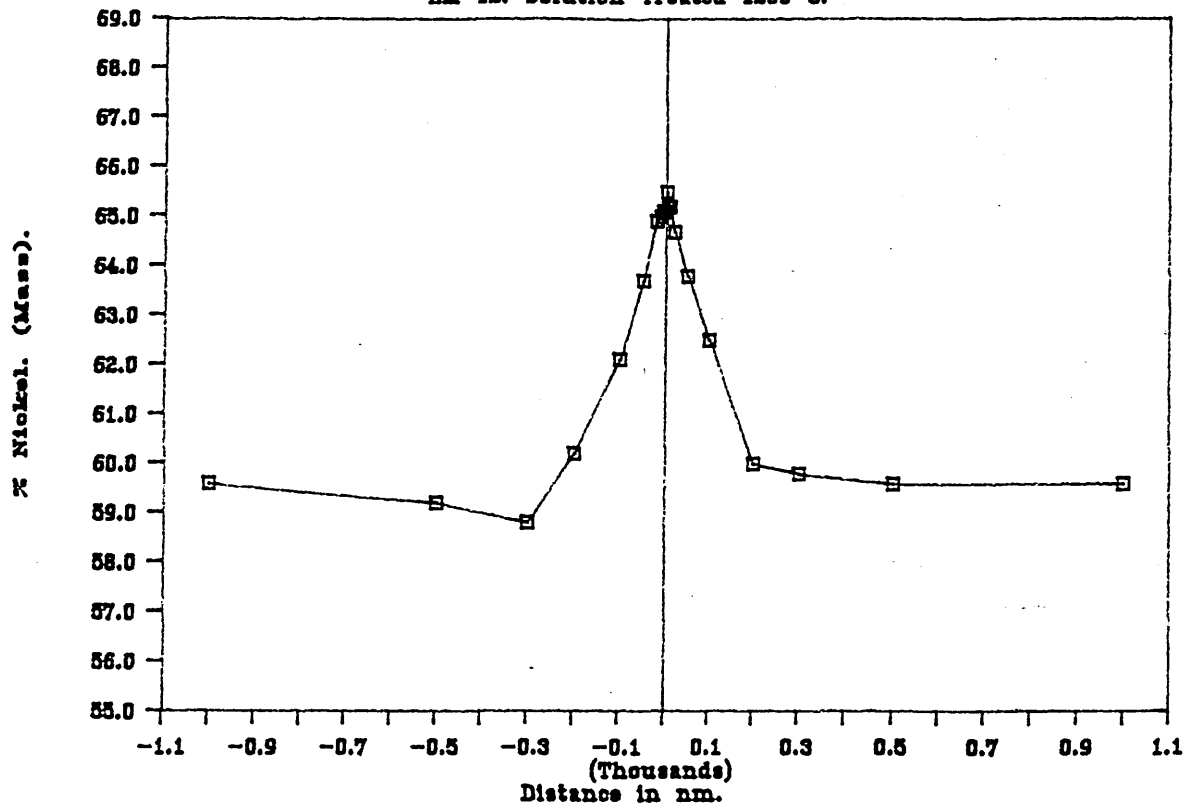


FIG.45

Chromium Depletion Profile. 720 C/5 hr.

HM 12. Solution Treated 1200 C.

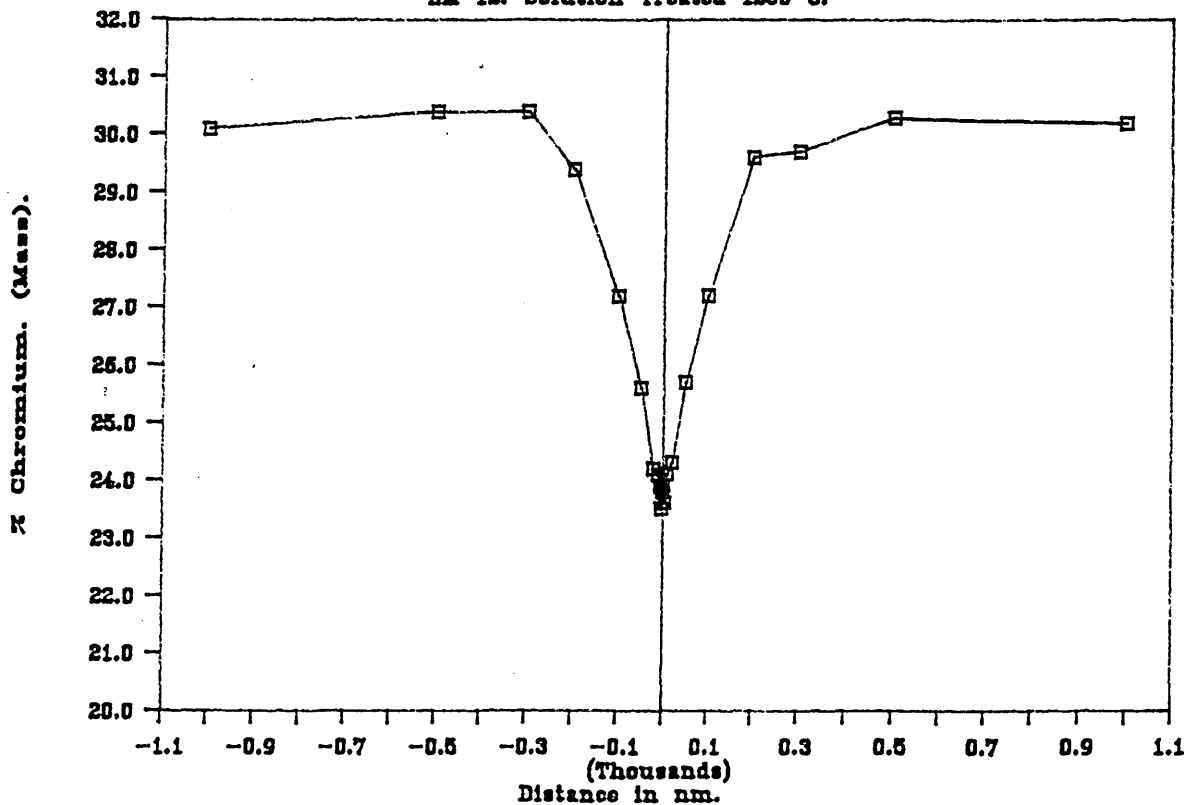


FIG. 46

Nickel Enrichment Profile. 720 C/10 hr.

EM 12. Solution Treated 1200 C.

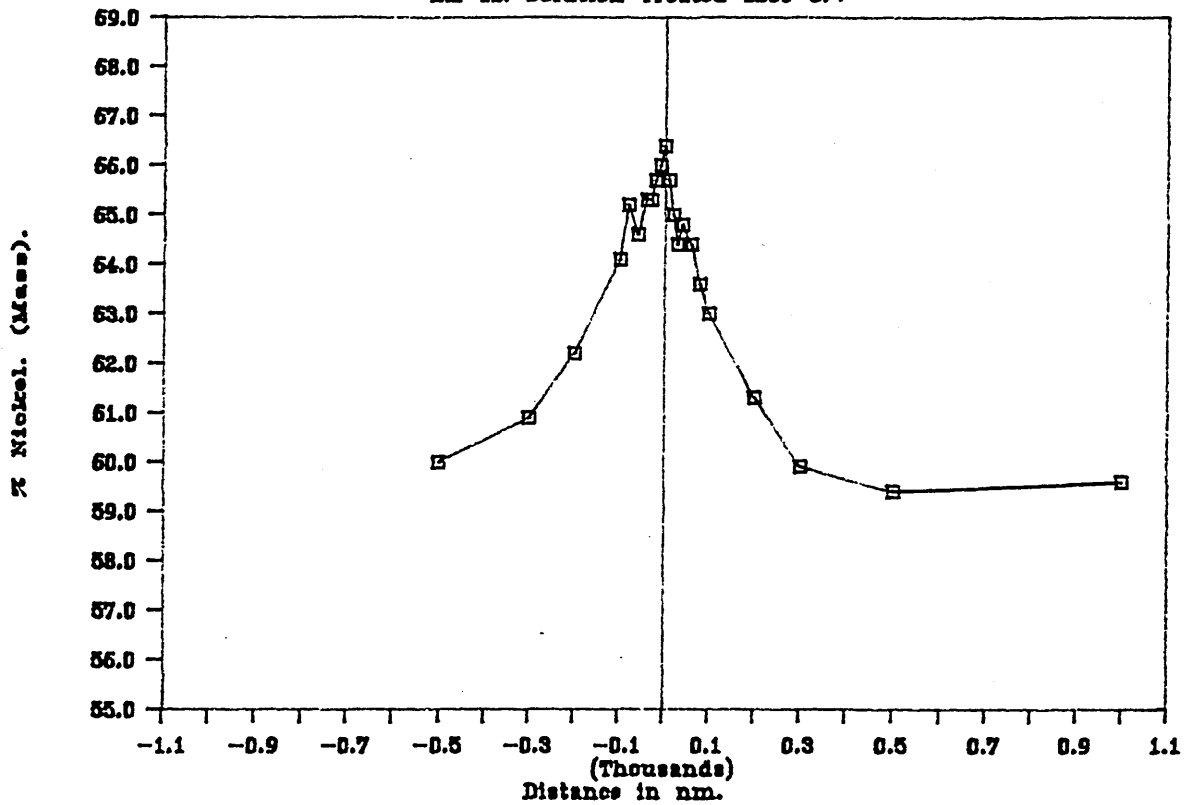


FIG. 47

Chromium Depletion Profile. 720 C/10 hr

EM 12. Solution Treated 1200 C.

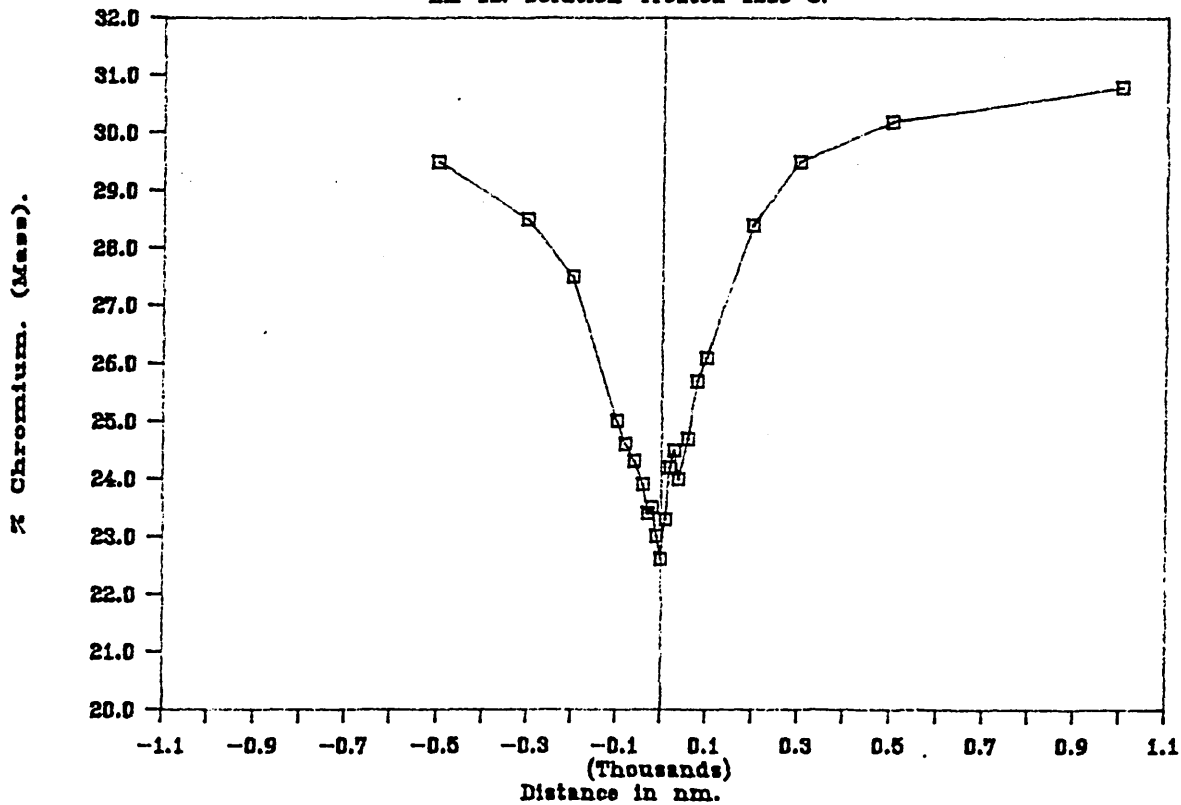


FIG.48

Nickel Enrichment Profile. 720 C/15 hr.

EM 12. Solution Treated 1200 C.

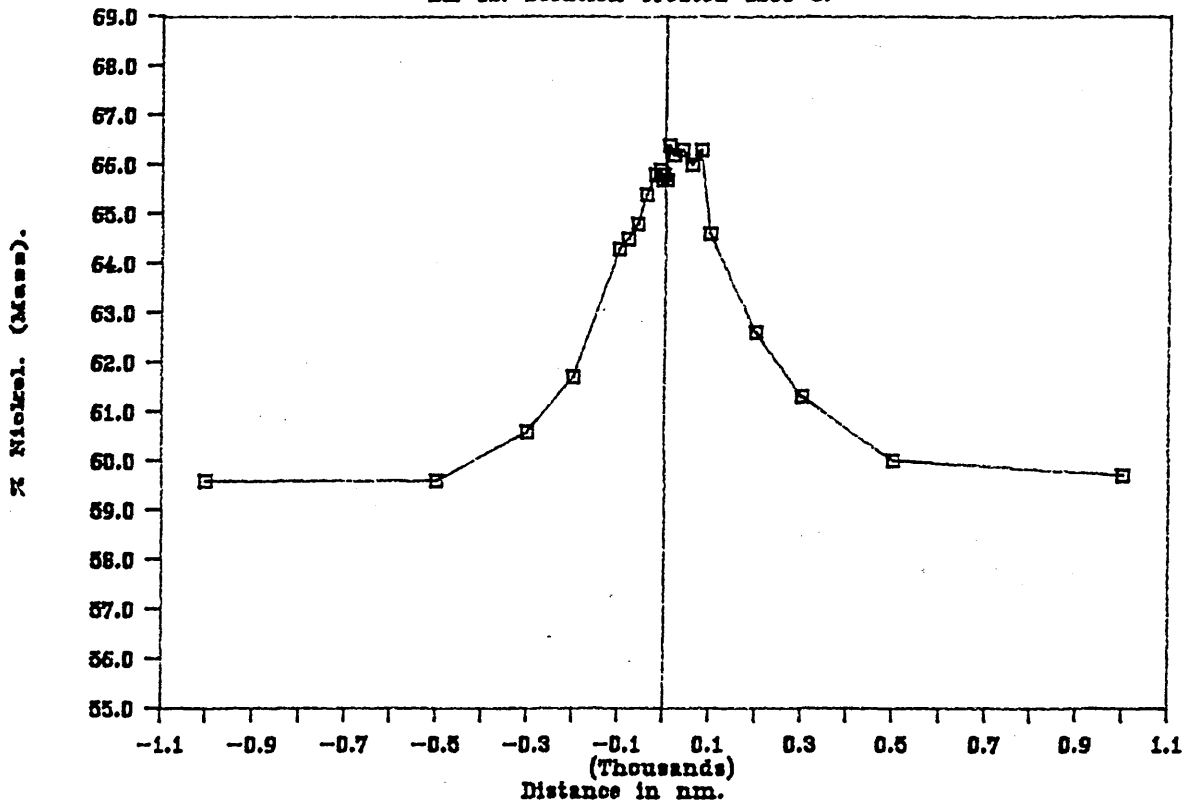


FIG.49

Chromium Depletion Profile. 720 C/15 hr

EM 12. Solution Treated 1200 C.

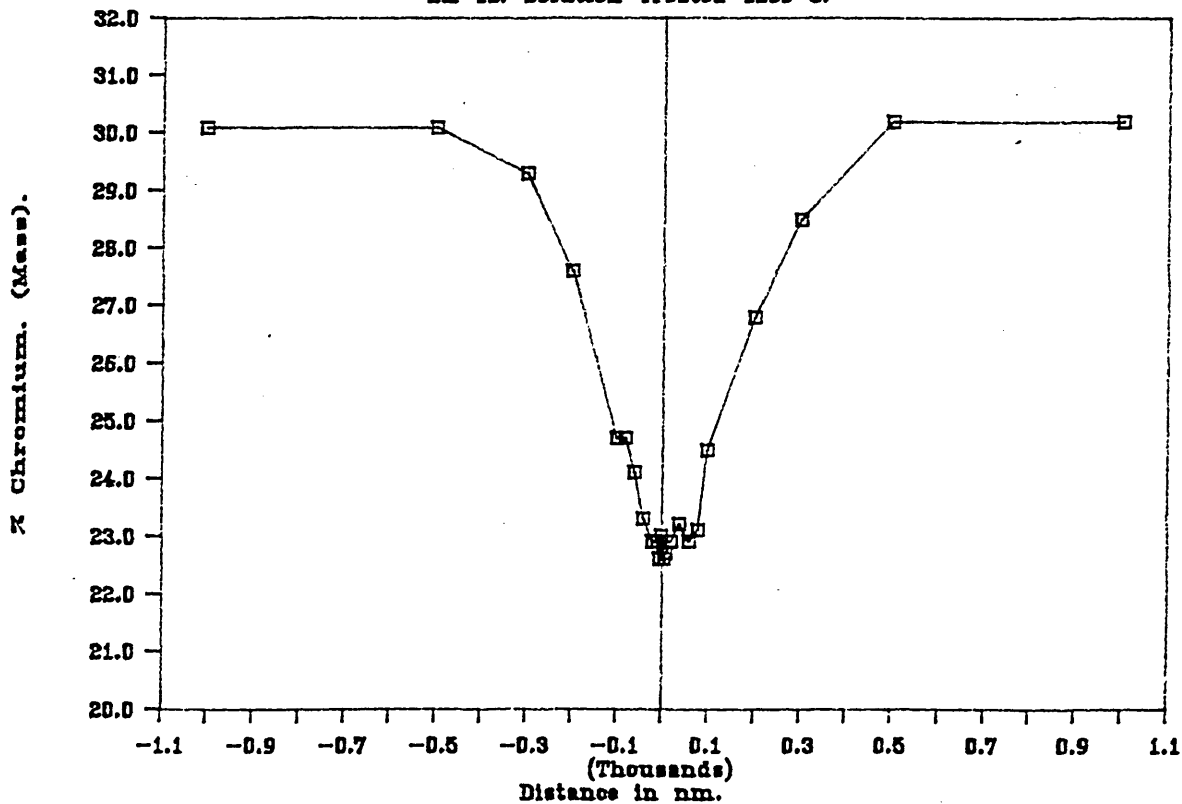


FIG.50

Nickel Enrichment Profile. Tube C.

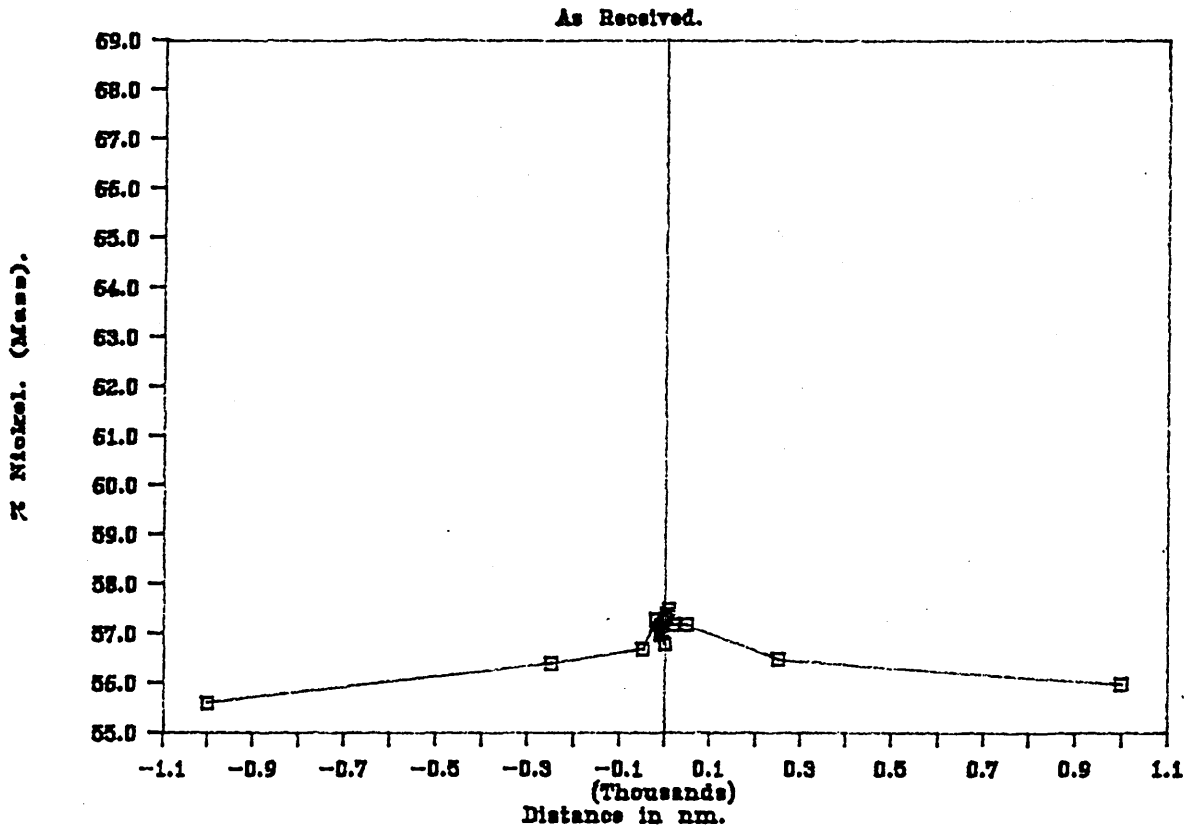


FIG.51

Chromium Depletion Profile. Tube C.

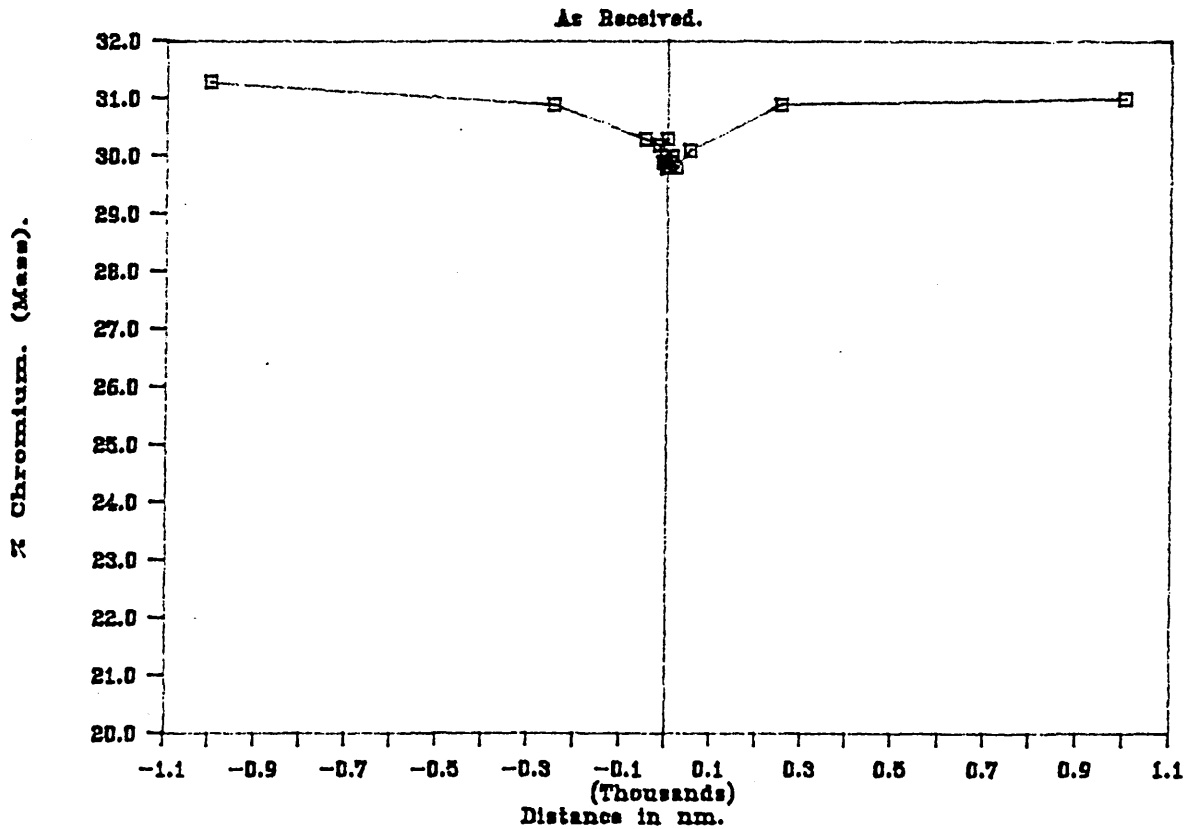


FIG.52 Tube E. Exposed to a 50% deaerated NaOH environment at 340°C for 1800 hours. Intergranular attack occurring on inside edge (compressive) of C ring specimen. (450x mag)



FIG.53 As above, but cracks are on outer (tensile) edge of C ring. (550x mag)

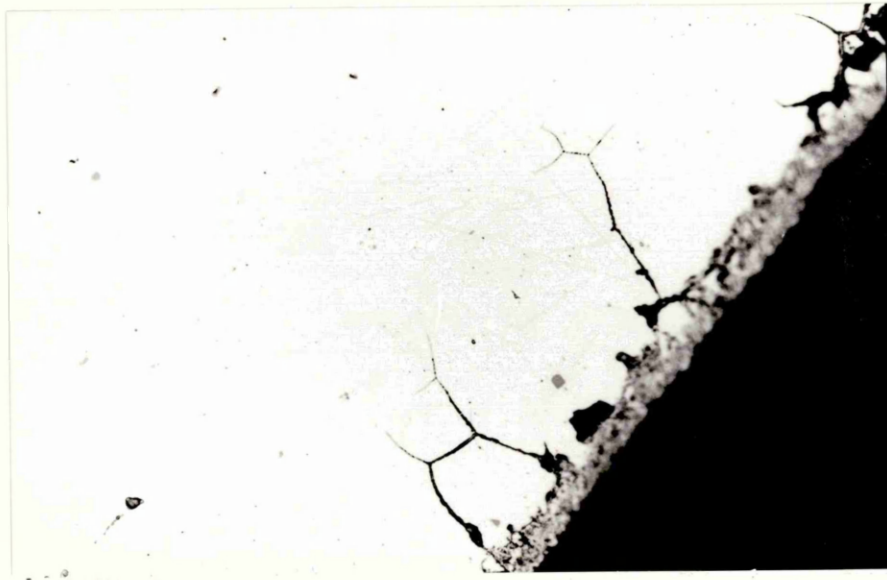


FIG.54 Striations due to belt polishing running perpendicular to the tube length on the outside diameter of Tube E. (1280x mag) S.E.M.

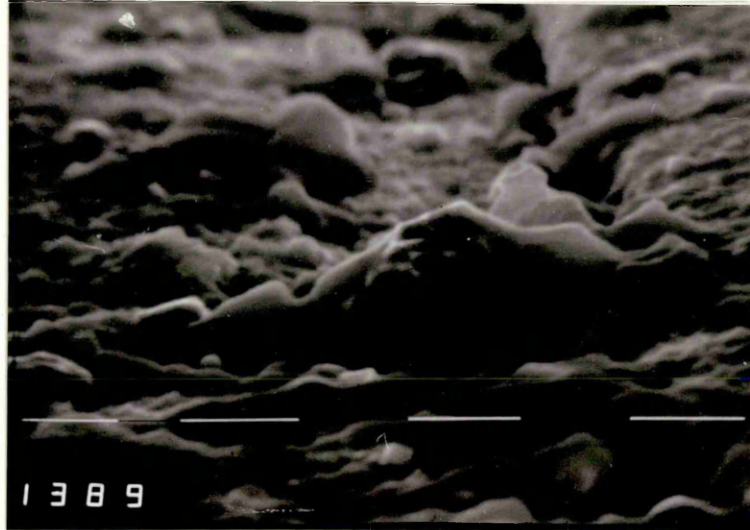


FIG.55 Alloy 600. SCC root of bolt thread. Exposed to a 50% deaerated NaOH environment at 340°C for 1800 hours. Etched in Kollings reagent. (375x mag)



FIG.56 Alloy 600. Intergranularly attacked areas on nut and bolt section. Total penetration had occurred in many places, especially highly stressed areas. (50x mag)

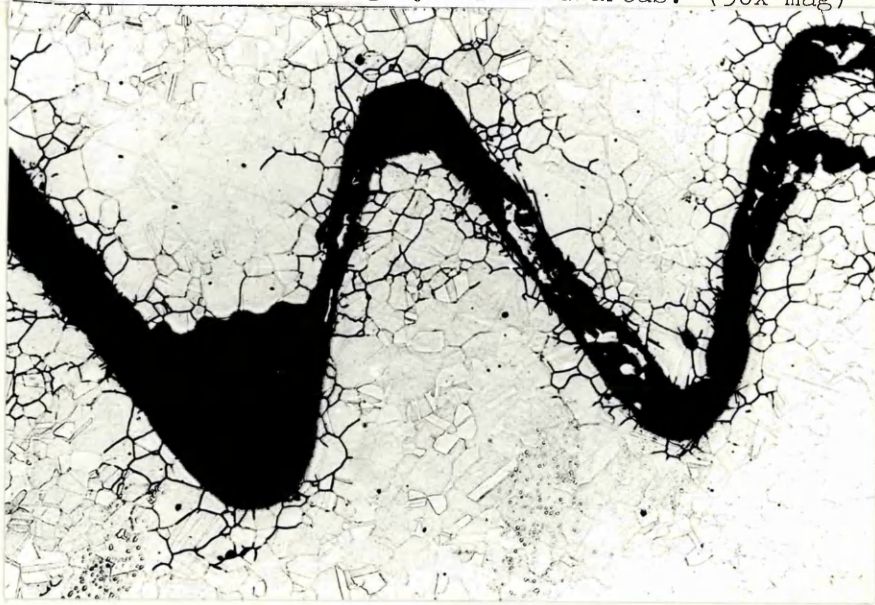


FIG.57 Alloy 600. Bolt thread completely penetrated. Exposed to 30% NaOH + 10% Na₂SO₄ environment at 340°C.

x150

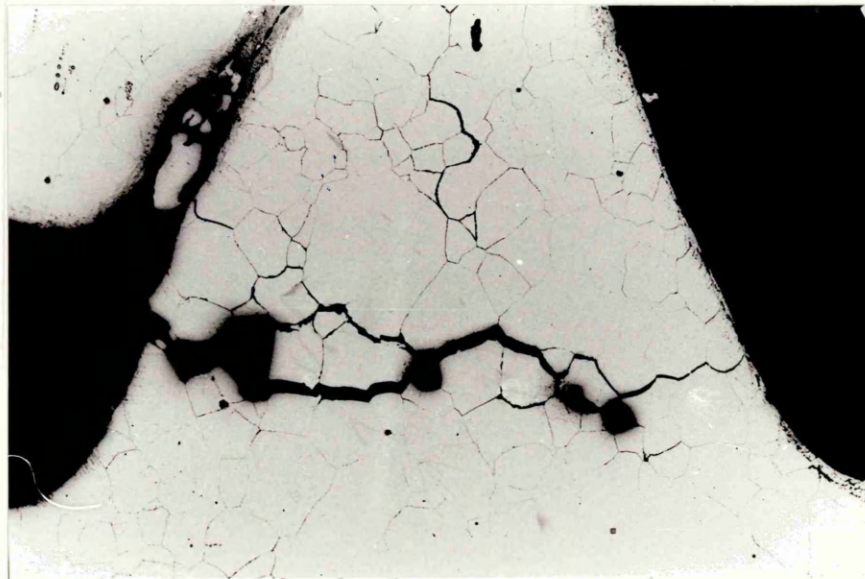


FIG.58 The effect of prior deformation between 10% and 35% on recrystallisation temperature for mill annealing temperature between 1000°C and 1100°C

Hardness vs % Deformation. EM 12.

Annealed between 1000 - 1100°C

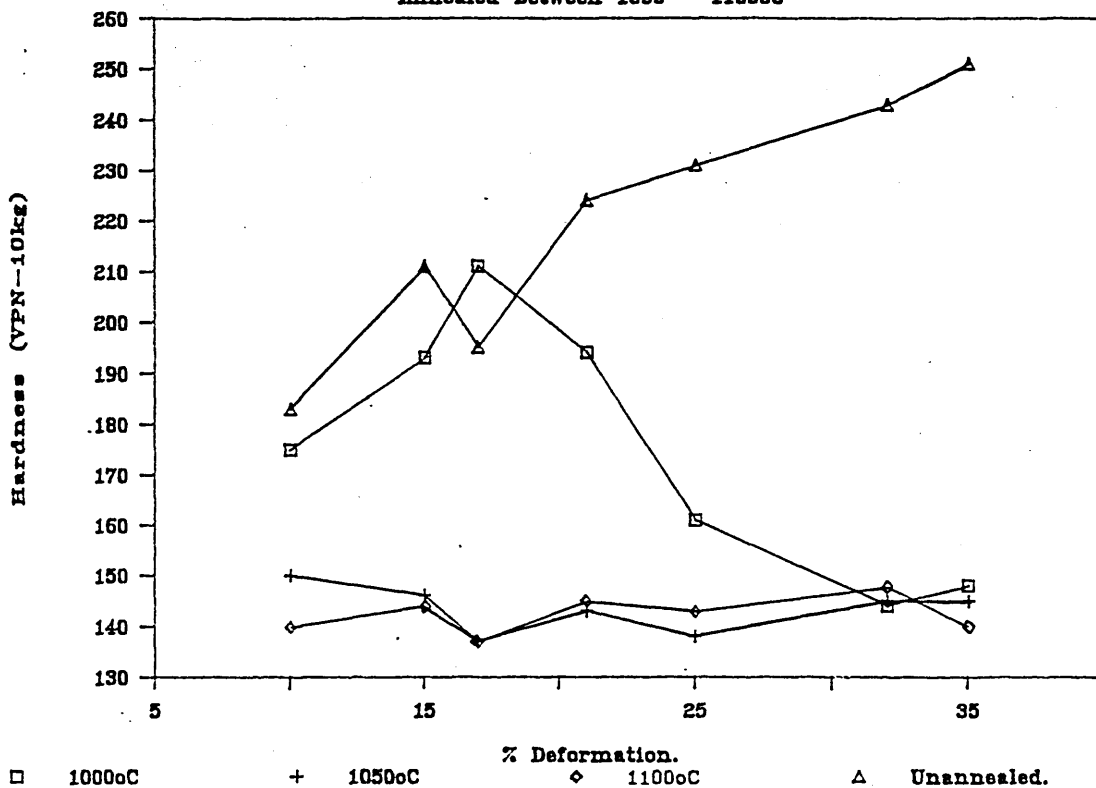


FIG.59(a)

Relationship Between Mass Fraction of Undissolved Cr^{236} and Grain Size.

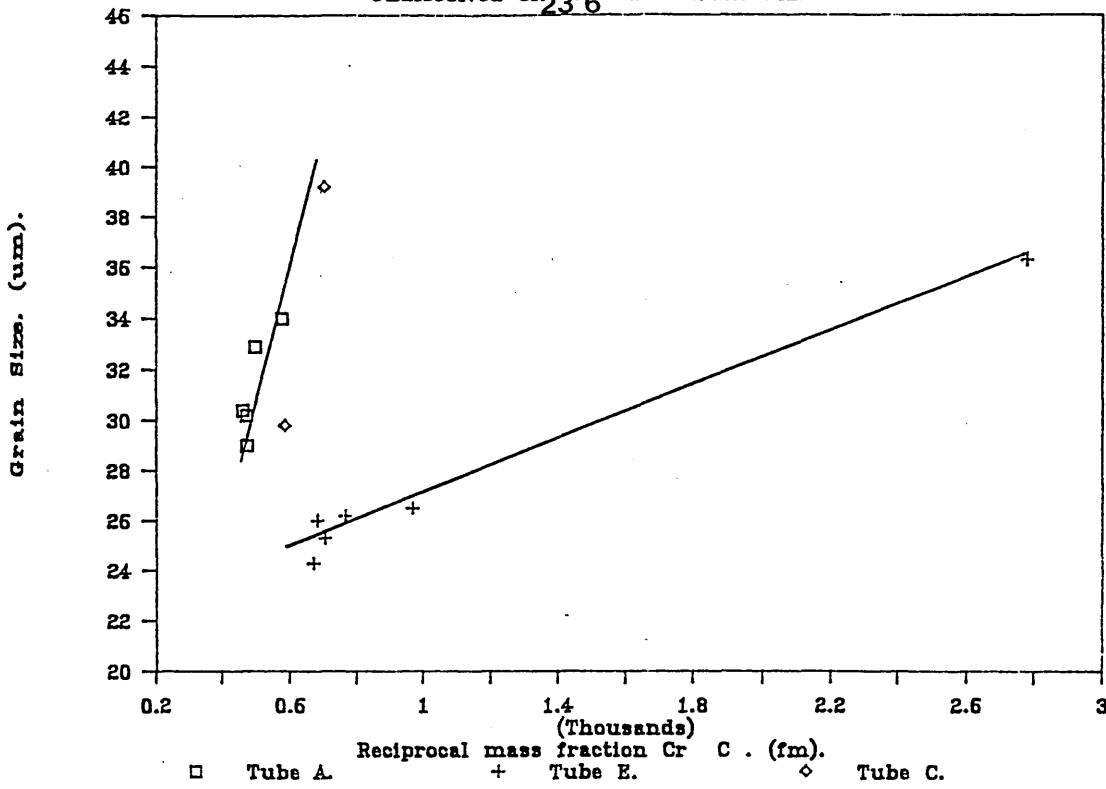


FIG.59(b)

Relationship Between Reciprocal of mass % Undissolved TIC and Grain Size.

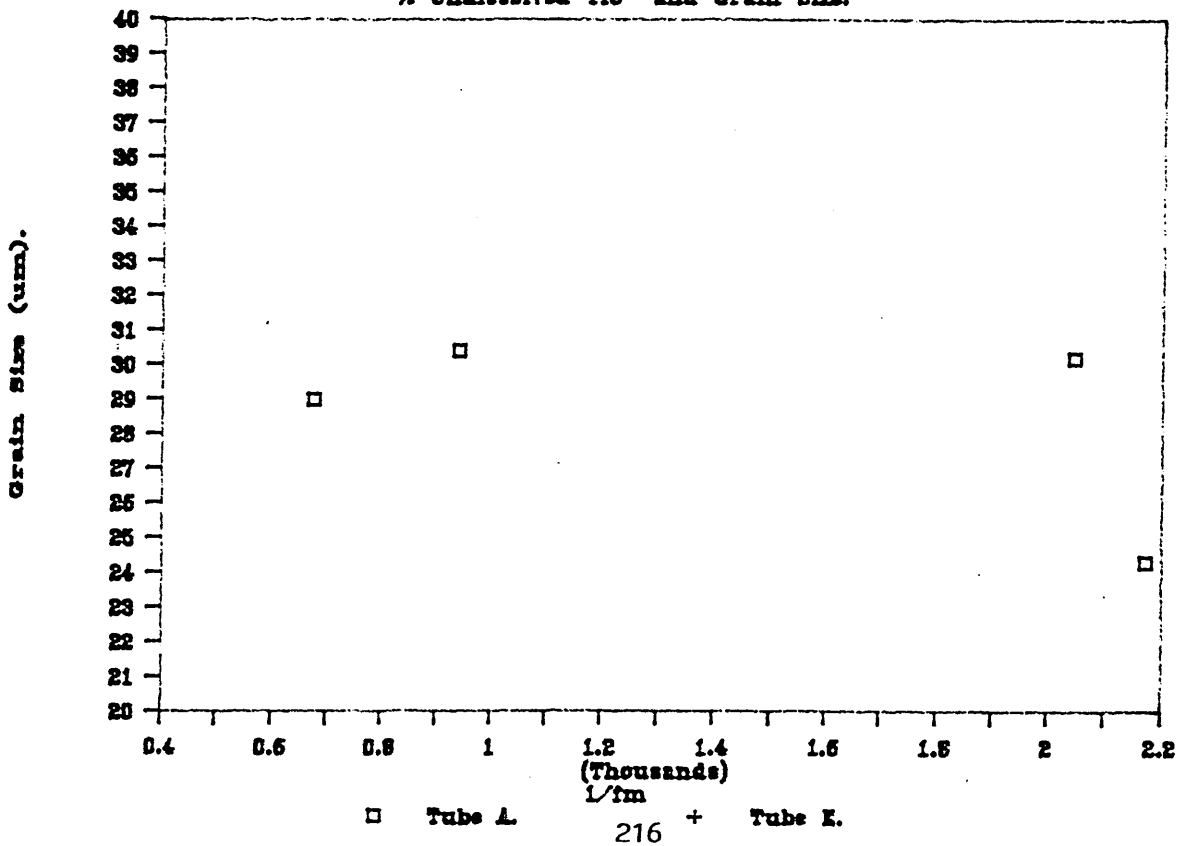


FIG.60 Grain size inhomogeneity in as-received Tube A.
Outer edge. (160x mag)

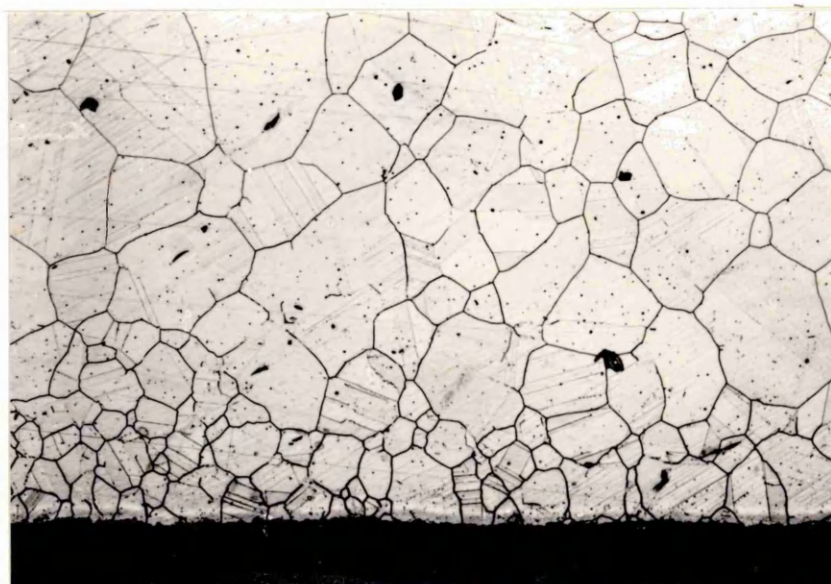
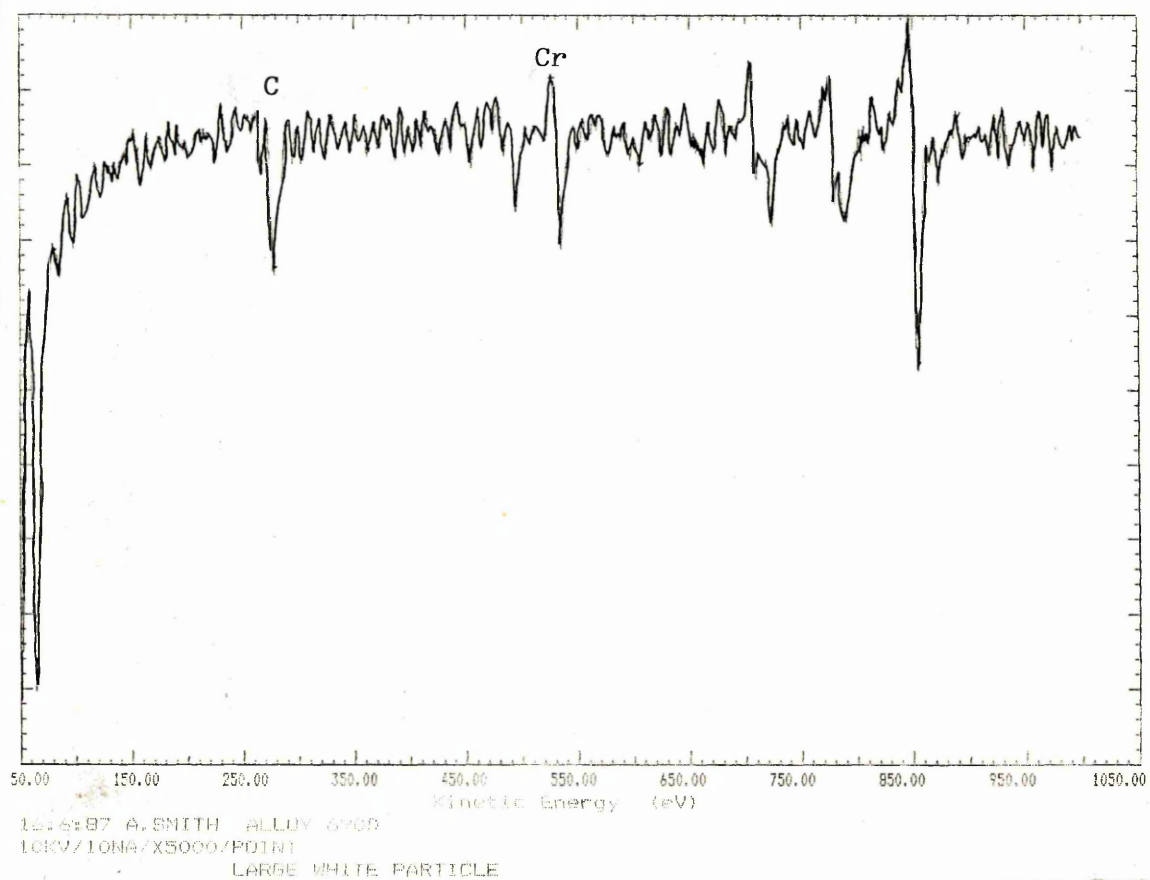
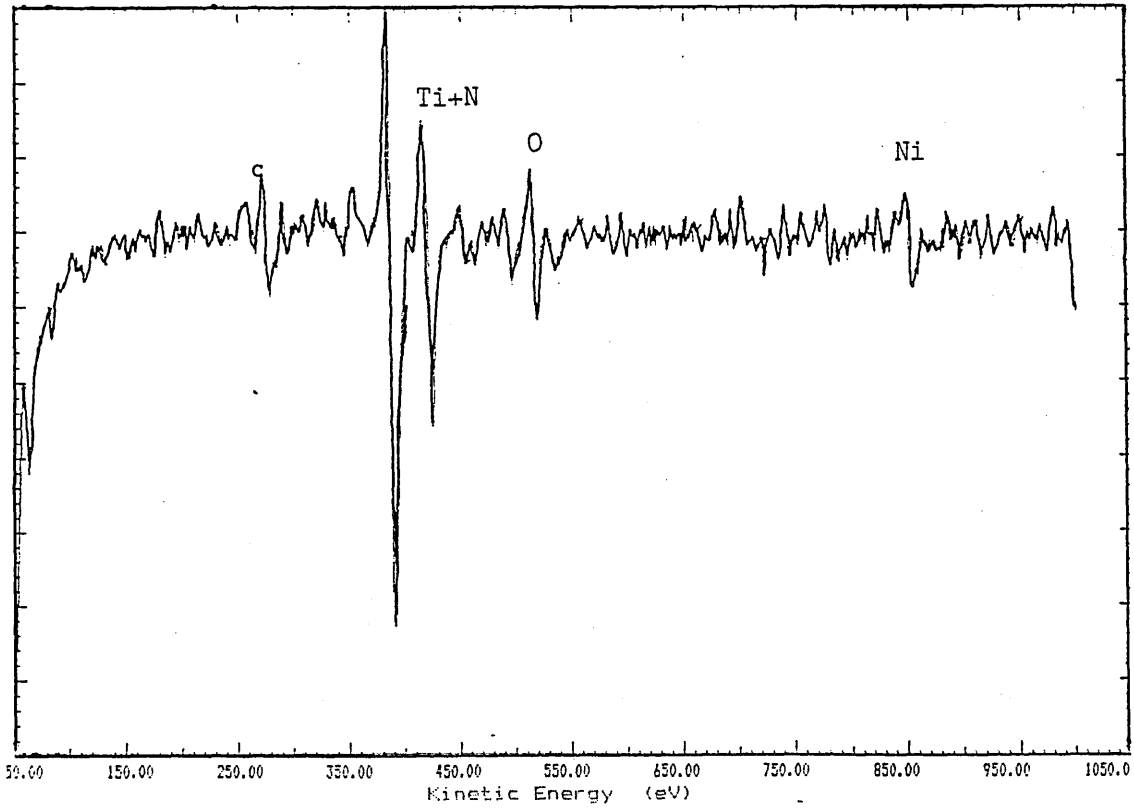


FIG.61 Chromium carbides

Relard Ratio = 4 Max Plotted Count Rate = 6766
Step Size = 0.25 eV. 3 Scans of 3800 channels at 20 ms per chan

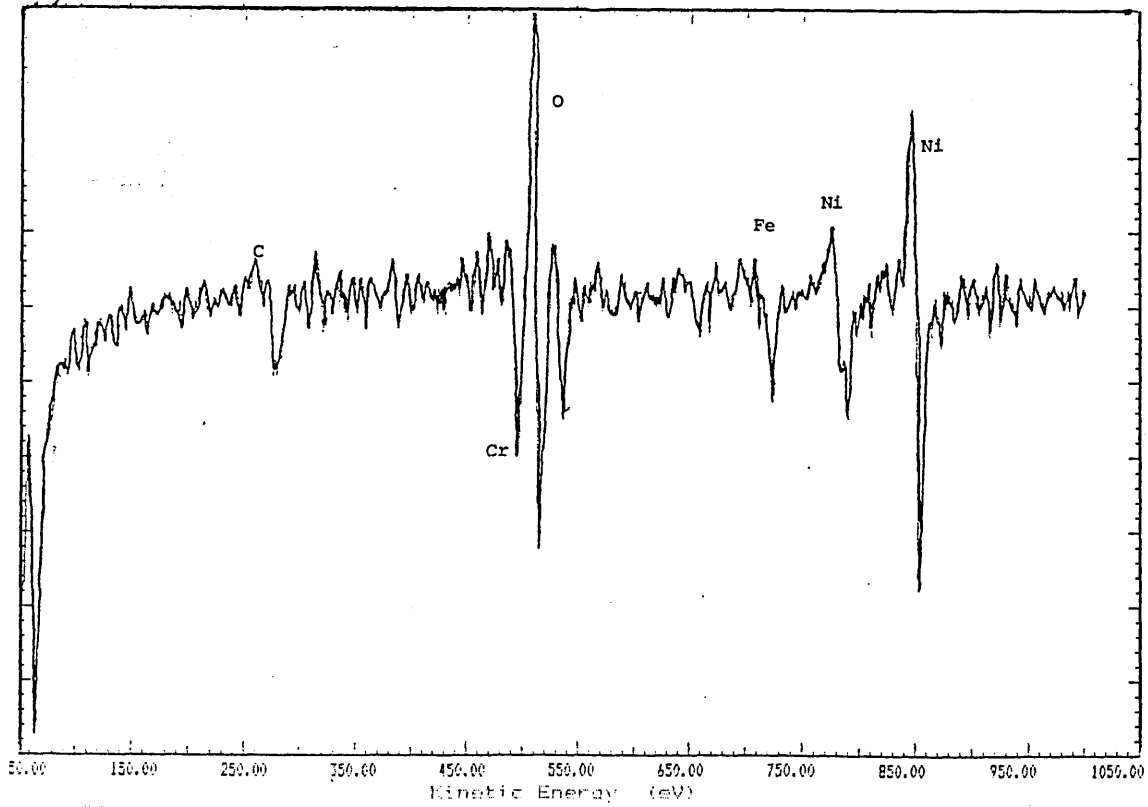


10000 Titanium Nitride
 Total Counts = 5400
 Step Size = 0.25 eV. 3 Scans of 3800 channels at 20 ms per chan



1e:4:07 A. SMITH ALLOY 690D
 10KV/10NA/X5000/POINT
 ROUNDED PARTICLE

Total Counts = 3266
 Step Size = 0.25 eV. 3 Scans of 3800 channels at 20 ms per chan



1e:4:07 A. SMITH ALLOY 690D
 10KV/10NA/X5000/POINT
 WHITE STRINGER

FIG. 63 Stringer orientated in the direction of Pilgering
 identified as Cr-rich spinel

FIG.64 Typical grain size inhomogeneity of experimental melts (160x mag)

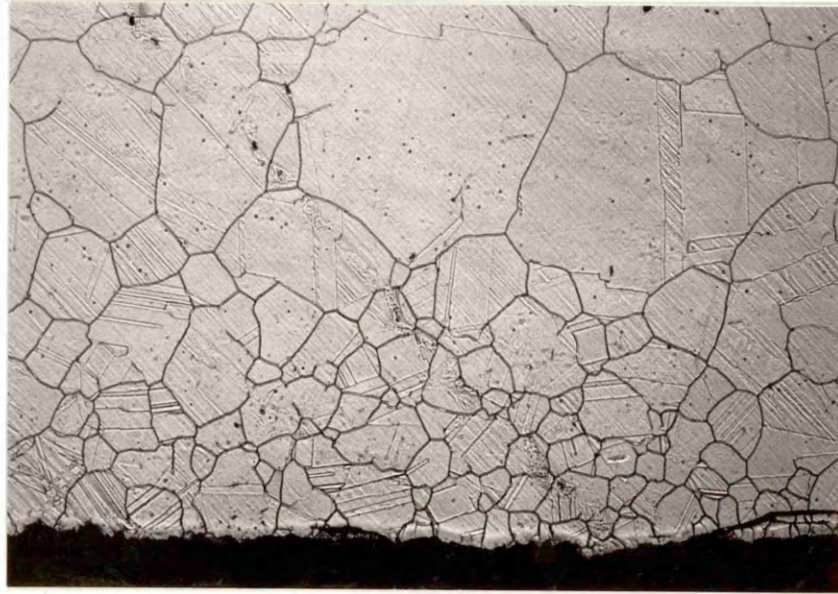


FIG.65

Log D vs 1/T. Tubes A and E with Experimental Melts 12 and 13.

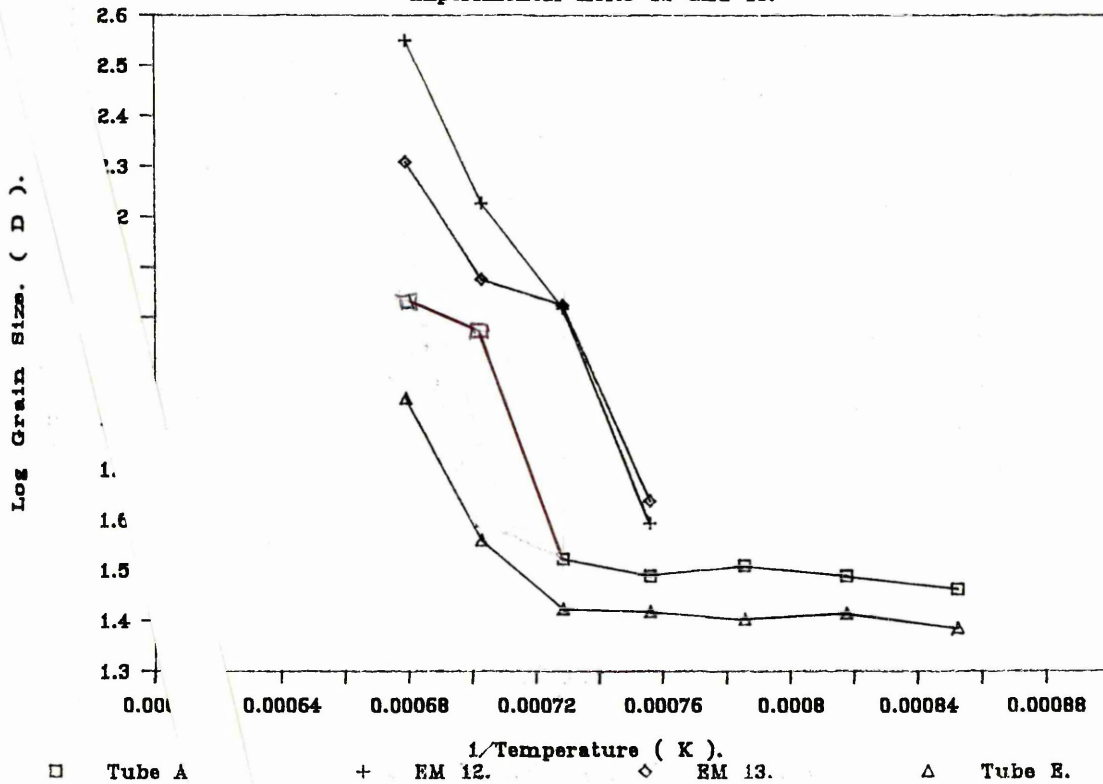


FIG. 66

Log D vs 1/T. Tube A.

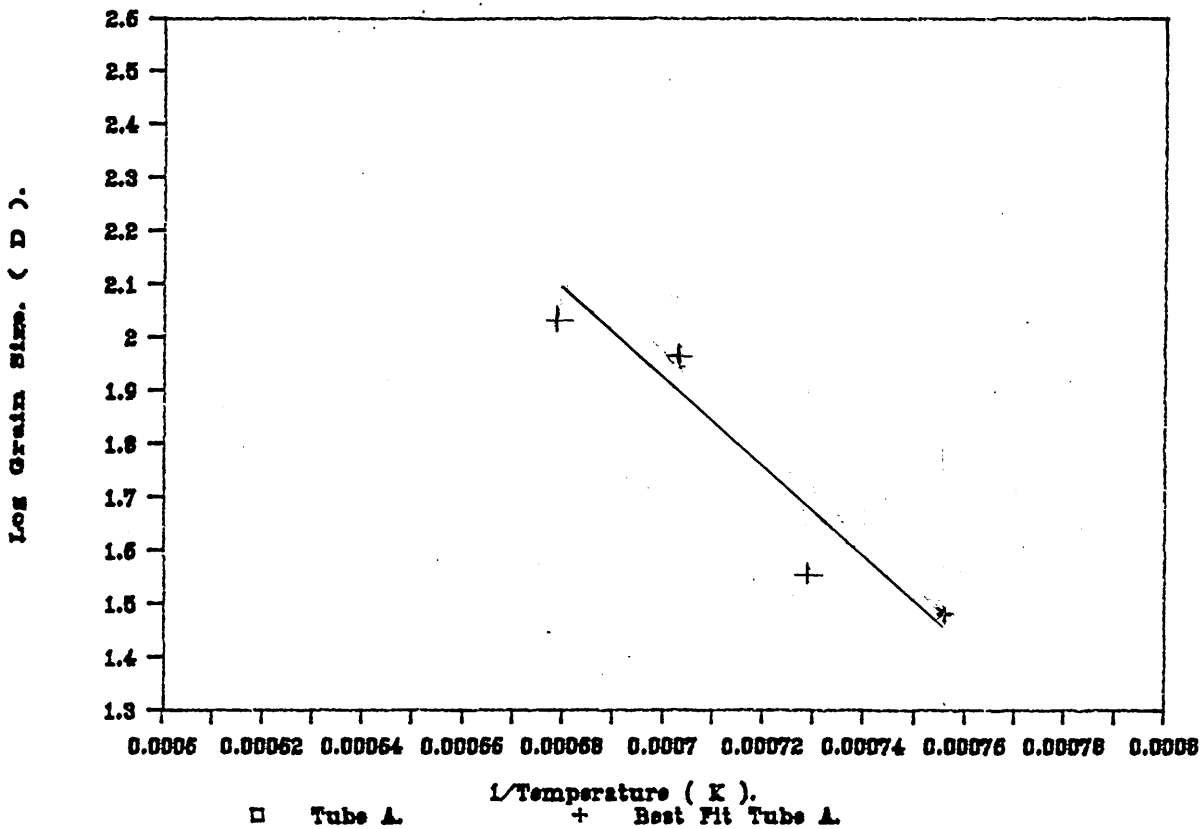


FIG. 67

Log D vs 1/T. Tube E.

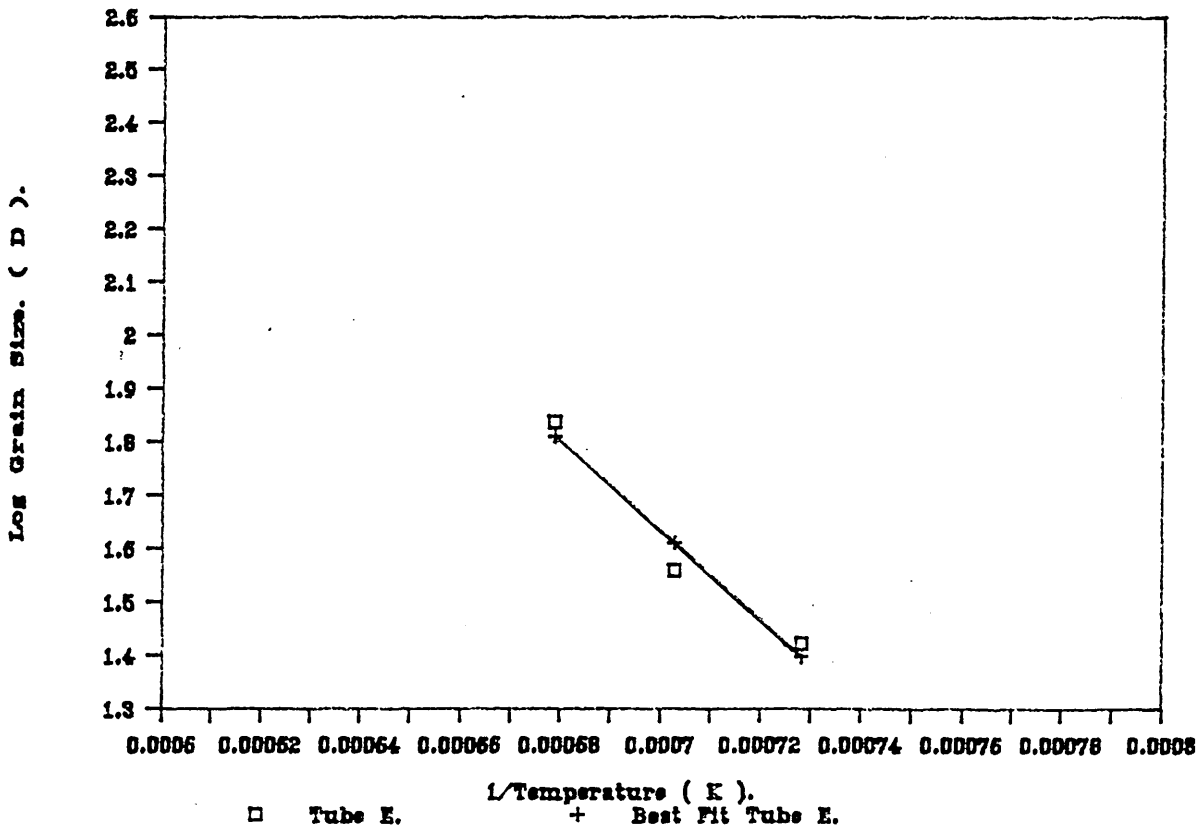


FIG.68(a)

Log D vs 1/T. EM 1.

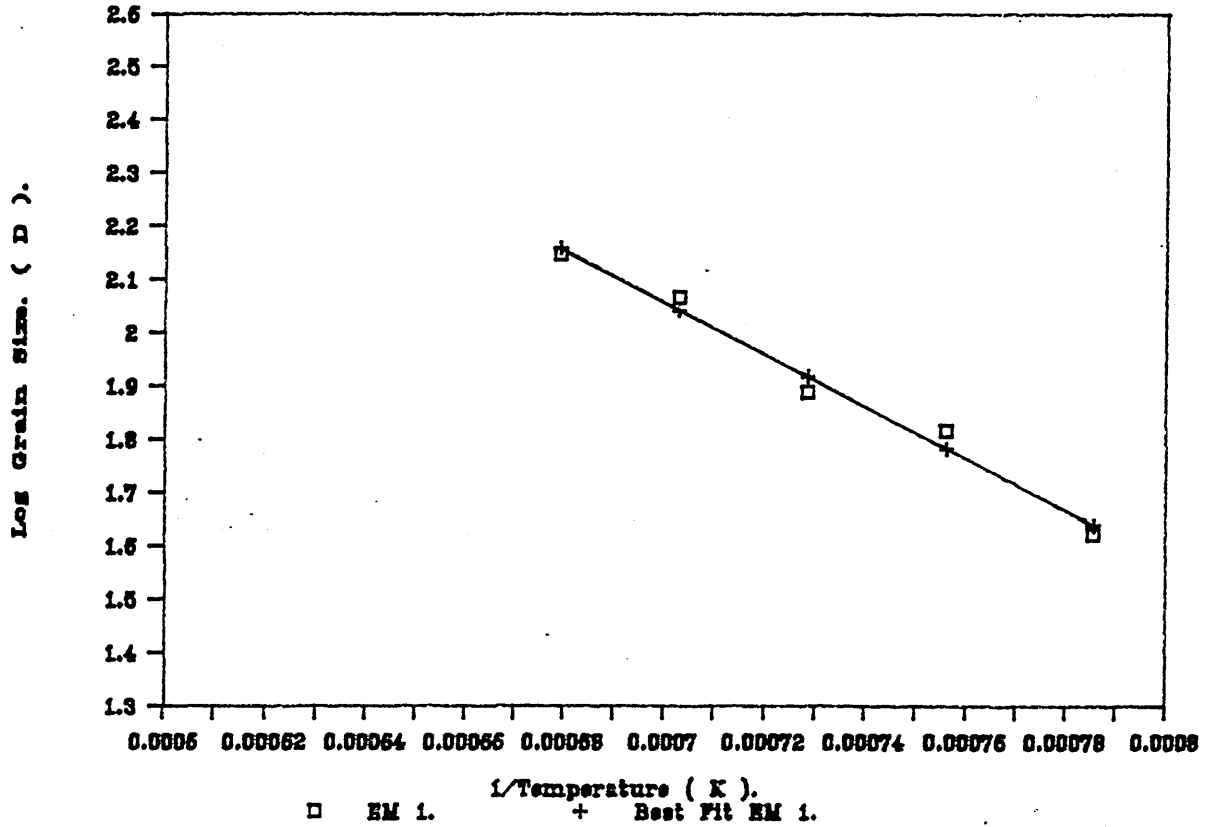


FIG.68(b)

Log D vs 1/T. EM 5.

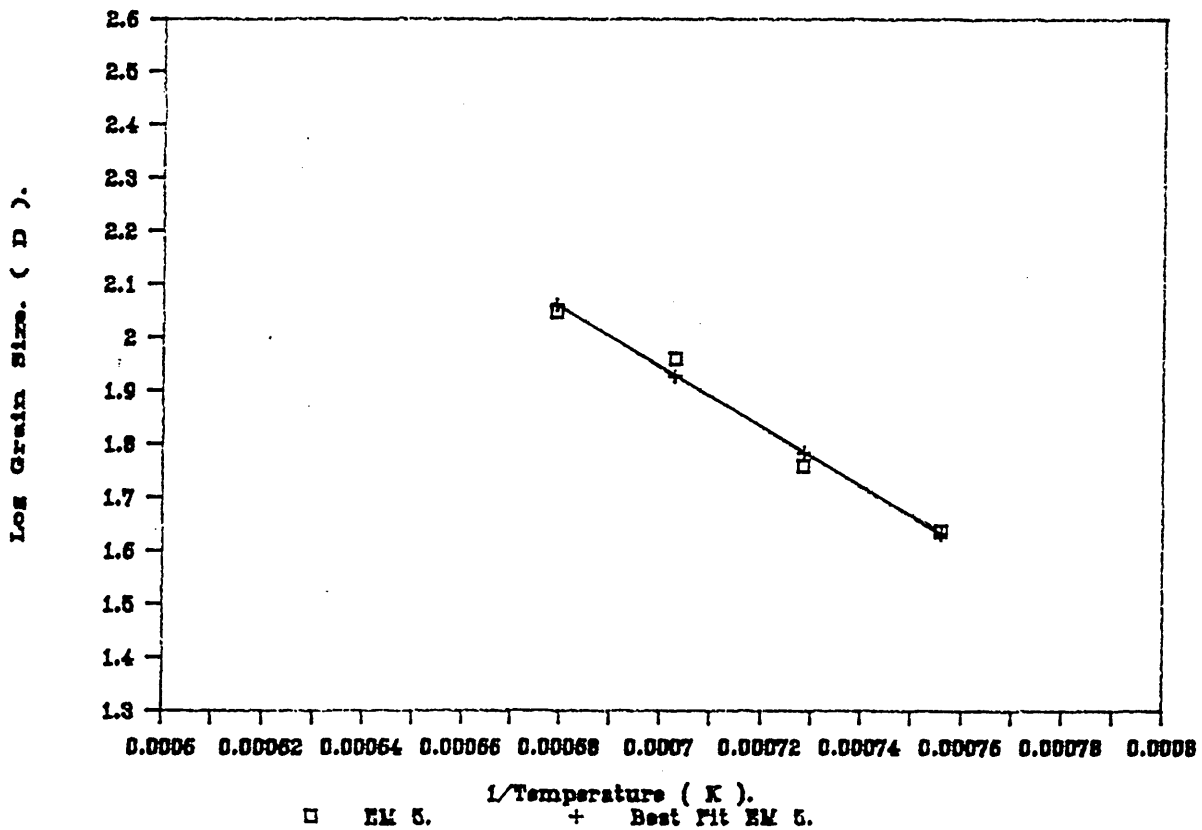


FIG.69

Log D vs 1/T. EM 12.

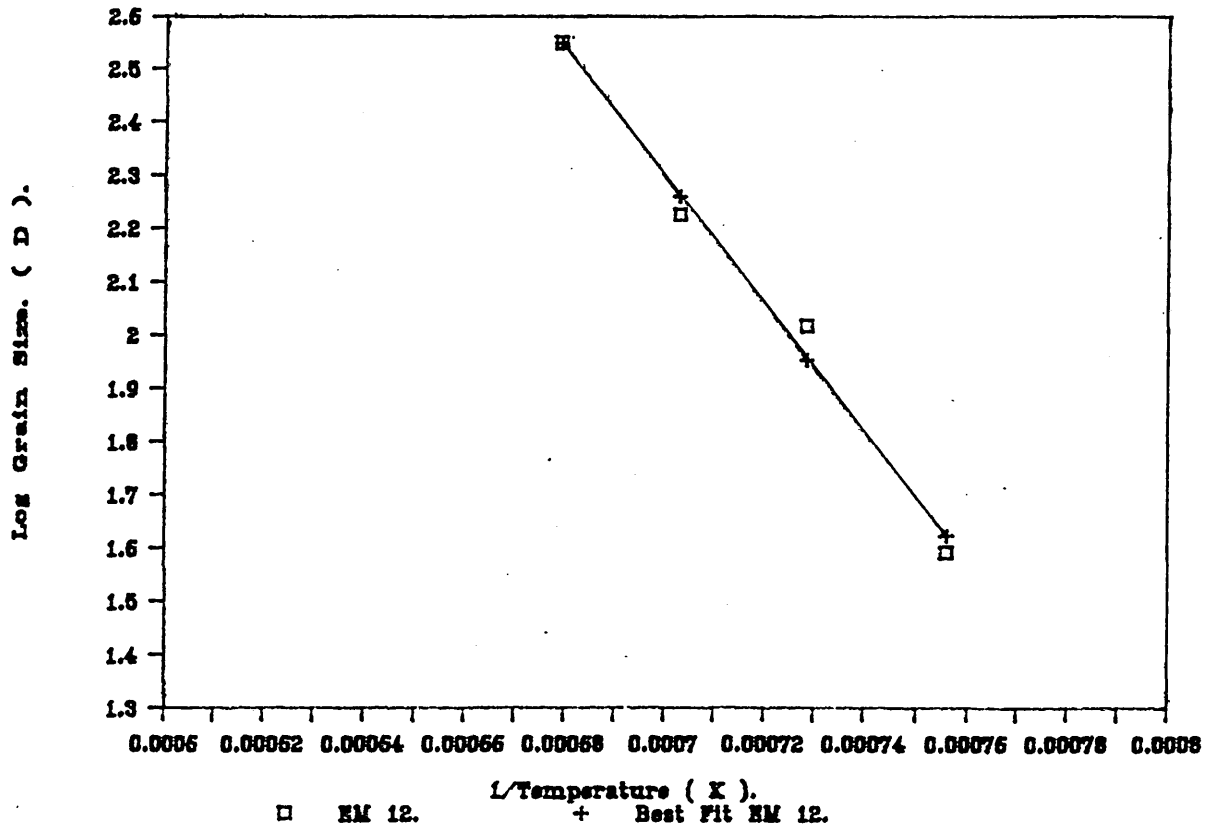


FIG.70

Log D vs 1/T. EM 13.

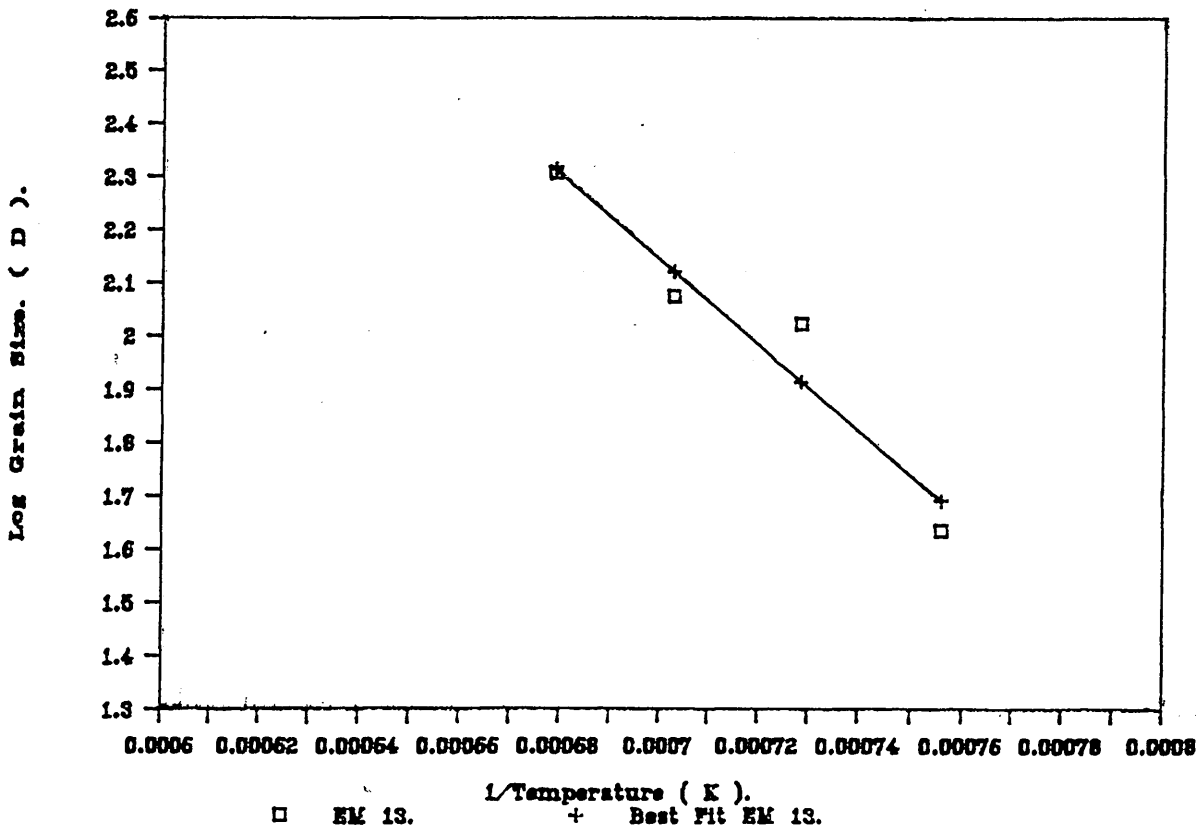


FIG.71

Log D vs 1/T. EM 7.

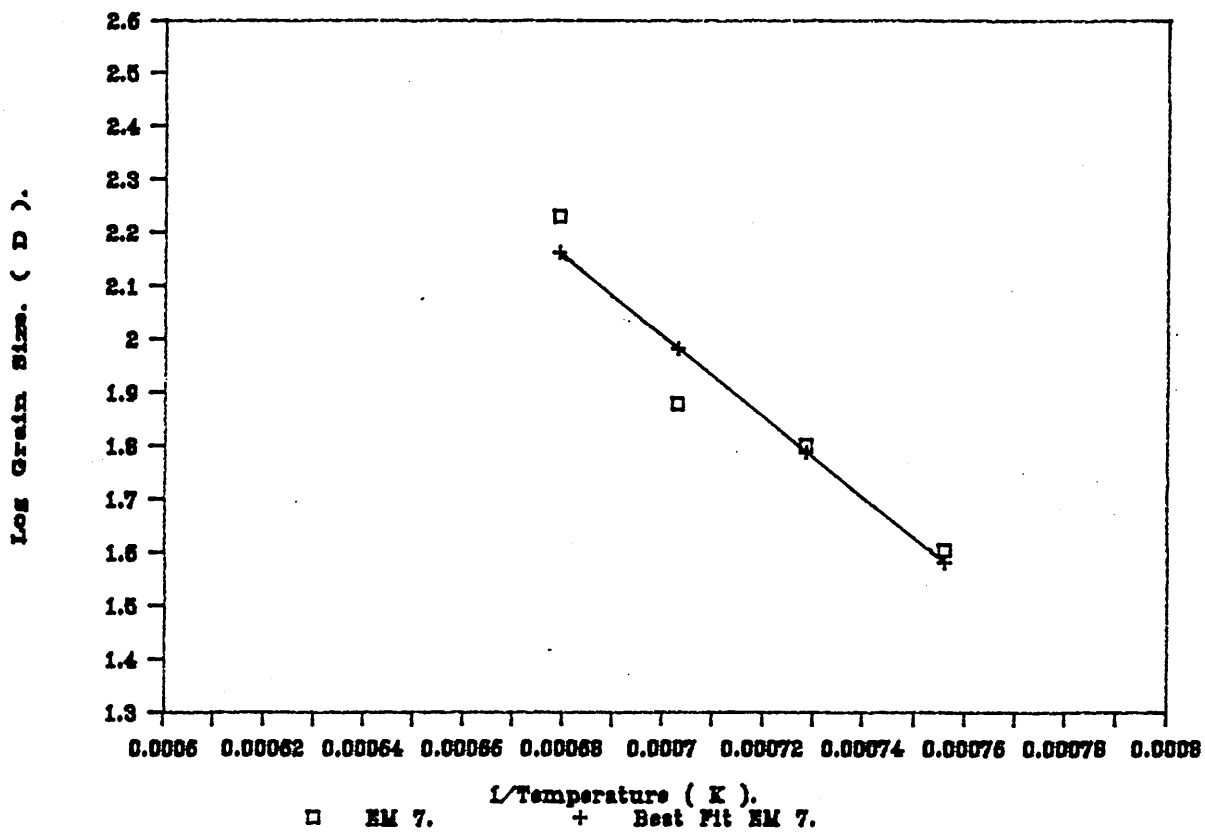


FIG.72

Log D vs 1/T. EM 11.

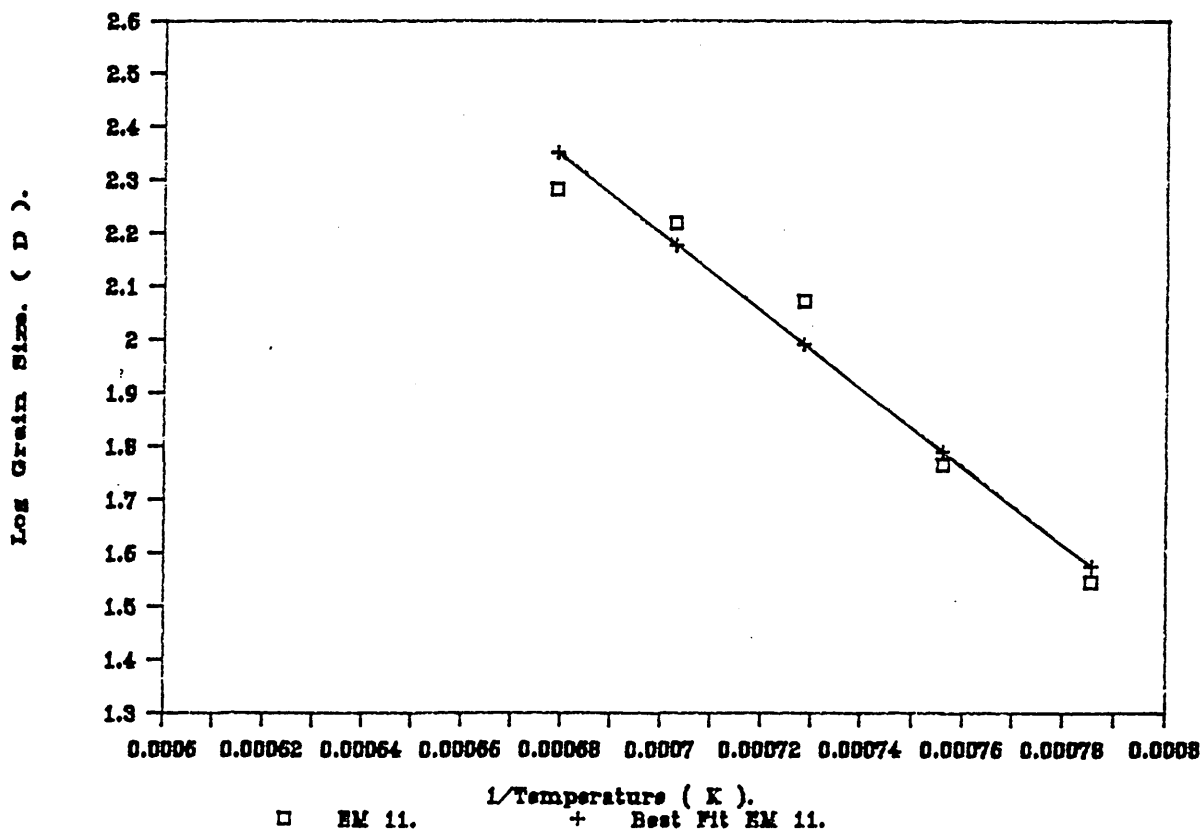


FIG.73

Log D vs 1/T. EM 8.

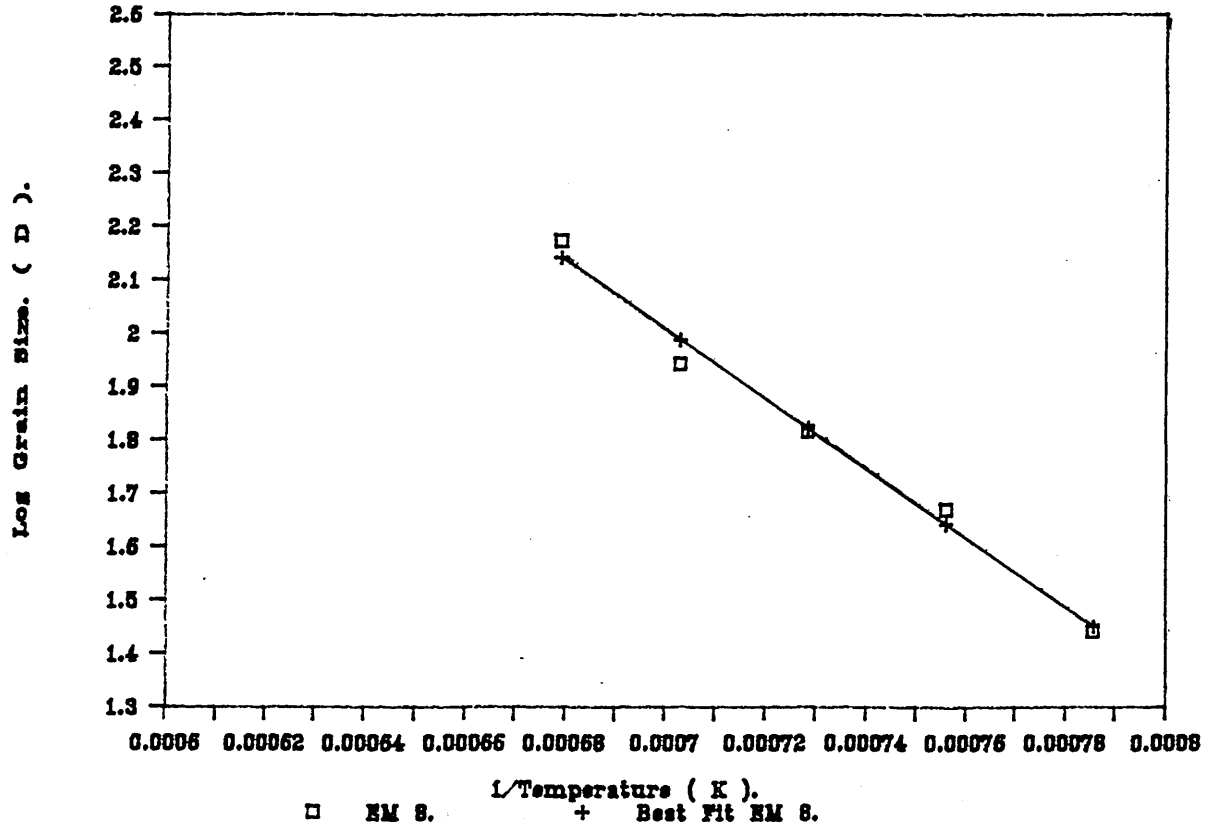


FIG.74

Log D vs 1/T. EM 10.

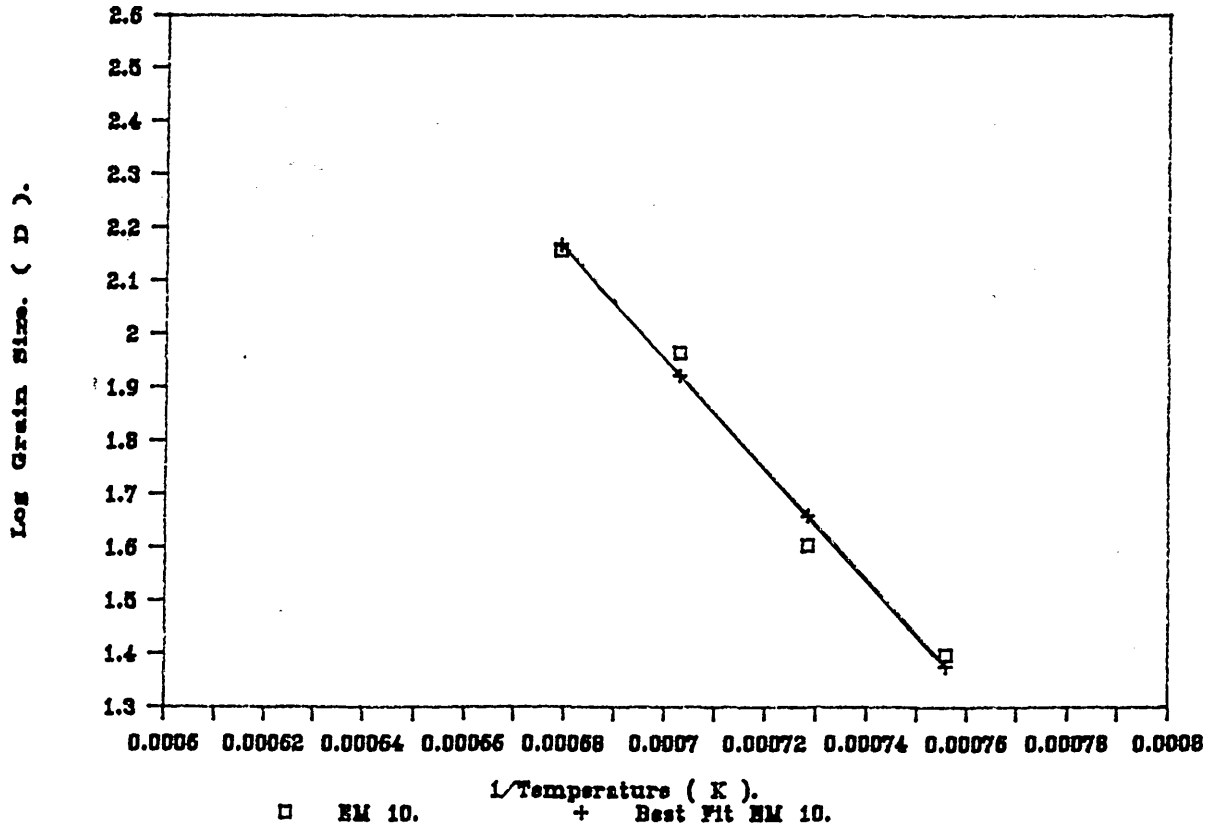
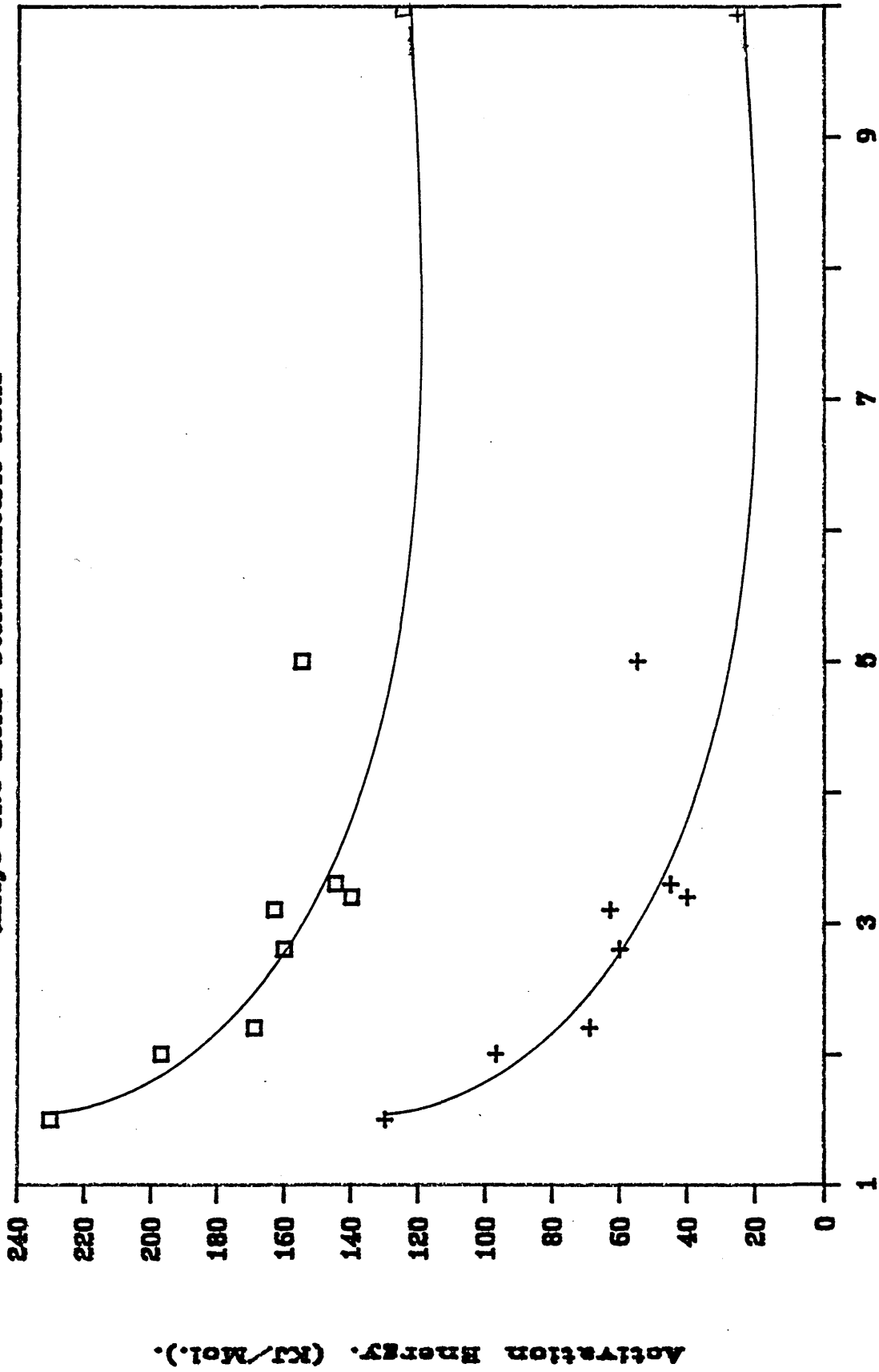


Fig. 75

Activation Energy for Grain Growth Vs.

Alloys Ti:C Molar Stoichiometric Ratio



Alloys Ti:C Molar Stoichiometric Ratio.
+ Effect of Ti:C Ratio

□ Total act. Energy.

Activation Energy. (KJ/Mol.)

FIG.76(a)

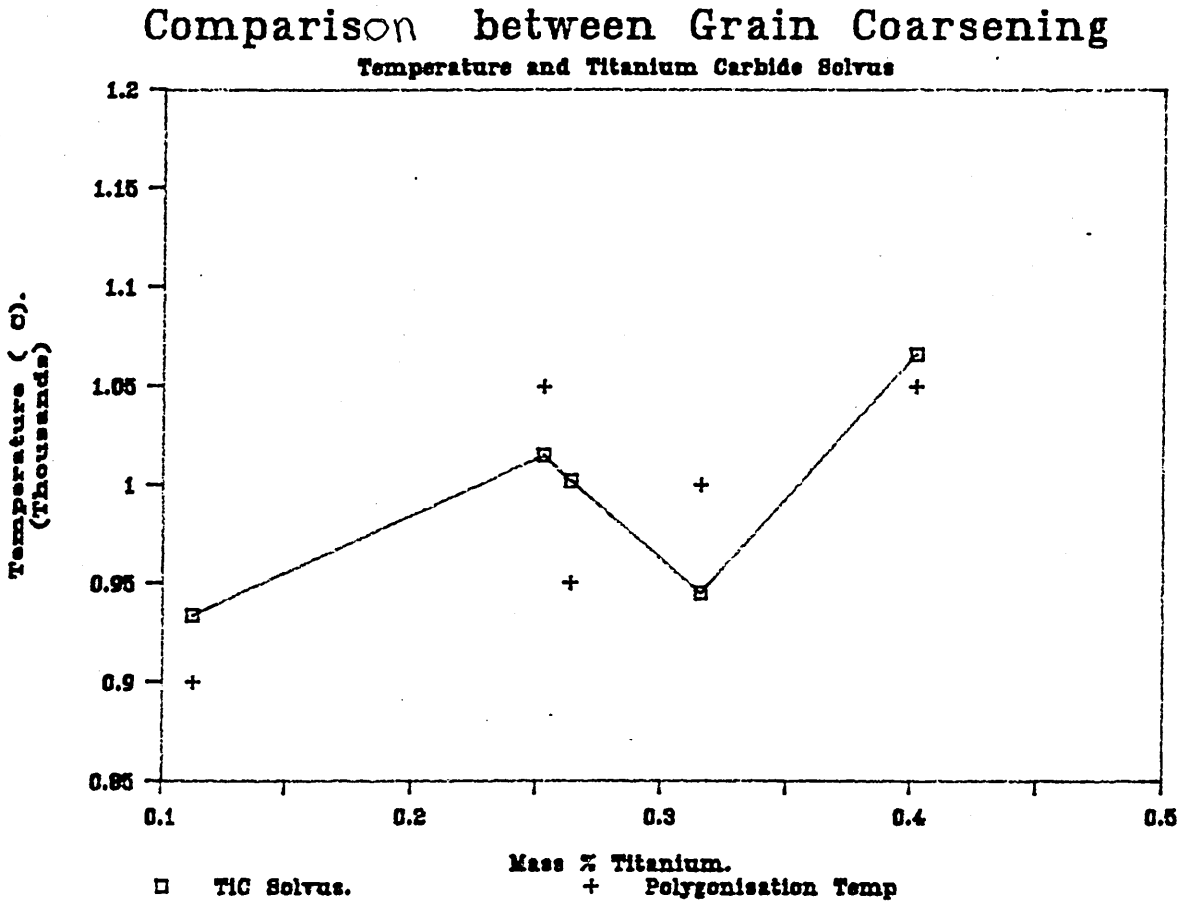


FIG.76(b) Comparison between Grain Coarsening
Temperature and Chromium Carbide Solvus

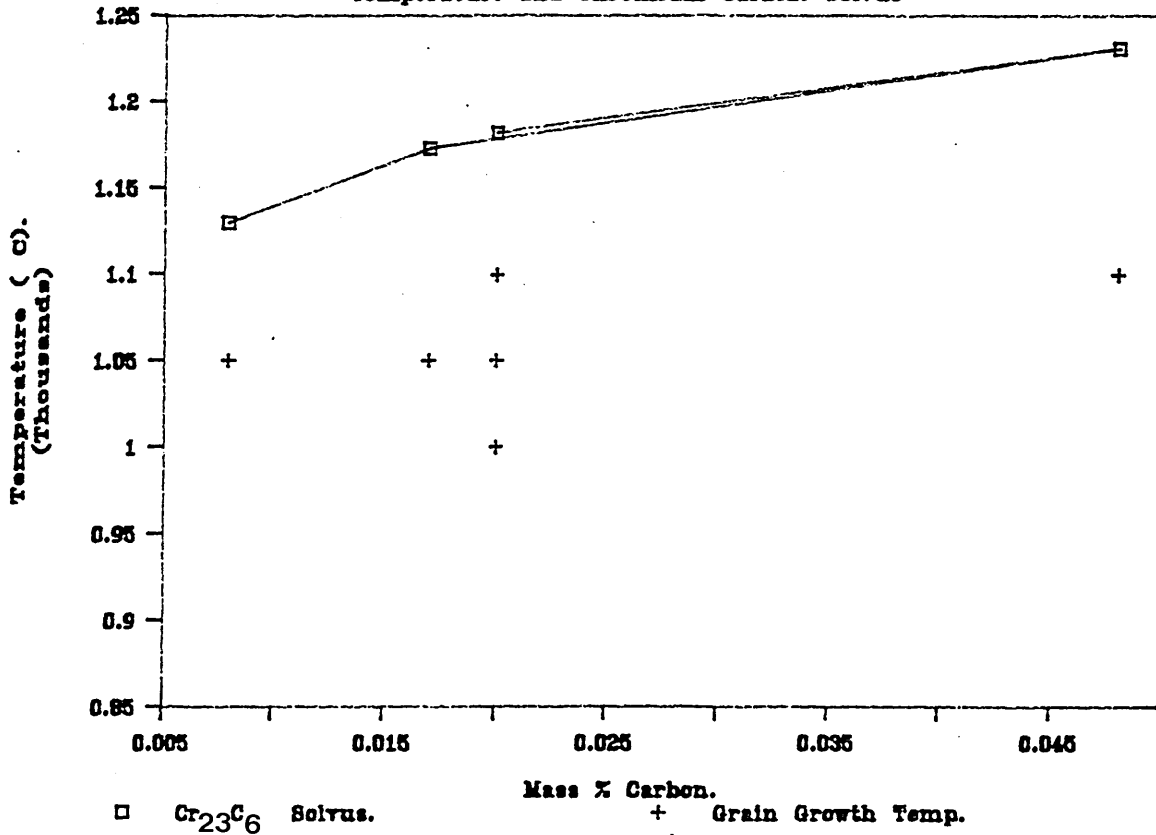
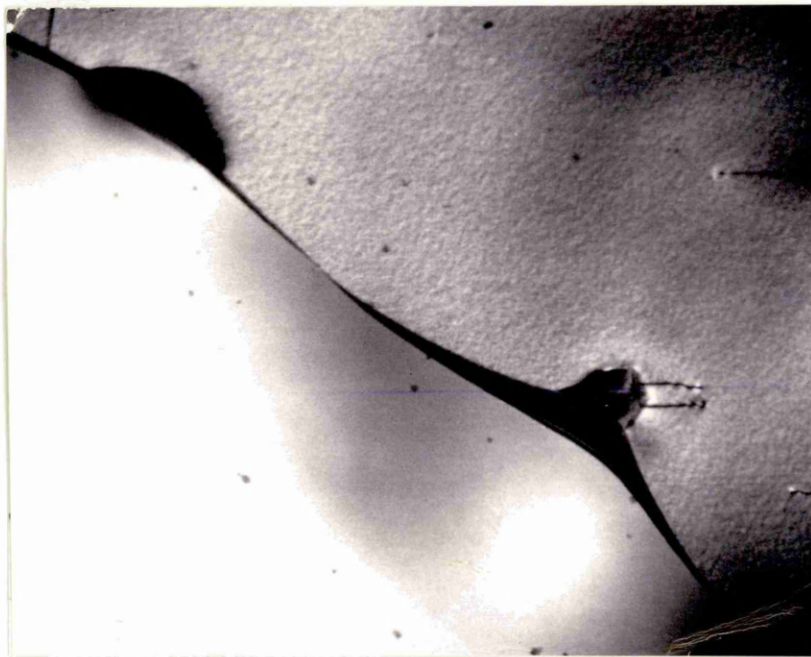


FIG.77



As-received Tube C. Evidence of dual pinning of grain boundary between Cr_{23}C_6 (upper LHS) and TiC (Lower RHS) S.T.E.M. $\times 50\text{K}$

FIG.78(a) Coarse Ti-rich grain boundary carbide. ST 1200°C
Aged at 700°C for 5 mins. S.T.E.M.

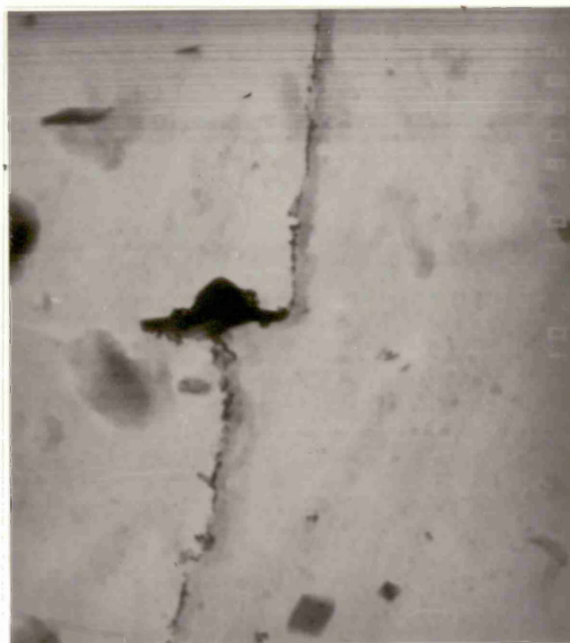


FIG.78(b) Coarse Ti-rich grain boundary carbide. ST 1200°C
Aged at 700°C for 5 mins. S.T.E.M.

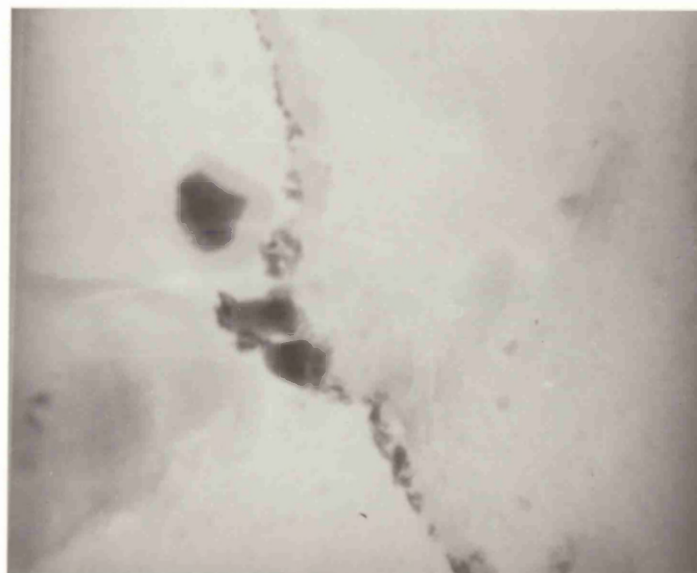


FIG.79 EDX analysis taken from the matrix of an alloy 600 bolt used to stress C ring specimens in a 50% NaOH deaerated environment at 340°C

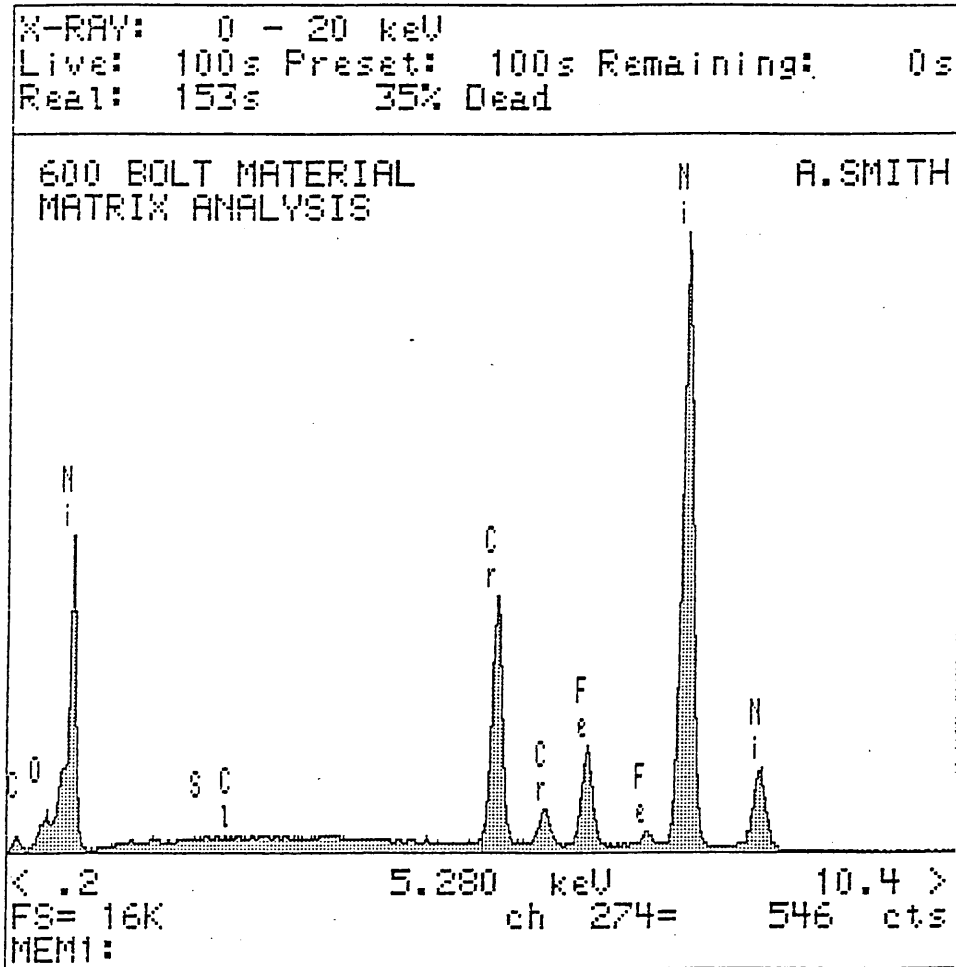


FIG.80 EDX analysis taken from an intergranularly attacked area of an alloy 600 bolt (see Fig.79) for matrix composition

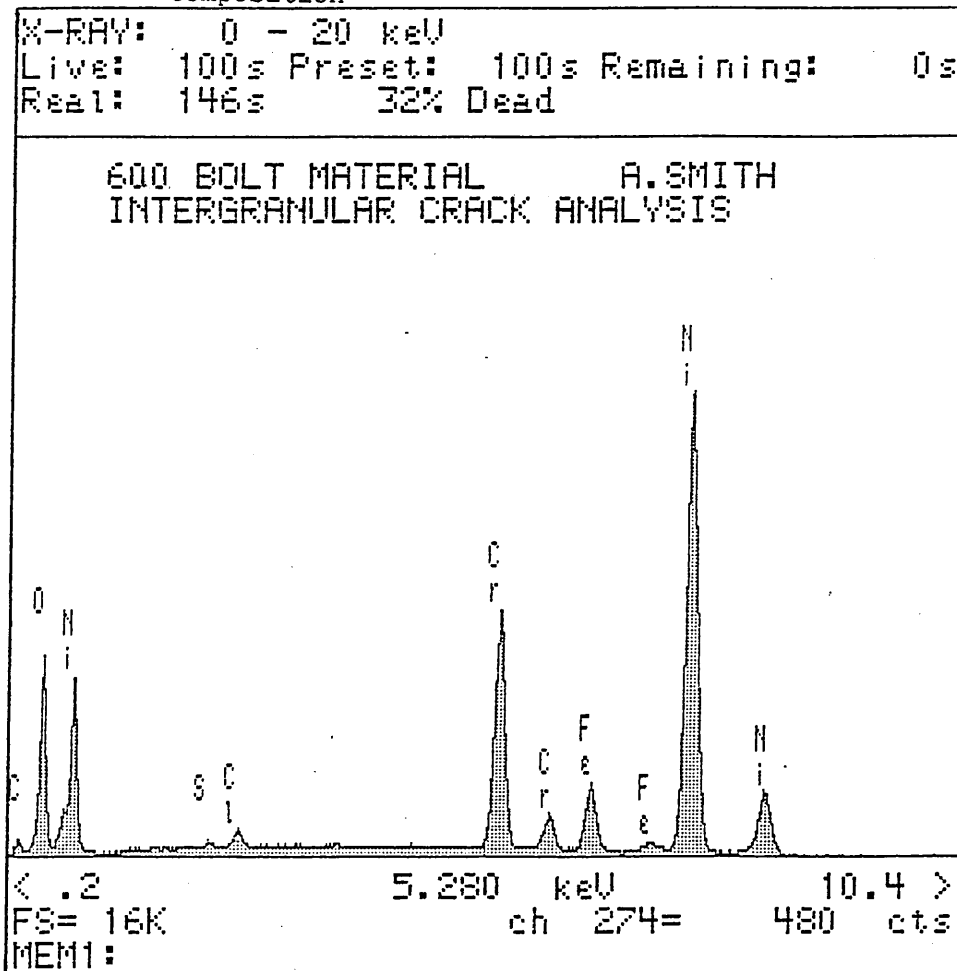


FIG.81 EDX analysis taken from the matrix of an alloy 690 C ring specimen which had been exposed to a 50% deaerated NaOH environment at 340°C

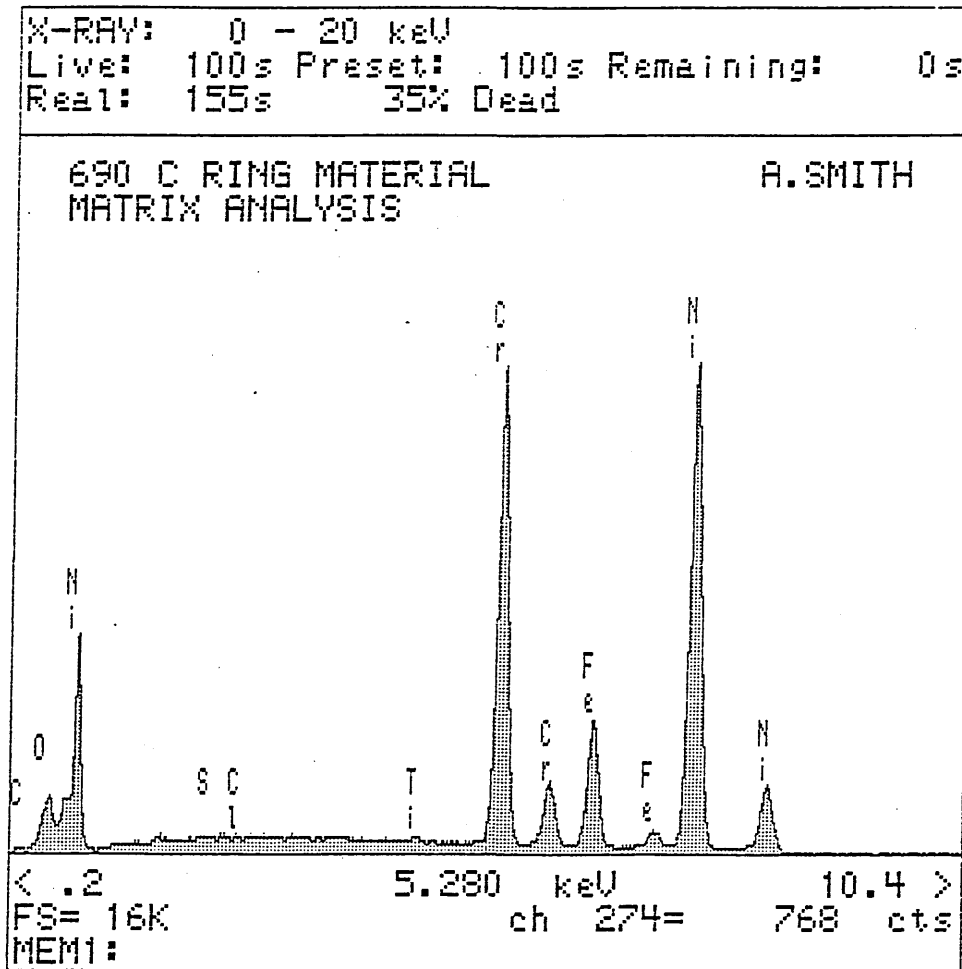
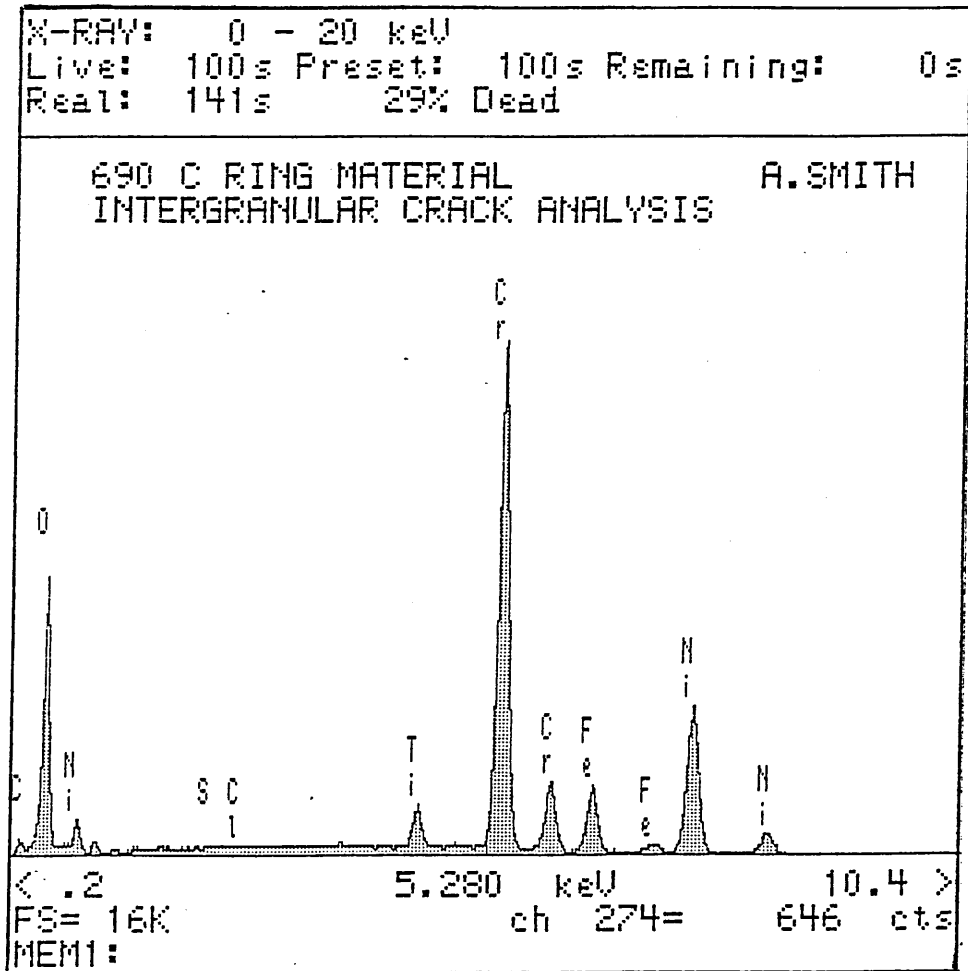


FIG.82 EDX analysis taken from an intergranularly attacked C ring specimen of alloy 690 (See Fig.81) for matrix composition



APPENDIX A.

The Effect of Composition and Thermal Treatment on the Corrosion Resistance of Selected Experimental Alloys in a Deaerated 30% NaOH + 10% Na₂SO₄ environment at 350°C.

Introduction.

The alloy compositions were chosen to examine the effects of:

- (1) Varying carbon content in the absence of both Al and Ti
- (2) Varying the Ti:C ratio for constant Al.
- (3) Varying the Al content.

All the samples were subjected to solution treatment of 1200°C for 30 minutes prior to the thermal treatment at 700°C. The thermal treatment times were 1, 5, 10, and 15 hours. Two samples from each alloy were corrosion tested in the as solution treated condition. The corrosive test environment chosen was deaerated 30 wt% NaOH + 10 wt% Na₂SO₄ at 350°C. The test duration was 1283 hours.

Results.

The results of the corrosion tests are given in table (AI).

All the samples were attacked intergranularly, fig. A1 and A2.

Measurements were taken from the edge of the crack not the surface of the corrosion product.

Discussion.

It is clear from fig. A1 that alloy 690 is not intergranularly attacked in the same way as alloy 600. It would appear that once intergranular attack in alloy 690 has moved a certain distance down a grain boundary the tip of the advancing IGA becomes "blunted". The attack then occurs perpendicular to the original direction resulting in general corrosion across the surface of the sample. It is similar in appearance to the acid wastage reported in alloy 600.

Measurements of the corrosion product varied from approximately zero to approximately $25\mu\text{m}$. Measurement of depth of IGA + corrosion product would thus be susceptible to unacceptable levels of scatter. It is for this reason that measurements were taken from the edge of the advancing IGA rather than the corrosion product, the corrosion product having exfoliated, to a lesser or greater degree, from around the periphery of the sample.

It is felt that since the main source of material loss is from uniform attack a more appropriate measurement to ascertain the effect of thermal treatment and chemical composition would be by weight loss. However since samples were not weighed before exposure this method cannot be used. It is interesting to note that the maximum crack depth in the stressed C ring samples (table XXI) was as much as three times deeper than those measured in the unstressed condition. The deepest attack of any of the samples measured in the unstressed condition was $26\mu\text{m}$. If the progression of the IGA relies on the exfoliation of the

corrosion product then it is possible that stressing the sample will encourage that exfoliation and thus allow further attack.

The Effect of Thermal Treatment on the Corrosion Resistance of Selected Experimental Alloys in Deaerated 30% NaOH + 10% Na₂SO₄ at 350°C.

The results given in table A1 confirm those given in Table XXII. After solution treating at 1200°C, a thermal treatment at 700°C for 1, 5, 10 and 15 hours appears to have no effect on corrosion resistance under the conditions of test. Further, the solution treated only alloys under went a similar depth of attack to those thermally treated. This is based on the assumption that the average corrosion product thickness measured represents the effect of the 1283 hour exposure. However, if the test continued, it must be assumed that exfoliation would occur across the entire surface of the sample and simple measurements of corrosion product thickness and depth of IGA may not be adequate.

The Effect of Composition on the Corrosion Resistance of Selected Experimental Alloys in Deaerated 30% NaOH + 10% Na₂SO₄.

The results given in table (A1) suggest that under the conditions of test and within the compositional bounds specified there is no clear effect of Al, C or Ti on the IGA resistance of 690. The possibility that an effect of composition could be observed at longer exposures or under stressed conditions cannot be ruled out.

Though these results do not support the hypothesis that Al may be exerting some influence over the IGA resistance of 690, they do

not entirely disprove it either. The previous results were obtained after a longer exposure to the corrosive environment and it may be that the effects of compositional variations are time dependant.

These results confirm that alloy 690 must be considered a most suitable material for steam generator applications.

Conclusions.

- (A1) There appears to be no effect of increasing the aluminium content from <0.05% to 0.14% on the corrosion resistance of experimental melts of alloy 690 under the conditions of test.
- (A2) Increasing the carbon content of an experimental melt of 690 from 0.004% to 0.05% in the absence of both Al and Ti appears to have no pronounced effect on the alloys corrosion resistance under the conditions of test.
- (A3) An alloy with a Ti:C ratio close to that of the stoichiometric ratio does not demonstrate a lesser or greater corrosion resistance when compared to the other alloys tested under the same conditions.
- (A4) Thermal treatments ranging from solution treated only (1200^o) to solution treated + thermal ageing for 1, 5, 10 and 15 hours at 700^oC had no effect on the corrosion resistance of any of the alloys examined.

Further Work.

The above test should be continued to examine what effect increased exposure will have on the growth rate of the IGA and general corrosion. During longer exposures a measurement of sample weight loss may be more a appropriate guide to a given alloys performance.

It is possible that in the working environment of a steam generator tube the corrosion product will be susceptible to removal by erosion and vibration. If the IGA growth is "stunted" by the corrosion product formation then its continual removal by vibration or erosion may have considerable effect on the IGA growth rate. A more appropriate test procedure should be devised to take account of this.

Table (A1).

Material	Thermal Treatment Time (h)	Average Crack Length (μ)	Standard Deviation
EM 7	0	15.31	3.76
	1	14.76	1.53
	5	16.68	1.68
	10	13.37	2.08
	15	11.47	2.67
EM 11	0	13.50	0.87
	1	14.58	2.42
	5	14.01	1.34
	10	18.30	2.61
	15	15.43	1.95
EM 5	0	13.87	1.89
	1	15.43	2.20
	5	18.48	2.42
	10	14.94	1.34
	15	16.97	2.01
EM 6	0	14.76	2.35
	1	17.43	1.84
	5	16.95	1.96
	10	15.45	2.03
	15	12.45	1.15
EM 12	0	13.22	3.76
	1	16.22	2.04
	5	16.48	0.67
	10	14.92	2.71
	15	13.37	2.08
EM 13	0	15.13	2.53
	1	16.67	1.69
	5	15.18	0.93
	10	13.47	1.96
	15	14.37	2.23

Fig.(A1) EM 7. Exposed to deaerated 30% NaOH + 10% Na₂SO₄ at 350°C for 1283 hours. The attack appears to be by intergranular penetration followed by a period of general attack similar to the acid wastage reported in alloy 600. (200X Mag)

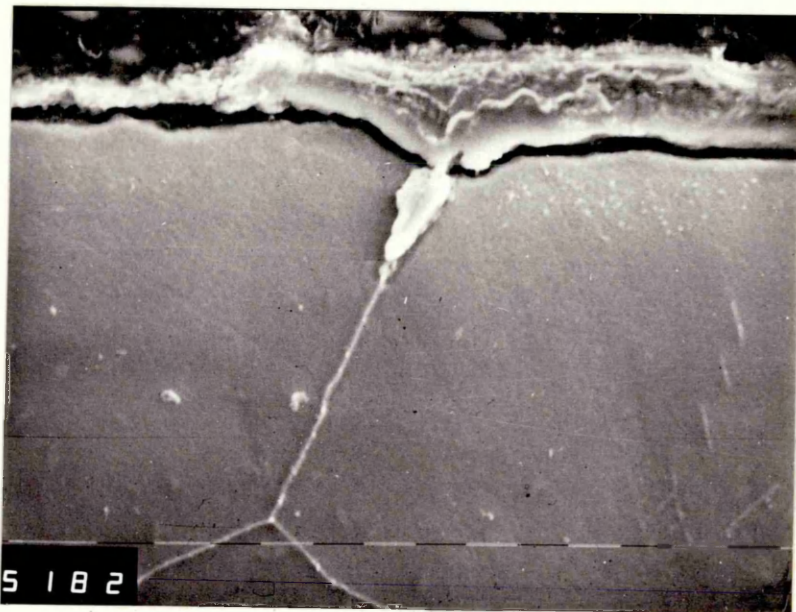
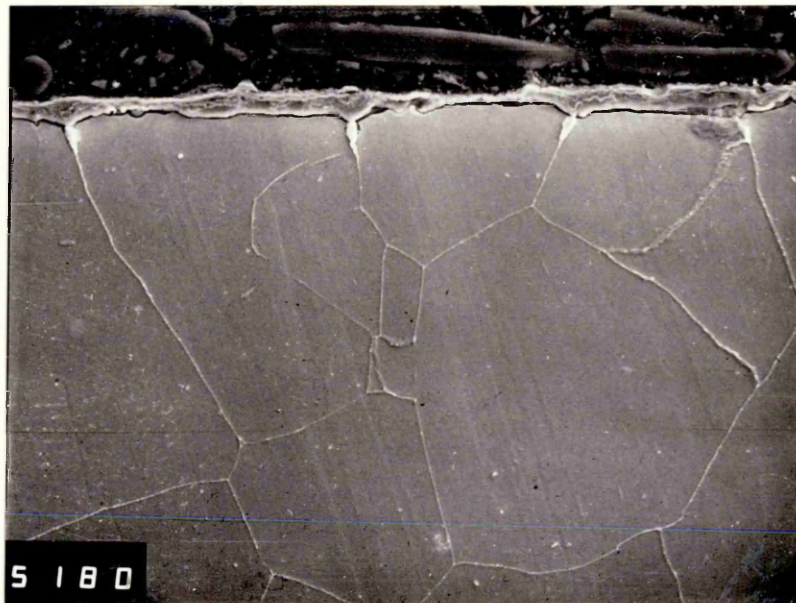


Fig.(A2). EM 12. Test conditions as above. Clear evidence of corrosion product build up in those boundaries penetrated, as well as more general corrosion above the IGA. (1400X mag).